

**Copyright**  
**By**  
**Jeffrey Roger Diephuis**  
**2004**

**Factors Affecting Bond in Multi-Strand Post-Tensioning Tendons  
Including the Effect of Emulsifiable Oils**

by

**Jeffrey Roger Diephuis, BSCE**

**Thesis**

Presented to the Faculty of the Graduate School of  
The University of Texas at Austin  
in Partial Fulfillment  
of the Requirements  
for the Degree of

**Master of Science in Engineering**

**The University of Texas at Austin**

**August 2004**

**Factors Affecting Bond in Multi-Strand Post-Tensioning Tendons**  
**Including the Effect of Emulsifiable Oils**

**APPROVED BY**  
**SUPERVISING COMMITTEE:**

---

**John E. Breen, Supervisor**

---

**Sharon L. Wood**

## **Dedication**

To my Family and to the Lord.

## **Acknowledgements**

I would like to express deep and sincere thanks to Dr. John E. Breen for the insight, guidance, and support he continually offered in his role as supervising professor. I also wish to express the same thanks to Dr. Michael E. Kreger who, in the early stages of the project, provided nearly day-to-day advice, encouragement, and direction. The things I learned from them will forever pay dividends in my professional life.

I express sincere thanks to Juan José Icaza, my partner in this research from the very beginning. Sharing each other's successes and failures as if they were our own, we shared not only a project, but a friendship. His continual input and effort to this work was invaluable. My sincere thanks also belong to Tanya Luthi who helped immensely in the completion of my testing and the revision of this document. I wish her good luck as she finishes the work I started.

I wish to thank Dr. Sharon Wood for her valuable input in the revision of this document.

I wish to acknowledge the assistance of the technical and administrative staff of the Ferguson Structural Engineering Laboratory. Hortensia Peoples, Mary Jo Moore, Michelle Santos, Regina Forward, Mike Bell, Dennis Phillip, and Blake Stasney and contributed immensely to the completion of this work. Likewise, I wish to thank our undergraduate

assistant Andrew Chronister for his work on this project, without which we never could have accomplished all that we did.

Many thanks are due to the students at the Ferguson Structural Engineering Laboratory. I am sure that each one contributed to my success in one way or another. Their friendship and support will always be remembered. Those deserving special mention include Mike, Christin, Michael, Rubén, and Will.

I gratefully acknowledge the Texas Department of Transportation and the Federal Highway Administration who provided the funding which made the work reported in this thesis possible.

Special thanks to my parents for their faithful support and loving encouragement. In teaching me by example the value of hard work and the satisfaction of a job well done, they gave me the discipline and inspiration to travel this far.

Thanks also to my brother, sister and the rest of my family for their encouragement and prayers.

Finally I thank God for his guiding hand, faithful provision, and most of all, for his gift of grace.

**Jeffrey Roger Diephuis**

**August, 2004**

# **Factors Affecting Bond in Multi-Strand Post-Tensioning Tendons Including the Effect of Emulsifiable Oils**

Jeffrey Roger Diephuis, M.S.E.

The University of Texas at Austin, 2004

SUPERVISOR: John E. Breen

Recent corrosion problems worldwide have brought increased attention to the issues of durability and corrosion resistance of post-tensioned tendons. While the overall experience in the United States has been good, there is a desire to implement further measures to ensure the adequate protection of post-tensioning systems.

This thesis is part of a broad research program evaluating both temporary and long-term corrosion protection solutions. In particular, this thesis addresses the effect of emulsifiable oils used for temporary corrosion protection on bond in multi-strand post-tensioning tendons. The effect of duct type on bond behavior is also investigated.

Overall findings indicate that while the force developed by oiled strands is satisfactory, the reduced adhesion between the steel and the grout results in excessive slip. Additionally, galvanized steel pipes tended to allow the grout to slip relative to the duct or the duct to slip relative to the concrete at significantly reduced loads. Corrugated ducts eliminated this slip. Of the corrugated ducts, galvanized metal ducts provided somewhat better bond performance than high density polyethylene ducts.



## Table of Contents

<b>CHAPTER 1 INTRODUCTION.....</b>	<b>1</b>
1.1 Background .....	1
1.2 Research Objectives and Scope.....	2
1.2.1 Project Statement.....	2
1.2.2 Project Objectives .....	4
1.2.3 Project Scope.....	5
1.2.4 Thesis Scope.....	6
<b>CHAPTER 2 BACKGROUND.....</b>	<b>7</b>
2.1 Bond Mechanics for Prestressing Strand and Multi-Strand Tendons .....	7
2.2 Previous Single Strand Research.....	9
2.3 Previous Multi-Strand Research.....	11
2.3.1 Calculation of Bond Stress .....	11
2.3.2 Trost et al.....	13
2.3.3 Braverman .....	13
2.3.4 Osborne .....	15
2.3.5 Radloff.....	15
2.3.6 Schupack and Johnston .....	17
2.3.7 Losinger.....	17
2.3.8 VSL .....	17
2.3.9 Limitations of Previous Research .....	18

<b>CHAPTER 3 EXPERIMENTAL PROGRAM.....</b>	<b>19</b>
3.1 Introduction .....	19
3.2 Development of Test Specimens.....	19
3.2.1 Review of Typical Post-Tensioning Systems.....	20
3.2.2 Selection of Variables .....	21
3.2.3 Description of Specimens.....	22
3.3 Materials.....	24
3.3.1 Prestressing Strand .....	24
3.3.2 Duct .....	24
3.3.3 Grout.....	26
3.3.4 Emulsifiable Oil .....	26
3.3.5 Post-Tensioning Hardware.....	26
3.3.6 Concrete and Reinforcing Steel.....	27
3.4 Fabrication of Bond Test Specimens .....	28
3.4.1 Reinforcing Steel.....	28
3.4.2 Formwork and Placement of Concrete.....	29
3.5 Preparation of Bond Test Specimens .....	30
3.5.1 Installation of Tendon .....	30
3.5.2 Pre-grout Stressing .....	34
3.5.3 Tendon Sealing.....	34
3.5.4 Grouting .....	37
3.6 Instrumentation.....	39
3.6.1 Force Measurements .....	39
3.6.2 Displacement Measurements.....	40
3.6.3 Data Acquisition Equipment .....	40
3.7 Testing Sequence.....	42
3.7.1 Overview .....	42

3.7.2 Loading Procedure .....	43
3.8 Specimen Summary.....	43
3.8.1 Specimen Naming Scheme.....	43
3.9 Recommendations for Future Testing.....	47
<b>CHAPTER 4 TEST RESULTS .....</b>	<b>48</b>
4.1 Introduction .....	48
4.2 Test Data .....	48
4.2.1 Galvanized Steel Pipe Specimens .....	52
4.2.1.1 0-SP-20°-1 .....	52
4.2.1.2 0-SP-15°-1 .....	55
4.2.1.3 0-SP-10°-1 .....	58
4.2.1.4 0-SP-10°-2 .....	61
4.2.1.5 0-SP-7.5°-1 .....	63
4.2.1.6 0-SP-7.5°-2 .....	66
4.2.1.7 1-SP-7.5°-1 .....	69
4.2.1.8 1-SP-7.5°-2 .....	72
4.2.2 Galvanized Metal Duct Specimens .....	75
4.2.2.1 0-GD-20°-1 .....	75
4.2.2.2 0-GD-15°-1 .....	77
4.2.2.3 0-GD-10°-1 .....	79
4.2.2.4 0-GD-10°-2 .....	81
4.2.2.5 0-GD-7.5°-1 .....	83
4.2.2.6 0-GD-7.5°-2 .....	86
4.2.2.7 0-GD-7.5°-3 .....	89
4.2.2.8 0-GD-5°-1 .....	92
4.2.2.9 1-GD-7.5°-1 .....	95
4.2.2.10 1-GD-7.5-2 .....	98

4.2.3 High Density Polyethylene Duct Specimens .....	101
4.2.3.1 0-HD-20°-1.....	101
4.2.3.2 0-HD-15°-1.....	103
4.2.3.3 0-HD-10°-1.....	105
4.2.3.4 0-HD-10°-2.....	107
4.2.3.5 0-HD-10°-3.....	110
4.2.3.6 0-HD-7.5°-1.....	113
4.2.3.7 0-HD-7.5°-2.....	115
4.2.3.8 0-HD-7.5°-3.....	118
4.2.3.9 1-HD-7.5°-1.....	121
4.2.3.10 1-HD-7.5°-2.....	124

<b>CHAPTER 5 COMPARISON OF BEHAVIOR AND EFFECT OF VARIABLES .....</b>	<b>127</b>
5.1 Introduction .....	127
5.1.1 Modes of Failure .....	127
5.1.2 Summary of Data .....	128
5.2 Comparisons Within Duct Types .....	132
5.2.1 Galvanized Steel Pipe Specimens .....	132
5.2.1.1 Comparison with Previous Results .....	134
5.2.2 Galvanized Metal Duct Specimens .....	135
5.2.2.1 Comparison with Previous Results .....	137
5.2.3 High Density Polyethylene Duct Specimens .....	137
5.3 Comparisons Among Duct Types .....	142
5.4 Comparisons Between Oiled and Unoiled Specimens.....	144
5.5 Summary of Findings .....	147
5.5.1 Effect of Duct Type.....	147
5.5.2 Effect of Emulsifiable Oil .....	147

5.5.3 Effect of Confinement.....	148
<b>CHAPTER 6 SUMMARY AND CONCLUSIONS.....</b>	<b>149</b>
6.1 Introduction.....	149
6.2 Summary and Conclusions.....	150
6.2.1 Effect of Duct Type.....	150
6.2.2 Effect of Tendon Surface Condition.....	150
6.2.3 Effect of Confining Reinforcement.....	151
6.3 Overall Conclusions and Suggestions for Implementation.....	151
6.4 Directions for Future Research.....	152
<b>APPENDIX B ORIGINAL AND MODIFIED TEST DATA.....</b>	<b>153</b>
A.1 Galvanized Steel Pipe Specimen Data.....	153
A.2 Galvanized Metal Duct Specimen Data.....	165
A.3 HDPE Duct Specimen Data.....	181
<b>APPENDIX B SPECIMEN</b>	
<b>SUMMARY.....</b>	<b>197</b>
<b>REFERENCES.....</b>	<b>199</b>
<b>VITA.....</b>	<b>202</b>

## **List of Tables**

Table 2-1 Trost et al. Tests and Results .....	14
Table 2-2 Radloff Test Results.....	16
Table 3-1 Specimen Size Details .....	22
Table 3-2 Specimen Summary .....	45
Table 5-1 Data Summary for Galvanized Steel Pipe Specimens .....	129
Table 5-2 Data Summary for Galvanized Metal Duct Specimens .....	130
Table 5-3 Data Summary for HDPE Duct Specimens .....	131

## List of Figures

Figure 2-1 Hoyer Effect .....	8
Figure 3-1 Specimen Profiles .....	23
Figure 3-2 Galvanized Steel Duct .....	25
Figure 3-3 HDPE Duct .....	25
Figure 3-4 Galvanized Steel Pipe .....	25
Figure 3-5 Post-Tensioning Anchor Head and Wedges .....	27
Figure 3-6 Reinforcing Steel Cage Type S .....	28
Figure 3-7 Reinforcing Steel Cage Type H .....	29
Figure 3-8 Assembled Specimen Cage, Duct, and Formwork .....	30
Figure 3-9 Tension Ring Bearing Plate .....	31
Figure 3-10 Prestressing Equipment on Supports .....	32
Figure 3-11 Specimen Ready for Installation of Tendon .....	32
Figure 3-12 Oil Application .....	33
Figure 3-13 Prestressing Setup .....	33
Figure 3-14 Completed Initial Foaming .....	35
Figure 3-15 Specimen Ready for Final Foaming .....	36
Figure 3-16 Completed Final Foaming .....	36
Figure 3-17 Hand Grout Pump .....	38
Figure 3-18 Live End Linear Potentiometer Placement .....	41
Figure 3-19 Dead End Linear Potentiometer Placement .....	41

Figure 3-20 A Specimen Ready For Testing.....	42
Figure 4-1 Live End Data Requiring Large Modification.....	50
Figure 4-2 Dead End Data Requiring Large Modification .....	50
Figure 4-3 Live End Data Requiring Average Modification .....	51
Figure 4-4 Dead End Data Requiring Average Modification .....	51
Figure 4-5 Live End Load-Displacement and Dead End Load-Slip Response for Specimen 0-SP-20°-1 .....	53
Figure 4-6 Dead End Load-Slip Response for Specimen 0-SP-20°-1, Amplified Scale.....	53
Figure 4-7 Live End of Specimen 0-SP-20°-1 after Testing.....	54
Figure 4-8 Live End Load-Displacement and Dead End Load-Slip Response for Specimen 0-SP-15°-1 .....	56
Figure 4-9 Dead End Load-Slip Response for Specimen 0-SP-15°-1, Amplified Scale.....	56
Figure 4-10 Live End of Specimen 0-SP-15°-1 after Testing.....	57
Figure 4-11 Live End Load-Displacement and Dead End Load-Slip Response for Specimen 0-SP-10°-1, Normal Range .....	59
Figure 4-12 Dead End Load-Slip Response for Specimen 0-SP-10°-1, Amplified Scale.....	59
Figure 4-13 Live End Load-Displacement Response for Specimen 0-SP-10°-1, Full Range .....	60
Figure 4-14 Live End of Specimen 0-SP-10°-1 after Testing.....	60
Figure 4-15 Live End Load-Displacement and Dead End Load-Slip Response for Specimen 0-SP-10°-2 .....	62
Figure 4-16 Dead End Load-Slip Response for Specimen 0-SP-10°-2, Amplified Scale.....	62



Figure 4-17 Live End Load-Displacement and Dead End Load-Slip Response for Specimen 0-SP-7.5°-1 .....	64
Figure 4-18 Dead End Load-Slip Response for Specimen 0-SP-7.5°-1, Amplified Scale .....	64
Figure 4-19 Live End of Specimen 0-SP-7.5°-1 after Testing .....	65
Figure 4-20 Live End Load-Displacement and Dead End Load-Slip Response for Specimen 0-SP-7.5°-2 .....	67
Figure 4-21 Dead End Load-Slip Response for Specimen 0-SP-7.5°-2, Amplified Scale .....	67
Figure 4-22 Live End of Specimen 0-SP-7.5°-2 after Testing .....	68
Figure 4-23 Live End Load-Displacement and Dead End Load-Slip Response for Specimen 1-SP-7.5°-1 .....	70
Figure 4-24 Dead End Load-Slip Response for Specimen 1-SP-7.5°-1, Amplified Scale .....	70
Figure 4-25 Photo of Specimen 1-SP-7.5°-1 after Testing .....	71
Figure 4-26 Live End Load-Displacement and Dead End Load-Slip Response for Specimen 1-SP-7.5°-2 .....	73
Figure 4-27 Dead End Load-Slip Response for Specimen 1-SP-7.5°-2, Amplified Scale .....	73
Figure 4-28 Photo of Specimen 1-SP-7.5°-2 after Testing .....	74
Figure 4-29 Live End Load-Displacement and Dead End Load-Slip Response for Specimen 0-GD-20°-1 .....	76
Figure 4-30 Dead End Load-Slip Response for Specimen 0-GD-20°-1, Amplified Scale .....	76
Figure 4-31 Live End Load-Displacement and Dead End Load-Slip Response for Specimen 0-GD-15°-1 .....	78
Figure 4-32 Dead End Load-Slip Response for Specimen 0-GD-15°-1, Amplified Scale .....	78

Figure 4-33	Live End Load-Displacement and Dead End Load-Slip Response for Specimen 0-GD-10°-1 .....	80
Figure 4-34	Dead End Load-Slip Response for Specimen 0-GD-10°-1, Amplified Scale .....	80
Figure 4-35	Live End Load-Displacement and Dead End Load-Slip Response for Specimen 0-GD-10°-2 .....	82
Figure 4-36	Dead End Load-Slip Response for Specimen 0-GD-10°-2, Amplified Scale .....	82
Figure 4-37	Live End Load-Displacement and Dead End Load-Slip Response for Specimen 0-GD-7.5°-1 .....	84
Figure 4-38	Dead End Load-Slip Response for Specimen 0-GD-7.5°-1, Amplified Scale .....	84
Figure 4-39	Profile of Specimen 0-GD-7.5°-1 after Testing .....	85
Figure 4-40	Live End Load-Displacement and Dead End Load-Slip Response for Specimen 0-GD-7.5°-2 .....	87
Figure 4-41	Dead End Load-Slip Response for Specimen 0-GD-7.5°-2, Amplified Scale .....	87
Figure 4-42	Photo of Specimen 0-GD-7.5°-2 after Testing .....	88
Figure 4-43	Live End Load-Displacement and Dead End Load-Slip Response for Specimen 0-GD-7.5°-3 .....	90
Figure 4-44	Dead End Load-Slip Response for Specimen 0-GD-7.5°-3, Amplified Scale .....	90
Figure 4-45	Profile of Specimen 0-GD-7.5°-3 after Testing .....	91
Figure 4-46	Live End Load-Displacement and Dead End Load-Slip Response for Specimen 0-GD-5°-1 .....	93
Figure 4-47	Dead End Load-Slip Response for Specimen 0-GD-5°-1, Amplified Scale .....	93
Figure 4-48	Photo of Specimen 0-GD-5°-1 after Testing .....	94

Figure 4-49	Live End Load-Displacement and Dead End Load-Slip Response for Specimen 1-GD-7.5°-1 .....	96
Figure 4-50	Dead End Load-Slip Response for Specimen 1-GD-7.5°-1, Amplified Scale .....	96
Figure 4-51	Photo of Specimen 1-GD-7.5°-1 after Testing .....	97
Figure 4-52	Live End Load-Displacement and Dead End Load-Slip Response for Specimen 1-GD-7.5°-2 .....	99
Figure 4-53	Dead End Load-Slip Response for Specimen 1-GD-7.5°-2, Amplified Scale .....	99
Figure 4-54	Photo of Specimen 1-GD-7.5°-2 after Testing .....	100
Figure 4-55	Live End Load-Displacement and Dead End Load-Slip Response for Specimen 0-HD-20°-1 .....	102
Figure 4-56	Dead End Load-Slip Response for Specimen 0-HD-20°-1, Amplified Scale .....	102
Figure 4-57	Live End Load-Displacement and Dead End Load-Slip Response for Specimen 0-HD-15°-1 .....	104
Figure 4-58	Dead End Load-Slip Response for Specimen 0-HD-15°-1, Amplified Scale .....	104
Figure 4-59	Live End Load-Displacement and Dead End Load-Slip Response for Specimen 0-HD-10°-1 .....	106
Figure 4-60	Dead End Load-Slip Response for Specimen 0-HD-10°-1, Amplified Scale .....	106
Figure 4-61	Live End Load-Displacement and Dead End Load-Slip Response for Specimen 0-HD-10°-2 .....	108
Figure 4-62	Dead End Load-Slip Response for Specimen 0-HD-10°-2, Amplified Scale .....	108
Figure 4-63	Photo of Specimen 0-HD-10°-2 after Testing .....	109

Figure 4-64 Live End Load-Displacement and Dead End Load-Slip Response for Specimen 0-HD-10°-3 .....	111
Figure 4-65 Dead End Load-Slip Response for Specimen 0-HD-10°-3, Amplified Scale .....	111
Figure 4-66 Side View of Specimen 0-HD-10°-3 after Testing.....	112
Figure 4-67 Top View of Specimen 0-HD-10°-3 after Testing .....	112
Figure 4-68 Live End Load-Displacement and Dead End Load-Slip Response for Specimen 0-HD-7.5°-1 .....	114
Figure 4-69 Dead End Load-Slip Response for Specimen 0-HD-7.5°-1, Amplified Scale .....	114
Figure 4-70 Live End Load-Displacement and Dead End Load-Slip Response for Specimen 0-HD-7.5°-2 .....	116
Figure 4-71 Dead End Load-Slip Response for Specimen 0-HD-7.5°-2, Amplified Scale .....	116
Figure 4-72 Photo of Specimen 0-HD-7.5°-2 after Testing .....	117
Figure 4-73 Live End Load-Displacement and Dead End Load-Slip Response for Specimen 0-HD-7.5°-3 .....	119
Figure 4-74 Dead End Load-Slip Response for Specimen 0-HD-7.5°-3, Amplified Scale .....	119
Figure 4-75 Photo of Specimen 0-HD-7.5°-3 after Testing .....	120
Figure 4-76 Photo of Specimen 0-HD-7.5°-3 after Testing .....	120
Figure 4-77 Live End Load-Displacement and Dead End Load-Slip Response for Specimen 1-HD-7.5°-1 .....	122
Figure 4-78 Dead End Load-Slip Response for Specimen 1-HD-7.5°-1, Amplified Scale .....	122
Figure 4-79 Photo of Specimen 1-HD-7.5°-1 after Testing .....	123
Figure 4-80 Live End Load-Displacement and Dead End Load-Slip Response for Specimen 1-HD-7.5°-2 .....	125

Figure 4-81 Dead End Load-Slip Response for Specimen 1-HD-7.5°-2, Amplified Scale.....	125
Figure 4-82 Photo of Specimen 1-HD-7.5°-2 after Testing.....	126
Figure 5-1 Failure Load vs. Bonded Length for Galvanized Pipe Specimens...	133
Figure 5-2 Bond Stress vs. Bonded Length for Galvanized Pipe Specimens ....	133
Figure 5-3 Failure Load vs. Bonded Length for Galvanized Metal Duct Specimens.....	136
Figure 5-4 Tendon-Grout Bond Stress vs. Bonded Length for Galvanized Metal Duct Specimens .....	136
Figure 5-5 Failure Load vs. Bonded Length for HDPE Duct Specimens .....	139
Figure 5-6 Tendon-Grout Bond Stress vs. Bonded Length for HDPE Duct Specimens.....	139
Figure 5-7 Peak Failure Load vs. Bonded Length for Different Transverse Reinforcement Spacings.....	141
Figure 5-8 Tendon-Grout Bond Stress vs. Bonded Length for Different Transverse Reinforcement Spacings .....	141
Figure 5-9 Average Failure Loads for 7.5° Specimens with Different Duct Types .....	142
Figure 5-10 Average Failure Loads for 7.5° Specimens with Oiled and Unoiled Tendons .....	144
Figure 5-11 Peak Loads for 7.5° Specimens with Oiled and Unoiled Tendons in Galvanized Metal and HDPE Ducts.....	146

# CHAPTER 1

## Introduction

### 1.1 BACKGROUND

Durability and design life are important aspects of any engineered structure. Recent experiences worldwide have heightened attention to these issues when considering the design and safety of post-tensioned structures, particularly long-span bridges. The 1992 collapse of the Ynys-y-Gwas bridge in Wales, U.K. (Woodward, 2001); the discovery of significant corrosion of post-tensioning tendons in several Florida, U.S.A. bridges (Pielstick, 2002); and other instances of corrosion have highlighted the importance of the durability and reliability of post-tensioning systems and techniques. The fact that most post-tensioning systems cannot be easily inspected or replaced after construction lends increased consequence to their durability (Ganz, 2002). While these cases of severe corrosion seem alarming, they represent only a very small fraction of the post-tensioned structures currently in service (Freyermuth, 2001). The experience in the United States has overall been very good, and many states with large numbers of post-tensioned bridges have reported no problems to date (ASBI, 2002).

An outgrowth of this increased scrutiny has been the introduction of a host of new materials and construction techniques intended to improve the long-term performance of post-tensioning systems. New materials have been suggested for every part of the post-tensioning system including the strand, anchorages, duct, duct couplers, grout, and so on (fib, 2000; Ganz, 2002; Tourneur, 2002). Construction techniques including improved grouting methods and training of

grouting personnel, certification of grouters, grouting sooner after stressing, applying temporary corrosion inhibitors to the strands, increasing construction inspection, and more have also been suggested (ASBI, 2002; PTI, 2001; Schokker et al., 1999).

Often engineers rush to implement these new and often unproven materials and techniques out of fear, or at the insistence of an uninformed owner. Many aspects of these innovative materials and techniques have yet to be physically evaluated for their merit in improving the safety and durability of post-tensioned structures. This evaluation is necessary for both engineers and owners to make intelligent decisions about the design and construction of post-tensioned structures.

## **1.2 RESEARCH OBJECTIVES AND SCOPE**

This section provides an overview of the larger project, of which this thesis is part.

### **1.2.1 Project Statement**

The research presented in this thesis is part of The University of Texas at Austin, Center for Transportation Research Project 0-4562: “Effect of Emulsifiable Oils Used as Temporary Corrosion Protection in Grouted Post-Tensioned Tendons, and Investigation of Alternate Corrosion-Resistant Post-Tensioning Systems.” Work on this project is being performed at Pennsylvania State University and at the Phil M. Ferguson Structural Engineering Laboratory at The University of Texas at Austin. The project is sponsored by the Texas Department of Transportation (TxDOT) and the Federal Highway Administration (FHWA).

As the project title indicates, there are two distinct facets to this project: the investigation into the effect of emulsifiable oils used for temporary corrosion

protection, and the assessment of alternative post-tensioning systems used to provide long-term corrosion resistance. Due to the distinctness of each aspect, the project is divided into two phases.

The first phase addresses the desire of contractors to increase economy by delaying grouting operations until a significant amount of work is ready and can be completed at once. Owners, on the other hand, are very reluctant to relax the stringent restrictions set forth by the Post-Tensioning Institute (PTI, 2000) and the American Association of State Highway and Transportation Officials (AASHTO, 2002) which limit the length of time ungrouted strands may be in ducts. Additionally, the use of a temporary corrosion protection system would provide a margin of safety against unforeseen construction delays which could postpone grouting. Potential side effects of using oils for temporary corrosion protection are a reduction in both bond and friction. This phase of the project addresses the effect of temporary corrosion protection on corrosion rate, bond strength, and friction losses of post-tensioning tendons.

The second phase of the project reflects the desire of designers and owners to have reliable information about the benefits, if any, of using new technologies to provide enhanced durability for post-tensioning systems. Recently, the post-tensioning market has been flooded with new materials and technologies claiming improved durability. Many of these technologies are more costly than standard systems and materials, and independent observations of their relative performance are necessary to aid in the informed selection of appropriate post-tensioning systems and materials. This thesis does not address any of the issues related to the second phase of the project.



### **1.2.2 Project Objectives**

The primary objectives of TxDOT Project 0-4562 are as follows:

#### *Phase I*

1. Identify emulsifiable oils or other suitable products for providing temporary corrosion protection.
2. Assess the performance of the corrosion-inhibiting products.
3. Investigate how the products affect friction loss during post-tensioning.
4. Determine the impact of corrosion-inhibiting products on bond strength and behavior of multi-strand tendons.
5. Determine how flexural capacity is affected by any changes in bond strength or behavior and develop recommendations for the use of temporary corrosion protection.

#### *Phase II*

1. Identify alternate materials and systems for corrosion resistant post-tensioning systems.
2. Examine physical and mechanical properties of new materials.
3. Identify and evaluate potential accelerated corrosion test methods.
4. Plan and implement a series of tests examining the durability of different post-tensioning systems and materials.
5. Consider the constructability and behavior of corrosion resistant post-tensioning systems.
6. Develop recommendations for implementation of alternate post-tensioning systems.

In each phase, the final objective represents the culmination of the work, and the findings will be compiled into design guidelines.

### **1.2.3 Project Scope**

The objectives of this project are very broad and it was necessary to limit the scope of the project to a manageable size. For this reason, each phase of the project was divided into individual tasks of narrowly defined scope. This thesis will only discuss the tasks of phase I.

#### ***1.2.3.1 Phase I***

The tasks for Phase I of TxDOT Project 0-4562 are as follows:

1. Identification of Emulsifiable Oils
2. Accelerated Corrosion Testing
3. PTI/ASTM Single-Strand Pullout Tests
4. Tendon Friction Tests
5. Multiple-Span Beam Tests
6. Development of Specifications and Code Changes
7. Preparation of Reports

The first three tasks were carried out by Salcedo (2003) at Pennsylvania State University. The use of small-scale accelerated corrosion testing and single-strand pullout tests allowed Salcedo to evaluate a large number of emulsifiable oils quickly and inexpensively. His findings were reviewed by the research team and used to select the oils evaluated in the subsequent tasks.

Task four evaluated friction losses using large-scale test specimens and realistic tendon sizes, with a limited number of oils.

While it was initially envisioned that task five would test multiple-span beams to determine the bond performance of oiled multi-strand tendons, it

became clear to the research team that large-scale pullout testing would allow the investigation of a larger number of variables. While the work in the task does not directly address the effect of emulsifiable oils on flexural capacity or behavior, the results of the large-scale pullout tests provide insight into the nature of bond and the effect emulsifiable oils have on bond in multi-strand post-tensioning tendons. This information provides for an indirect assessment of flexural capacity and behavior. Initial findings for this task are reported in this thesis. To this point only large-scale pullout testing has been completed towards the fulfillment of this task, however, the research team reserves the option to test a small number of multiple-span beams to verify the conclusions drawn based on the results of the large-scale pullout testing.

Tasks six and seven will commence when the final results of tasks four and five have been compiled.

#### **1.2.4 Thesis Scope**

The author's involvement in Project 0-4562 began in August of 2002, and included work on many of the tasks in both phases. The scope of this thesis includes only work from task 5 of phase 1. The work of task 5 is not yet complete, and additional testing will take place beyond the completion of this thesis.

In Chapter 2, an overview of bond mechanics is given, as is a summary of previous research done in the area of bond of multi-strand post-tensioning tendons. Chapter 3 explains the variables and describes the test procedure employed in this research program. Chapter 4 provides the data collected in all completed large-scale pullout tests. A brief description of the results is also provided. Chapter 5 presents the findings of the research program to date, and Chapter 6 provides a summary and the conclusions.

## CHAPTER 2

### Background

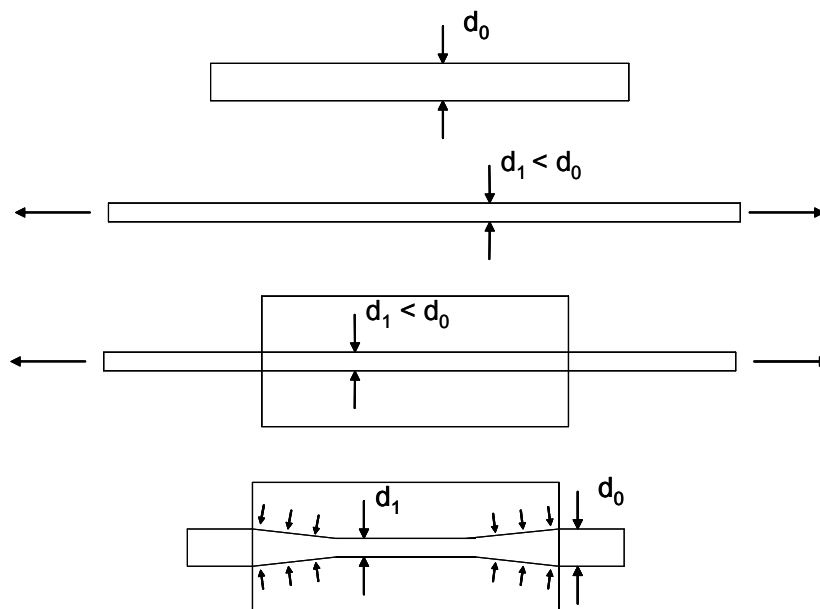
#### 2.1 BOND MECHANICS FOR PRESTRESSING STRAND AND MULTI-STRAND TENDONS

Bond transfer between prestressing strand and concrete or cementitious grout occurs through three primary mechanisms: adhesion, friction, and mechanical restraint. Adhesion is the microscopic physical and chemical interlock between steel and concrete. Adhesion exists between concrete and steel only until relative slip occurs between the two materials, shearing the bonds. (Laldji and Young, 1988) Friction occurs with a decrease in steel strain and a corresponding increase in strand diameter. This action, commonly termed the Hoyer effect, causes radial pressure against the concrete or grout and a resulting friction force resistant to slip of the strand. Mechanical restraint occurs as the irregular shape of a strand attempts to move through the surrounding concrete or grout. The strand surface bears against the material causing resistance to slip. This mechanism is similar to, but less effective than, that caused by the lugs in ordinary reinforcing steel. (Janney, 1954; Hanson and Kaar, 1959)

There are two primary actions requiring the development of bond stress: transfer bond and flexural bond. Transfer bond is most applicable to pretensioned concrete members, while flexural bond exists in any concrete member reinforced with steel.

Transfer bond imparts the prestress force into a pretensioned member at release. It is developed through the actions of friction and mechanical restraint. Janney (1954) showed that in the transfer zone, the reduction in steel strain does

not equal the compressive strain in the concrete at the same point. Adhesion therefore cannot contribute to transfer bond, since slip has occurred in this region. Both friction and mechanical interlock play important roles in the development of transfer bond. When a strand is stressed, its diameter decreases according to Poisson's ratio. After the concrete cast around the strand hardens, the external restraint on the strand is released, and the stress at the ends of the strand returns to zero. The strand near the ends then attempts to return to its initial diameter, exerting a radial pressure against the hardened concrete that in turn creates a clamping force on the strand. (Collins and Mitchell, 1997) This clamping force or pressure creates a corresponding frictional resistance to slip. Figure 2-1 provides a pictorial representation of this action, often called the Hoyer effect. Mechanical resistance also occurs as slippage in the transfer zone changes the pitch of the strand, and the helical shape of the prestressing strand develops resistance against its impression in the concrete. (Janney, 1954; Hanson and Kaar, 1959)



**Figure 2-1 Hoyer Effect**

Flexural bond develops due to bending action on a flexural element. Localized bond stresses occur in the vicinity of flexural cracking. As the strand stress increases, adhesion is lost and slip occurs adjacent to the crack. Since the strand is loaded in increasing tension, radial contraction according to Poisson's ratio results in reduced frictional resistance to slip. This loss of frictional resistance is compensated for by changes in the pitch of the helical wires relative to the impression in the concrete. (Salmons and McCrate, 1977) This mechanical resistance is not as effective in prestressing steel as it is in regular reinforcing steel, which has ribs or lugs; however, it is sufficient to maintain the load carrying capacity of the member. (Hanson and Kaar, 1959)

## **2.2 PREVIOUS SINGLE STRAND RESEARCH**

Much experimental research has been done investigating the complex nature of bond between prestressing strand and concrete or grout. Single strand research has shown several important parameters affecting this behavior including the following:

### **1) Strand Surface Condition**

Janney (1954) and Hanson and Kaar (1959) showed that bond performance of rusted strand is as much as 30% better than that of clean, bright strand. Recent work by Barnes et al. (2003) confirmed this finding. However, the former also found that there was higher variability in the transfer lengths of rusted strand, and concluded that it could not be relied on to provide reduced transfer lengths.

Anderson and Anderson (1976) claimed that strands coated in oil did not show any reduction in bond performance. More recent research by Kittleman (1992) and Salcedo (2003) showed that the bond capacities of strands coated in

emulsifiable oil are reduced up to 97%. Kittleman also showed that while flushing oil from strands prior to grouting provided slightly better bond performance, the bond reduction compared to unoiled strands was significant.

## 2) Concrete or Grout Strength

Kaar et al. (1963) did a comprehensive study of prestress transfer lengths for strands with nominal diameters up to 1/2 in. and with concrete compressive strengths ranging from 1600 to 5000 psi. It was concluded that concrete strength had little effect on transfer bond. Flexural and pullout tests performed by Janney (1954) and Salmons and McCrate (1977) verified this conclusion. Most other research has, however, contradicted this conclusion, and it is generally accepted today that the compressive strength of concrete or grout has an influence on bond. Work done by Stocker and Sozen (1970) with concrete compressive strengths ranging from 2400 to 5000 psi showed a 10% increase in bond strength for every additional 1000 psi of concrete compressive strength. More recent work by Barnes et al. (2003) found that transfer length was proportional to the ratio of the strand stress at transfer and the square root of the concrete compressive strength at transfer.

## 3) Concrete or Grout Confinement

While most researchers concede that confinement plays a role in the bond behavior of prestressing strand, there is little available data quantifying this effect.

## 4) Rate of Loading

Karr et al. (1963) determined that the rate of release had a moderate effect on the transfer length of pretensioned elements. They found a 20% reduction in bond strength for 1/2-in. strand released by flame cutting rather than slow release.

For 0.6-in. diameter strand, the reduction was higher, around 30%. This finding was confirmed by Russell and Burns (1997). However, Barnes et al. (2003) showed that for concrete compressive strengths in excess of 7000 psi, the prestress release method had no effect on the transfer length for clean bright strands. Rusted strands, however, had longer transfer lengths when released suddenly. Work done by Vos and Reinhardt (1982) showed no significant effect of loading rate on pullout behavior of strand.

## **2.3 PREVIOUS MULTI-STRAND RESEARCH**

The body of research in the field of bond of multi-strand tendons is more limited than that of single strands. This section will review results of large-scale bond tests conducted using multi-strand tendons.

### **2.3.1 Calculation of Bond Stress**

In order to compare test results, a bonded area for various tendon sizes must be calculated. There are many ways to make the calculation, each one yielding a different result. The most common way of calculating a bonded area for a tendon is to calculate an equivalent tendon circumference,  $C_e$ , based on the steel area of the tendon. The bonded area is then the bonded length times the equivalent circumference. The bond stress is then the load divided by the bonded area. The following equations illustrate these calculations.

$$A_{ps} = \pi \cdot r_e^2 \quad \text{Equation 1}$$

$$r_e = \sqrt{\frac{A_{ps}}{\pi}} \quad \text{Equation 2}$$

$$C_e = 2 \cdot \pi \cdot r_e \quad \text{Equation 3}$$



$$C_e = 2\pi \cdot \sqrt{\frac{A_{ps}}{\pi}} \quad \text{Equation 4}$$

$$A_b = C_e \cdot L \quad \text{Equation 5}$$

$$\sigma_b = \frac{P}{A_b} \quad \text{Equation 6}$$

Where:

$C_e$  = Equivalent Tendon Circumference

$A_{ps}$  = Tendon Steel Area

$r_e$  = Equivalent Tendon Radius

$L$  = Bonded Length

$A_b$  = Equivalent Bonded Area

$P$  = Axial Load Applied to the Tendon

$\sigma_b$  = Bond Stress

In order to calculate the bonded area between the duct wall and the grout or the duct wall and the concrete, the actual inner or outer diameter of the duct, as appropriate, is used in place of the equivalent tendon circumference in Equation 5. The bond stress is then calculated as usual using Equation 6.

All bond stress results provided in this chapter are reported based on this method for calculating the bonded area. Results that were not originally reported using this format have been converted for consistency.

### **2.3.2 Trost et al.**

A large testing program was carried out by Trost et al. (1978, 1980) to evaluate the performance of a range of multi-strand tendon arrangements grouted in straight, corrugated, steel ducts. The results of the monotonic pullout tests, which were compiled by Radloff (1990), are summarized in Table 2-1.

In test series A, Trost achieved stable pullout for all specimens. Stable pullout was defined as dead end slip accumulating without a significant reduction in load. Specimens where the tendon was located adjacent to the duct wall exhibited greater slip and a 68% lower bond capacity than specimens where the tendon was located in the center of the duct.




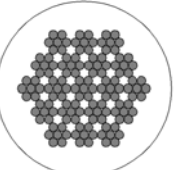
In test series B stable pullout was again achieved, with bond stresses similar to those observed in series A.

In test series C, bursting cracks developed at unloaded end displacements in the range of 0.1 – 0.3 mm, and bond failure occurred suddenly. For these tests, stable pullout was not observed.

### **2.3.3 Braverman**

Braverman (1985) conducted pullout tests of 1, 3, and 5-strand tendons with 3/8-in. diameter strands, grouted in the center of straight, smooth, steel ducts. The purpose of the research program was to investigate the effect of a variable tendon area to duct cross-sectional area ratio. The program evaluated ratios of 5%, 14%, and 24%, and tested specimens with 12 in. bonded lengths. The largest bond stress developed was 1.07 ksi and was achieved in the 3-strand tendon, which corresponded to the 14% area ratio. The larger tendon, which occupied 24% of the duct cross-sectional area, failed at the duct-grout interface at a significantly reduced load. The bond stress developed between the duct wall and the grout averaged 0.548 ksi in the two 5-strand tests.

**Table 2-1 Trost et al. Tests and Results**

Test Series	A-9	A-10	B	C-4
Strand Pattern				
Test Details	Tendon in Center of Duct	Tendon Against Wall of Duct	Tendon in Center of Duct	Tendon in Center of Duct
Strand Size/Number	4 – 0.6”	4 – 0.6”	3 – 0.6”	19 – 0.6”
Steel Area, $A_{ps}$ (in. <sup>2</sup> )	0.864	0.864	0.648	2.28
Equivalent Bond Circumference, $C_e$ (in.)	3.3	3.3	2.85	7.16
Bonded Length (in.)	5.25	5.25	4.5	11.6
Equivalent Bonded Area, $A_b$ (in. <sup>2</sup> )	17.3	17.3	13.0	83.1
Number of Tests	4	4	1	3
Duct Inner Diameter (in.)	1.77	1.77	1.57	3.54
Steel Area/Duct Area (%)	35	35	33	41
Avg. Grout Strength (psi)	8090	8225	7370	5180
Avg. Bond Stress at 0.1mm Unloaded End Slip (ksi)	1.22	0.804	1.28	1.04
Avg. Bond Stress at 0.5mm Unloaded End Slip (ksi)	1.55	1.11	1.28	Not Measured

#### **2.3.4 Osborne**

Osborne (1986) undertook a program similar to Braverman's. He considered 1, 3, 5, 7, and 11-strand tendons with 3/8-in. diameter strands, which provided areas ranging from 3% to 30% of the duct area. All specimens had a bonded length of 24 in. and were grouted in the center of a straight, smooth, steel duct. The largest bond stress of 1.56 ksi was achieved with the tendon of five strands, which occupied 14% of the duct cross-sectional area. The seven and 11-strand tendons failed at significantly lower loads either at the grout-duct interface or the duct-concrete interface. These tendon sizes corresponded to 19% and 30% of the duct cross-sectional area, respectively. With the exception of one 7-strand test, the pullout loads were very similar for both tendon sizes. The average bond stress developed between the duct and the grout in these tests was 0.240 ksi.

#### **2.3.5 Radloff**

Radloff (1990) conducted bond tests intended to replicate deviators in externally post-tensioned girders. The testing consisted of seven and twelve strand tendons using 1/2-in. diameter strands, grouted in nominal 3-in. diameter steel pipes (3.068" ID). Both straight and curved pipes were tested, and all tendons were located against the duct wall. The specimens that were curved were bent on a circular radius such that the desired tendon angle change was accommodated within the standard specimen length.

Rather than doing a standard pullout test, each tendon was stressed to 50% of its ultimate tensile capacity and then grouted. Three days after grouting, the load was slowly released and monitored until slip occurred at the opposite end. Table 2-2 summarizes the results of the testing program.

In the tests with the straight pipes, failure occurred at the duct-grout interface for both tendon sizes. The highest bond stresses were observed for the

6° deviation specimen. Similar bond stresses were observed for each deviation angle, independent of tendon size or the ratio of tendon area to duct cross-sectional area, suggesting that tendon profile is a more important factor than tendon size.

**Table 2-2 Radloff Test Results**

Deviation	Straight		6°		12°	
	7 – 1/2"	12 – 1/2"	7 – 1/2"	12 – 1/2"	7 – 1/2"	12 – 1/2"
Strand Size/Number	7 – 1/2"	12 – 1/2"	7 – 1/2"	12 – 1/2"	7 – 1/2"	12 – 1/2"
Steel Area, $A_{ps}$ (in. <sup>2</sup> )	1.071	1.836	1.071	1.836	1.071	1.836
Equivalent Bond Circumference, $C_e$ , at Failure Surface (in.)	9.638	9.638	3.669	4.803	3.669	4.803
Bonded Length (in.)	24	24	24	24	24	24
Equivalent Bonded Area, $A_b$ (in. <sup>2</sup> )	231.3	231.3	88.06	115.3	88.06	115.3
Number of Tests	1	1	1	1	1	1
Duct Inner Diameter (in.)	3.068	3.068	3.068	3.068	3.068	3.068
Steel Area/ Duct Area (%)	14.5	25	14.5	25	14.5	25
Grout Strength (psi)	2760	2555	2530	2590	1550	2710
Failure Type	Duct-Grout	Duct-Grout	Tendon-Grout	Tendon-Grout	Tendon-Grout	Tendon-Grout
Avg. Bond Stress on Failure Surface (ksi)	0.16	0.28	0.64	0.57	0.35	0.39

### **2.3.6 Schupack and Johnston**

Schupack and Johnston (1974) investigated the bond transfer length of a 54-strand tendon using 1/2-in. diameter strands. This tendon was stressed and grouted in a curved beam. The duct used was smooth-walled and flexible, with an inside diameter of 5.5 in. Concrete strains were measured before and after release to determine the transfer length of the tendon. The researchers estimated the transfer length to be approximately 10 ft, which corresponds to a bond stress of 1.47 ksi. Grout strength was in the range of 3500 psi in this test.

### **2.3.7 Losinger**

A single test on a 52-strand, rock anchor using 0.6-in. diameter strands and grouted in a 10.7 in. diameter steel pipe resulted in bond failure between the grout and the duct (Losinger 1977). The bonded length was 32.8 ft, and the maximum load achieved was 1926 kip, which corresponds to a bond stress of 0.15 ksi between the duct and the grout. This information was compiled by Radloff (1990).

### **2.3.8 VSL**

VSL International, under the supervision of Rostasy (VSL International), conducted a pullout test to determine whether ribbed polyethylene ducts could successfully transfer forces from a tendon to a concrete element. A 16-strand tendon using 1/2-in. diameter strands was grouted in a polyethylene duct with an inner diameter of 3.15 in. After the grout had cured the tendon was stressed to failure. Failure occurred at 496 kip, which corresponds to a bond stress of 0.88 ksi between the tendon and the grout. From this test, it was concluded that bond stress at the duct-grout interface was not critical for ribbed polyethylene ducts.

### **2.3.9 Limitations of Previous Research**

Previous research on bond of multi-strand tendons has not addressed several key aspects of their performance. The test done by VSL indicating that corrugated plastic duct was capable of satisfactorily transferring prestress forces has led the post-tensioning community to assume that plastic and galvanized metal ducts perform equally well. The bond performance of different duct types has not, however, been compared side-by-side. Additionally, research has indicated that coating single strands with emulsifiable oils significantly inhibits the adhesive bond mechanism. However, whether and how this reduced adhesion affects multi-strand tendon bond behavior is unknown.

## **CHAPTER 3**

### **Experimental Program**

#### **3.1 INTRODUCTION**

This test program consisted of monotonic pullout tests performed on multi-strand tendons grouted in curved ducts. Each tendon was initially stressed to a fairly low level to ensure contact between the tendon and the duct wall and then grouted before testing. Large-scale specimens were used to eliminate modeling questions and thus provide an accurate representation of actual behavior. The primary variables were the bonded length, the duct type, and the surface condition of the tendon. The first objective of this test program was to determine an appropriate length test specimen that would not fully develop the tendon. The second objective was to use that size test specimen to compare the performance of uncoiled tendons with that of tendons treated with emulsifiable oils.

#### **3.2 DEVELOPMENT OF TEST SPECIMENS**

The bond strength and mechanism of a multi-strand tendon grouted in a post-tensioning duct depends on the following parameters:

1. Bonded length
2. Surface condition of the prestressing strand
3. Tendon steel area to duct cross-sectional area ratio
4. Tendon radius
5. Duct type and properties
6. Grout properties
7. Location of tendon in duct
8. Duct confinement



In order to limit the testing program to a manageable size, only a few main variables were considered. Every effort was made to keep the remaining factors constant.

The main variables considered were the bonded length, the duct type, and the surface condition of the prestressing steel (i.e. oiled or unoiled). Initial tests used varying bonded lengths in order to determine the most appropriate length for the test program. Three different duct types were considered, covering the range of materials currently in standard use. Two different surface conditions were considered: unoiled and oiled with an emulsifiable oil.

### **3.2.1 Review of Typical Post-Tensioning Systems**

Post-tensioning system manufacturers were contacted to determine available tendon and duct sizes. Multi-strand tendons were available in standard sizes up to 55 strands. A wide range of duct sizes were available depending on the tendon size selected. Standard ducts were available in both galvanized steel and high density polyethylene (HDPE). Another option was to use galvanized steel pipes representative of deviator regions in externally post-tensioned elements. Many different patterns of duct corrugation or extrusion were available and generally varied by manufacturer. In addition to standard HDPE duct, specially vented ducts were available that suppliers claimed provided improved grout quality. In order to determine the size range of tendons typically in use, TxDOT officials were consulted and some design drawings for recent segmental bridges were reviewed.

### 3.2.2 Selection of Variables

a) Tendon Size; Duct Type and Size. A twelve-strand tendon was selected for testing because it represented the smallest tendon which would typically be used for segmental construction and could be economically tested. Nominal 1/2-in. diameter strand was selected for the same reasons. Industry standard galvanized metal duct and high density polyethylene (HDPE) duct were selected for testing because of their wide use and availability. A 3-in. nominal duct size was selected because it was the standard size for a 12-strand tendon made up of 1/2-in. diameter strand. A 3-in. nominal diameter galvanized steel pipe was also selected for testing.

b) Tendon Radius. Curved tendons were selected because they are more representative of actual post-tensioned geometries; straight tendons are very rarely used for multi-strand post-tensioning. A 30-ft radius was chosen for testing because it is the typical boundary separating the use of standard ducts and pipes. Generally galvanized metal and HDPE ducts are used with 30-ft radii and larger, while galvanized steel pipes are used with 30-ft radii and smaller. Furthermore this radius allowed for an appreciable angle change in a relatively short specimen.

c) Position of Tendon in Duct. A small prestressing force was applied to the tendon, resulting in a lateral force on the duct surface. This force caused the tendon to gather into a tightly packed, irregularly shaped bundle against the inside surface of the curved duct. This configuration simulated the actual position of a tendon in a post-tensioned element away from the anchorage.

d) Duct Confinement. The spacing of transverse reinforcement was constant in all but two specimens. The specimens were fairly heavily reinforced to control splitting cracking. A more complete discussion of the transverse reinforcement can be found in Section 3.4.1.

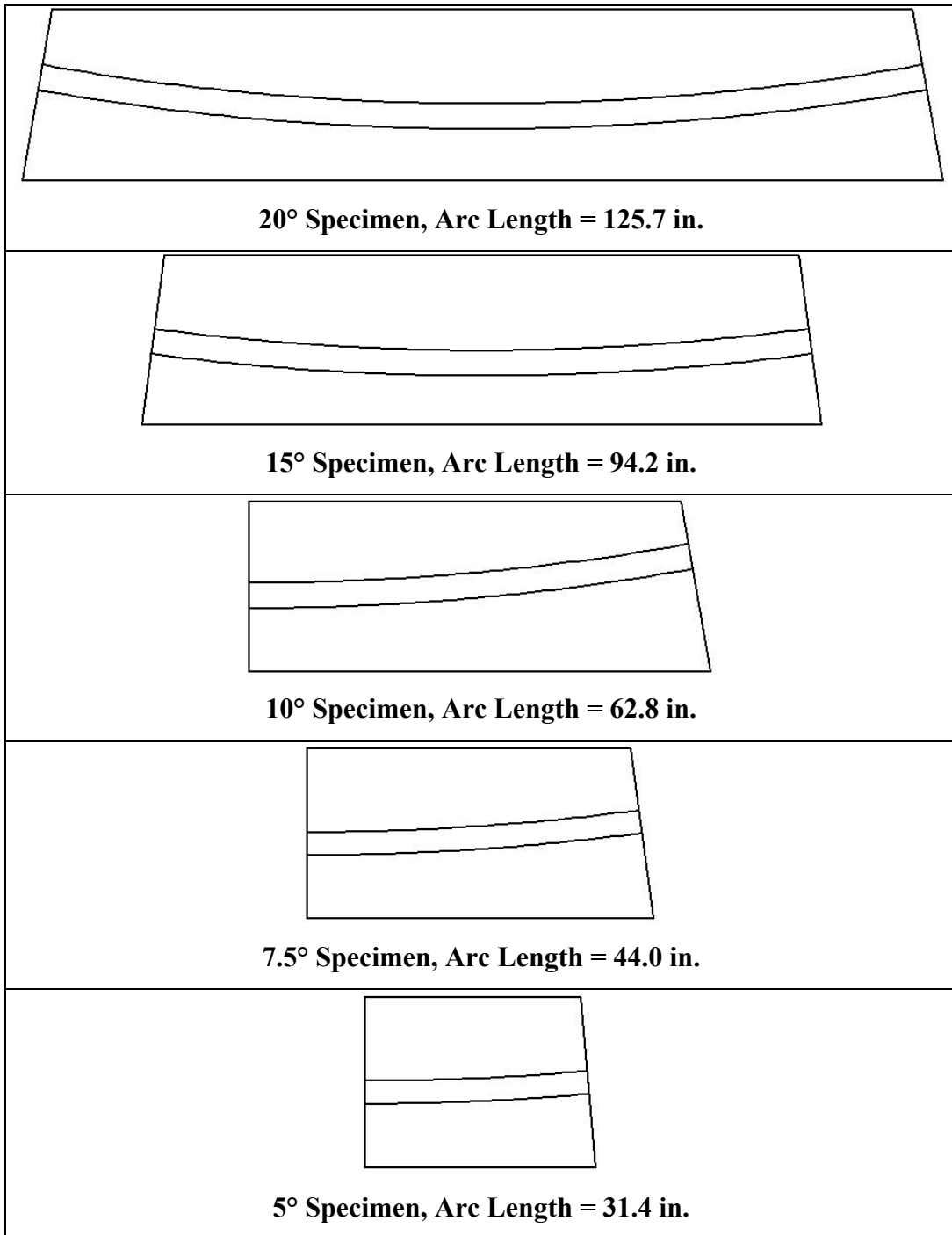
### 3.2.3 Description of Specimens

Five different length specimens corresponding to five different tendon angle changes were used in this testing program. Tendon angle changes ranged from 5° to 20°, providing bonded lengths varying from approximately 31 in. to approximately 126 in. Table 3-1 shows each tendon angle change and the corresponding centerline bonded length. The specimens tested earliest in the program had the largest angle changes. As testing progressed, the strands in many of the specimens with these large angle changes were being fully developed and bond failure was not realized. Progressively smaller specimens were tested until pullout could be achieved for all duct types. (Full development of strands is desirable in actual applications but precludes the comparison of the effect of variables in pullout tests.)

*Table 3-1 Specimen Size Details*

Tendon Angle Change	Centerline Bonded Length (in.)
20°	125.7
15°	94.2
10°	62.8
7.5°	44.0
5°	31.4

All specimens were 24 in. square in cross-section, and each end was constructed perpendicular to the tangent of the duct. In the 15° and 20° specimens, both ends of the specimen were inclined in order to preserve a 2 ft. by 2 ft. cross-section. In these cases, the tendon angle change was equally distributed between the two ends; that is, the tendon profile was symmetrical



*Figure 3-1 Specimen Profiles*

about the center of the specimen. In the remaining specimens, the tendon angle change could be accommodated in the cross-section with a horizontal tangent at one end of the specimen and an inclined tangent at the other, equal to the entire tendon angle change. Figure 3-1 shows each specimen and its tendon profile.

### **3.3 MATERIALS**

This section provides specific details about all of the materials used in the testing program.

#### **3.3.1 Prestressing Strand**

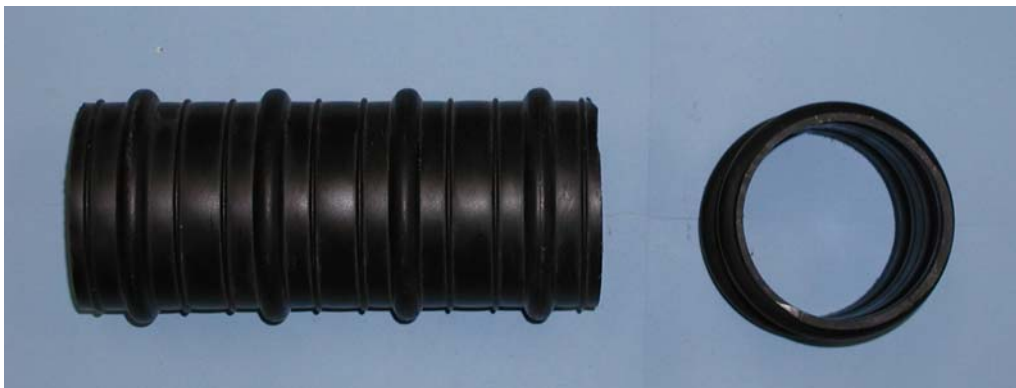
Seven-wire prestressing strand with a nominal diameter of 1/2 in. was used for each tendon. The strand was low-relaxation and conformed to ASTM A416-Grade 270 specifications. The same reel of strand was used for all specimens and the strand was clean, with negligible surface rust.

#### **3.3.2 Duct**

Three types of duct were tested in this program: industry standard galvanized metal duct, industry standard HDPE duct, and galvanized steel pipe. Each duct had a nominal diameter of 3 in. The galvanized metal duct had an inner diameter of 2.92 in. and an outer diameter of 3.20 in. The industry standard HDPE duct had an inner diameter of 2.92 in. and an outer diameter of 3.18 in. The outer diameter of the ribs was 3.55 in. The galvanized steel pipes consisted of Schedule 40 steel pipe bent to the appropriate centerline radius and galvanized by hot-dipping. The inner diameter of the final product was 3.06 in. and the outer diameter was 3.53 in. Both the inner and outer surfaces of the pipe were smooth and free of deformations induced by the bending process. Figure 3-2, Figure 3-3, and Figure 3-4 show the galvanized metal duct, HDPE duct, and galvanized steel pipe, respectively.



*Figure 3-2 Galvanized Steel Duct*



*Figure 3-3 HDPE Duct*



*Figure 3-4 Galvanized Steel Pipe*

### **3.3.3 Grout**

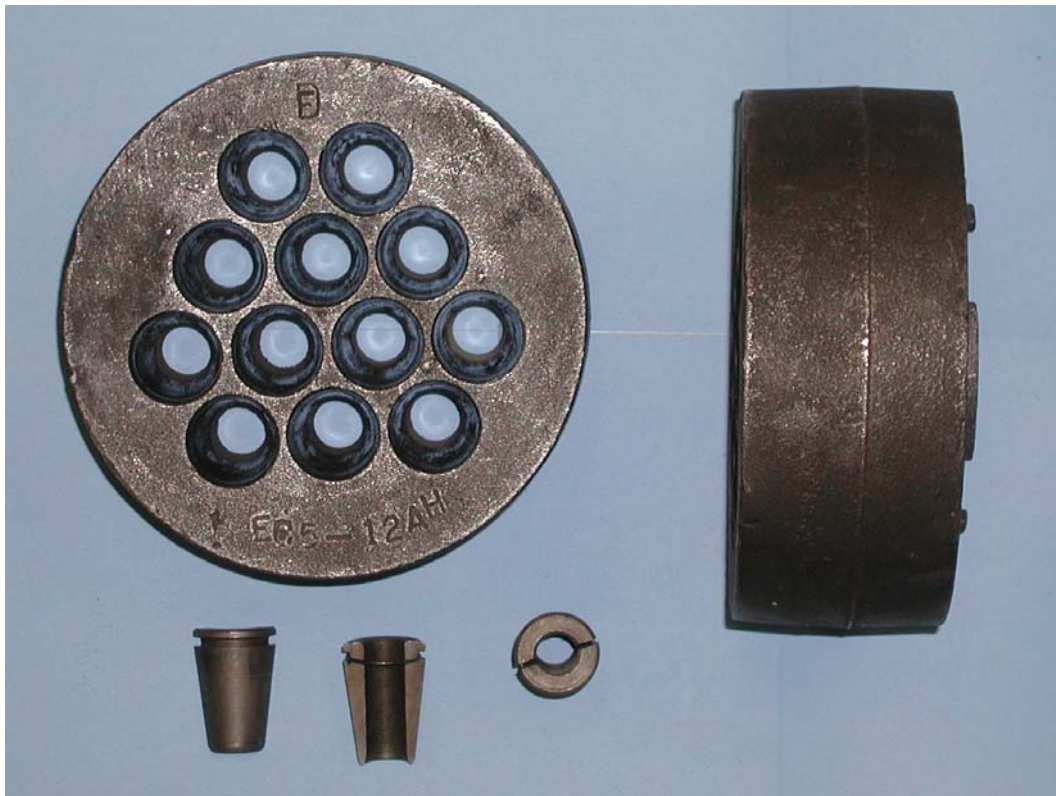
SikaGrout<sup>®</sup> 300PT, a pre-packaged grout available from the Sika Corporation, was used for all specimens in this testing program. This grout conformed to the PTI Guide Specifications for Grouting of Post-Tensioned Structures (PTI, 2000). The grout was non-sanded and resistant to bleed and shrinkage. The nominal 28-day strength was given by the manufacturer as 8,000 psi. Actual grout compressive strength was measured as described in Section 3.5.4.

### **3.3.4 Emulsifiable Oil**

The emulsifiable oil used in this testing program was Citgo Trukut NC 205. This oil was selected based on the results of the preliminary work done at Pennsylvania State University by Salcedo (2003). The oil performed satisfactorily in the corrosion evaluation and provided the least reduction in bond in the single strand pullout testing. Salcedo performed his testing without mixing the oil with water. For the sake of consistency, this testing program did the same.

### **3.3.5 Post-Tensioning Hardware**

Standard 12-strand anchor heads and the appropriate wedges were purchased from a post-tensioning supplier. Each anchor head was reused multiple times. However, new wedges were used for each pullout test. Figure 3-5 shows a sample of the anchor head and wedges used in the testing program.



*Figure 3-5 Post-Tensioning Anchor Head and Wedges*

### **3.3.6 Concrete and Reinforcing Steel**

Mild reinforcing steel was provided to resist forces induced by the loading during testing. Adequate reinforcement was provided to ensure that failure of the specimen would occur at the tendon-grout or grout-duct interface only. All mild steel reinforcement conformed to the ASTM A615 standard and was Grade 60.

Concrete was supplied by a local ready-mix plant. The concrete mix was designed for a 3/4-in. maximum aggregate size and a 28-day compressive strength of 5,000 psi. Standard 6 x 12 in. cylinders were tested to assure that the concrete strength was at least 5,000 psi prior to performing the pullout tests.

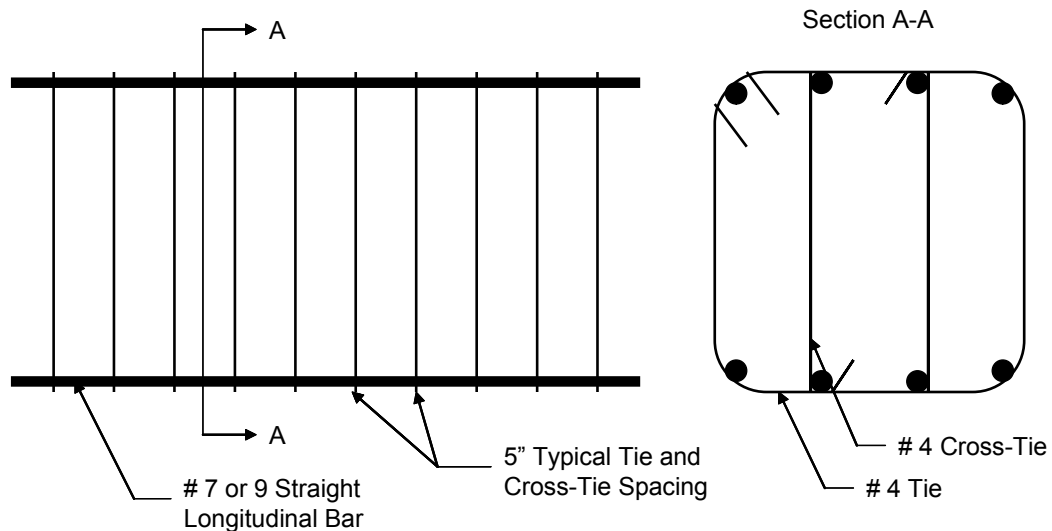


### 3.4 FABRICATION OF BOND TEST SPECIMENS

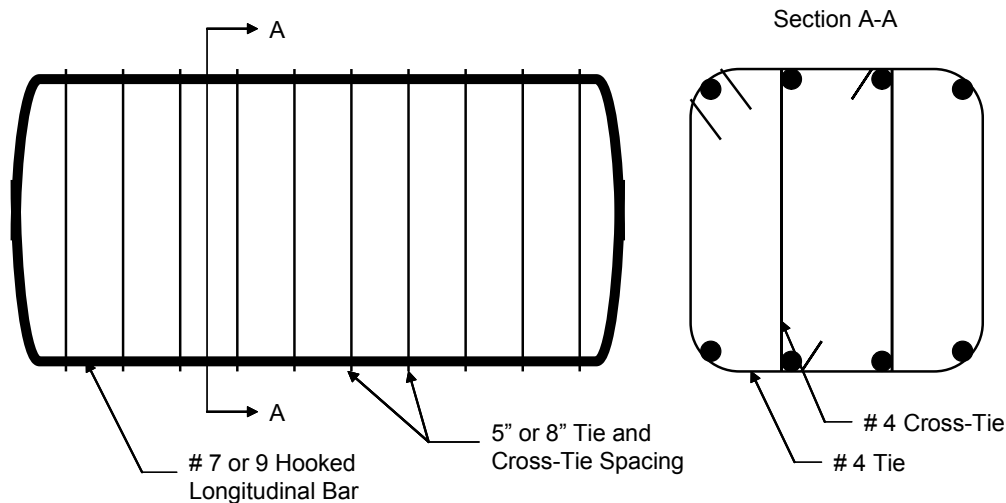
This section details the construction of the specimens, including the assembly of the reinforcing steel cages and the formwork, installation of the duct, and placement of the concrete.

#### 3.4.1 Reinforcing Steel

Reinforcing steel was provided by a local supplier and tied in the lab. Figure 3-6 and Figure 3-7 show the two typical reinforcing steel cage arrangements: cage type S and cage type H. The only difference between the two cage types is that cage type S had straight longitudinal bars while cage type H had longitudinal bars with 90° hooks. All specimens with tendon angle changes of 20° and 15° had cages of type H and #9 longitudinal bars. Specimens with tendon angle changes of 10°, 7.5°, and 5° had #7 longitudinal bars with cages of either type S or H. The specific parameters of each specimen are summarized in Table 3-2 in Section 3.8.1.



*Figure 3-6 Reinforcing Steel Cage Type S*



**Figure 3-7 Reinforcing Steel Cage Type H**

### 3.4.2 Formwork and Placement of Concrete

Between two and six specimens were cast concurrently to speed the testing process. After the reinforcing cage was placed in the forms, the duct was installed. The duct protruded through the end wall of the form and was sealed with duct tape to prevent debris from entering the duct during the placement of concrete. Care was taken to align the duct vertically and horizontally by tying it to the reinforcing cage with wire. Figure 3-8 shows a 15° tendon angle change specimen with HDPE duct prior to placing the last form wall.

After sealing the forms, concrete was delivered from the ready-mix truck to the forms with a bucket and overhead crane. The concrete was placed in several lifts and vibrated to provide acceptable consolidation. The forms were typically stripped within three days.



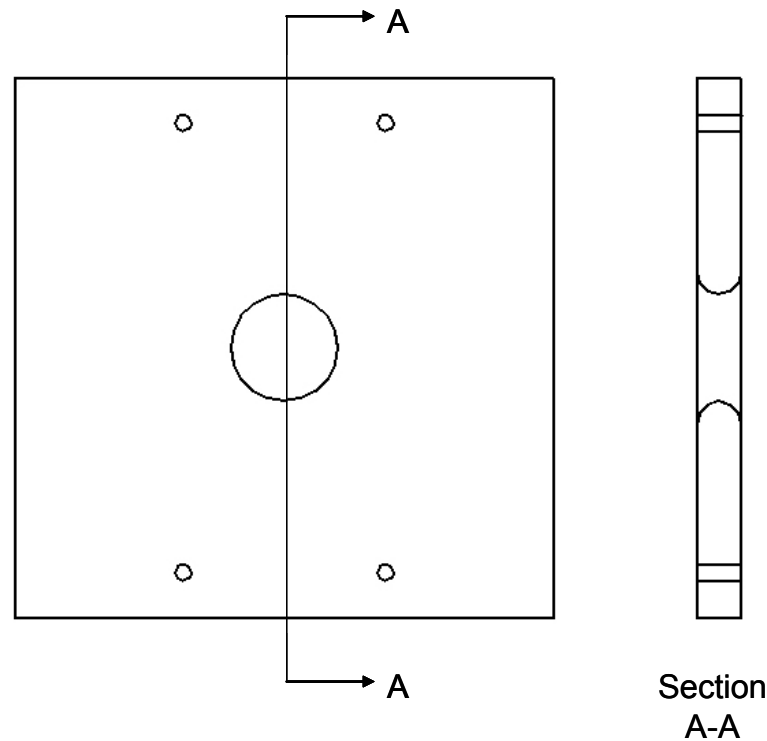
*Figure 3-8 Assembled Specimen Cage, Duct, and Formwork*

### **3.5 PREPARATION OF BOND TEST SPECIMENS**

This section details the preparation of each specimen for testing. It includes the installation of the tendon; the prestressing, sealing and grouting of the tendon; and the releasing of the prestressing force.

#### **3.5.1 Installation of Tendon**

After stripping the forms, the duct was cut flush with the face of the specimen and ground smooth. A 12-in. by 12-in. bearing plate with a machined circular hole was placed over each end of the duct to act as a tension ring for reducing the strand bundle from the large diameter of the anchor head to a smaller diameter suitable for entering the duct. In addition to the machined circular hole, the plate had four holes drilled and tapped for the attachment of a U-shaped frame of 2x4 lumber necessary for the sealing the tendon ends before grouting, as explained in Section 3.5.3. Prior to placing the plate, a bead of caulk was laid around the perimeter of the hole on the face which would be in contact with the concrete. The caulk helped to prevent grout from escaping between the bearing plate and the concrete. A schematic of the bearing plate is shown in Figure 3-9.



***Figure 3-9 Tension Ring Bearing Plate***

After placing the tension ring bearing plate, a hydraulic ram and chair were placed on either side of the duct in front of a beam upon which the anchor head beared. This equipment was used in the prestressing operation detailed in Section 3.5.2, and was held in place by timber supports which were customized depending on the angle of the face and the elevation of the duct. Figure 3-10 shows the prestressing equipment in place on the supports for the inclined end of a specimen with  $7.5^\circ$  of tendon deviation. Figure 3-11 shows the tension ring bearing plate and 2x4 frame in place on the same specimen. At this point the specimen is ready for installation of the tendon.



*Figure 3-10 Prestressing Equipment on Supports*



*Figure 3-11 Specimen Ready for Installation of Tendon*

After positioning the equipment, the 12-strand tendon was fed through the specimen, and anchor heads were installed on each end. If the specimen was to be coated with oil, the oil was applied to the tendon with a garden-type sprayer as it was fed into the duct. Figure 3-12 shows the application of oil. Figure 3-13 shows the profile of a specimen with prestressing equipment in place on both ends and a tendon installed.



*Figure 3-12 Oil Application*



*Figure 3-13 Prestressing Setup*

### **3.5.2 Pre-grout Stressing**

After installing the tendon and anchor heads, a plastic grout tube was inserted through the tension ring bearing plate such that it penetrated approximately 1 in. into the specimen. The tendon was then ready to be stressed. Each pair of rams was connected in parallel and isolated from the others with a valve. In this way the load in each pair of rams could be controlled by closing off the valve and isolating the pressurized rams.

Each specimen was prestressed to a load of approximately 6.3 kip. The purpose of this prestressing was to draw the tendon into a tightly packed bundle along the upper surface of the duct. Because the prestressing force was very small compared to the ultimate tensile capacity of the tendon, the tendon is considered initially unstressed for all purposes of this research.

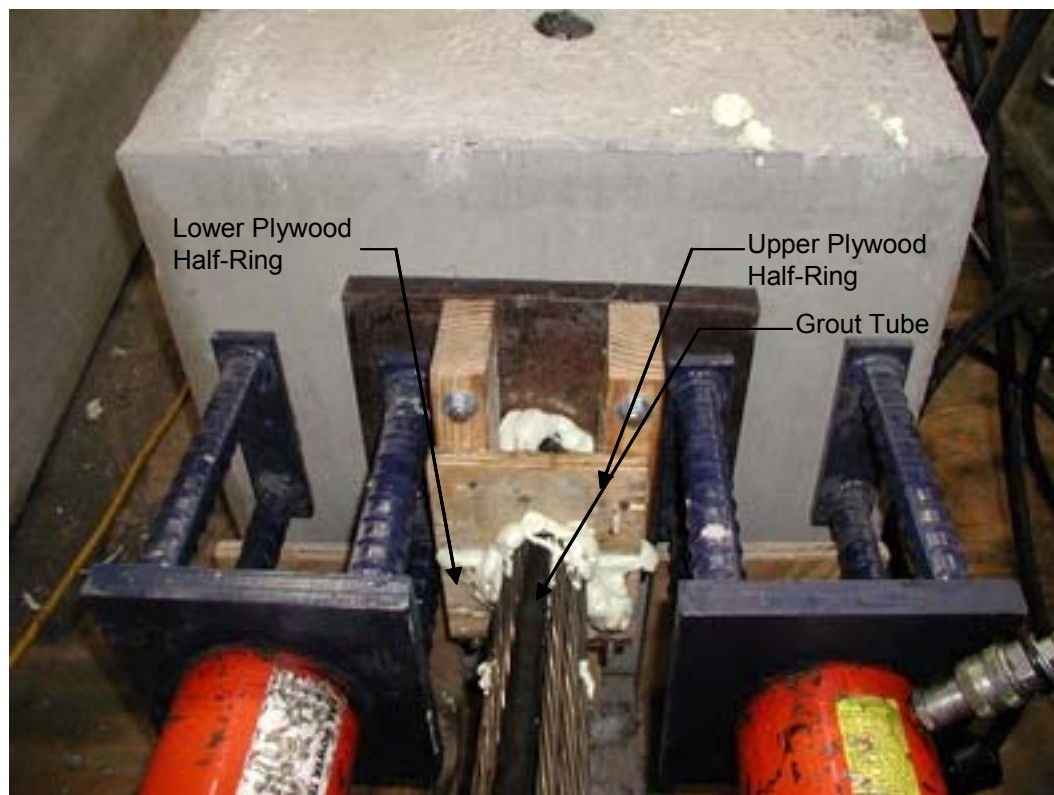
In the first set of specimens, load cells and dial gauges were used to monitor the prestressing force and elongation over a period of days. This additional work was done to verify that the equipment and procedure employed would adequately maintain the prestressing force. The load was satisfactorily maintained and varied slightly with thermal cycles in the lab.

### **3.5.3 Tendon Sealing**

In order to grout the tendon, both ends had to be well-sealed in order to contain the grout while in its fresh state. This procedure involved multiple steps.

After the tendon was stressed, the gaps between the hole in the tension ring bearing plate and the tendon and grout tube were filled with expanding foam insulation delivered from a pressurized can applied through a straw. Care was taken to keep the foam from penetrating too deeply into the specimen and filling the first part of the duct or blocking the end of the grout tube.

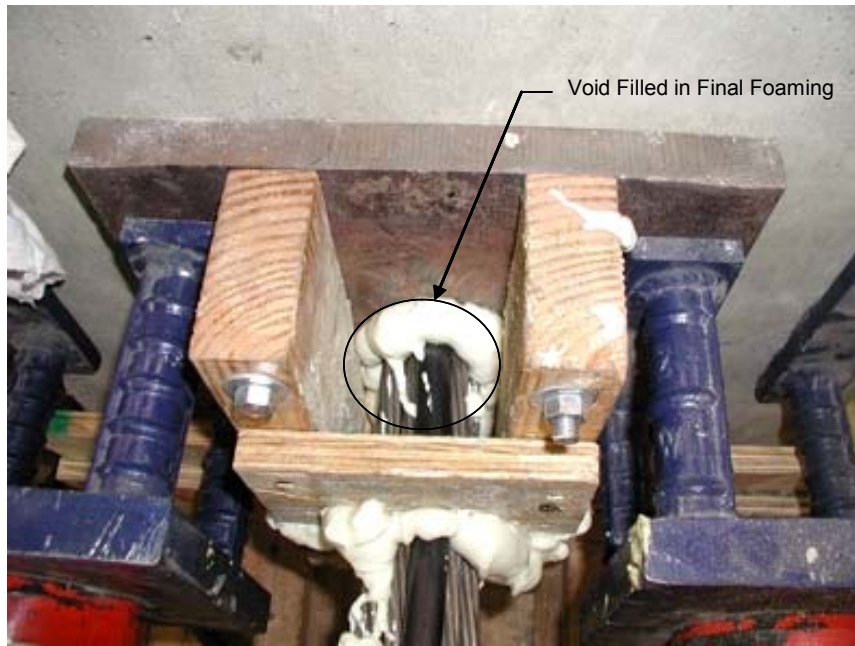
After sealing the inner hole, two half-rings cut from plywood were placed around the tendon and grout tube and screwed onto the face of the 2x4 frame. Expanding insulating foam was again used to seal the gaps between this hole and the tendon bundle and grout tube. At this point, an effort was made to fill the gaps between individual strands as much as possible. The foaming activities up to this point were called “initial foaming”. Figure 3-14 shows this step completed with important items labeled.



***Figure 3-14 Completed Initial Foaming***

After the initial foaming had cured for about a day, the void remaining in the 2x4 frame was completely filled with foam. This operation was called “final foaming”. Figure 3-15 shows the tendon ready for final foaming, and Figure 3-16 shows the final foaming completed.





*Figure 3-15 Specimen Ready for Final Foaming*



*Figure 3-16 Completed Final Foaming*

The purpose of the initial foaming was to seal the duct as well as possible using a controlled amount of foam, so as not to block a significant portion of the duct or the grout tube. Making the second hole with the plywood half-rings for the tendon to pass through was an effort to seal off the block area for the final foaming.

The purpose of the final foaming was to reinforce the initial foaming, keeping it from blowing out under the pressure from the pumping of grout, and also to seal up any holes which remained after the initial foaming. The final foaming was also very important because it allowed foam to expand into the spaces between the individual strands to completely seal off the tendon. After the final foaming had cured, the tendon was ready to be grouted.

Removal of the foam and blocks prior to testing often revealed evidence that grout had escaped beyond the initial seal around the tension ring bearing plate. These small leaks were particularly a problem in the small areas between each strand. The secondary foaming, however, generally arrested the leaks and created a successful seal. Early attempts at sealing the tendon were generally successful, but leakage did occur on occasion. After fine-tuning this procedure and practice applying the foam, reliable sealing of the tendon was achieved.

#### **3.5.4 Grouting**

Grout was mixed one 50-lb bag at a time according to the specifications of the manufacturer. Water was batched by weight according to the minimum amount specified by the manufacturer. The grout material was slowly added to the water while being mixed with a drill and paddle bit. Mixing continued until the grout was uniform in consistency.

A hand grout pump, shown in Figure 3-17, was attached to the grout tube using typical garden hose connections. Care was taken to ensure that the hopper on the grout pump remained full, preventing air from being drawn into the system. When grouting tendons which had unequal end elevations, grout was always pumped from the lower end of the tendon. Once grout began to flow evenly from the vent at the far end, it was capped and pumping ceased. The grout pump was then disconnected from the grout tube and the tube was capped.



*Figure 3-17 Hand Grout Pump*

After grouting of the specimens was complete, grout was pumped into 4x6 in. cylinders for compressive strength testing. Grouting took place approximately 48 hours after the application of oil for oiled specimens.

Five days after grouting, the pressure on the hydraulic rams was released and the prestressing equipment was removed. After release, grout cylinders were broken to determine the compressive strength of the grout. At the dead end, the tendon was cut so that it protruded from the face of the specimen end approximately 1 in. The foam was removed as much as possible and the specimen was ready for testing. On the live end, the tendon was left uncut, extending approximately 42 in. so that it could accommodate the hydraulic ram and an anchor head for the pullout test. The foam was removed as much as possible and the specimen was ready for testing. Pullout testing generally took place six days after grouting. Additionally, grout cylinders were broken to measure the compressive strength of the grout at the time of testing.

### **3.6 INSTRUMENTATION**

All data were collected electronically during testing. Mechanical measuring devices and visual references were used to verify the electronic readings throughout testing. This section details the electronic equipment and its placement during testing.

#### **3.6.1 Force Measurements**

The load on the tendon was measured based on the hydraulic pressure in the stressing ram. A 2000-psi electronic pressure transducer was used to monitor the pressure at all times. Before beginning the testing program, the pressure transducer was calibrated to determine the correct calibration factor. After calibration, the stressing ram was placed in a 600-kip testing machine with a reference load cell to verify the effective area of the ram and the accuracy of the

pressure transducer. During pullout testing, a mechanical pressure gauge was used to verify the readings of the pressure transducer.

### **3.6.2 Displacement Measurements**

Displacements of the live and dead end were recorded using linear potentiometers. The live end displacement was measured with a 5-in. potentiometer attached to the bearing plate on the cylinder of the ram and extending to the body of the ram. Figure 3-18 shows the placement of the live end potentiometer. On the dead end, a single 2-in. potentiometer was placed against the cut tendon end. Because of the size of the tendon bundle, using more than one potentiometer was impractical. The potentiometer was typically placed such that its tip was bearing on one of the internal strands in the tendon bundle. Figure 3-19 shows a typical dead end linear potentiometer placement. In all pullout tests, there was no visually perceptible differential movement between individual strands at the tendon's dead end. Before beginning the testing program, each linear potentiometer was calibrated to determine the correct calibration factor.

### **3.6.3 Data Acquisition Equipment**

All data from the pressure transducer and linear potentiometers were read by a Hewlett-Packard scanner model HP7500. A desktop-type IBM compatible personal computer with National Instruments LabVIEW software was used to control scanning functions. The software logged the data and also provided real-time monitoring. The software was also used to check the entire system prior to testing.



*Figure 3-18 Live End Linear Potentiometer Placement*



*Figure 3-19 Dead End Linear Potentiometer Placement*

### 3.7 TESTING SEQUENCE

This section details the procedure for the testing of each specimen, including the procedure for loading.

#### 3.7.1 Overview

Figure 3-20 shows a specimen ready for testing. The following is a summary of the test procedure:

- 1) The hydraulic ram was fit over the tendon and placed against the specimen.
- 2) An anchor head was placed on the tendon and the wedges were seated by hand.
- 3) All instrumentation was installed and tested for proper operation.
- 4) The tendon was loaded in a controlled manner until pullout and significant tendon displacement occurred, or a limiting load was reached.
- 5) The ram was retracted and the anchor head was cut off. The ram was then removed and the tendon was cut off near the face of the specimen. The specimen was then discarded.



*Figure 3-20 A Specimen Ready For Testing*

### **3.7.2 Loading Procedure**

Each specimen was loaded incrementally, with each load step being between 5 and 10 kip. After each load step, the potentiometers and pressure transducer were scanned and the data logged in the computer. In general, load was not increased beyond 80% of the ultimate tensile capacity of the tendon, or roughly 400 kip. This limit ensured that tendons did not rupture, which would present a potentially dangerous situation. In a few cases, the load was increased beyond this limiting load, and testing proceeded until individual wires in the tendon began to rupture. At this point testing was halted, and the specimen was unloaded. If the tendon failed in bond, readings were taken every few seconds until the load and displacement stabilized. The tendon was then loaded further, and testing continued until displacements of several inches had occurred.

## **3.8 SPECIMEN SUMMARY**

This section summarizes the details of each specimen, and outlines the naming schemes employed throughout.

### **3.8.1 Specimen Naming Scheme**

Specimens were initially named in a purely chronological manner. Since the amount of available equipment was limited, only two specimens could be tested at a time. The two specimens were often, but not always, a matching set. The format of the name was, for example, BT2-1. “BT” represented “Bond Test”, the number preceding the dash corresponded to the set number, and the number following the dash indicated whether the specimen was tested first or second.

For reporting and comparing test results, a more informative specimen name was desired, and so a second naming scheme was devised. The naming scheme includes identifiers for the surface condition, the duct type, the angle change, and the specimen number.



The surface condition of the tendon is identified with the numeral 0 or 1. Zero corresponds to an unoiled surface condition, while 1 indicates a tendon coated with Citgo Trukut NC 205. The duct type is identified by two letters. “SP” indicates the specimen had a steel pipe for a duct, GD indicates that the specimen had a galvanized metal duct, and HD indicates that the specimen had a HDPE duct. The angle change of the specimen is identified simply with the numerical value of the angle change and the degree (°) symbol. The specimen number indicates whether it is the first, second, third, etc. specimen of that type to be tested.

An example of a specimen named with this scheme is 0-GD-7.5°-2. This would refer to the second 7.5° specimen with a galvanized metal duct that was tested without oil.

Table 3-2 provides details for every specimen tested in this program. Both naming schemes are included along with the duct type, surface condition, angle change, cage type, longitudinal bar size, transverse reinforcement spacing, and grout strength, both at release and at the time of testing.

*Table 3-2 Specimen Summary*

Specimen Name Scheme 1	Specimen Name Scheme 2	Duct Type	Surface Condition	Angle Change (deg)	Cage Type	Longitudinal Bar Size (#)	Transverse Reinforcement Spacing (in.)	Grout Strength Release (psi)	Grout Strength Test (psi)
BT2-1	0-SP-20°-1	SP	Dry	20	H	9	5	8130	8400
BT2-2	0-SP-15°-1	SP	Dry	15	H	9	5	8130	8400
BT3-1	0-GD-20°-1	GD	Dry	20	H	9	5	7880	8400
BT3-2	0-HD-20°-1	HD	Dry	20	H	9	5	7880	8400
BT4-1	0-HD-15°-1	HD	Dry	15	H	9	5	7520	8140
BT4-2	0-GD-15°-1	GD	Dry	15	H	9	5	7520	8140
BT5-1	0-HD-10°-1	HD	Dry	10	S	7	8	7660	7980
BT5-2	0-HD-7.5°-1	HD	Dry	7.5	S	7	8	7660	7980
BT6-1	0-GD-10°-1	GD	Dry	10	H	7	5	7200	8440
BT6-2	0-GD-10°-2	GD	Dry	10	H	7	5	7200	8440
BT7-1	0-HD-10°-2	HD	Dry	10	H	7	5	8280	8580
BT7-2	0-HD-10°-3	HD	Dry	10	H	7	5	8280	8580
BT8-1	0-SP-10°-1	SP	Dry	10	H	7	5	8350	8660
BT8-2	0-SP-10°-2	SP	Dry	10	H	7	5	8350	8660
BT9-1	0-GD-7.5°-1	GD	Dry	7.5	S	7	5	8210	8530
BT9-2	0-GD-5°-1	GD	Dry	5	S	7	5	8210	8530
BT10-1	0-GD-7.5°-2	GD	Dry	7.5	S	7	5	8380	8655
BT10-2	0-GD-7.5°-3	GD	Dry	7.5	S	7	5	8380	8655
BT11-1	0-HD-7.5°-2	HD	Dry	7.5	S	7	5	8520	8370
BT11-2	0-HD-7.5°-3	HD	Dry	7.5	S	7	5	8520	8370
BT12-1	0-SP-7.5°-1	SP	Dry	7.5	S	7	5	8680	9110
BT12-2	0-SP-7.5°-2	SP	Dry	7.5	S	7	5	8680	9110

*Table 3-2 (Cont.) Specimen Summary*

Specimen Name Scheme 1	Specimen Name Scheme 2	Duct Type	Surface Condition	Angle Change (deg)	Cage Type	Longitudinal Bar Size (#)	Transverse Reinforcement Spacing (in.)	Grout Strength Release (psi)	Grout Strength Test (psi)
BT13-1	1-GD-7.5°-1	GD	NC 205	7.5	S	7	5	8620	7600
BT13-2	1-GD-7.5°-2	GD	NC 205	7.5	S	7	5	8620	7600
BT14-1	1-HD-7.5°-1	HD	NC 205	7.5	S	7	5	8560	9780
BT14-2	1-HD-7.5°-2	HD	NC 205	7.5	S	7	5	8560	9780
BT15-1	1-SP-7.5°-1	SP	NC 205	7.5	S	7	5	8360	8290
BT15-2	1-SP-7.5°-2	SP	NC 205	7.5	S	7	5	8360	8290

Note: The interested reader may refer to Appendix B for a similar table which includes additional details and data for each specimen.

### **3.9 RECOMMENDATIONS FOR FUTURE TESTING**

After completing the testing program, several recommendations were developed to improve the testing procedure described herein. Any one interested in undertaking a similar program may wish to consider these recommendations.

The pre-grout stressing operation used in this program was time consuming and laborious. The procedure could likely be eliminated or significantly simplified by installing the duct concave down. This would allow the tendon to be in contact with the inner radius of the duct without requiring the application of force to lift it.

There was evidence that the ram confined the live end of the specimen due to bearing. Other test specimens or methods of testing should be investigated to try and eliminate this situation. The main reason such a simple test specimen was selected in this program was to facilitate the pre-grout stressing. Eliminating that step would allow more freedom in the selection of a test specimen.

# CHAPTER 4

## Test Results

### 4.1 INTRODUCTION

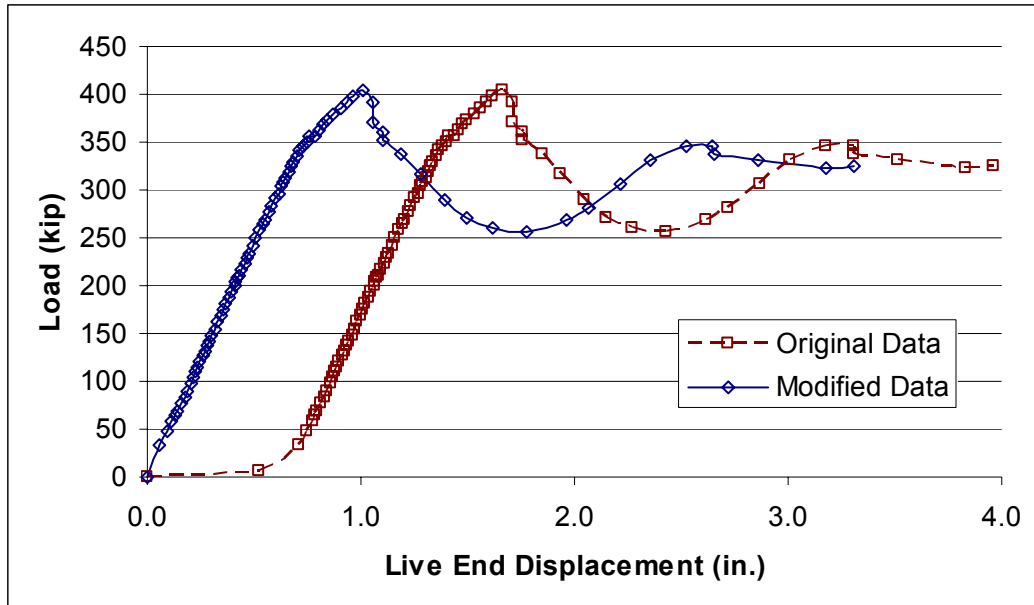
This chapter presents the data from each of the specimens tested in this program. In general, there are two plots shown for each specimen, one showing live end load-displacement and dead end load-slip behavior, and one showing dead-end load-slip behavior on an amplified scale. The specimens are identified according to the naming scheme outlined in Section 3.8.1.

### 4.2 TEST DATA

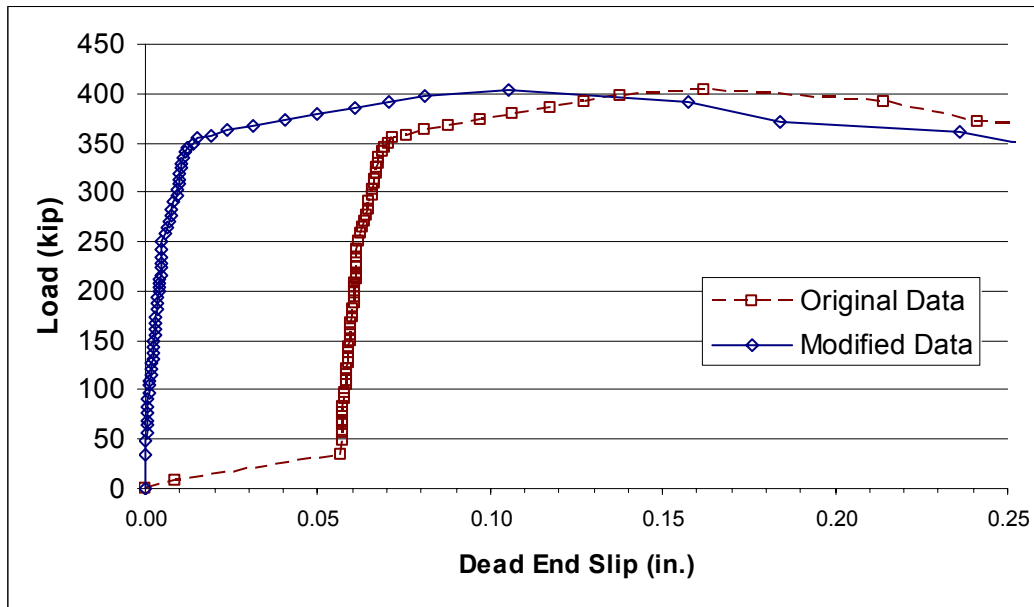
Because the specimens were free-standing, small displacements were often registered in the initial stages of loading, as the hydraulic ram came into full contact with the specimen. For this reason, the data for many of the specimens required minor modifications so that the load-displacement and load-slip curves passed through the origin. In general, the only modification to the data has simply been to shift them along the displacement axis to eliminate the seating displacement. Figure 4-1 and Figure 4-2 show the magnitude of relatively large modifications applied to the data from specimen 0-HD-10°-2. Figure 4-3 and Figure 4-4 show data requiring average modification, in these cases from specimen 0-HD-10°-1. Data from some specimens required no modification at all. All other plots of data in this chapter will contain modified data only, as applicable. Plots showing original and modified data for all test specimens are available in Appendix A. Live end displacement data were collected to slips on the order of 4 in., while dead end data were collected to slips on the order of 2 in. Less data were taken at the dead end due to the difficulty of collecting

displacement data after the end of the tendon had displaced a significant distance into the specimen.

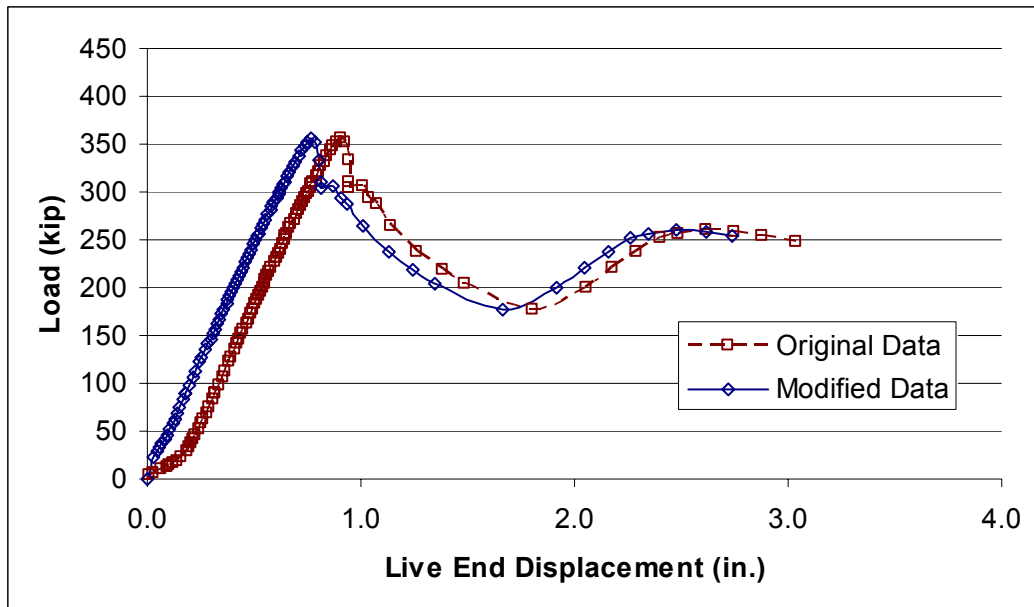
For the purposes of this chapter failure is defined as a peak load followed by a sudden drop in resistance and accumulation of significant dead end slip. The load at a dead end slip of 0.02 in. is also reported in this chapter because it is used in the subsequent chapters to make comparisons. A more thorough discussion of failure modes is provided in Section 5.1.1.



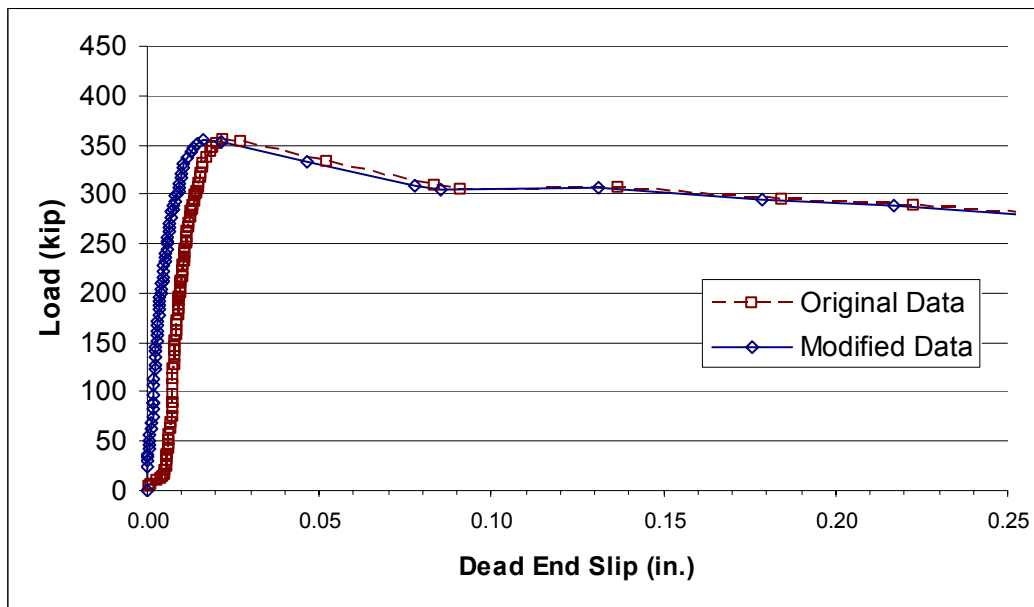
*Figure 4-1 Live End Data Requiring Large Modification*



*Figure 4-2 Dead End Data Requiring Large Modification*



*Figure 4-3 Live End Data Requiring Average Modification*



*Figure 4-4 Dead End Data Requiring Average Modification*

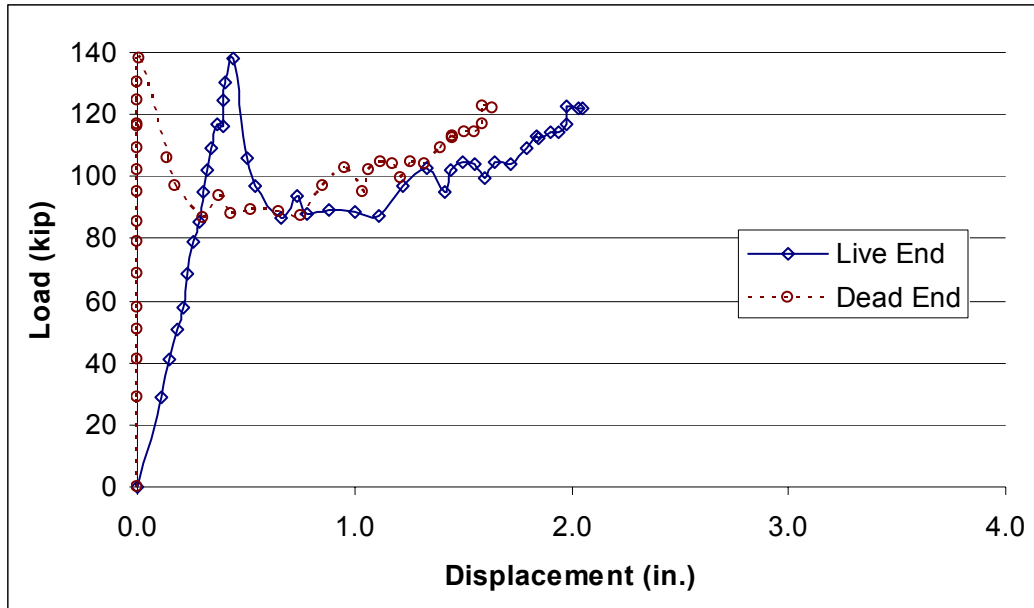


## **4.2.1 Galvanized Steel Pipe Specimens**

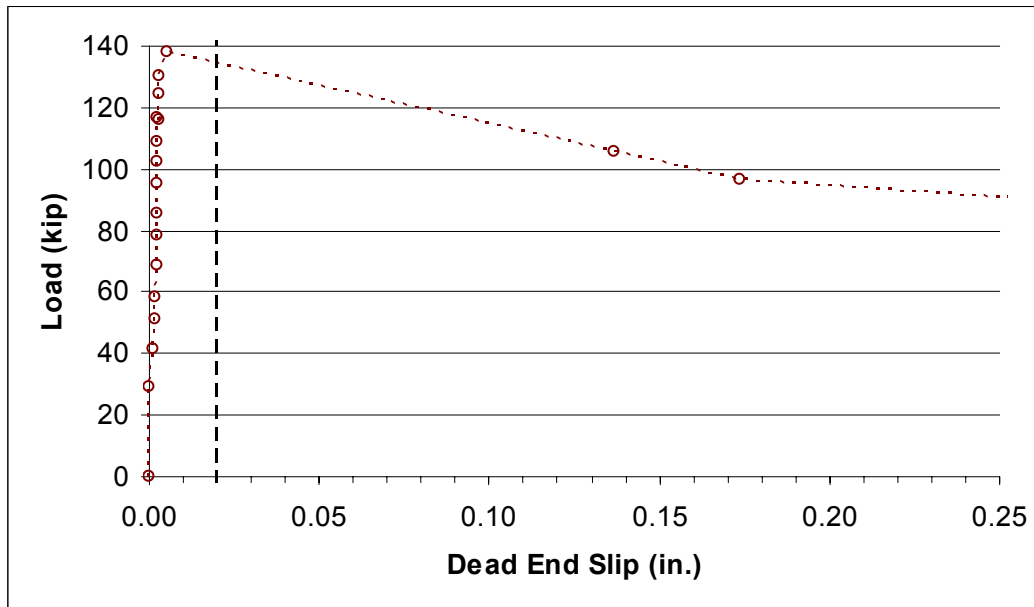
The response of the galvanized pipe specimens will be presented in order of decreasing length, with the unoiled specimen data preceding the oiled specimen data. No cracking of the concrete was observed in any of the specimens containing galvanized steel pipes.

### ***4.2.1.1 0-SP-20°-1***

Figure 4-5 is the load vs. live end displacement and load vs. dead end slip plot for specimen 0-SP-20°-1. The figure indicates that the peak load achieved was 138 kip, at which point an extremely pronounced reduction in resistance occurred. Figure 4-6 is the load vs. dead end slip plot for the specimen. It shows slip behavior at an amplified scale over a smaller range of displacement values. This highlights the slip behavior prior to and just after failure. The figure shows that very little slip occurred prior to the maximum load. The maximum load corresponds to the point where the first appreciable dead end slip occurred, after which substantial displacement accumulated on both the live and dead ends at lower load levels. Failure occurred at the grout-duct interface for this specimen prior to a dead end slip of 0.02 in. Figure 4-7 shows the specimen after testing, with the tendon and grout pulled several inches out of the specimen.



**Figure 4-5 Live End Load-Displacement and Dead End Load-Slip Response for Specimen 0-SP-20°-1**



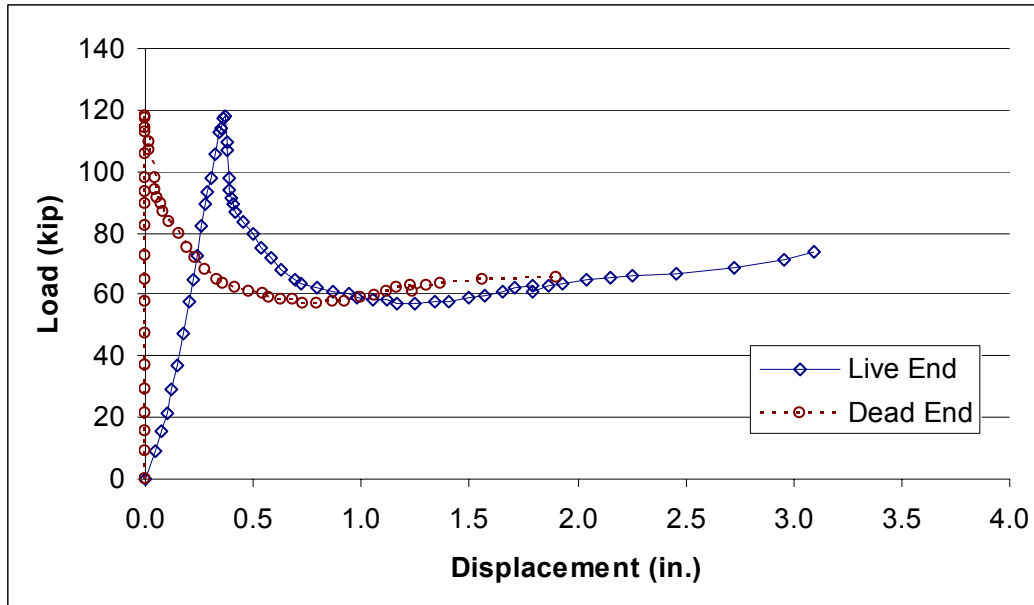
**Figure 4-6 Dead End Load-Slip Response for Specimen 0-SP-20°-1, Amplified Scale**



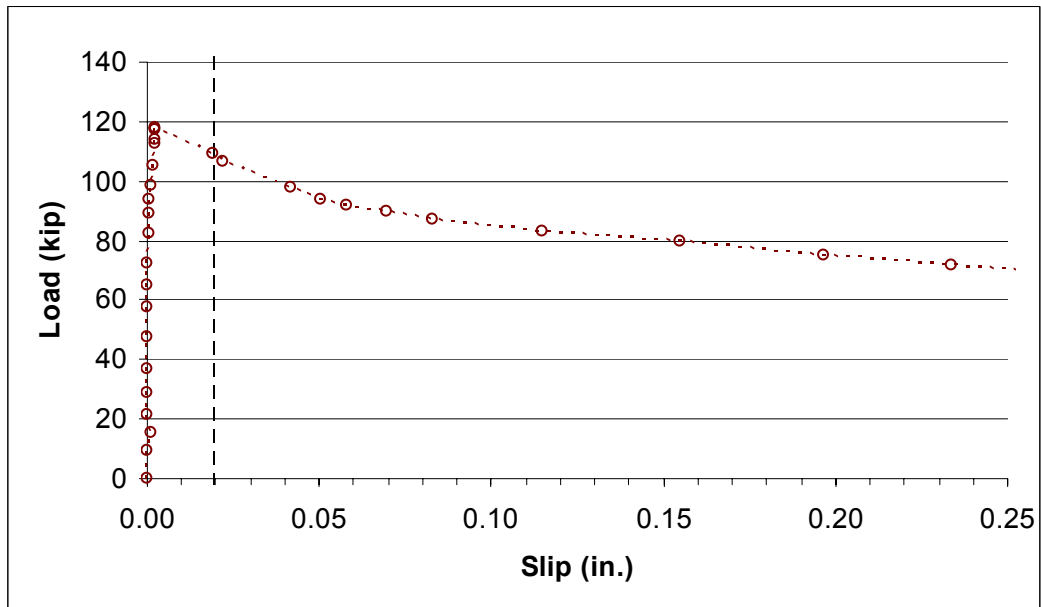
*Figure 4-7 Live End of Specimen 0-SP-20°-1 after Testing*

#### ***4.2.1.2 0-SP-15°-1***

Figure 4-8 is the load vs. live end displacement and load vs. dead end slip plot for specimen 0-SP-15°-1. The figure indicates that the peak load achieved was 118 kip, at which point an extremely pronounced reduction in resistance occurred. Figure 4-9 is the load vs. dead end slip plot for the specimen. It shows slip behavior at an amplified scale over a smaller range of displacement values. This highlights the slip behavior prior to and just after failure. The figure shows that very little slip occurred prior to the maximum load. The maximum load corresponds to the point where the first appreciable dead end slip occurred, after which substantial displacement accumulated on both the live and dead ends at lower load levels. Failure occurred at the grout-duct interface for this specimen prior to a dead end slip of 0.02 in. Figure 4-10 shows the specimen after testing, with the tendon and grout pulled several inches out of the specimen.



*Figure 4-8 Live End Load-Displacement and Dead End Load-Slip Response for Specimen 0-SP-15°-1*



*Figure 4-9 Dead End Load-Slip Response for Specimen 0-SP-15°-1, Amplified Scale*

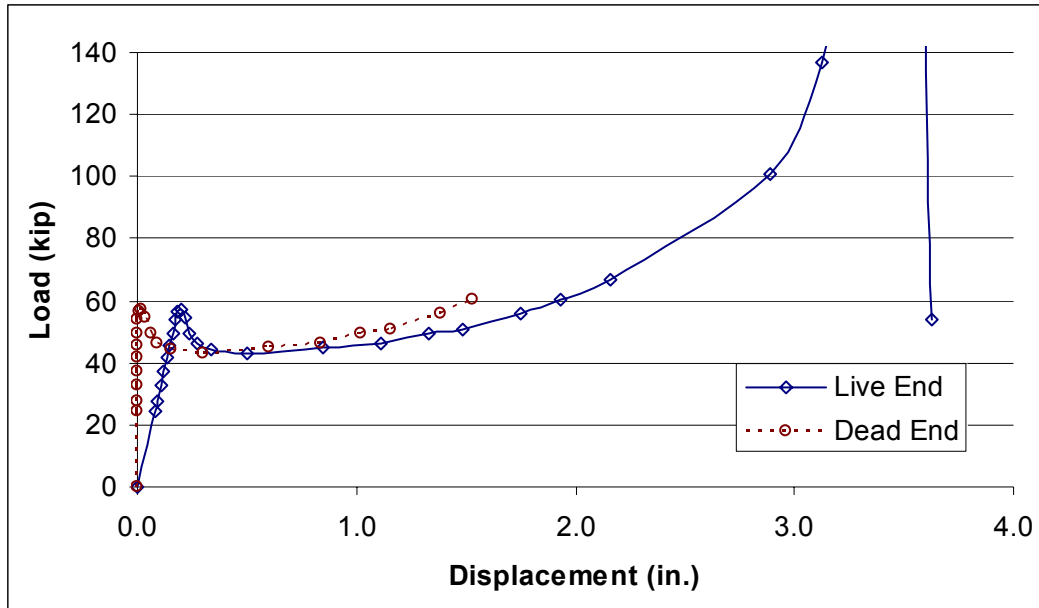


*Figure 4-10 Live End of Specimen 0-SP-15°-1 after Testing*

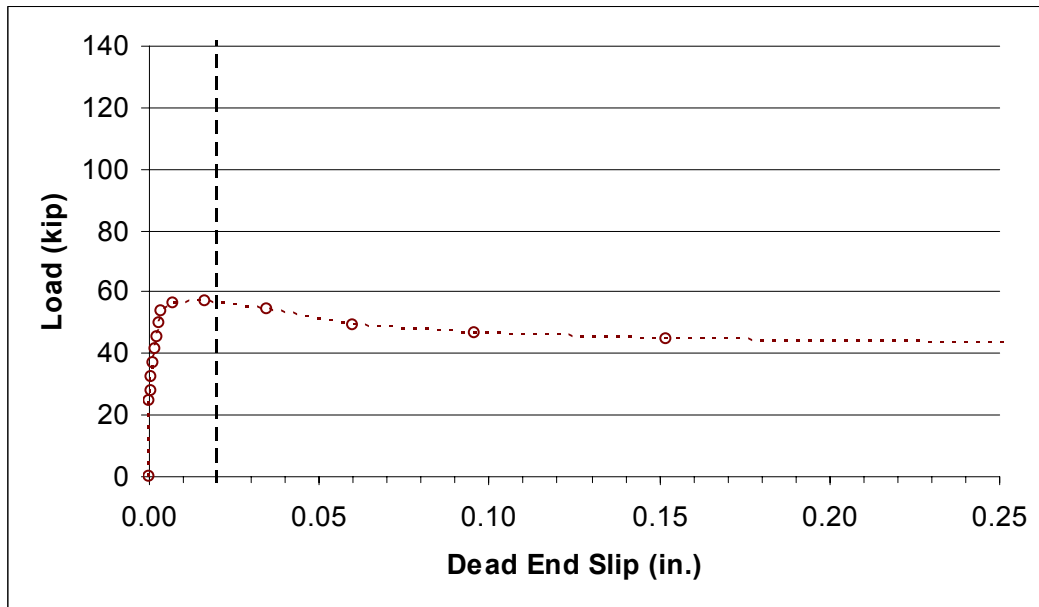
#### **4.2.1.3 0-SP-10°-1**

Figure 4-11 is the load vs. live end displacement and load vs. dead end slip plot for specimen 0-SP-10°-1 on the standard scale used for all pipe specimens. This figure indicates that an initial peak load of 57.2 kip was achieved, at which point a pronounced reduction in resistance occurred. Figure 4-12 is the load vs. dead end slip plot for the specimen. It shows slip behavior at an amplified scale over a smaller range of displacement values. This highlights the slip behavior prior to and just after the initial failure. The figure shows that very little slip occurred prior to the initial reduction in load. This load corresponds to the point where the first appreciable dead end slip occurred, after which substantial displacement accumulated on both the live and dead ends at lower load levels. The initial failure occurred at the grout-duct interface for this specimen with a dead end slip of less than 0.02 in.

With continued displacement, the load began to increase at a rapid rate, reaching a maximum load of 233 kip at a live end displacement of over 3 in., as indicated by Figure 4-13. An extremely pronounced reduction in resistance occurred as the pipe broke away from the concrete. This behavior is believed to result from the solid tendon and grout plug binding up as it tried to rotate as a rigid body out of the specimen. Because of its orientation, the hydraulic ram continued to pull the tendon and grout normal to the face of the specimen. This misalignment caused the tendon and grout to kink against the pipe and the load to increase until a bond failure occurred between the pipe and the concrete. Figure 4-14 shows the specimen after testing, with the tendon and grout pulled several inches out of the pipe, and the pipe pulled about 1/4 in. out of the specimen.

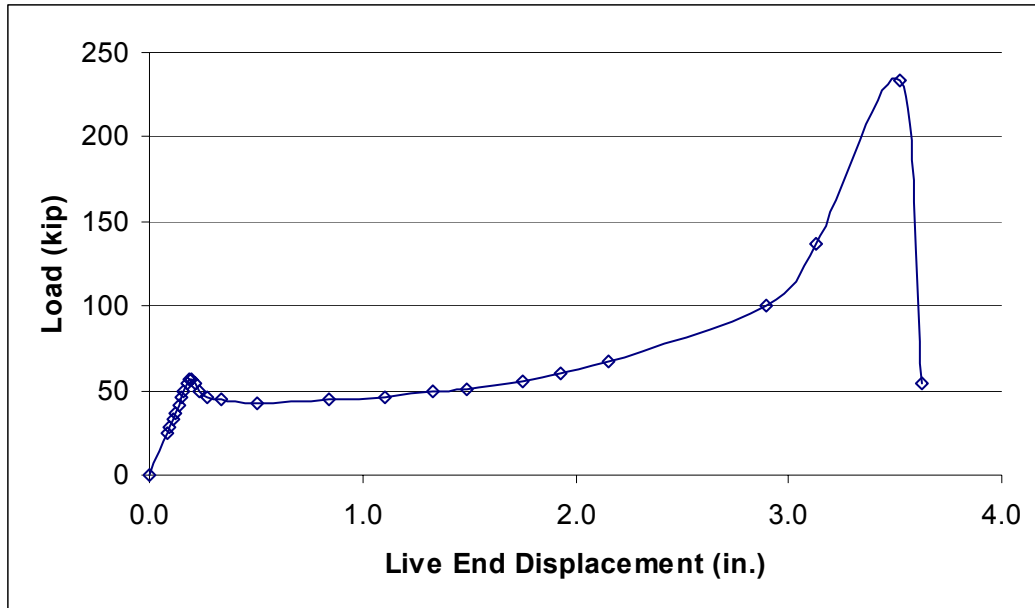


*Figure 4-11 Live End Load-Displacement and Dead End Load-Slip Response for Specimen 0-SP-10°-1, Normal Range*



*Figure 4-12 Dead End Load-Slip Response for Specimen 0-SP-10°-1, Amplified Scale*





**Figure 4-13** *Live End Load-Displacement Response for Specimen 0-SP-10°-1, Full Range*

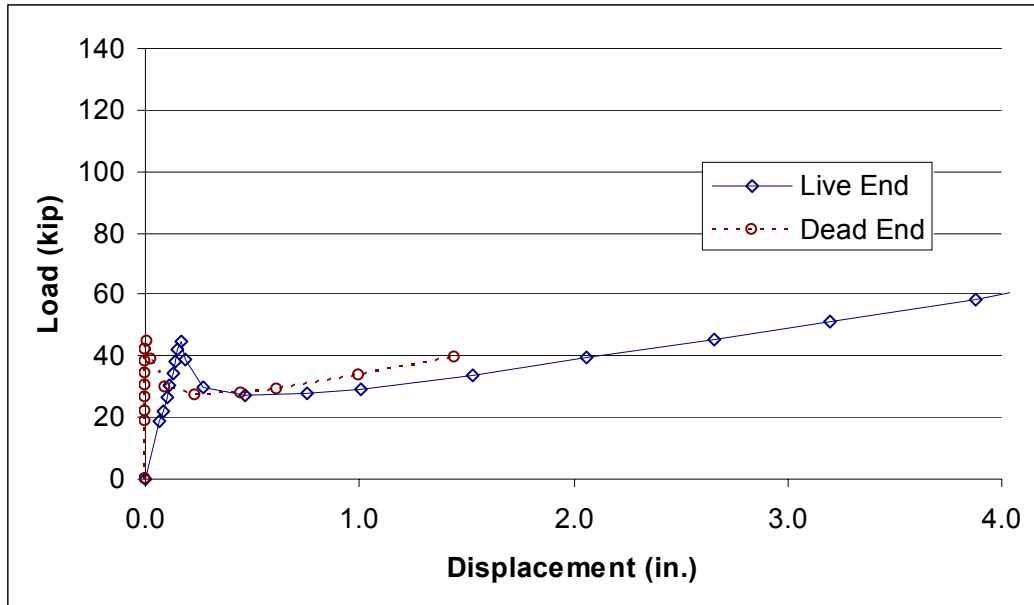


**Figure 4-14** *Live End of Specimen 0-SP-10°-1 after Testing*

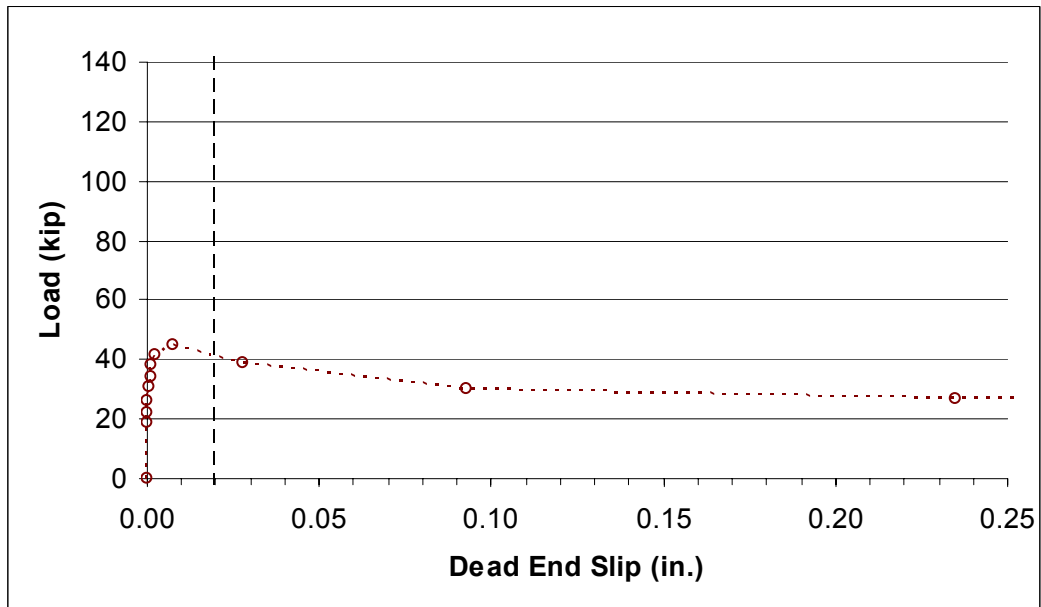
#### **4.2.1.4 0-SP-10°-2**

Figure 4-15 is the load vs. live end displacement and load vs. dead end slip plot for specimen 0-SP-10°-2. The figure indicates that the ultimate load achieved was 44.6 kip, at which point an extremely pronounced reduction in resistance occurred. Figure 4-16 is the load vs. dead end slip plot for the specimen. It shows slip behavior at an amplified scale over a smaller range of displacement values. This highlights the slip behavior prior to and just after failure. The figure shows that very little slip occurred prior to the failure load. The failure load corresponds to the point where the first appreciable dead end slip occurred, after which substantial displacement accumulated on both the live and dead ends at lower load levels. Failure occurred at the grout-duct interface for this specimen with a dead end slip of less than 0.02 in.

This specimen also showed a recovery of load similar to that observed in its companion specimen, 0-SP-10°-1. However, the increase in strength was not as large, and did not result in a failure between the pipe and the concrete. A photograph of this specimen after testing was not available. The specimen did, however, look very similar to Figure 4-14 except that the duct did not protrude from the face of the live end.



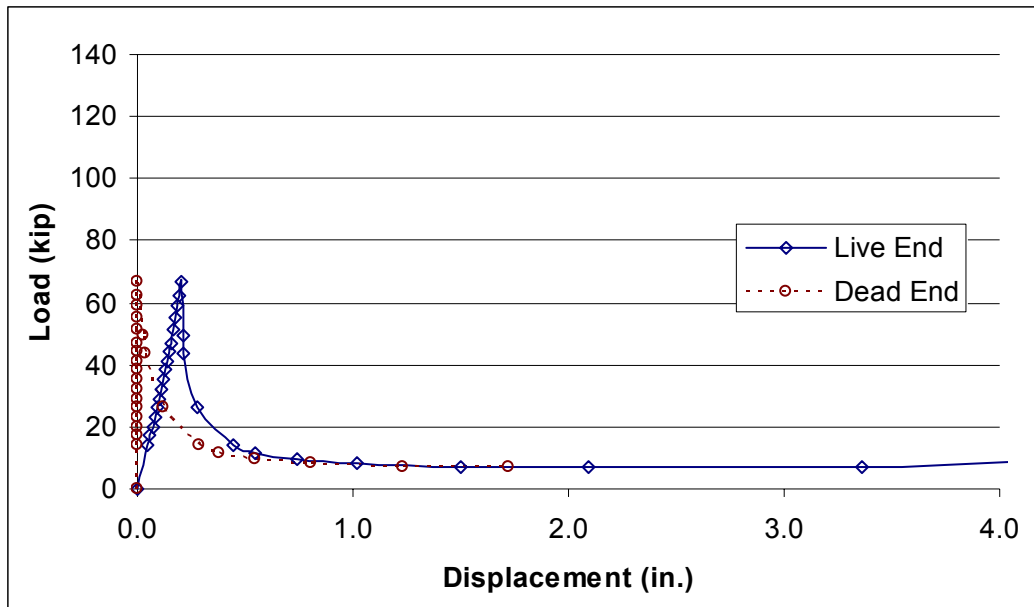
**Figure 4-15 Live End Load-Displacement and Dead End Load-Slip Response for Specimen 0-SP-10°-2**



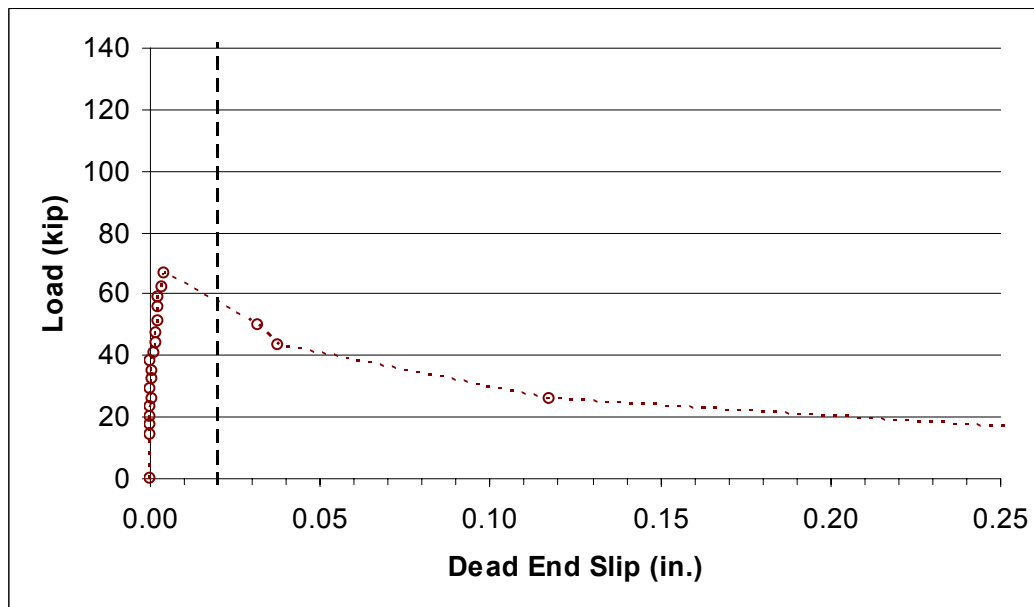
**Figure 4-16 Dead End Load-Slip Response for Specimen 0-SP-10°-2, Amplified Scale**

#### ***4.2.1.5 0-SP-7.5°-1***

Figure 4-17 is the load vs. live end displacement and load vs. dead end slip plot for specimen 0-SP-7.5°-1. The figure indicates that the peak load achieved was 67.1 kip, at which point an extremely pronounced reduction in resistance occurred. Figure 4-18 is the load vs. dead end slip plot for the specimen. It shows slip behavior at an amplified scale over a smaller range of displacement values. This highlights the slip behavior prior to and just after failure. The figure shows that very little slip occurred prior to the maximum load. The maximum load corresponds to the point where the first appreciable dead end slip occurred, after which substantial displacement accumulated on both the live and dead ends at lower load levels. Failure occurred at the duct-concrete interface for this specimen with a dead end slip of less than 0.02 in. Figure 4-19 shows the specimen after testing, with the duct and tendon pulled several inches out of the specimen.



*Figure 4-17 Live End Load-Displacement and Dead End Load-Slip Response for Specimen 0-SP-7.5°-1*



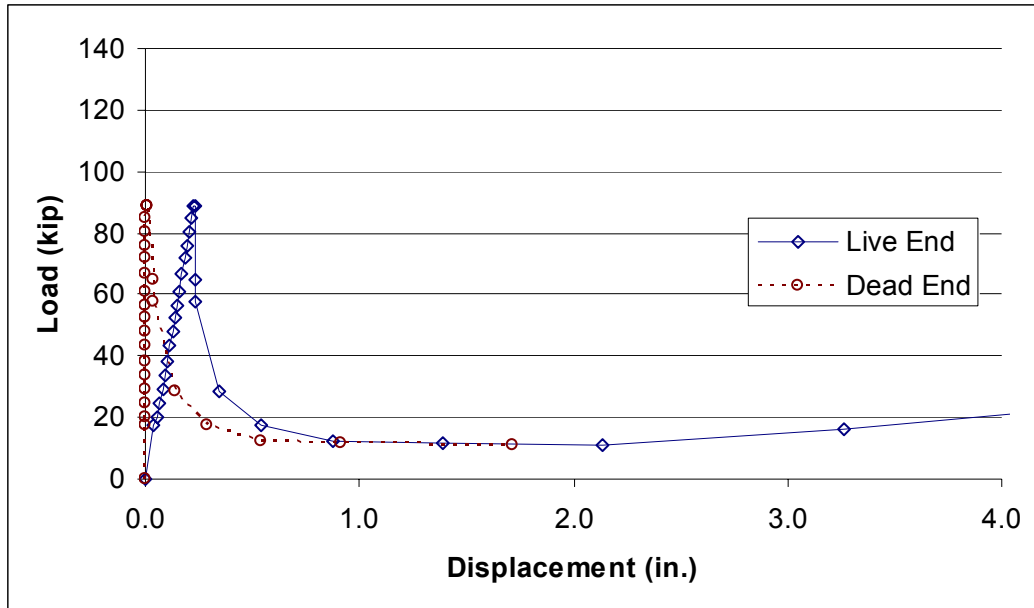
*Figure 4-18 Dead End Load-Slip Response for Specimen 0-SP-7.5°-1, Amplified Scale*



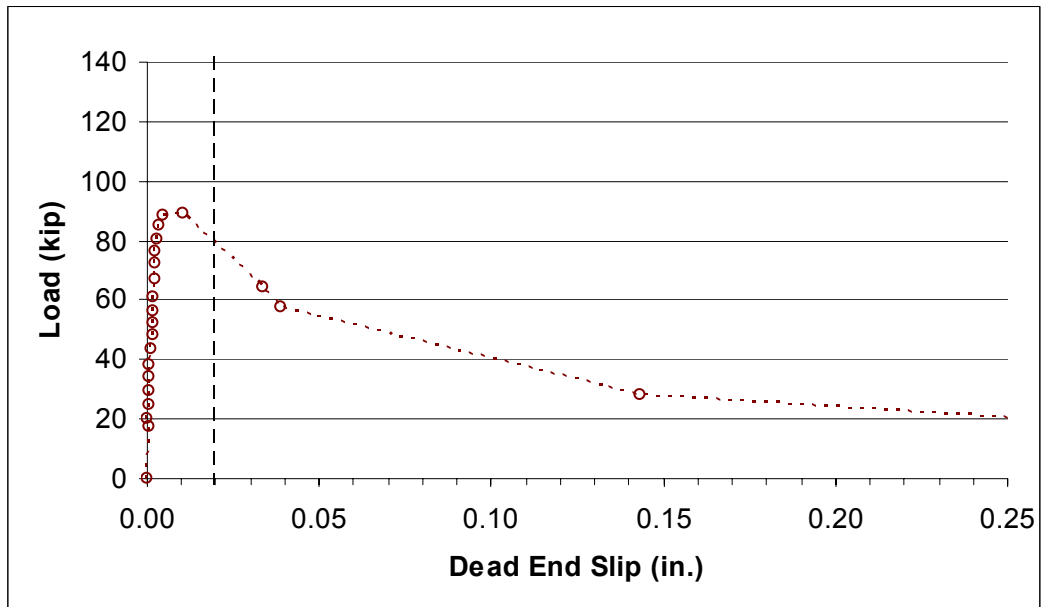
*Figure 4-19 Live End of Specimen 0-SP-7.5°-1 after Testing*

#### **4.2.1.6 0-SP-7.5°-2**

Figure 4-20 is the load vs. live end displacement and load vs. dead end slip plot for specimen 0-SP-7.5°-2. The figure indicates that the peak load achieved was 89.1 kip, at which point an extremely pronounced reduction in resistance occurred. Figure 4-21 is the load vs. dead end slip plot for the specimen. It shows slip behavior at an amplified scale over a smaller range of displacement values. This highlights the slip behavior prior to and just after failure. The figure shows that very little slip occurred prior to the maximum load. The maximum load corresponds to the point where the first appreciable dead end slip occurred, after which substantial displacement accumulated on both the live and dead ends at lower load levels. Failure occurred at the duct-concrete interface for this specimen with a dead end slip of less than 0.02 in. Figure 4-22 shows the specimen after testing, with the duct and tendon pulled several inches out of the specimen.



**Figure 4-20** *Live End Load-Displacement and Dead End Load-Slip Response for Specimen 0-SP-7.5°-2*



**Figure 4-21** *Dead End Load-Slip Response for Specimen 0-SP-7.5°-2, Amplified Scale*





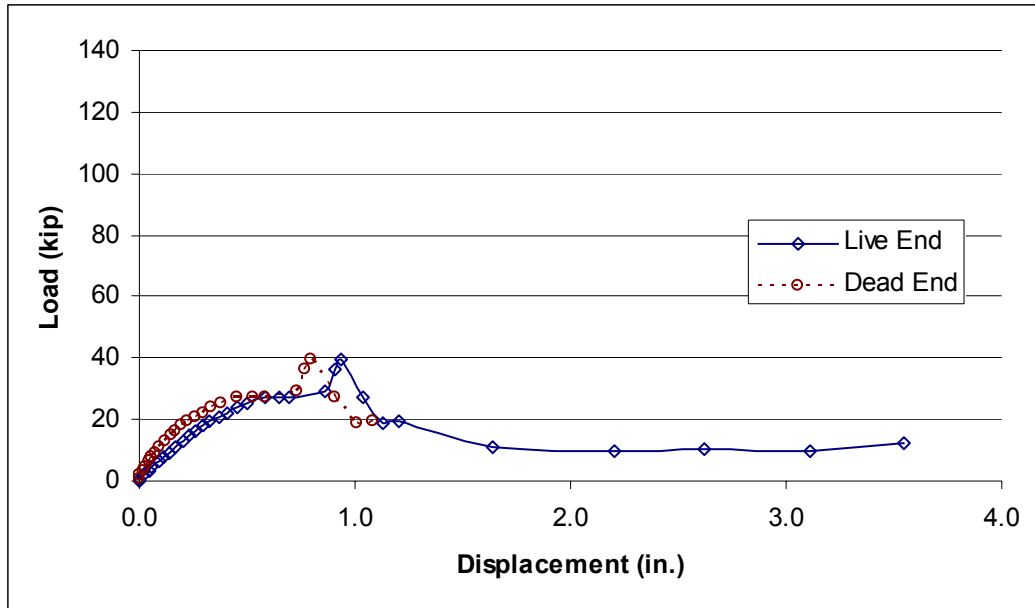
*Figure 4-22 Live End of Specimen 0-SP-7.5°-2 after Testing*

#### ***4.2.1.7 1-SP-7.5°-1***

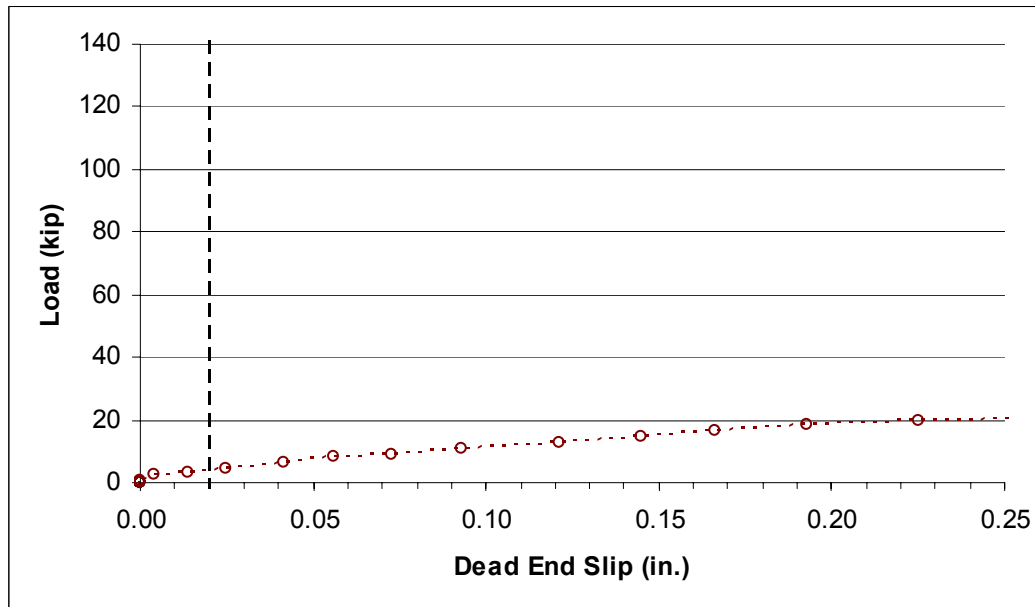
Figure 4-23 is the load vs. live end displacement and load vs. dead end slip plot for specimen 1-SP-7.5°-1. The figure indicates that a peak load of 39.3 kip was achieved, at which point a pronounced reduction in resistance occurred. Figure 4-24 is the load vs. dead end slip plot for the specimen. The figure shows that significant dead end slip began accumulating immediately upon loading.

This specimen exhibited very strange behavior with regard to failure mode. Immediately upon loading, the tendon began to slip relative to the grout. After a small slip, on the range of 0.1 in., the grout began to slip relative to the pipe. Finally, the maximum load occurred as the pipe broke free from the concrete, and a resultant reduction in resistance occurred. The load at a cumulative dead end slip of 0.02 in was 4.1 kip.

Upon inspection of the specimen after testing, a dark slimy residue was observed on the grout plug. This residue is most likely residual oil that collected on the lower surface of the duct since it was not observed on any of the uncoiled specimens. It is highly likely that this residual oil contributed to the loss of adhesion that was observed between the grout and the duct in this specimen. Figure 4-25 is a picture of the live end of the specimen after testing. The tendon and grout are pulled about 1 in. out of the pipe, and the pipe is pulled about 2.5 in. out of the specimen.



**Figure 4-23 Live End Load-Displacement and Dead End Load-Slip Response for Specimen 1-SP-7.5°-1**



**Figure 4-24 Dead End Load-Slip Response for Specimen 1-SP-7.5°-1, Amplified Scale**



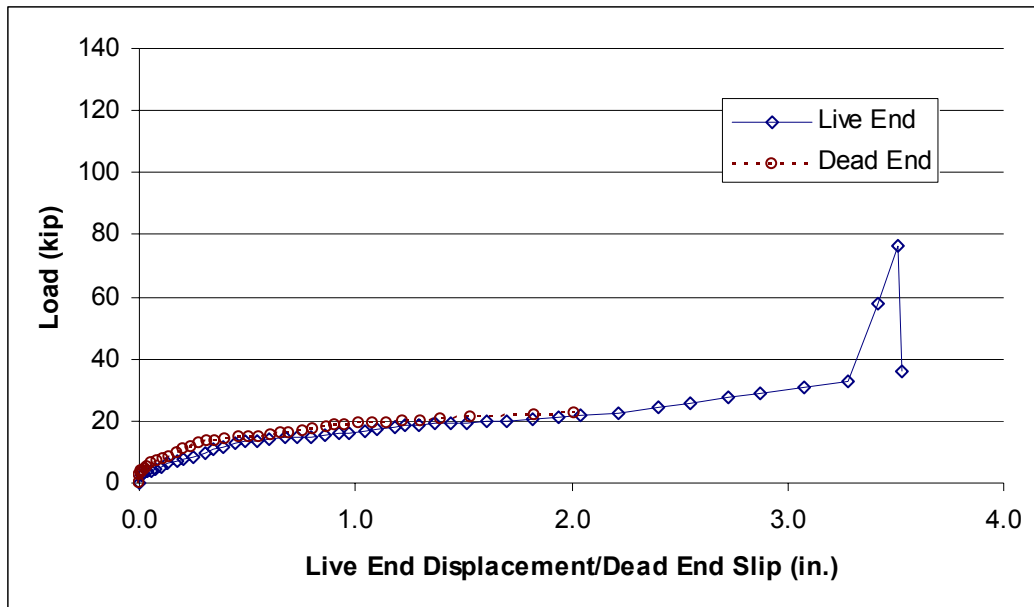
*Figure 4-25 Photo of Specimen 1-SP-7.5°-1 after Testing*

#### **4.2.1.8 1-SP-7.5°-2**

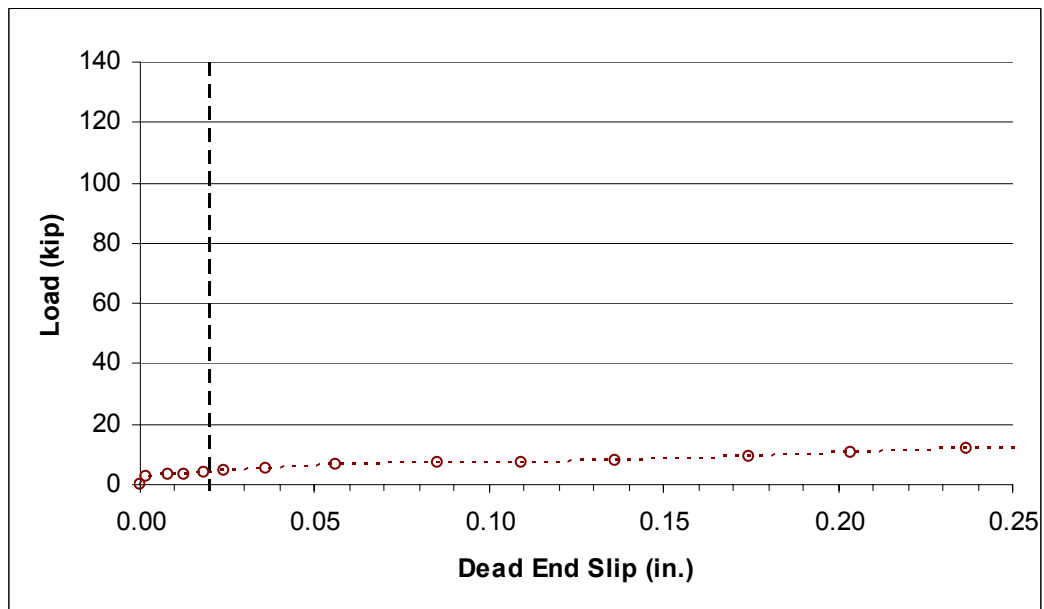
Figure 4-26 is the load vs. live end displacement and load vs. dead end slip plot for specimen 1-SP-7.5°-2. The figure indicates that a load of 32.9 kip was achieved before a significant spike in the load occurred. After a peak load of 76.3 kip was attained, the pipe broke free from the concrete and a reduction in resistance was observed. It is believed that the tendon and grout kinked in the pipe as discussed in Section 4.2.1.3. Figure 4-27 is the load vs. dead end slip plot for the specimen. The figure shows that significant dead end slip began accumulating immediately upon loading.

The tendon in this specimen began to slip at the grout-duct interface. The load at 0.02 in. of dead end slip was 4.1 kip. After a displacement of over 3 in., the load spiked and a secondary failure at the duct-concrete interface occurred.

Upon inspection of the specimen after testing, a dark slimy residue was noted on the underside of the grout plug. This residue is most likely residual oil that collected on the lower surface of the duct since it was not observed on any of the unoiled specimens. It is highly likely that this residual oil contributed to the loss of adhesion observed between the grout and the duct in this specimen. Figure 4-28 is a picture of the live end of the specimen after testing with the tendon and grout pulled about 3 in. out of the pipe and the pipe pulled about 1/4 in. out of the specimen.



**Figure 4-26** *Live End Load-Displacement and Dead End Load-Slip Response for Specimen 1-SP-7.5°-2*



**Figure 4-27** *Dead End Load-Slip Response for Specimen 1-SP-7.5°-2, Amplified Scale*



*Figure 4-28 Photo of Specimen 1-SP-7.5°-2 after Testing*

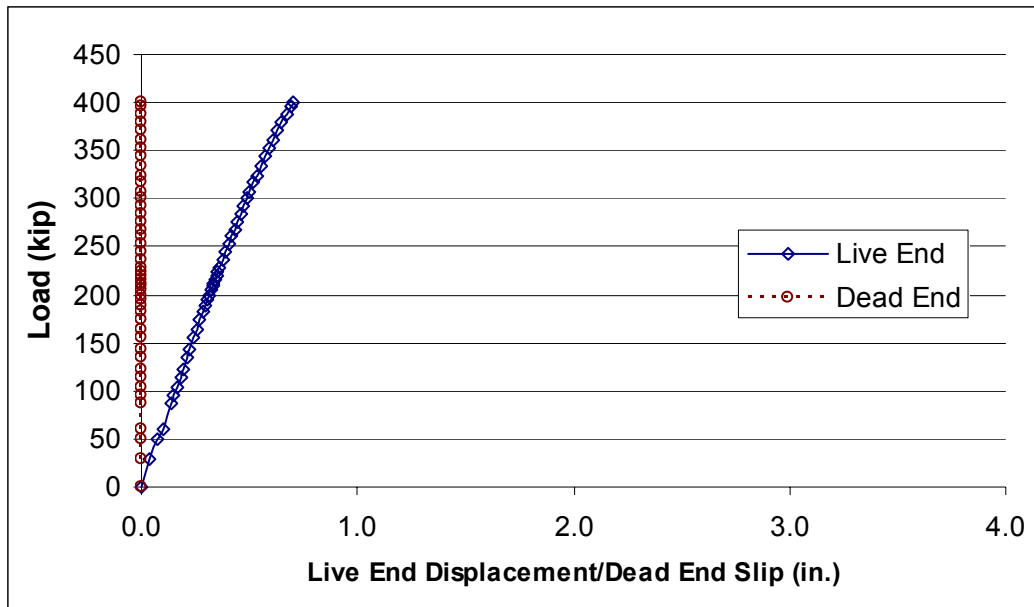
## **4.2.2 Galvanized Metal Duct Specimens**

The data from the galvanized metal duct specimens will be presented in order of decreasing length, with the unoiled specimen data preceding the oiled specimen data.

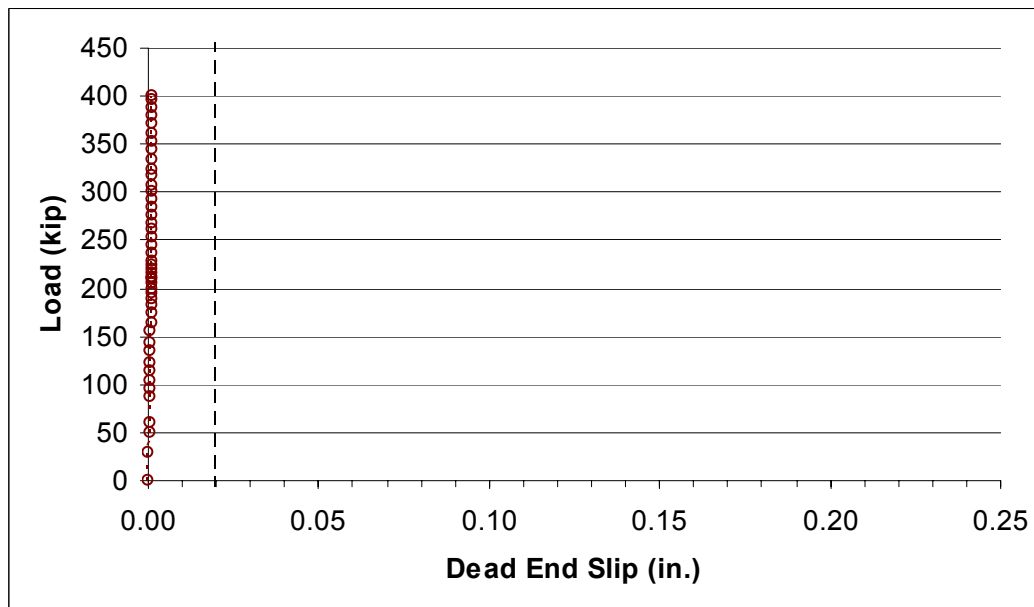
### ***4.2.2.1 0-GD-20°-1***

Figure 4-29 is the load vs. live end displacement and load vs. dead end slip plot for specimen 0-GD-20°-1. The figure indicates that a load of 400 kip was achieved without a pullout failure. Figure 4-30 is the load vs. dead end slip plot for the specimen. The maximum dead end slip recorded was less than 0.02 in. No cracking of the concrete was observed during this test.





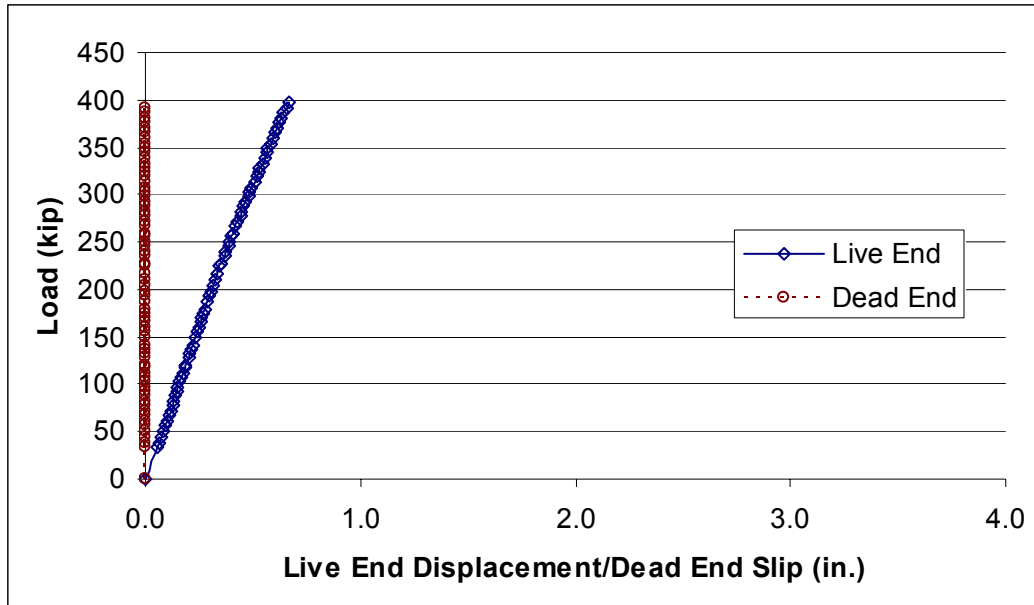
*Figure 4-29 Live End Load-Displacement and Dead End Load-Slip Response for Specimen 0-GD-20°-1*



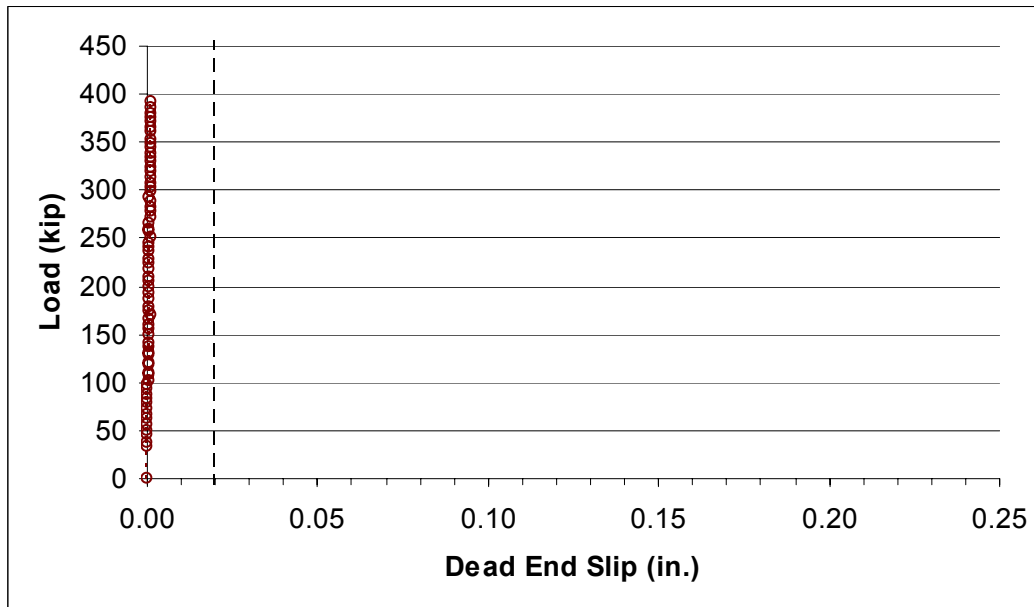
*Figure 4-30 Dead End Load-Slip Response for Specimen 0-GD-20°-1, Amplified Scale*

#### **4.2.2.2 0-GD-15°-1**

Figure 4-31 is the load vs. live end displacement and load vs. dead end slip plot for specimen 0-GD-15°-1. The figure indicates that a load of 400 kip was achieved without a pullout failure. Figure 4-32 is the load vs. dead end slip plot for the specimen. A maximum dead end slip of less than 0.02 in. was recorded. No cracking of the concrete was observed during this test.



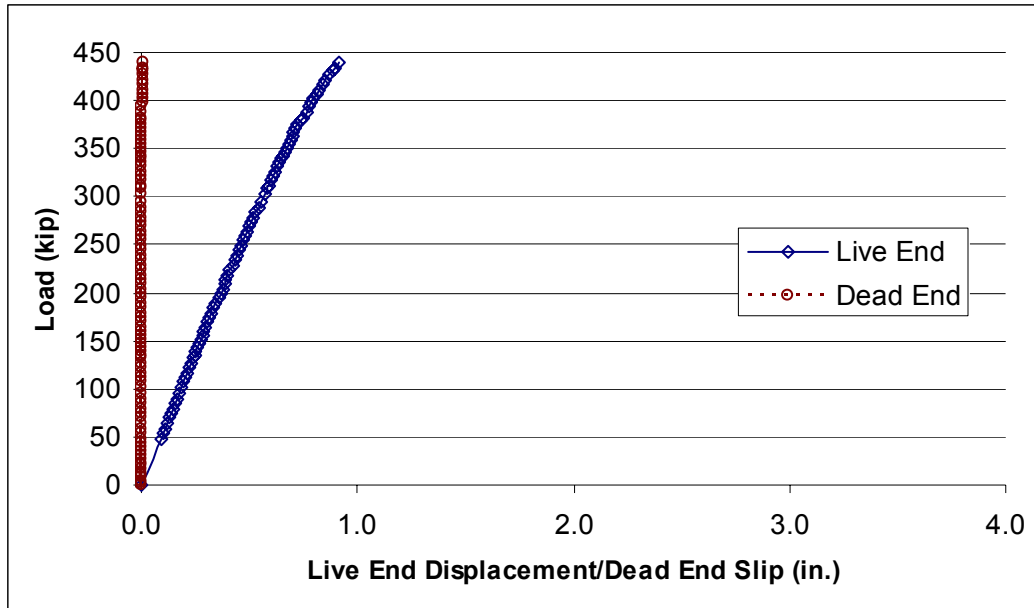
*Figure 4-31 Live End Load-Displacement and Dead End Load-Slip Response for Specimen 0-GD-15°-1*



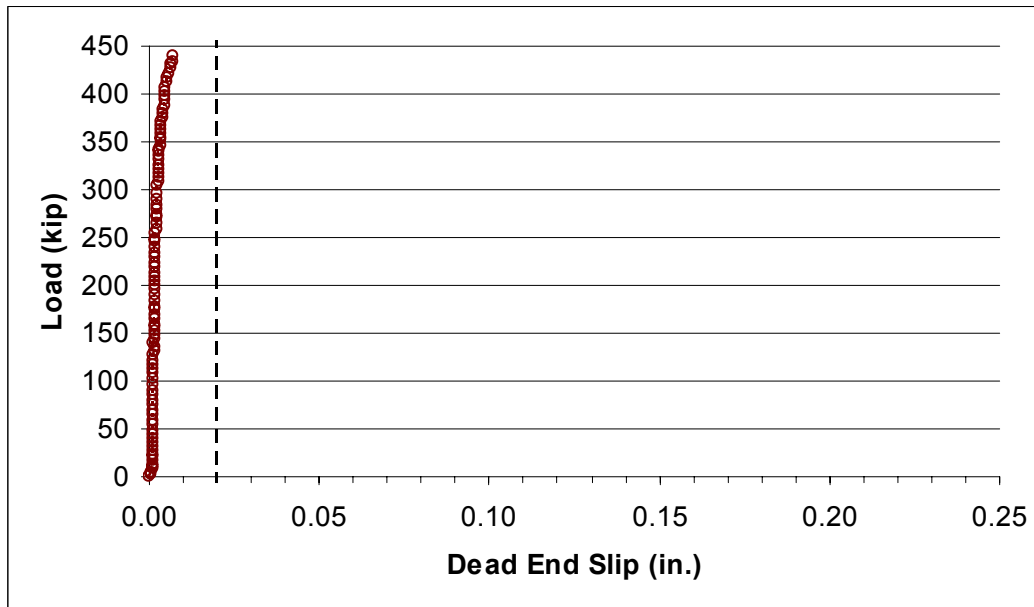
*Figure 4-32 Dead End Load-Slip Response for Specimen 0-GD-15°-1, Amplified Scale*

#### **4.2.2.3 0-GD-10°-1**

Figure 4-33 is the load vs. live end displacement and load vs. dead end slip plot for specimen 0-GD-10°-1. The figure indicates that a load of 438 kip was achieved without a pullout failure. The loading was halted when individual wires in the tendon began to break. Figure 4-34 is the load vs. dead end slip plot for the specimen. The figure shows that the maximum dead end slip achieved during testing was less than 0.02 in. No cracking of the concrete was observed during this test.



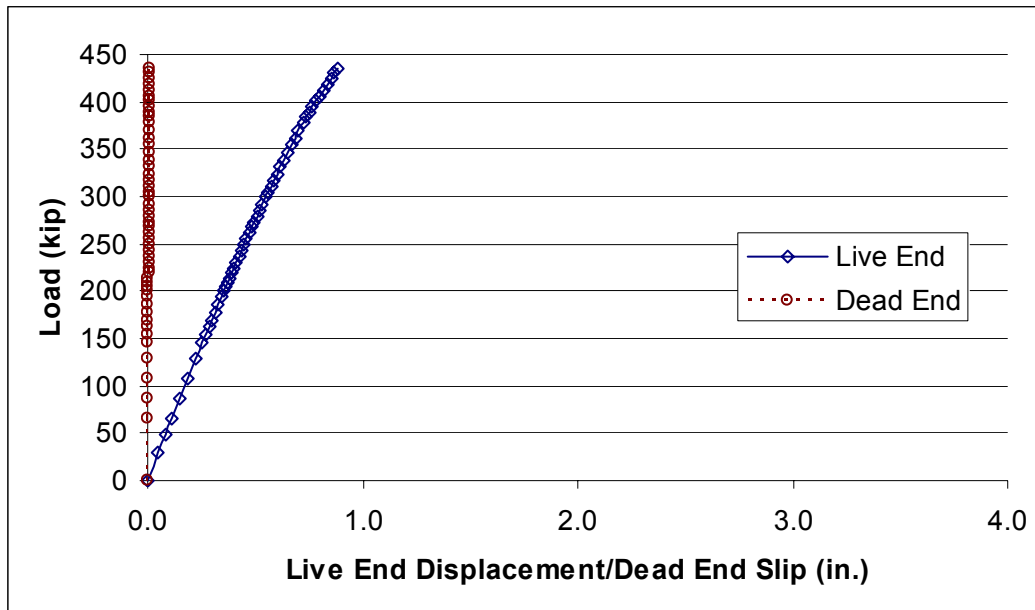
*Figure 4-33 Live End Load-Displacement and Dead End Load-Slip Response for Specimen 0-GD-10°-1*



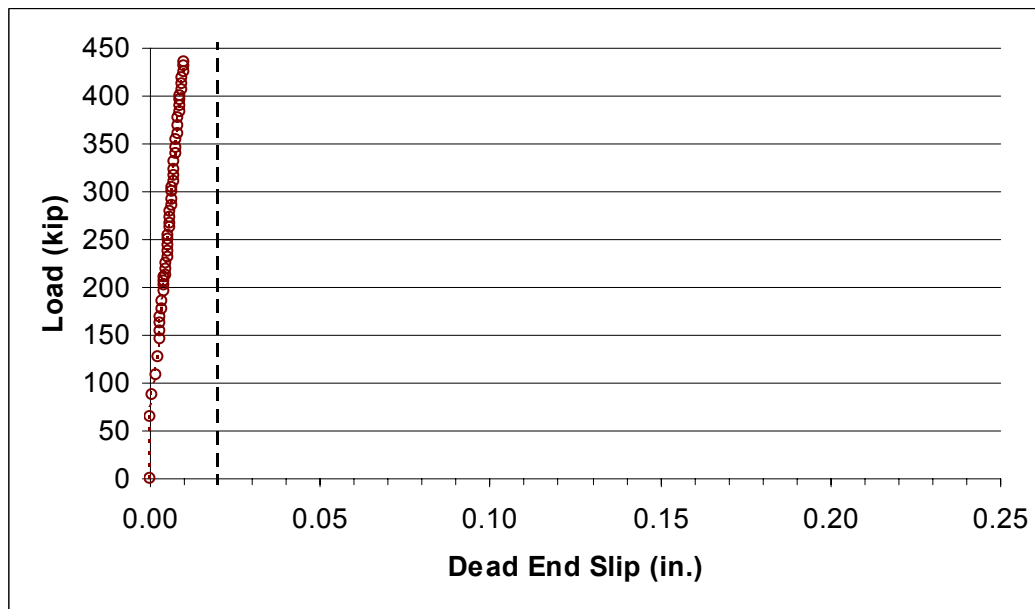
*Figure 4-34 Dead End Load-Slip Response for Specimen 0-GD-10°-1, Amplified Scale*

#### **4.2.2.4 0-GD-10°-2**

Figure 4-35 is the load vs. live end displacement and load vs. dead end slip plot for specimen 0-GD-10°-2. The figure indicates that a load of 436 kip was achieved without a pullout failure. The loading was halted when individual wires in the tendon began to break. Figure 4-36 is the load vs. dead end slip plot for the specimen. The figure shows that the maximum dead end slip achieved during testing was less than 0.02 in. No cracking of the concrete was observed during this test.



*Figure 4-35 Live End Load-Displacement and Dead End Load-Slip Response for Specimen 0-GD-10°-2*



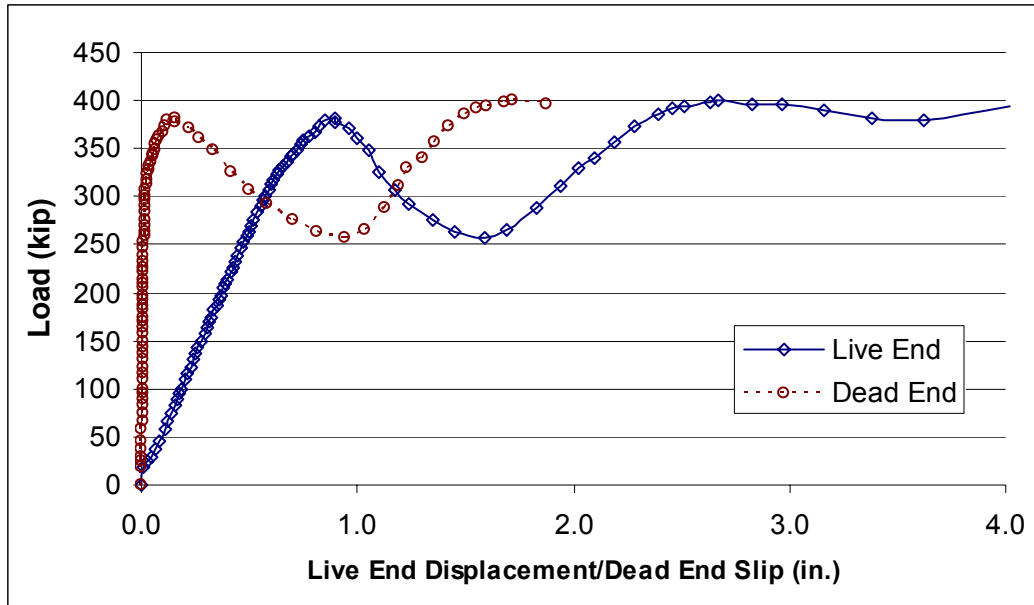
*Figure 4-36 Dead End Load-Slip Response for Specimen 0-GD-10°-2, Amplified Scale*

#### **4.2.2.5 0-GD-7.5°-1**

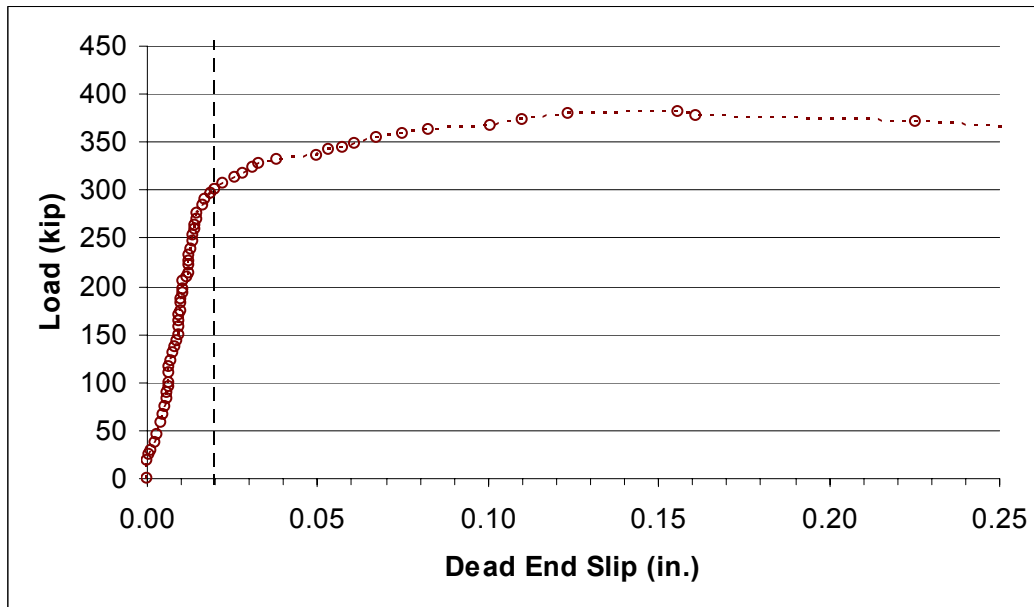
Figure 4-37 is the load vs. live end displacement and load vs. dead end slip plot for specimen 0-GD-7.5°-1. The figure indicates that an initial peak load of 382 kip was achieved, at which point a pronounced reduction in resistance occurred. Figure 4-38 is the load vs. dead end slip plot for the specimen. It shows slip behavior at an amplified scale over a smaller range of displacement values. This highlights the slip behavior prior to and just after failure. The figure shows that significant slip occurred prior to the initial peak load. The load at 0.02 in. of dead end slip was 302 kip. The peak load was accompanied by a marked increase in dead end displacements. After the initial maximum load, substantial displacement accumulated on both the live and dead ends. Failure of this specimen occurred at the tendon-grout interface. With continued loading, a maximum load of 400 kip was achieved at a dead end slip of over 1.5 in. The maintenance of load carrying capacity was likely due to interlocking at the irregular interface between the tendon and the grout as the tendon moved through the specimen.

Significant cracking of the concrete occurred simultaneously with the initial maximum load in the specimen. Figure 4-39 shows a profile of the specimen after testing with the dead end in the foreground. The figure shows the pattern of cracking observed in the specimen, with splitting cracks spreading radially out from the duct. The crack on the top of the specimen extended all the way to the live end of the specimen, while the cracks on the sides extended from the dead end about three quarters of the length of the specimen.





*Figure 4-37 Live End Load-Displacement and Dead End Load-Slip Response for Specimen 0-GD-7.5°-1*



*Figure 4-38 Dead End Load-Slip Response for Specimen 0-GD-7.5°-1, Amplified Scale*

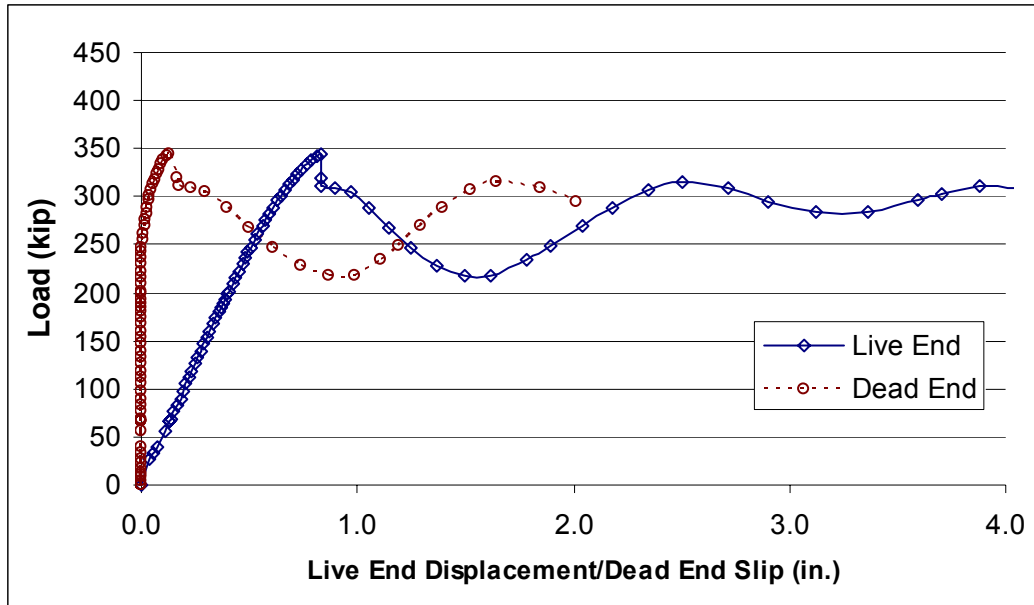


*Figure 4-39 Profile of Specimen 0-GD-7.5°-1 after Testing*

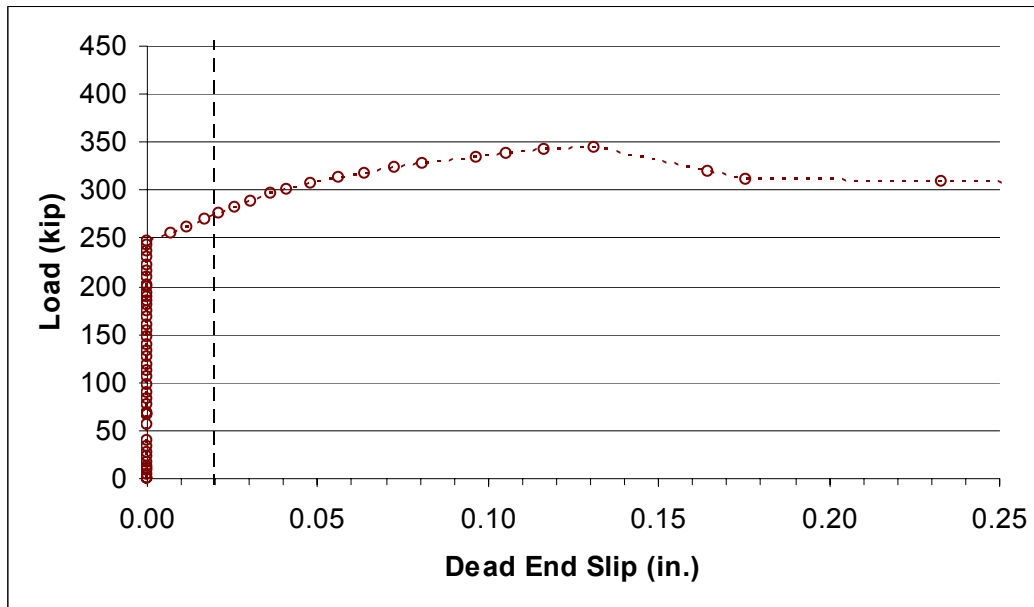
#### **4.2.2.6 0-GD-7.5°-2**

Figure 4-40 is the load vs. live end displacement and load vs. dead end slip plot for specimen 0-GD-7.5°-2. The figure indicates a maximum load of 345 kip was achieved, at which point a pronounced reduction in resistance occurred. Figure 4-41 is the load vs. dead end slip plot for the specimen. It shows slip behavior at an amplified scale over a smaller range of displacement values. This highlights the slip behavior prior to and just after failure. The figure shows that significant slip occurred prior to the peak load. The load at 0.02 in. of dead end slip was 274 kip. The peak load was accompanied by a marked increase in the magnitude of dead end displacements. After the maximum load, substantial displacement accumulated on both the live and dead ends. Failure occurred at the tendon-grout interface for this specimen. With continued displacement, a significant fraction of the load carrying capacity was maintained. The maintenance of load carrying capacity was likely due to interlocking at the irregular interface between the tendon and the grout as the tendon moved through the specimen.

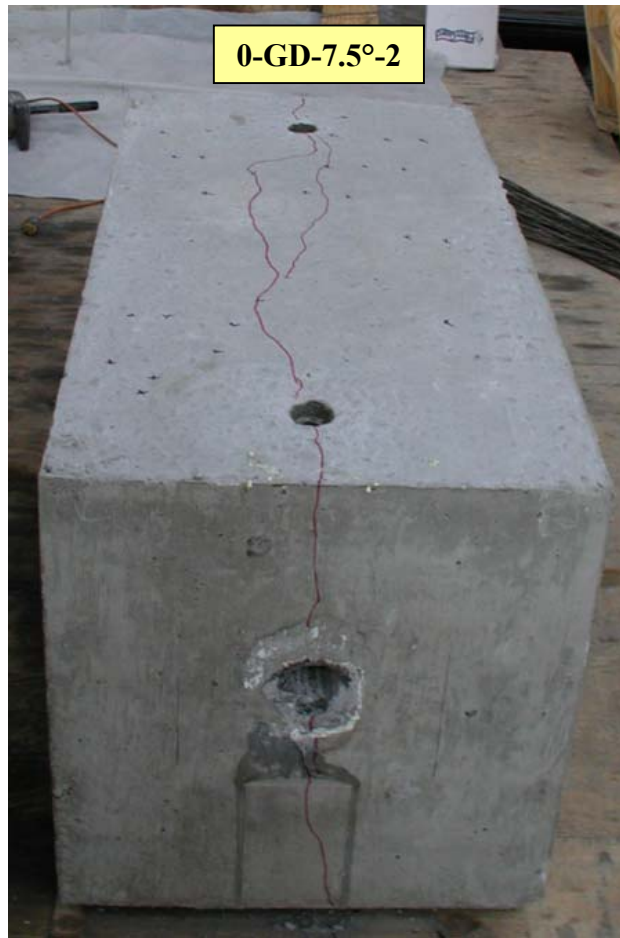
Significant cracking of the concrete occurred simultaneously with the maximum load in the specimen. Figure 4-42 shows the specimen after testing with the dead end in the foreground. The figure shows the pattern of cracking observed in the specimen, with a single splitting crack running down the center. The crack extended along the entire length of the specimen.



*Figure 4-40 Live End Load-Displacement and Dead End Load-Slip Response for Specimen 0-GD-7.5°-2*



*Figure 4-41 Dead End Load-Slip Response for Specimen 0-GD-7.5°-2, Amplified Scale*

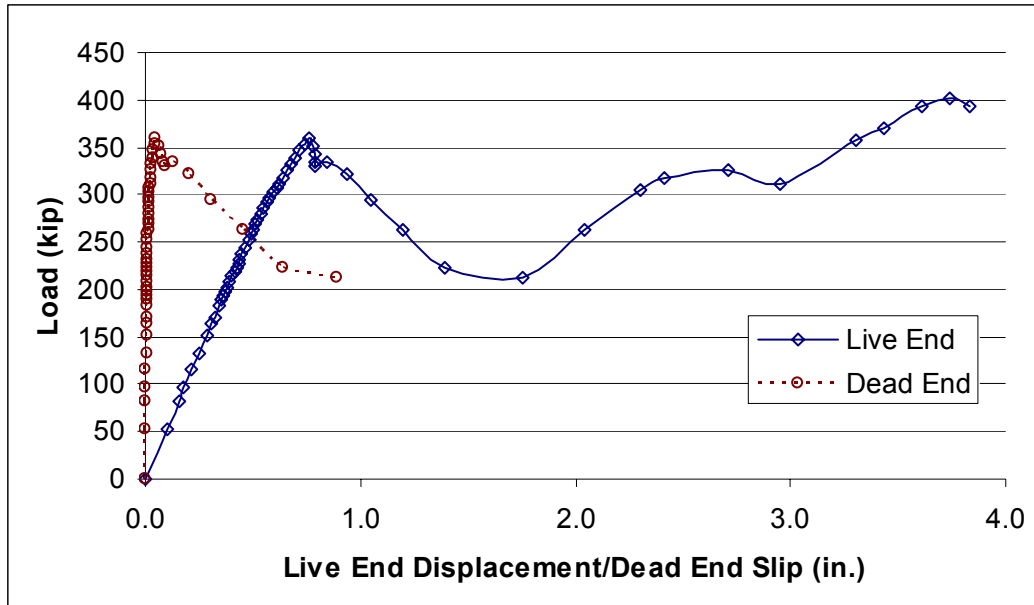


*Figure 4-42 Photo of Specimen 0-GD-7.5°-2 after Testing*

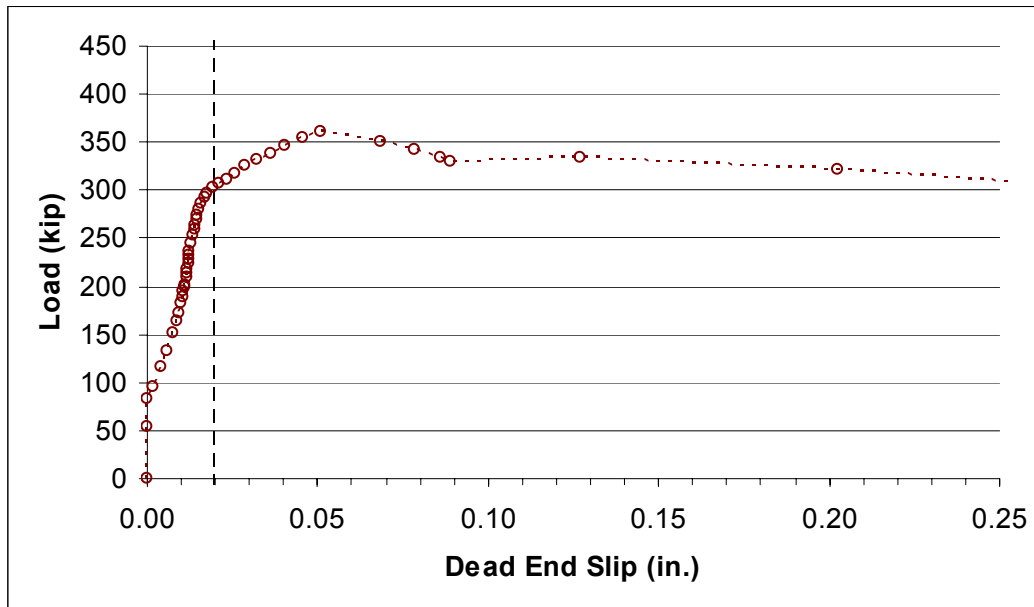
#### **4.2.2.7 0-GD-7.5°-3**

Figure 4-43 is the load vs. live end displacement and load vs. dead end slip plot for specimen 0-GD-7.5°-3. The figure indicates that an initial peak load of 360 kip was achieved, at which point a pronounced reduction in resistance occurred. Figure 4-44 is the load vs. dead end slip plot for the specimen. It shows slip behavior at an amplified scale over a smaller range of displacement values. This highlights the slip behavior prior to and just after failure. The figure shows that slip began occurring at relatively low loads, and significant slip occurred prior to the initial peak load. The load at 0.02 in. of dead end slip was 304 kip. The peak load was accompanied by a significant increase in dead end displacements. After the initial maximum load, substantial displacement accumulated on both the live and dead ends. Failure occurred at the tendon-grout interface for this specimen. With continued loading, a maximum load of 402 kip was achieved at a live end displacement of over 3.5 in. The maintenance of load carrying capacity was likely due to interlocking at the irregular interface between the tendon and the grout as the tendon moved through the specimen.

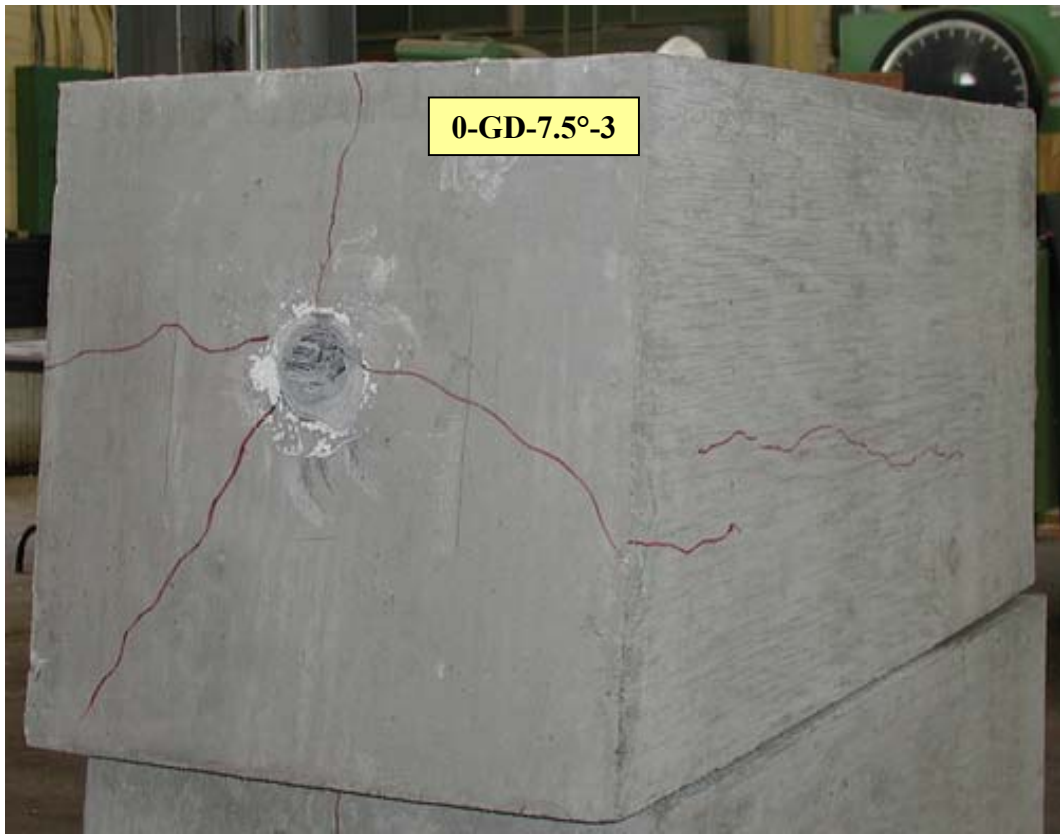
Significant cracking of the concrete occurred simultaneously with the initial maximum load. Figure 4-45 shows a profile of the specimen after testing with the dead end in the foreground. The figure shows the pattern of cracking observed in the specimen, with splitting cracks spreading radially out from the duct. A crack on the top of the specimen extended the entire length, while cracks on the sides extended from the dead end about three quarters of the length of the specimen.



**Figure 4-43 Live End Load-Displacement and Dead End Load-Slip Response for Specimen 0-GD-7.5°-3**



**Figure 4-44 Dead End Load-Slip Response for Specimen 0-GD-7.5°-3, Amplified Scale**



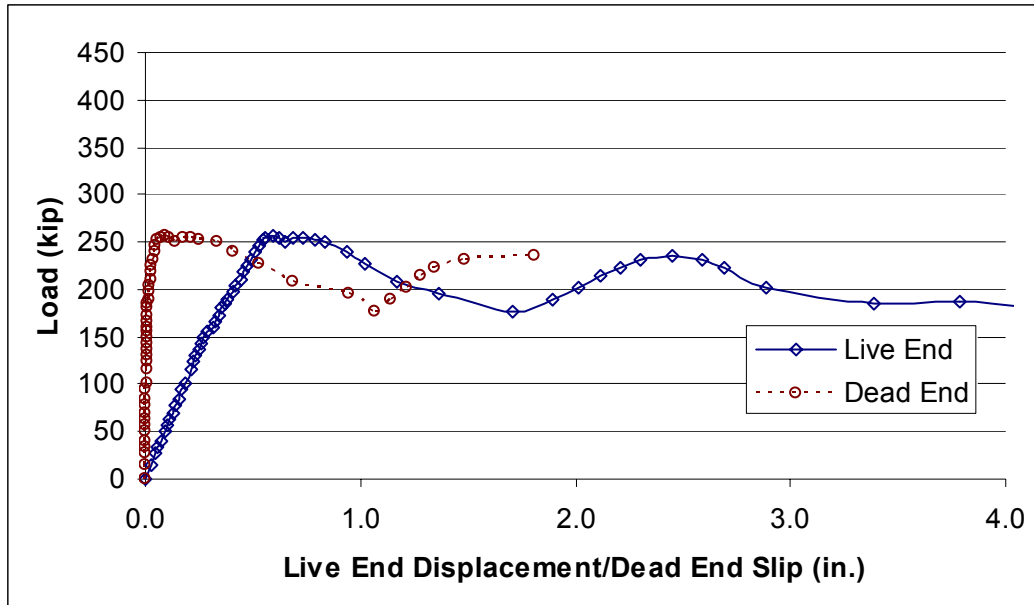
*Figure 4-45 Profile of Specimen 0-GD-7.5°-3 after Testing*



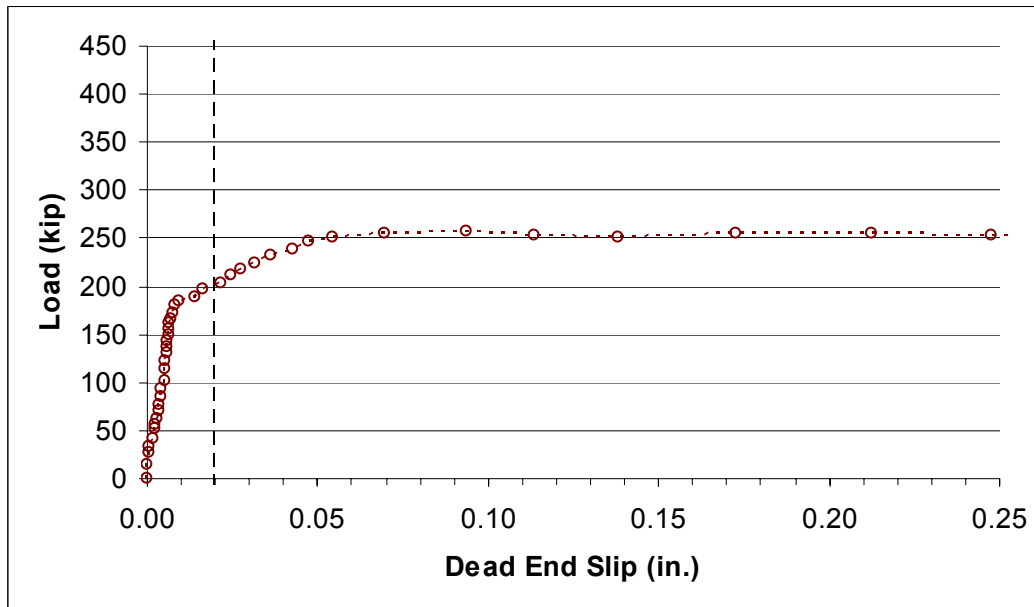
#### **4.2.2.8 0-GD-5°-1**

Figure 4-46 is the load vs. live end displacement and load vs. dead end slip plot for specimen 0-GD-5°-1. The figure indicates a maximum load of 257 kip was achieved, at which point a pronounced reduction in resistance occurred. Figure 4-47 is the load vs. dead end slip plot for the specimen. It shows slip behavior at an amplified scale over a smaller range of displacement values. This highlights the slip behavior prior to and just after failure. The figure shows that significant slip occurred prior to the peak load. The load at a dead end slip of 0.02 in was 202 kip. The peak load was accompanied by a marked increase in the magnitude of dead end displacements. After reaching the maximum load, substantial displacement accumulated on both the live and dead ends. Failure occurred at the tendon-grout interface for this specimen. With continued displacement, a significant fraction of the load carrying capacity was maintained. The maintenance of load carrying capacity was likely due to interlocking at the irregular interface between the tendon and the grout as the tendon moved through the specimen.

Significant cracking of the concrete occurred simultaneously with the maximum load in the specimen. Figure 4-48 shows a profile of the specimen after testing with the dead end in the foreground. The figure shows the pattern of cracking observed, with splitting cracks spreading radially out from the duct. A crack in the top extended the entire length of the specimen, as did the crack on the side of the specimen shown in the photo. A crack on the opposite side of the specimen extended from the dead end about three quarter of the length of the specimen.



**Figure 4-46 Live End Load-Displacement and Dead End Load-Slip Response for Specimen 0-GD-5°-1**



**Figure 4-47 Dead End Load-Slip Response for Specimen 0-GD-5°-1, Amplified Scale**



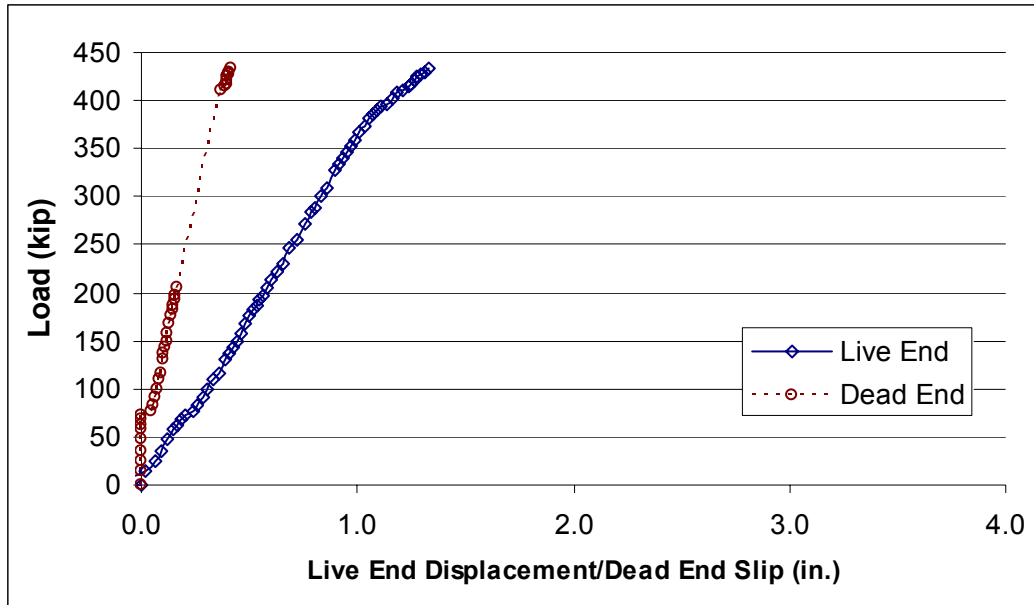
*Figure 4-48 Photo of Specimen 0-GD-5°-1 after Testing*

#### **4.2.2.9 1-GD-7.5°-1**

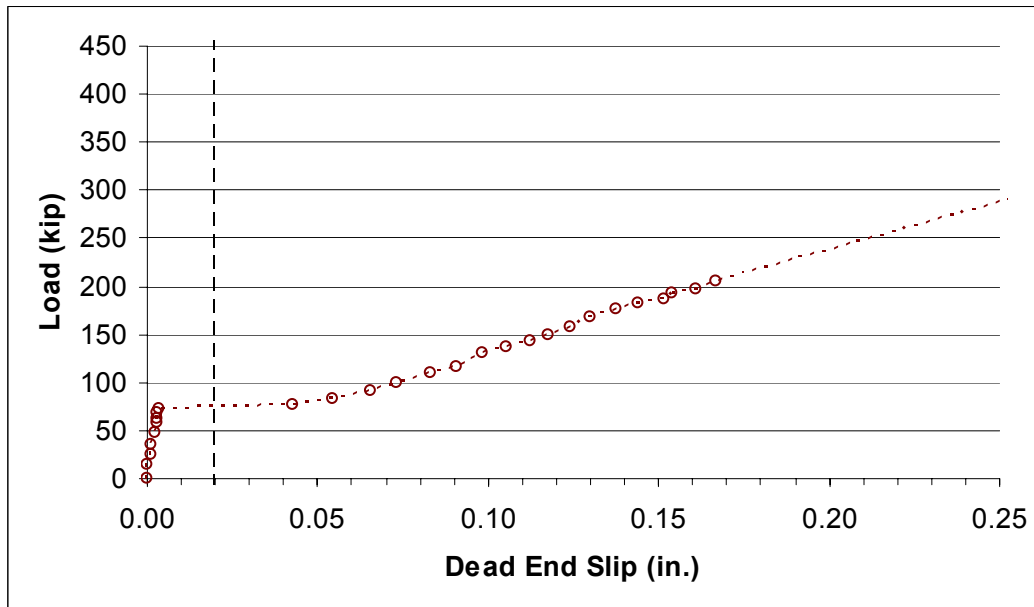
Figure 4-49 is the load vs. live end displacement and load vs. dead end slip plot for specimen 1-GD-7.5°-1. The figure indicates that a load of 434 kip was achieved without a pullout failure. The loading was halted when individual wires in the tendon began to break. Figure 4-50 is the load vs. dead end slip plot for the specimen. The figure shows that significant dead end slip began accumulating at very low loads. The load at a dead end slip of 0.02 in. was 74.4 kip.

Hairline cracking was not noticed in the concrete until after testing had been halted. For this reason it is not certain when cracking occurred. Figure 4-51 shows a profile of the specimen after testing with the live end in the foreground, illustrating the pattern of cracking observed. Splitting cracks spread out radially from the duct. Two longitudinal cracks formed in the specimen which extended from the live end about three quarters of the length of the specimen. Of the galvanized metal duct specimens, only this specimen and its companion, 1-GD-7.5°-2 exhibited cracks which propagated from the live end toward the dead.

The gap in the dead end slip data is due to the fact that the head of the linear potentiometer became caught on some of the grout at the dead end after the tendon began to slip. When the problem was recognized, the head of the potentiometer was freed and accurate readings were registered for the remainder of the test. The reader is reminded that original data can be found in Appendix A.



**Figure 4-49 Live End Load-Displacement and Dead End Load-Slip Response for Specimen 1-GD-7.5°-1**



**Figure 4-50 Dead End Load-Slip Response for Specimen 1-GD-7.5°-1, Amplified Scale**

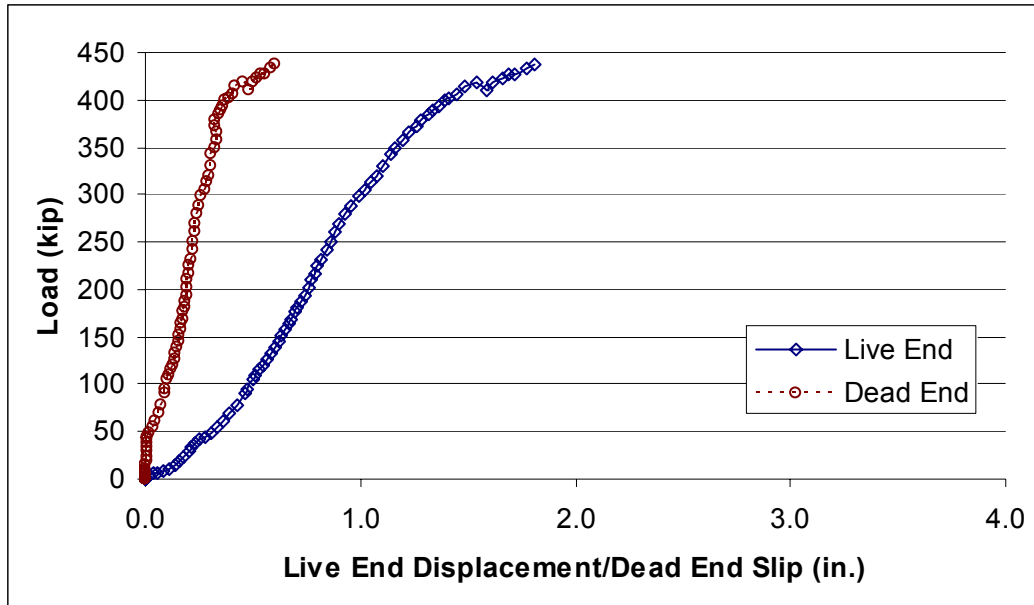


*Figure 4-51 Photo of Specimen 1-GD-7.5°-1 after Testing*

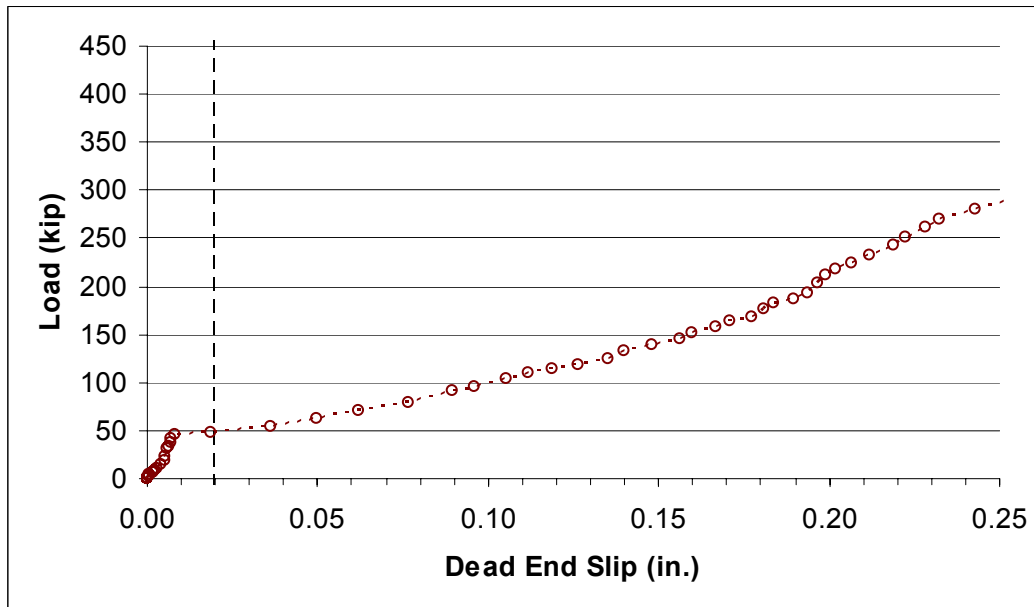
#### **4.2.2.10 1-GD-7.5-2**

Figure 4-52 is the load vs. live end displacement and load vs. dead end slip plot for specimen 1-GD-7.5-2. The figure indicates that a load of 437 kip was achieved without a pullout failure. The loading was halted when individual wires in the tendon began to break. Figure 4-53 is the load vs. dead end slip plot for the specimen. The figure shows that significant dead end slip began accumulating at very low loads. The load at a dead end slip of 0.02 in. was 48.1 kip.

Hairline cracking was not noticed in the concrete until after testing had been halted. For this reason it is not certain when cracking occurred. Figure 4-54 shows a profile of the specimen after testing with the live end in the foreground, illustrating the pattern of cracking observed. Splitting cracks spread out radially from the duct. Two longitudinal cracks formed in the specimen which extended from the live end about ninety percent of the length of the specimen. Of the galvanized metal duct specimens, only this specimen and its companion, 1-GD-7.5°-1 exhibited cracks which propagated from the live end toward the dead.



*Figure 4-52 Live End Load-Displacement and Dead End Load-Slip Response for Specimen 1-GD-7.5°-2*



*Figure 4-53 Dead End Load-Slip Response for Specimen 1-GD-7.5°-2, Amplified Scale*





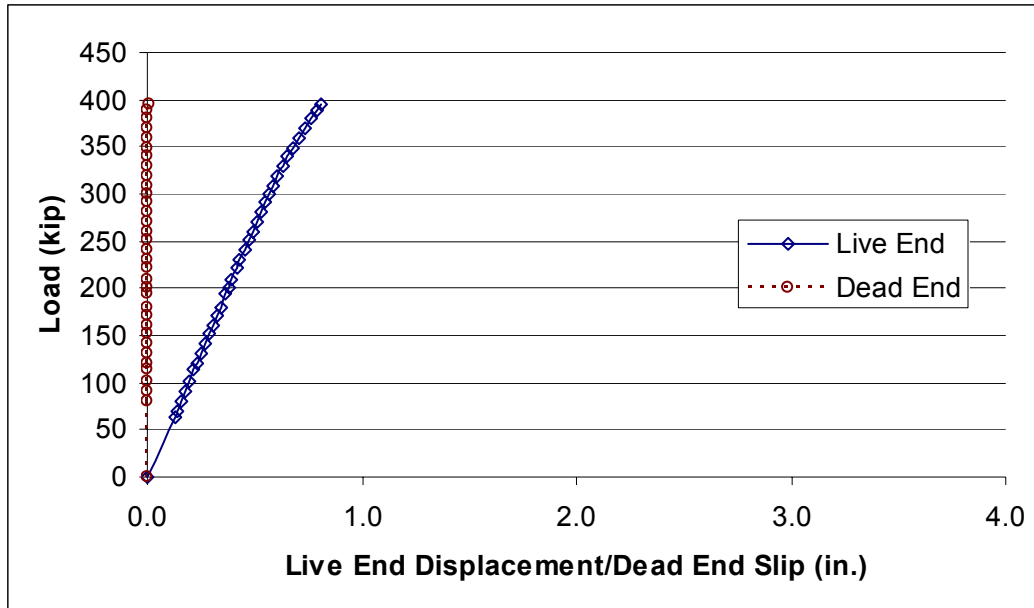
*Figure 4-54 Photo of Specimen 1-GD-7.5°-2 after Testing*

### **4.2.3 High Density Polyethylene Duct Specimens**

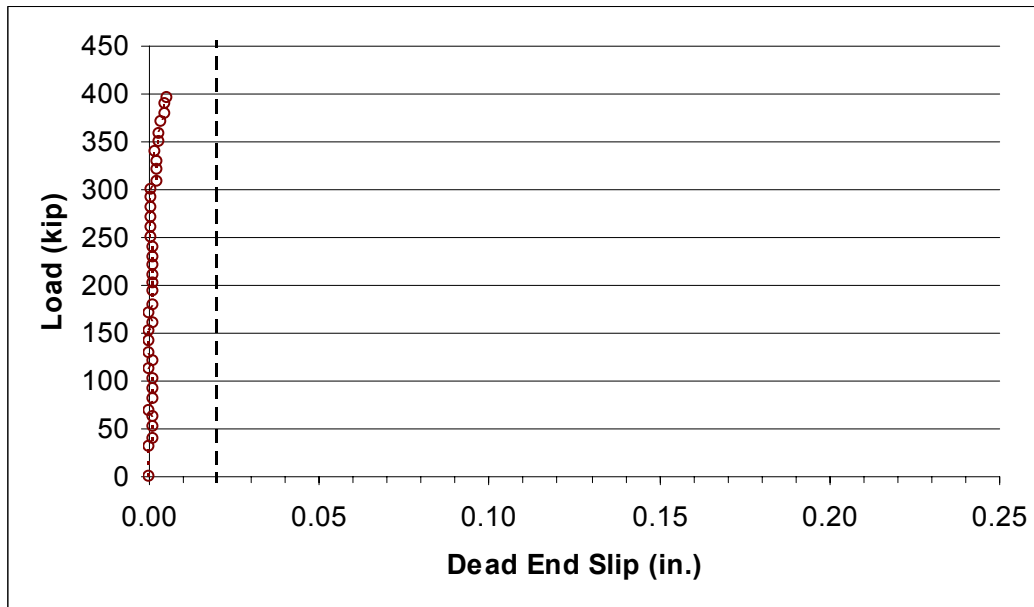
The data from the high density polyethylene duct specimens will be presented in order of decreasing length, with the unoiled specimen data preceding the oiled specimen data.

#### ***4.2.3.1 0-HD-20°-1***

Figure 4-55 is the load vs. live end displacement and load vs. dead end slip plot for specimen 0-HD-20°-1. The figure indicates that a load of 400 kip was achieved without a pullout failure. Figure 4-56 is the load vs. dead end slip plot for the specimen. The figure shows that no appreciable dead end slip occurred during testing. No cracking of the concrete was observed during this test.



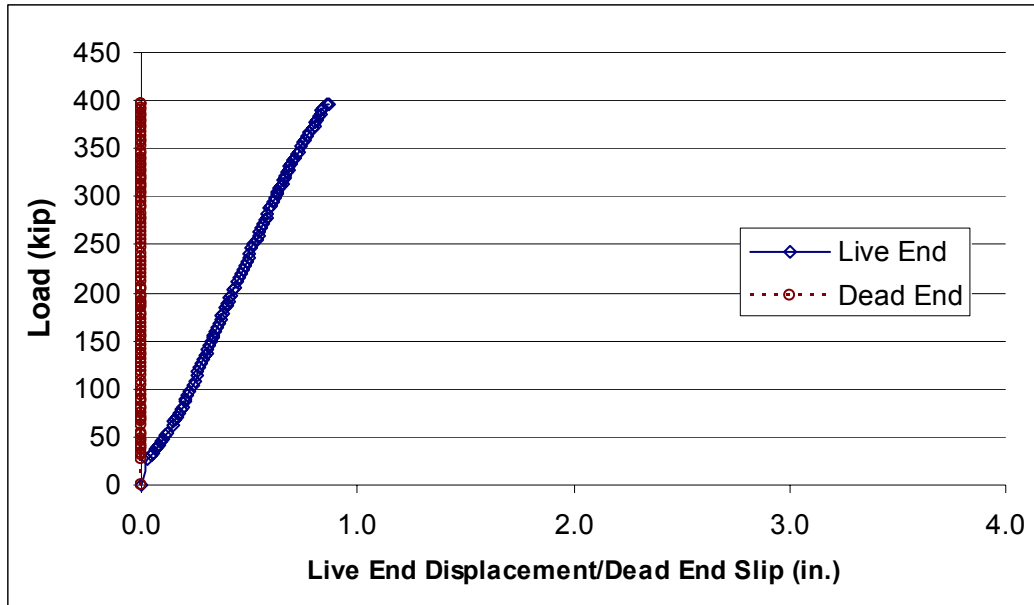
*Figure 4-55 Live End Load-Displacement and Dead End Load-Slip Response for Specimen 0-HD-20°-1*



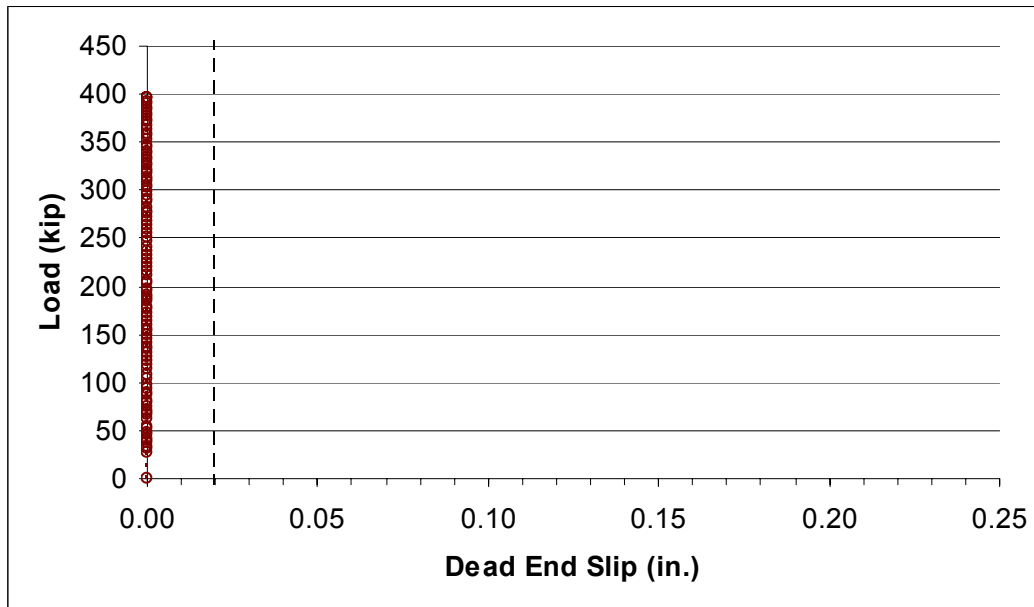
*Figure 4-56 Dead End Load-Slip Response for Specimen 0-HD-20°-1, Amplified Scale*

#### **4.2.3.2 0-HD-15°-1**

Figure 4-57 is the load vs. live end displacement and load vs. dead end slip plot for specimen 0-HD-15°-1. The figure indicates that a load of 400 kip was achieved without a pullout failure. Figure 4-58 is the load vs. dead end slip plot for the specimen. The figure shows that no dead end slip occurred during testing. No cracking of the concrete was observed during this test.



*Figure 4-57 Live End Load-Displacement and Dead End Load-Slip Response for Specimen 0-HD-15°-1*

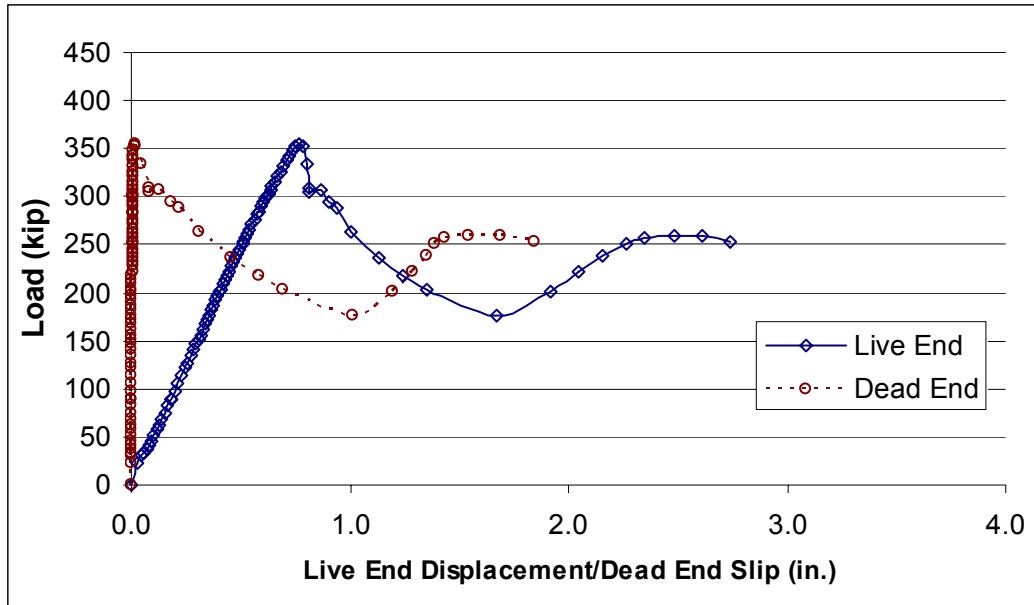


*Figure 4-58 Dead End Load-Slip Response for Specimen 0-HD-15°-1, Amplified Scale*

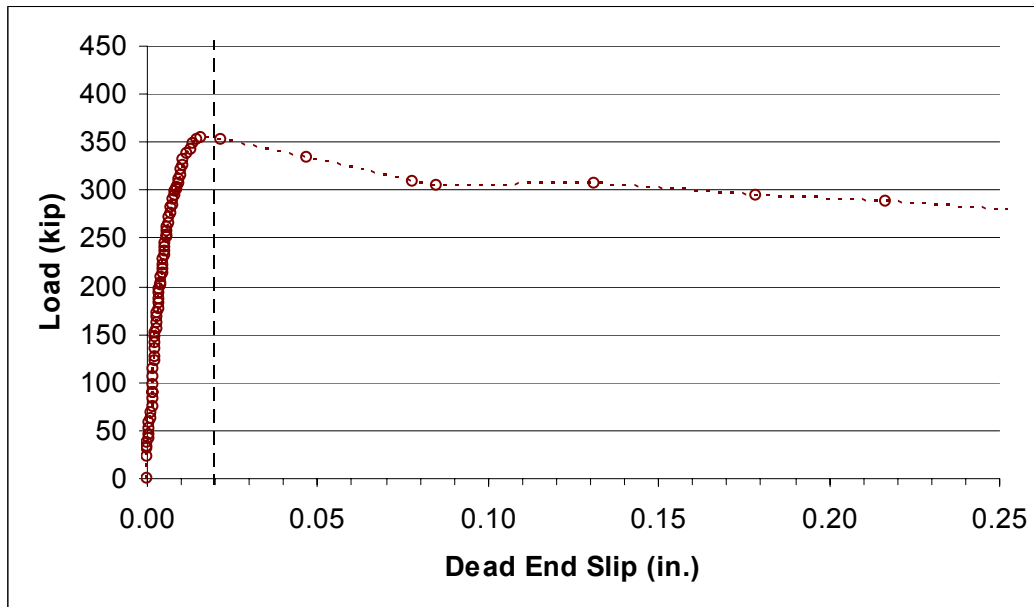
#### **4.2.3.3 0-HD-10°-1**

Figure 4-59 is the load vs. live end displacement and load vs. dead end slip plot for specimen 0-HD-10°-1. The figure indicates a peak load of 355 kip was achieved, at which point a pronounced reduction in resistance occurred. Figure 4-60 is the load vs. dead end slip plot for the specimen. It shows slip behavior at an amplified scale over a smaller range of displacement values. This highlights the slip behavior prior to and just after failure. The figure shows that measurable slip occurred prior to the peak load. However, the peak load was reached before 0.02 in. of dead end slip had occurred. The peak load was accompanied by a significant increase in the magnitude of dead end displacements. After the peak load, substantial displacement accumulated on both the live and dead ends. Failure occurred at the tendon-grout interface for this specimen. With continued displacement a significant fraction of the load carrying capacity was maintained. The maintenance of load carrying capacity is likely due to interlocking at the irregular interface between the tendon and the grout as the tendon moved through the specimen.

Significant cracking of the concrete occurred simultaneously with the maximum load in the specimen. This specimen was one of two specimens in the program which had less transverse reinforcement than was typical. For this reason, the cracking observed in this specimen was wider than that observed in the other cracked specimens with the standard transverse reinforcement spacing. A photograph of this specimen after testing was not available.



*Figure 4-59 Live End Load-Displacement and Dead End Load-Slip Response for Specimen 0-HD-10°-1*



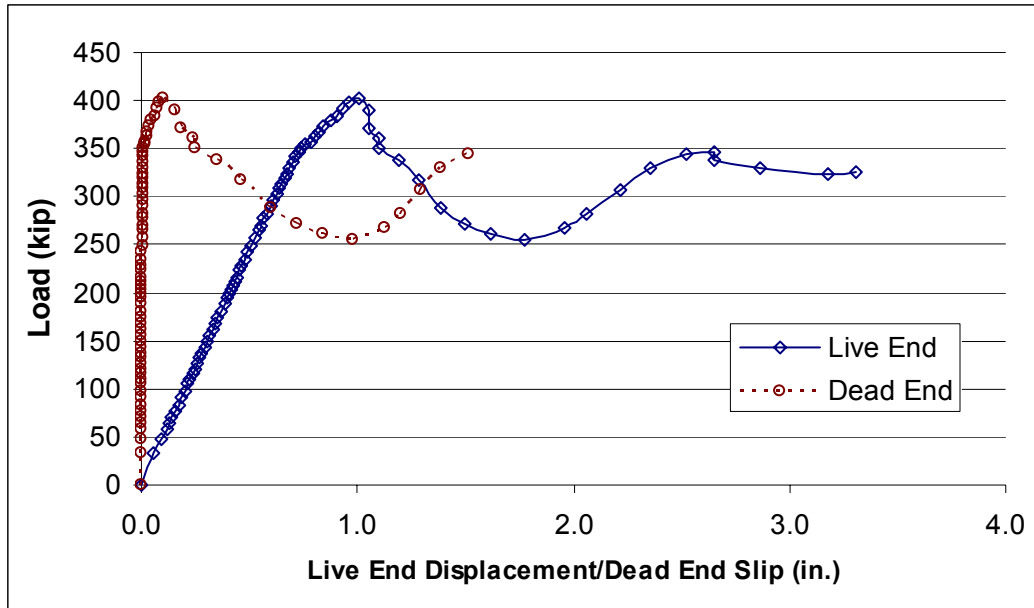
*Figure 4-60 Dead End Load-Slip Response for Specimen 0-HD-10°-1, Amplified Scale*

#### **4.2.3.4 0-HD-10°-2**

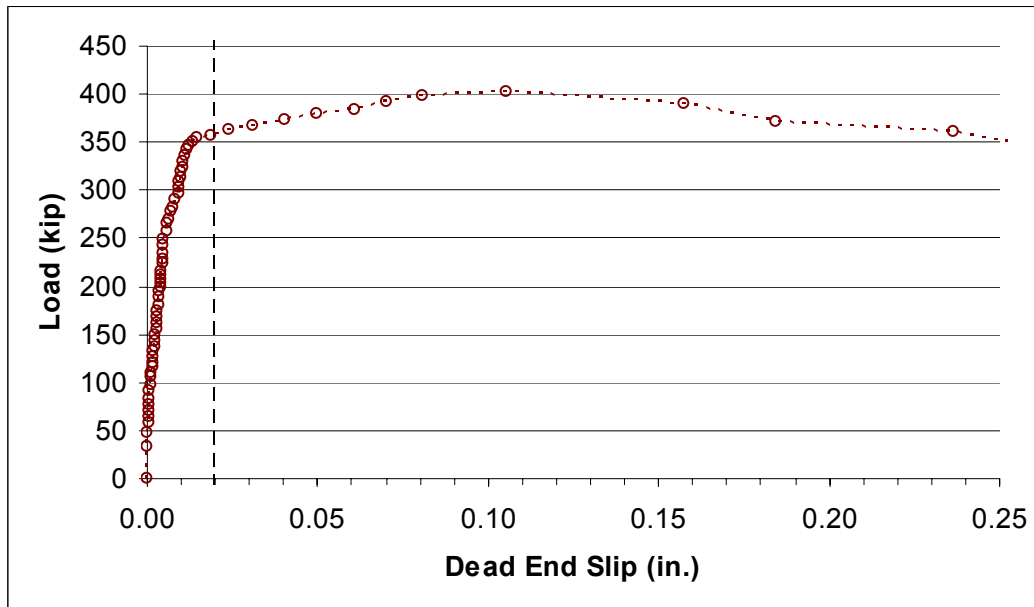
Figure 4-61 is the load vs. live end displacement and load vs. dead end slip plot for specimen 0-HD-10°-2. The figure indicates a peak load of 403 kip was achieved, at which point a pronounced reduction in resistance occurred. Figure 4-62 is the load vs. dead end slip plot for the specimen. It shows slip behavior at an amplified scale over a smaller range of displacement values. This highlights the slip behavior prior to and just after failure. The figure shows that significant slip occurred just prior to the peak load. The load at a dead end slip of 0.02 in. was 358 kip. The peak load was accompanied by a significant increase in the magnitude of dead end displacements. After reaching the maximum load, substantial displacement accumulated on both the live and dead ends. Failure occurred at the tendon-grout interface for this specimen. With continued displacement a significant fraction of the load carrying capacity was maintained. The maintenance of load carrying capacity was likely due to interlocking at the irregular interface between the tendon and the grout as the tendon moved through the specimen.

Significant cracking of the concrete occurred simultaneously with the peak load in the specimen. Figure 4-63 shows the specimen after testing with the dead end in the foreground. The figure shows the pattern of cracking observed, with splitting cracks spreading radially out from the duct. The crack seen in the top extended the entire length of the specimen, while a crack on the left side extended from the dead end about three quarters of the length of the specimen.





**Figure 4-61 Live End Load-Displacement and Dead End Load-Slip Response for Specimen 0-HD-10°-2**



**Figure 4-62 Dead End Load-Slip Response for Specimen 0-HD-10°-2, Amplified Scale**

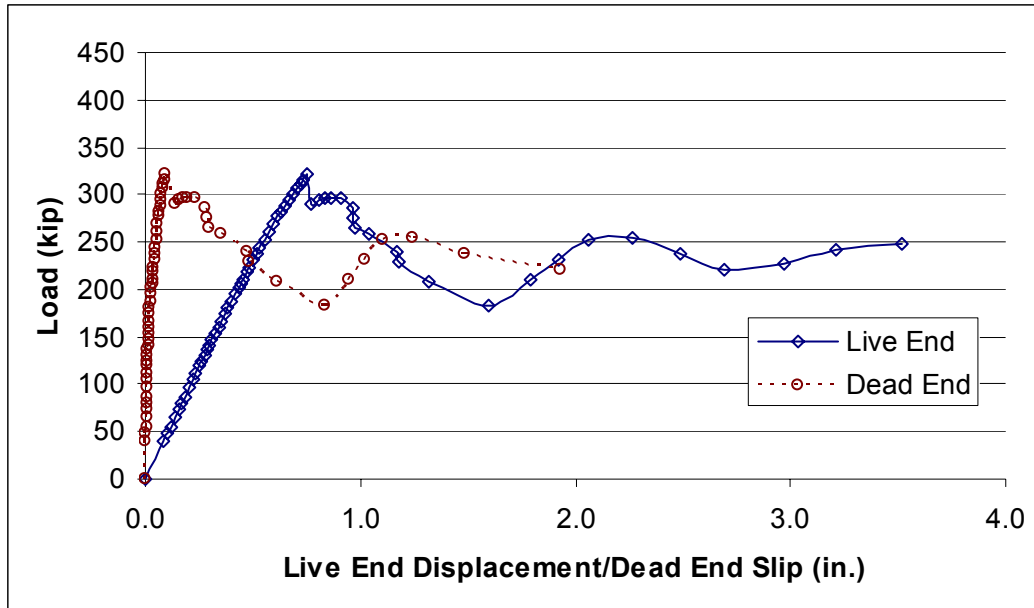


*Figure 4-63 Photo of Specimen 0-HD-10°-2 after Testing*

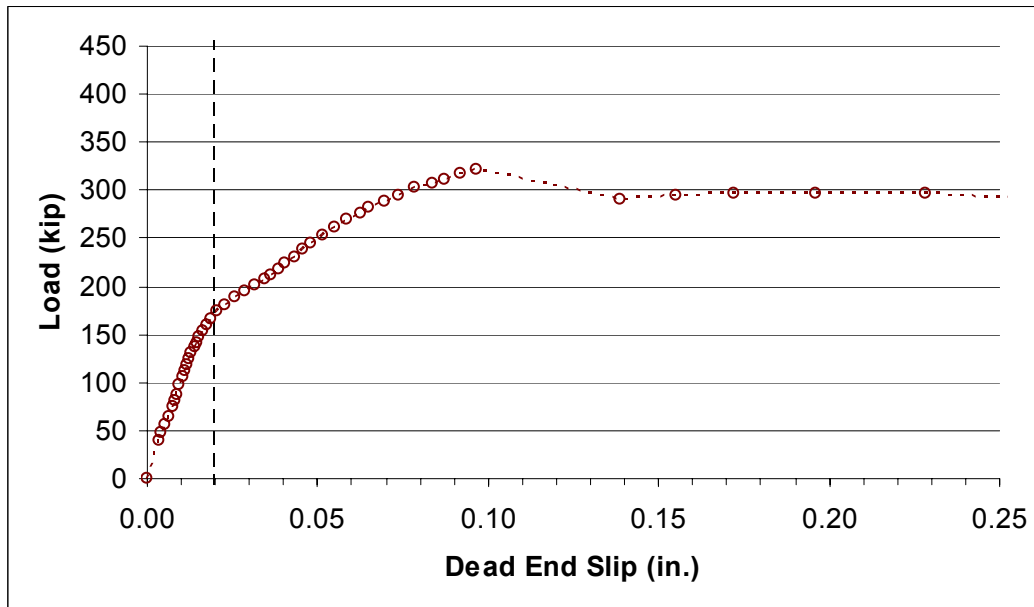
#### **4.2.3.5 0-HD-10°-3**

Figure 4-64 is the load vs. live end displacement and load vs. dead end slip plot for specimen 0-HD-10°-3. The figure indicates a peak load of 321 kip was achieved, at which point a pronounced reduction in resistance occurred. Figure 4-65 is the load vs. dead end slip plot for the specimen. It shows slip behavior at an amplified scale over a smaller range of displacement values. This highlights the slip behavior prior to and just after failure. The figure shows that significant slip occurred just prior to the peak load. The load at a dead end slip of 0.02 in. was 171 kip. The peak load was accompanied by a significant increase in the magnitude of dead end displacements. After reaching this load, substantial displacement accumulated on both the live and dead ends. Failure occurred at the tendon-grout interface for this specimen. With continued displacement a significant fraction of the load carrying capacity was maintained. The maintenance of load carrying capacity was likely due to interlocking at the irregular interface between the tendon and the grout as the tendon moved through the specimen.

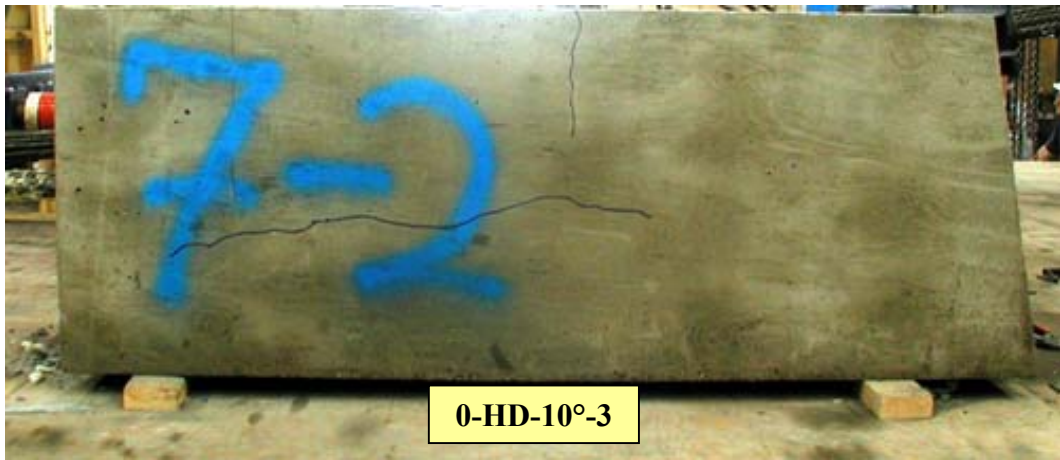
Significant cracking of the concrete occurred simultaneously with the maximum load in the specimen. Figure 4-66 shows a side view and Figure 4-67 shows a top view of the specimen after testing. In both photos, the dead end is on the right. The figures show that unlike most of the other specimens, the cracking was not initiated at the dead end. Rather, the cracking was initiated some distance away from the dead end and propagated toward the live end. As in the other uncoiled specimens, there were no splitting cracks observed on the face of the live end. This unusual behavior may have been caused by a void extending from the dead end some distance into the specimen which was a result of a leak during grouting. This void also likely explains the why the specimen failed at a reduced load as compared to its companion specimen, 0-HD-10°-2.



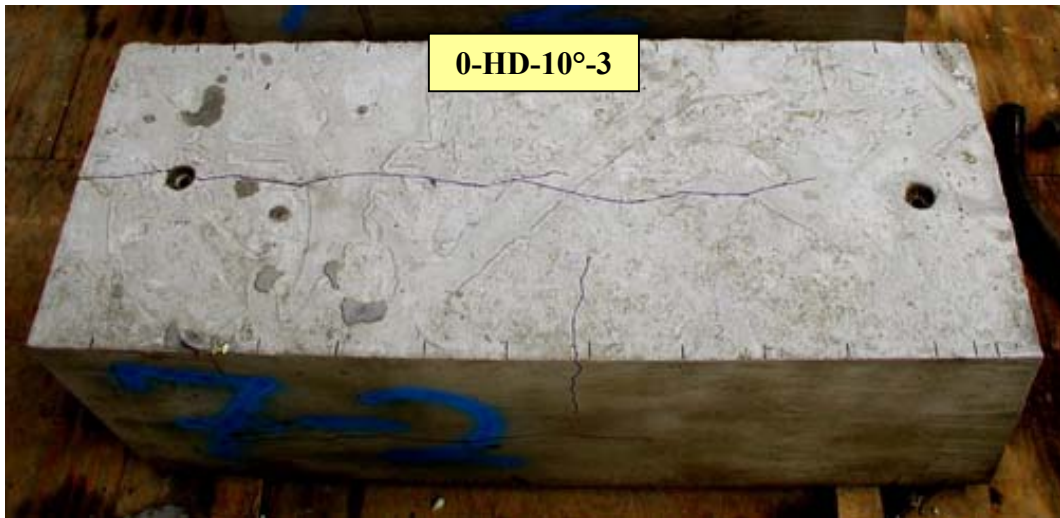
*Figure 4-64 Live End Load-Displacement and Dead End Load-Slip Response for Specimen 0-HD-10°-3*



*Figure 4-65 Dead End Load-Slip Response for Specimen 0-HD-10°-3, Amplified Scale*



*Figure 4-66 Side View of Specimen 0-HD-10°-3 after Testing*

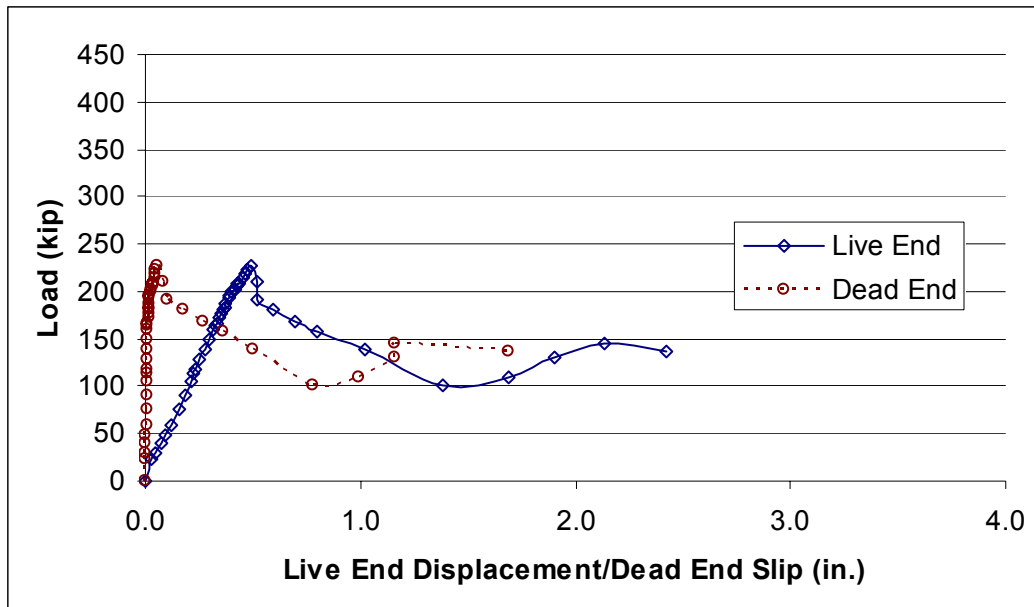


*Figure 4-67 Top View of Specimen 0-HD-10°-3 after Testing*

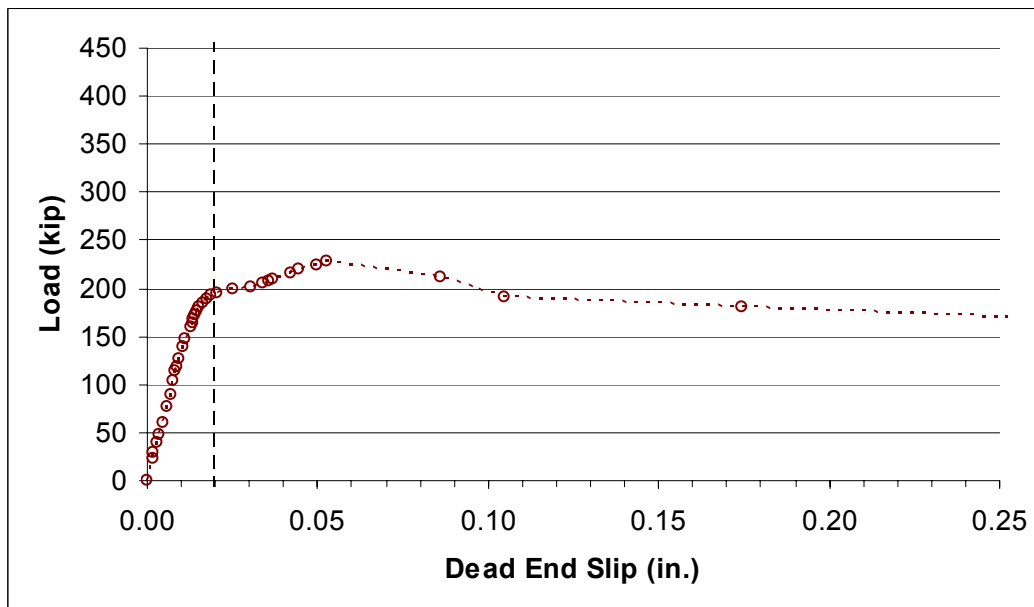
#### **4.2.3.6 0-HD-7.5°-1**

Figure 4-68 is the load vs. live end displacement and load vs. dead end slip plot for specimen 0-HD-7.5°-1. The figure indicates a peak load of 228 kip was achieved, at which point a pronounced reduction in resistance occurred. Figure 4-69 is the load vs. dead end slip plot for the specimen. It shows slip behavior at an amplified scale over a smaller range of displacement values. This highlights the slip behavior prior to and just after failure. The figure shows that significant slip occurred prior to the peak load. The load at a dead end slip of 0.02 in. was 195 kip. The peak load was accompanied by a significant increase in the magnitude of dead end displacements. After reaching the maximum load, substantial displacement accumulated on both the live and dead ends. Failure occurred at the tendon-grout interface for this specimen. With continued displacement a significant fraction of the load carrying capacity was maintained observed. The maintenance of load carrying capacity was likely due to interlocking at the irregular interface between the tendon and the grout as the tendon moved through the specimen.

Significant cracking of the concrete occurred simultaneously with the maximum load in the specimen. This specimen was one of two in the program which had less confining reinforcement than was typical. For this reason, the cracking observed in this specimen was wider than that observed in other cracked specimens with the standard transverse reinforcement spacing. A photograph of this specimen after testing was not available.



**Figure 4-68** *Live End Load-Displacement and Dead End Load-Slip Response for Specimen 0-HD-7.5°-1*



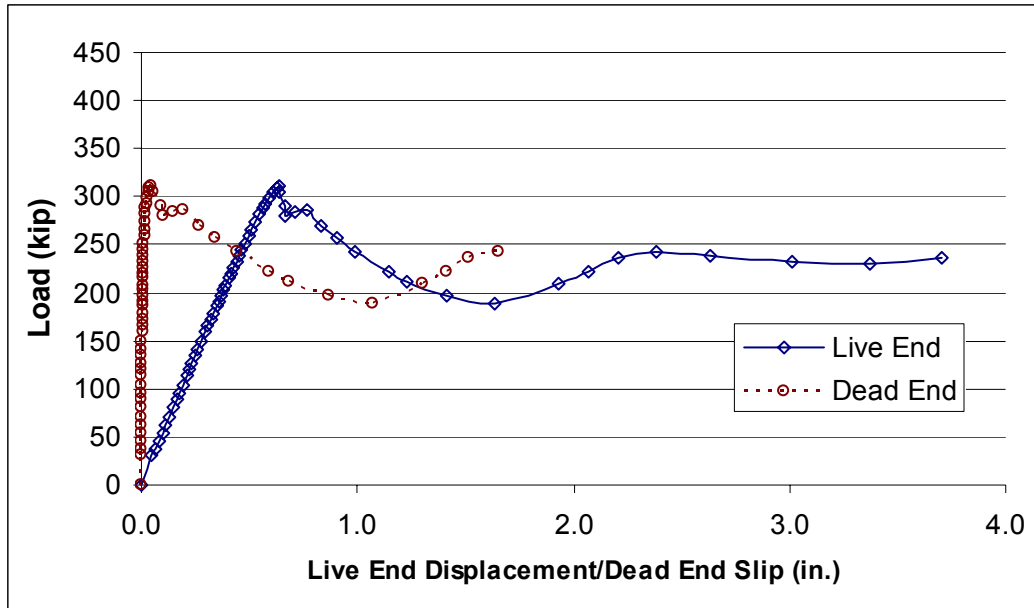
**Figure 4-69** *Dead End Load-Slip Response for Specimen 0-HD-7.5°-1, Amplified Scale*

#### **4.2.3.7 0-HD-7.5°-2**

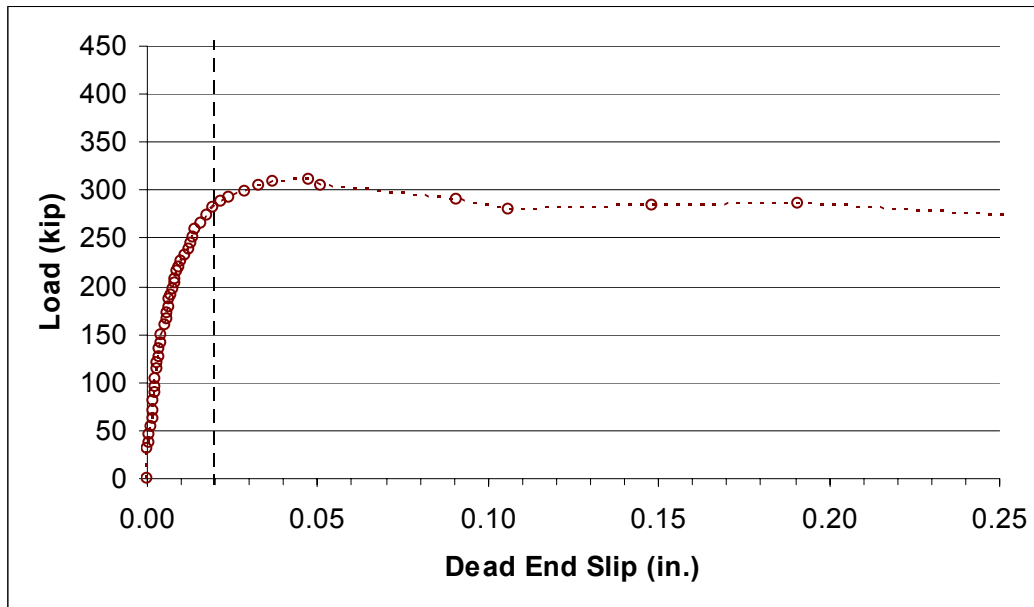
Figure 4-70 is the load vs. live end displacement and load vs. dead end slip plot for specimen 0-HD-7.5°-2. The figure indicates a peak load of 311 kip was achieved, at which point a pronounced reduction in resistance occurred. Figure 4-71 is the load vs. dead end slip plot for the specimen. It shows slip behavior at an amplified scale over a smaller range of displacement values. This highlights the slip behavior prior to and just after failure. The figure shows that significant slip occurred just prior to the peak load. The load at a dead end slip of 0.02 in. was 284 kip. The peak load was accompanied by a significant increase in the magnitude of dead end displacements. After reaching the peak load, substantial displacement accumulated on both the live and dead ends. Failure occurred at the tendon-grout interface for this specimen. With continued displacement a significant fraction of the load carrying capacity was maintained. The maintenance of load carrying capacity was likely due to interlocking at the irregular interface between the tendon and the grout as the tendon moved through the specimen.

Significant cracking of the concrete occurred simultaneously with the maximum load in the specimen. Figure 4-72 shows the dead end of the specimen after testing. The figure shows the pattern of cracking observed, with a splitting crack bisecting the cross-section vertically. The crack on the top extended the full length of the specimen.





**Figure 4-70 Live End Load-Displacement and Dead End Load-Slip Response for Specimen 0-HD-7.5°-2**



**Figure 4-71 Dead End Load-Slip Response for Specimen 0-HD-7.5°-2, Amplified Scale**

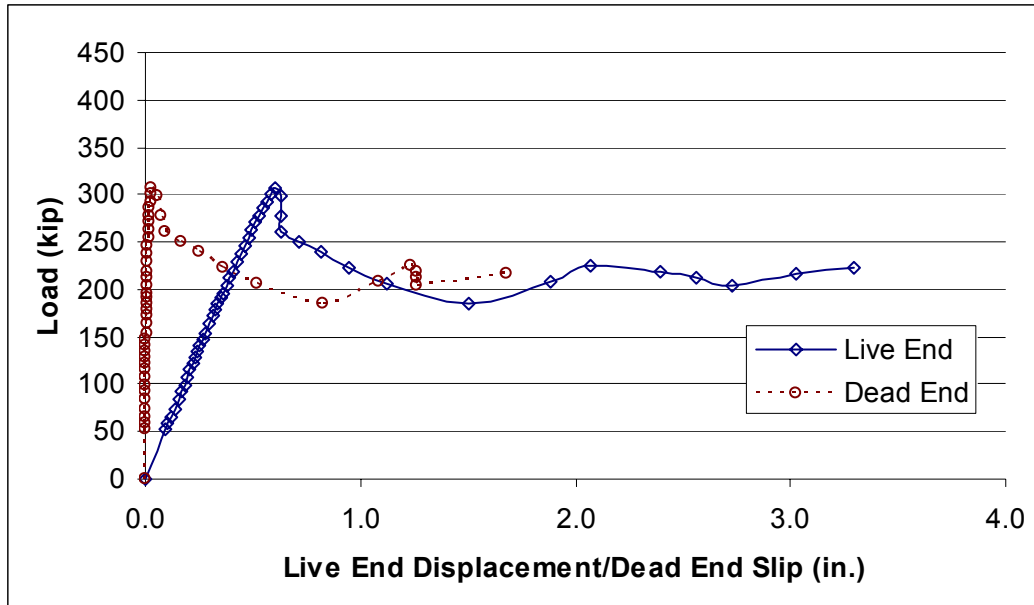


*Figure 4-72 Photo of Specimen 0-HD-7.5°-2 after Testing*

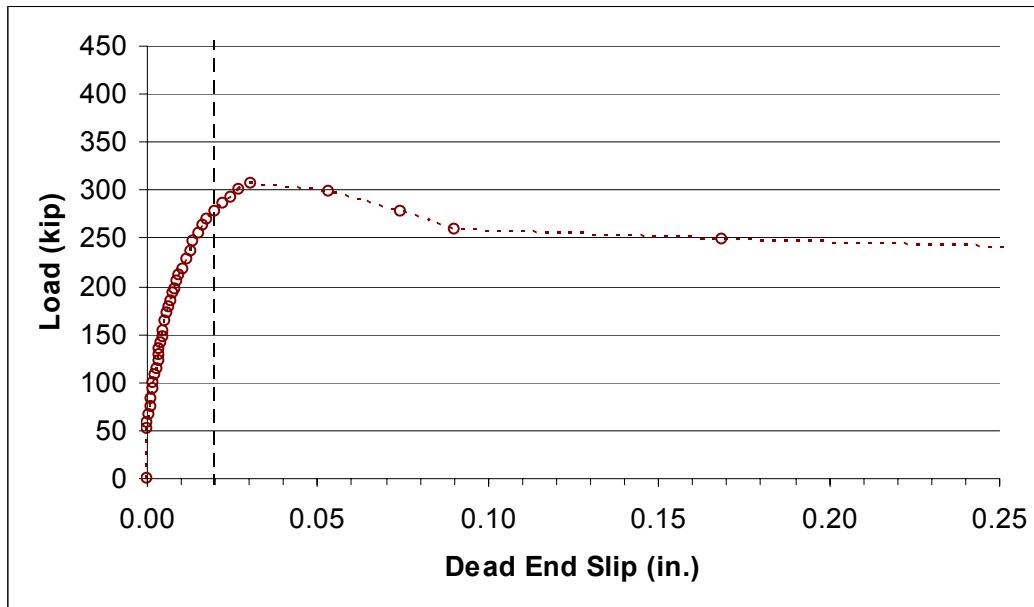
#### **4.2.3.8 0-HD-7.5°-3**

Figure 4-73 is the load vs. live end displacement and load vs. dead end slip plot for specimen 0-HD-7.5°-3. The figure indicates a peak load of 307 kip was achieved, at which point a pronounced reduction in resistance occurred. Figure 4-74 is the load vs. dead end slip plot for the specimen. It shows slip behavior at an amplified scale over a smaller range of displacement values. This highlights the slip behavior prior to and just after failure. The figure shows that significant slip occurred prior to the peak load. The load at a dead end slip of 0.02 in. was 279 kip. The peak load was accompanied by a significant increase in the magnitude of dead end displacements. After reaching the peak load, substantial displacement accumulated on both the live and dead ends. Failure occurred at the tendon-grout interface for this specimen. With continued displacement a significant fraction of the load carrying capacity was maintained. The maintenance of load carrying capacity was likely due to interlocking at the irregular interface between the tendon and the grout as the tendon moved through the specimen.

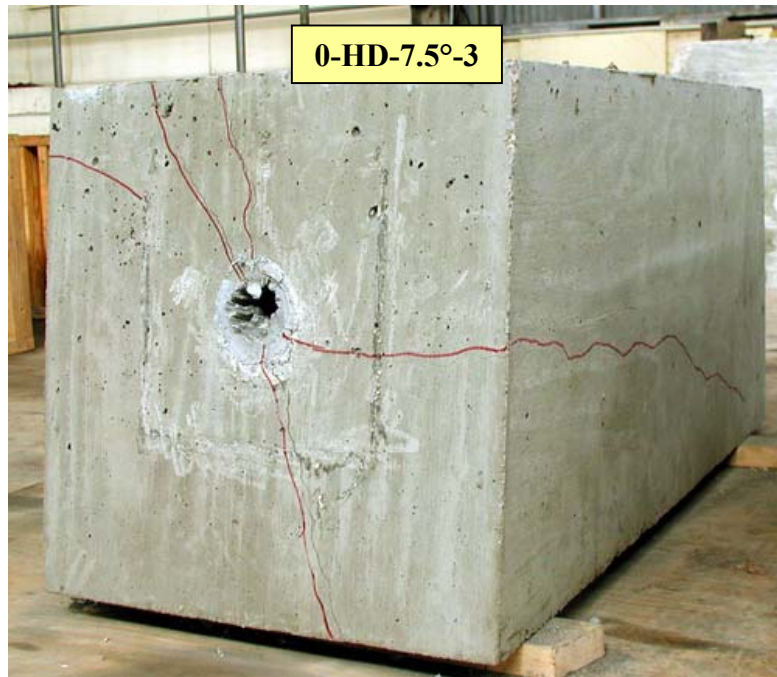
Significant cracking of the concrete occurred simultaneously with the maximum load in the specimen. Figure 4-75 and Figure 4-76 show the specimen after testing with the dead end in the foreground. The figures show the pattern of cracking observed, with splitting cracks spreading radially out from the duct. A crack in the top extended the entire length of the specimen, as did the crack on the left side of the specimen. A crack on the right side extended from the dead end nearly the entire length of the specimen.



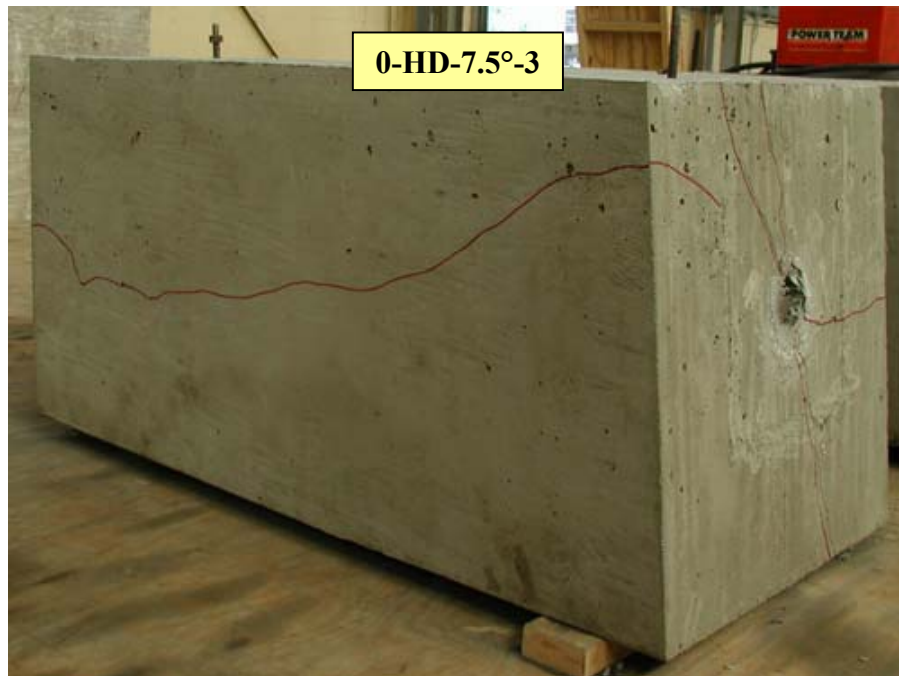
*Figure 4-73 Live End Load-Displacement and Dead End Load-Slip Response for Specimen 0-HD-7.5°-3*



*Figure 4-74 Dead End Load-Slip Response for Specimen 0-HD-7.5°-3, Amplified Scale*



*Figure 4-75 Photo of Specimen 0-HD-7.5°-3 after Testing*



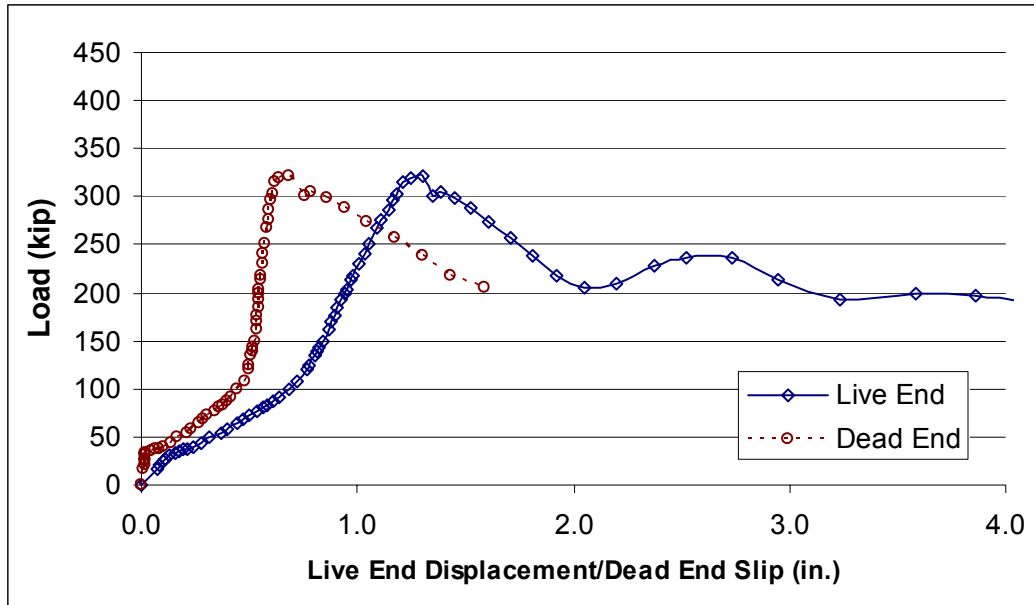
*Figure 4-76 Photo of Specimen 0-HD-7.5°-3 after Testing*

#### **4.2.3.9 1-HD-7.5°-1**

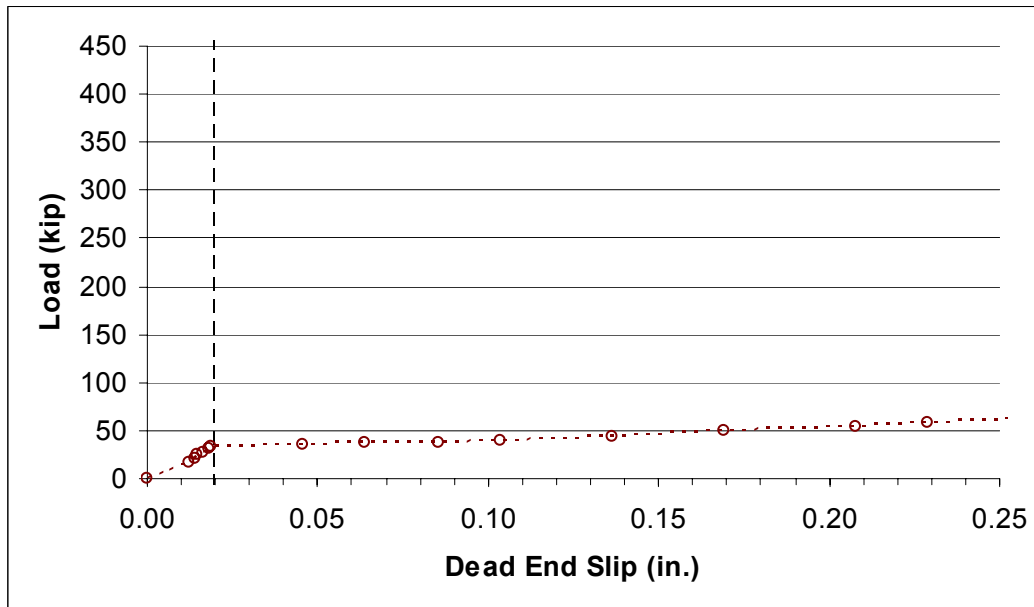
Figure 4-77 is the load vs. live end displacement and load vs. dead end slip plot for specimen 1-HD-7.5°-1. The figure indicates a peak load of 322 kip was achieved, at which point a pronounced reduction in resistance occurred. Figure 4-78 is the load vs. dead end slip plot for the specimen. It shows slip behavior at an amplified scale over a smaller range of displacement values. This highlights the slip behavior at low loads. The figure shows that significant slip occurred immediately upon the application of load. The load at a dead end slip of 0.02 in. was 34.2 kip. A peak load occurred after increased loading and was followed by an increase in the magnitude of dead end displacements. Failure occurred at the tendon-grout interface for this specimen. With continued displacement a fraction of the load carrying capacity was maintained. This behavior was likely due to interlocking at the irregular interface between the tendon and the grout.

This specimen and its companion, 1-HD-7.5°-2, exhibited behavior that was not observed in any of the other specimens. At a load between 100 and 150 kip, the stiffness of the load-displacement and load-slip plots changed and there was an increased resistance to pullout. The cause of this behavior is not entirely clear but one hypothesis is as follows. The oil destroyed the adhesion between the tendon and the grout and caused the tendon to move more freely than usual at low load levels. As significant displacements occurred, the irregular shape of the tendon became interlocked with the grout, and the resistance to pullout increased.

Significant cracking of the concrete occurred simultaneously with the peak load in the specimen. Figure 4-79 shows the specimen after testing with the dead end in the foreground. It illustrates the pattern of cracking observed in the specimen, with splitting cracks spreading radially out from the duct. The crack in the top extended the entire length of the specimen, while cracks on the sides extended from the dead end about three quarters of the length of the specimen.



**Figure 4-77** *Live End Load-Displacement and Dead End Load-Slip Response for Specimen 1-HD-7.5°-1*



**Figure 4-78** *Dead End Load-Slip Response for Specimen 1-HD-7.5°-1, Amplified Scale*



*Figure 4-79 Photo of Specimen 1-HD-7.5°-1 after Testing*

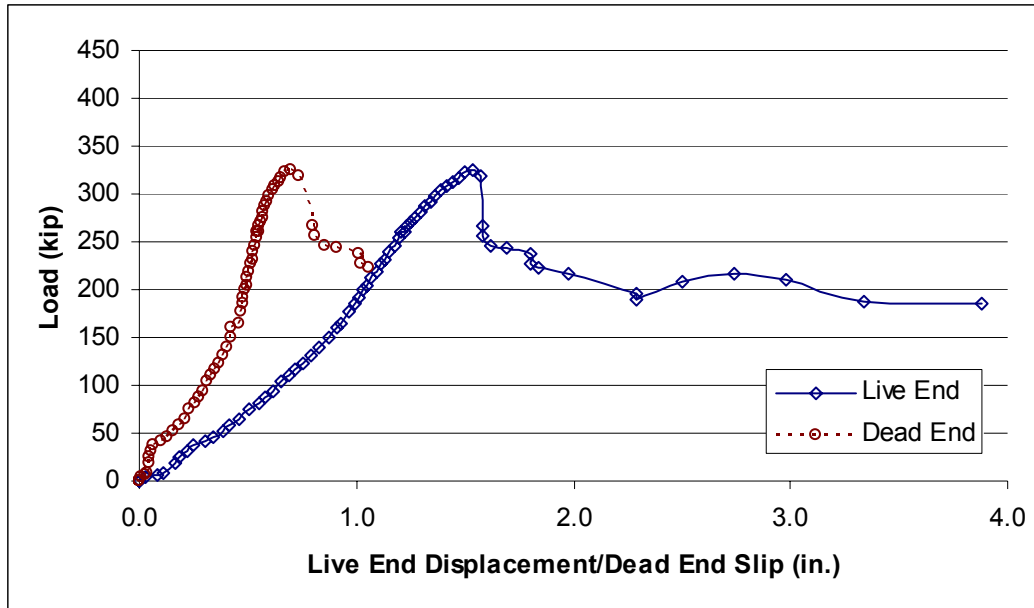


#### **4.2.3.10 1-HD-7.5°-2**

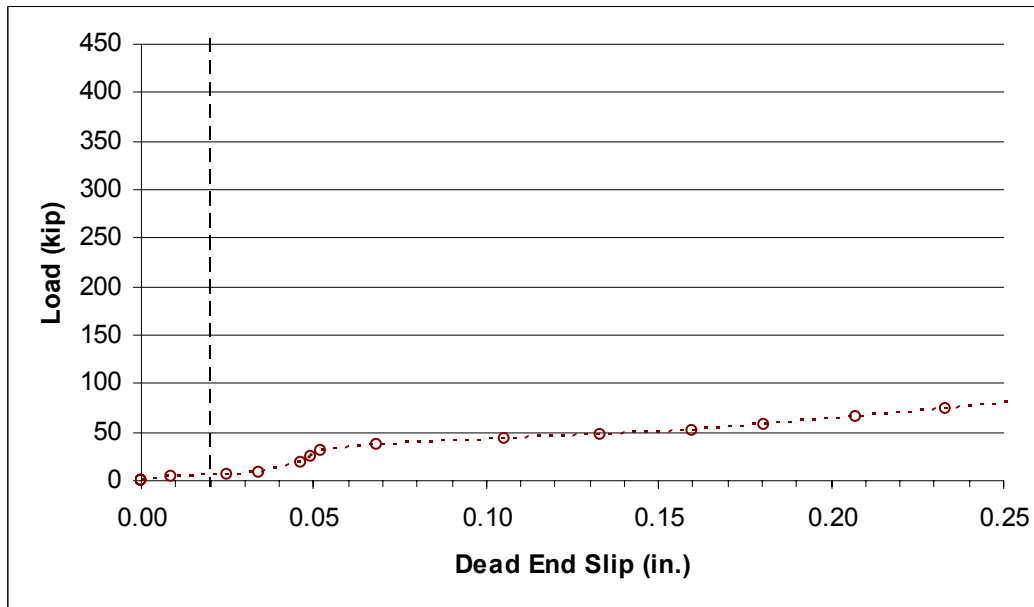
Figure 4-80 is the load vs. live end displacement and load vs. dead end slip plot for specimen 1-HD-7.5°-2. The figure indicates a peak load of 325 kip was achieved, at which point a pronounced reduction in resistance occurred. Figure 4-81 is the load vs. dead end slip plot for the specimen. It shows slip behavior at an amplified scale over a smaller range of displacement values. This highlights the slip behavior at low loads. The figure shows that significant slip occurred immediately with the application of load. The load at a dead end slip of 0.02 in. was 5.7 kip. A peak load occurred after increased loading and was followed by an increase in the magnitude of dead end displacements. Failure occurred at the tendon-grout interface for this specimen. With continued displacement a fraction of the load carrying capacity was maintained. This behavior was likely due to interlocking at the irregular interface between the tendon and the grout.

This specimen and its companion, 1-HD-7.5°-1, exhibited behavior that was not observed in any of the other specimens. At a load between 100 and 150 kip, the stiffness of the load-displacement and load-slip plots changed and there was an increased resistance to pullout. While this behavior was more pronounced in the companion specimen, it is also evident in this specimen. The cause of this behavior is not entirely clear, but may be explained by the hypothesis presented in the discussion of the companion specimen in Section 4.2.3.9.

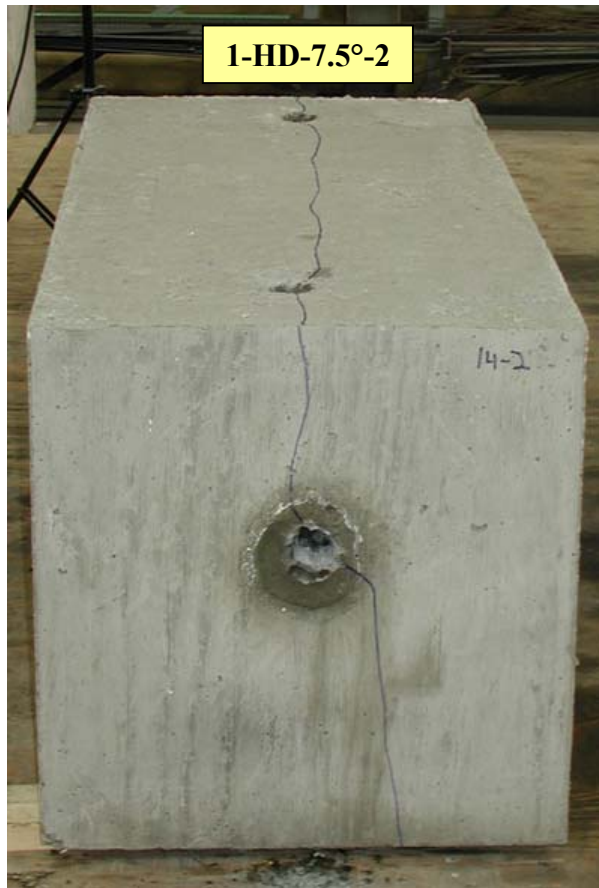
Significant cracking of the concrete occurred simultaneously with the maximum load in the specimen. Figure 4-82 shows the specimen after testing with the dead end in the foreground. The figure shows the pattern of cracking observed, with a single splitting crack vertically bisecting the specimen and extending its entire length.



**Figure 4-80 Live End Load-Displacement and Dead End Load-Slip Response for Specimen 1-HD-7.5°-2**



**Figure 4-81 Dead End Load-Slip Response for Specimen 1-HD-7.5°-2, Amplified Scale**



*Figure 4-82 Photo of Specimen 1-HD-7.5°-2 after Testing*

## CHAPTER 5

### Comparison of Behavior and Effect of Variables

#### 5.1 INTRODUCTION

This chapter will make comparisons to illustrate the effect of the variables discussed in Chapter 3 based on the data presented in Chapter 4.

##### 5.1.1 Modes of Failure

Two modes of failure were observed in this testing program. In the first, the resistance dropped suddenly following a peak load as the tendon or duct moved through the specimen. Most specimens clearly exhibited this type of behavior. The second mode of failure corresponded to a dead end slip of 0.02 in. Pullout testing of high-strength bars done by Ferguson et al. (1965) used a live end slip limitation as a failure criterion, realizing that excessive slip would lead to serviceability problems such as large crack widths. The ASTM A 981-97 standard for single strand pullout testing requires a limiting dead end slip of 0.01 in., while the North American Strand Producers Association has recommended a value of 0.1 in. (Salcedo 2003). A limiting value of 0.02 in. was selected for this program because the research team felt that it best represented the transition from linear to non-linear slip behavior in the unoiled specimens. Both peak load and critical dead end slip load values are reported in this chapter. When the mode of failure is not specifically identified, the load reported is the lowest failure load observed.

### 5.1.2 Summary of Data

Table 5-1, Table 5-2, and Table 5-3 are a summary of values reported in Chapter 4 as well as bond stresses calculated using those values. Specifically, the table includes the test specimen names, their observed failure mode and pullout load, the load at 0.02 in. of dead end slip, and various calculated bond stresses. Bond stresses are given at the tendon-grout interface, the duct-grout interface, and the duct-concrete interface. The table includes stresses computed using both the peak load and the load at 0.02 in. dead end slip. The tendon-grout bond stresses are calculated by dividing the failure load by the product of the bonded length and the equivalent tendon circumference. Duct-grout and concrete-duct bond stresses are calculated by dividing the failure load by the product of the bonded length and the inner or outer perimeter of the duct, respectively. The calculation of bond stresses is thoroughly outlined in Section 2.1.2.1. For specimens where the tendon was essentially fully developed, the load given is the maximum load resisted by the specimen. The shaded boxes indicate the bond stress which corresponds to the interface where peak load failure occurred.

*Table 5-1 Data Summary for Galvanized Steel Pipe Specimens*

Specimen Name Scheme 2	Peak Load Failure Interface	Bonded Length (in)	Peak Load (kips)	Load at 0.02 in. Slip (kips)	Maximum Bond Stress (ksi)			Bond Stress at 0.02 in. Slip (ksi)		
					Duct-Concrete	Grout-Duct	Tendon-Grout	Duct-Concrete	Grout-Duct	Tendon-Grout
0-SP-20°-1	Grout-Duct	126	138	NA	0.099	0.114	0.228	NA	NA	NA
0-SP-15°-1	Grout-Duct	94.2	118	NA	0.113	0.130	0.261	NA	NA	NA
0-SP-10°-1	Grout-Duct	62.8	57.2	NA	0.082	0.095	0.190	NA	NA	NA
0-SP-10°-2	Grout-Duct	62.8	44.6	NA	0.064	0.074	0.148	NA	NA	NA
0-SP-7.5°-1	Duct-Concrete	44.0	67.1	NA	0.138	0.159	0.318	NA	NA	NA
0-SP-7.5°-2	Duct-Concrete	44.0	89.1	NA	0.183	0.211	0.422	NA	NA	NA
1-SP-7.5°-1	Multiple	44.0	39.3	4.1	0.081	0.093	0.186	0.008	0.010	0.019
1-SP-7.5°-2	Grout-Duct	44.0	32.9	4.1	0.067	0.078	0.156	0.008	0.010	0.020

**Table 5-2 Data Summary for Galvanized Metal Duct Specimens**

Specimen Name Scheme 2	Peak Load Failure Interface	Bonded Length (in)	Peak Load (kips)	Load at 0.02 in. Slip (kips)	Maximum Bond Stress (ksi)			Bond Stress at 0.02 in. Slip (ksi)		
					Duct-Concrete	Grout-Duct	Tendon-Grout	Duct-Concrete	Grout-Duct	Tendon-Grout
0-GD-20°-1	No Pullout	126	400	NA	0.286	0.330	0.661	NA	NA	NA
0-GD-15°-1	No Pullout	94.2	400	NA	0.383	0.442	0.885	NA	NA	NA
0-GD-10°-1	No Pullout	62.8	438	NA	0.629	0.726	1.453	NA	NA	NA
0-GD-10°-2	No Pullout	62.8	436	NA	0.626	0.722	1.446	NA	NA	NA
0-GD-7.5°-1	Tendon-Grout	44.0	382	302	0.783	0.903	1.809	0.619	0.714	1.430
0-GD-7.5°-2	Tendon-Grout	44.0	345	274	0.707	0.816	1.634	0.562	0.648	1.297
0-GD-7.5°-3	Tendon-Grout	44.0	360	304	0.738	0.851	1.705	0.623	0.719	1.439
0-GD-5°-1	Tendon-Grout	31.4	257	202	0.738	0.851	1.705	0.580	0.669	1.340
1-GD-7.5°-1	No Pullout	44.0	434	74.4	0.889	1.026	2.055	0.152	0.176	0.352
1-GD-7.5°-2	No Pullout	44.0	437	48.1	0.896	1.033	2.069	0.099	0.114	0.228

**Table 5-3 Data Summary for HDPE Duct Specimens**

Specimen Name Scheme 2	Peak Load Failure Interface	Bonded Length (in)	Peak Load (kips)	Load at 0.02 in. Slip (kips)	Maximum Bond Stress (ksi)			Bond Stress at 0.02 in. Slip (ksi)		
					Duct-Concrete	Grout-Duct	Tendon-Grout	Duct-Concrete	Grout-Duct	Tendon-Grout
0-HD-20°-1	No Pullout	126	400	NA	0.286	0.330	0.661	NA	NA	NA
0-HD-15°-1	No Pullout	94.2	400	NA	0.383	0.442	0.885	NA	NA	NA
0-HD-10°-1	Tendon-Grout	62.8	355	NA	0.510	0.588	1.178	NA	NA	NA
0-HD-10°-2	Tendon-Grout	62.8	403	358	0.579	0.668	1.337	0.514	0.593	1.188
0-HD-10°-3 <sup>†</sup>	Tendon-Grout	62.8	321	171	0.461	0.532	1.065	0.246	0.283	0.567
0-HD-7.5°-1	Tendon-Grout	44.0	228	195	0.467	0.539	1.080	0.400	0.461	0.923
0-HD-7.5°-2	Tendon-Grout	44.0	311	284	0.637	0.735	1.473	0.582	0.671	1.345
0-HD-7.5°-3	Tendon-Grout	44.0	307	279	0.629	0.726	1.454	0.572	0.660	1.321
1-HD-7.5°-1	Tendon-Grout	44.0	322	34.2	0.660	0.761	1.525	0.070	0.081	0.162
1-HD-7.5°-2	Tendon-Grout	44.0	325	5.69	0.666	0.768	1.539	0.012	0.013	0.027

<sup>†</sup> Data from this specimen is not used in this chapter due its incomplete grouting



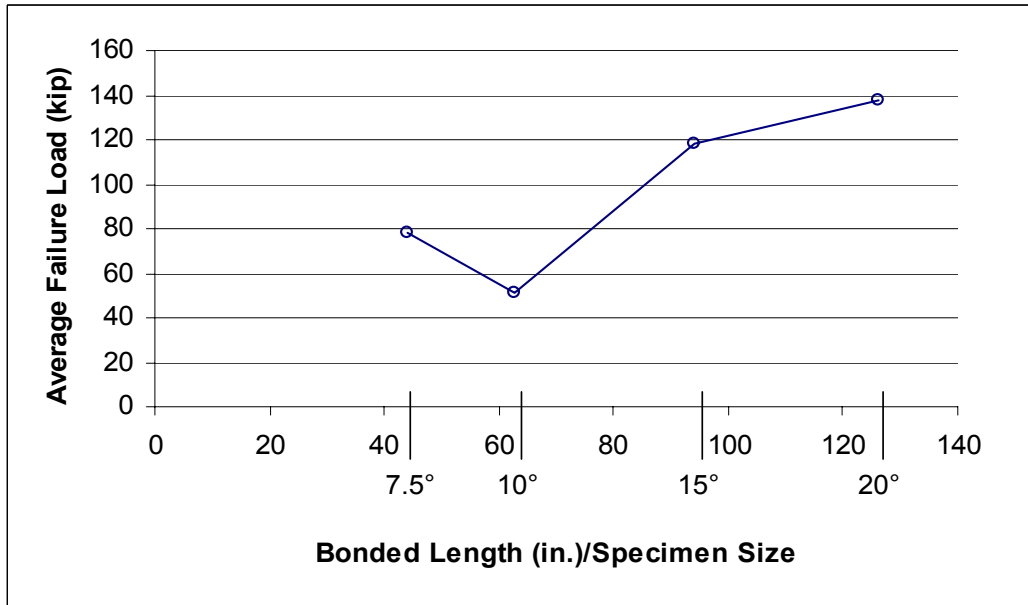
## **5.2 COMPARISONS WITHIN DUCT TYPES**

In this section each duct type will be considered independently, and observations will be made based on the behavior of different uncoiled specimens with the same duct type. The effect of the oil will be evaluated in Section 5.4.

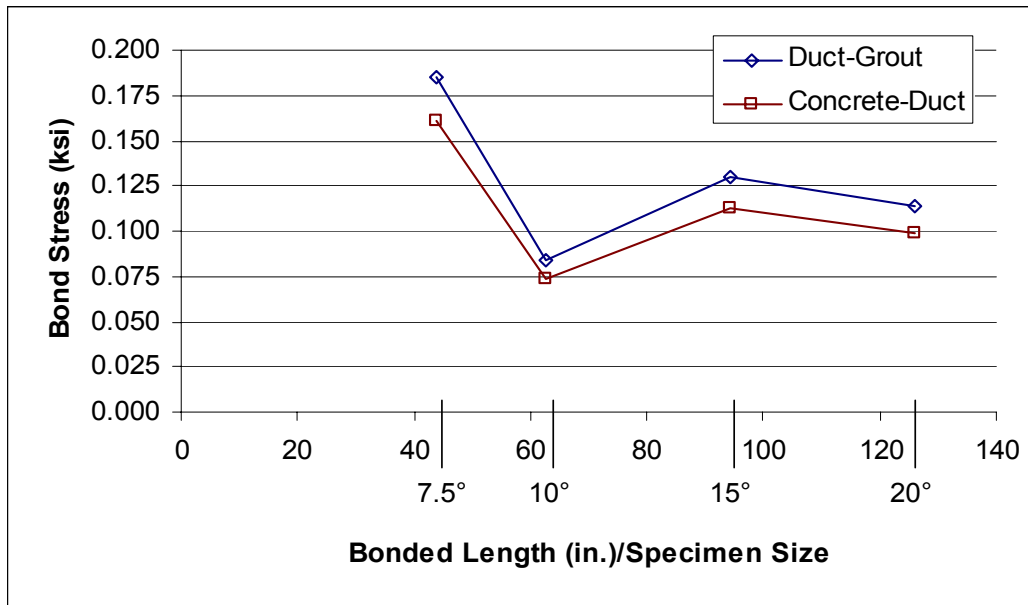
### **5.2.1 Galvanized Steel Pipe Specimens**

Failure was achieved in galvanized pipe specimens with deviations of 20°, 15°, 10°, and 7.5° (bonded lengths of 126 in., 94.2 in., 62.8 in., and 44.0 in., respectively). There were two specimens each of the 10° and 7.5° sizes. Since all galvanized steel pipe specimens experienced peak load failure at only a fraction of the ultimate tensile capacity of the tendon, it can be concluded that the development length for a 12 strand tendon in a nominal 3-in. galvanized steel pipe is much greater than 126 in.

Figure 5-1 is a plot of the failure load vs. bonded length for the galvanized steel pipe specimens. Each point on the plot represents the average load from all uncoiled specimens of the corresponding bonded length. All of the specimens except the 7.5° specimens failed at the duct-grout interface. The 7.5° specimens both failed at the concrete-duct interface. All galvanized steel pipe specimens failed suddenly with very low levels of dead end slip. Figure 5-2 is a plot of bond stress vs. bonded length for the galvanized steel pipe specimens. Each point on the plot represents the average bond stress from all uncoiled specimens of the corresponding bonded length. Both duct-grout and concrete-duct bond stresses are plotted.



*Figure 5-1 Failure Load vs. Bonded Length for Galvanized Pipe Specimens*



*Figure 5-2 Bond Stress vs. Bonded Length for Galvanized Pipe Specimens*

The results from the 7.5° specimens do not fit the trend of the other data. It would be expected that pullout load would decrease with bonded length, and that the bond stress at failure would be somewhat consistent regardless of length. In the 20°, 15°, and 10° specimens, the failure at the duct-grout interface occurred at bond stresses ranging from 0.084 to 0.130 ksi. The 7.5° specimens reached a significantly higher bond stress of 0.185 ksi at the duct-grout interface before failing at the concrete-grout interface. Since both specimens were fabricated from sections of the same pipe, the inner surface of the duct in both specimens may have been inconsistent with other tests. Prior to installing the tendon in these specimens, small chunks of residual galvanizing material were removed from the inside of these pipes. These two specimens will likely be retested before the conclusion of this research project to clear up this inconsistency.

#### ***5.2.1.1 Comparison with Previous Results***

These specimens failed at the interface which would have been expected based on some of the results from previous research done by Braverman (1985), Osborne (1986), and Radloff (1990). In this program, the ratio of tendon steel area to duct cross-sectional area for all specimens was 25%. This ratio is in the range where failures at the duct-grout interface have been observed in straight duct specimens. Radloff, however, tested curved ducts with a similar area ratio and observed failure at the tendon-grout interface.

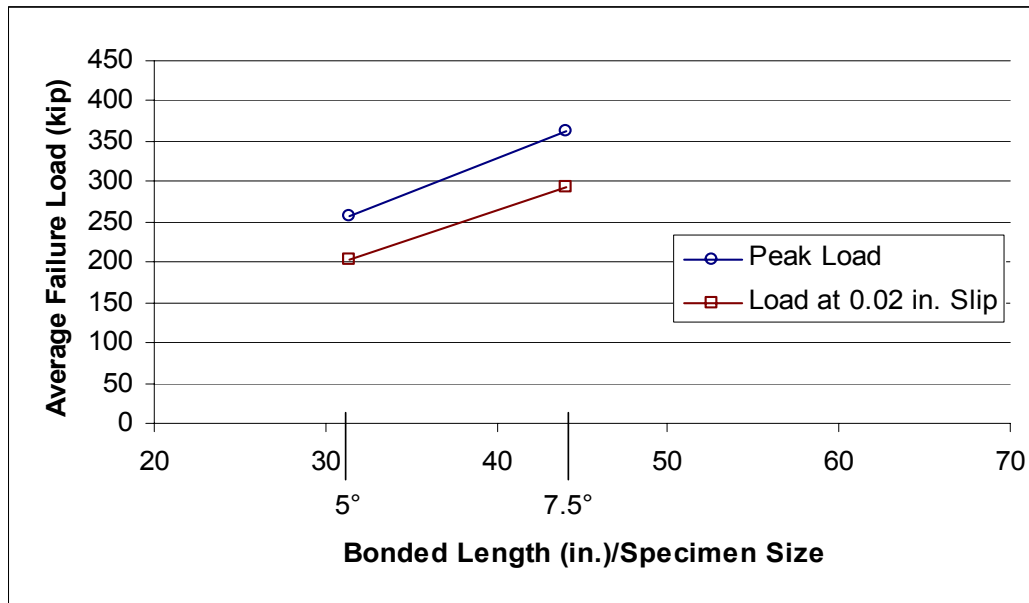
The bond stresses observed in this research program are significantly lower than those reported by Radloff for straight galvanized pipe specimens failing at the grout-duct interface. Radloff tested the same size tendon in a similar diameter steel pipe and reported a bond stress at failure on the grout-duct interface of 0.28 ksi. This research program has observed values as low as 0.084 ksi. While the specimens tested by Radloff were similar to specimens in this program,

the testing procedure employed by Radloff was significantly different than that used in this program. The test procedure employed by Radloff involved stressing the tendon to 50% of its tensile capacity and then grouting it. After the grout had cured, the tendon was slowly released. The force differential between the two ends of the specimen and the displacement of the tendon was recorded. The force differential across the specimen when the tendon began to slip was considered the ultimate load. This procedure varies significantly from a standard pullout test. In Radloff's test method, the Hoyer effect (Section 2.1) would tend to increase the bond capacity of the tendon. In a pullout test, however, the effect would tend to reduce the bond capacity since the diameter of the strands would tend to decrease rather than increase according to Poisson's ratio. The difference in testing procedures may explain the difference in bond stresses from the two programs.

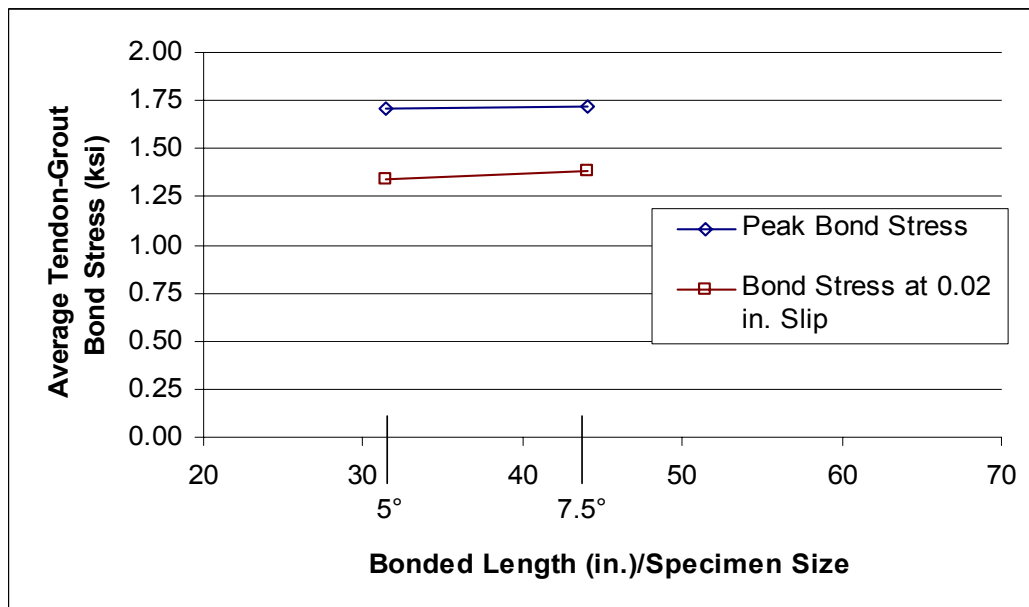
### **5.2.2 Galvanized Metal Duct Specimens**

Failure was achieved in galvanized metal duct specimens with deviations of 7.5° and 5° (bonded lengths of 44.0 in. and 31.4 in., respectively). Three 7.5° specimens were tested and one 5° specimen was tested. For this test procedure, it can be concluded that the development length for a 12-strand tendon in a corrugated galvanized metal duct is less than or equal to 62.8 in., since all specimens of that length or longer were essentially fully developed.

Figure 5-3 shows the failure loads for the different bonded lengths of galvanized metal duct specimens and Figure 5-4 shows the corresponding bond stresses at the tendon-grout interface. The results plotted in the figures include data from both failure modes. When more than one specimen of a bonded length was tested, the value plotted is the average of all tests. The loads corresponding to the dead end slip failure mode were roughly 20% lower than those corresponding to the peak failure mode.



**Figure 5-3 Failure Load vs. Bonded Length for Galvanized Metal Duct Specimens**



**Figure 5-4 Tendon-Grout Bond Stress vs. Bonded Length for Galvanized Metal Duct Specimens**

The figures show behavior that would be expected. The shorter bonded length had a lower ultimate load, while both bonded lengths had similar maximum bond stresses.

The peak load failures observed in the galvanized metal duct specimens were controlled by splitting of the concrete. Splitting cracks appeared in all specimens as the peak load was reached. The fact that the splitting cracks propagated from the dead end toward the live end, and did not always reach the face of the live end, indicates that the hydraulic ram likely provided a confining effect as it reacted against the specimen.

#### ***5.2.2.1 Comparison with Previous Results***

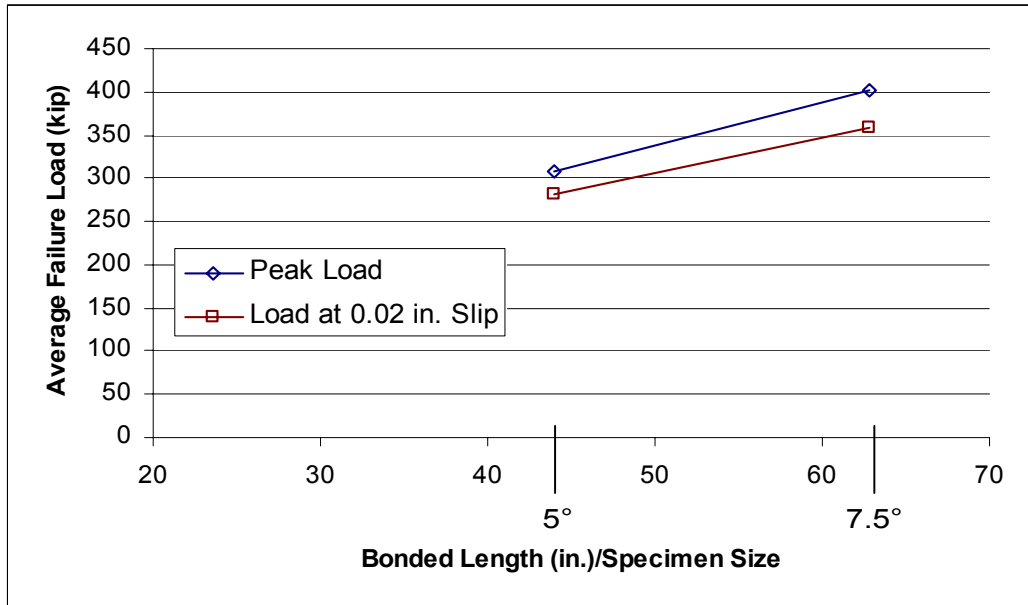
The results of the uncoiled galvanized metal duct tests are in good agreement with previous research by Trost et al (1978, 1980) with respect to the failure interface. The bond stresses achieved in this testing program are, however, about 24% higher than those reported for Trost's tests of tendons located against the duct wall. The bond stresses are also significantly higher than those reported by Braverman (1985) and Radloff (1990) for galvanized pipe specimens failing at the tendon-grout interface. It is possible that the confining effect provided by the hydraulic ram resulted in peak loads which were artificially high.

#### **5.2.3 High Density Polyethylene Duct Specimens**

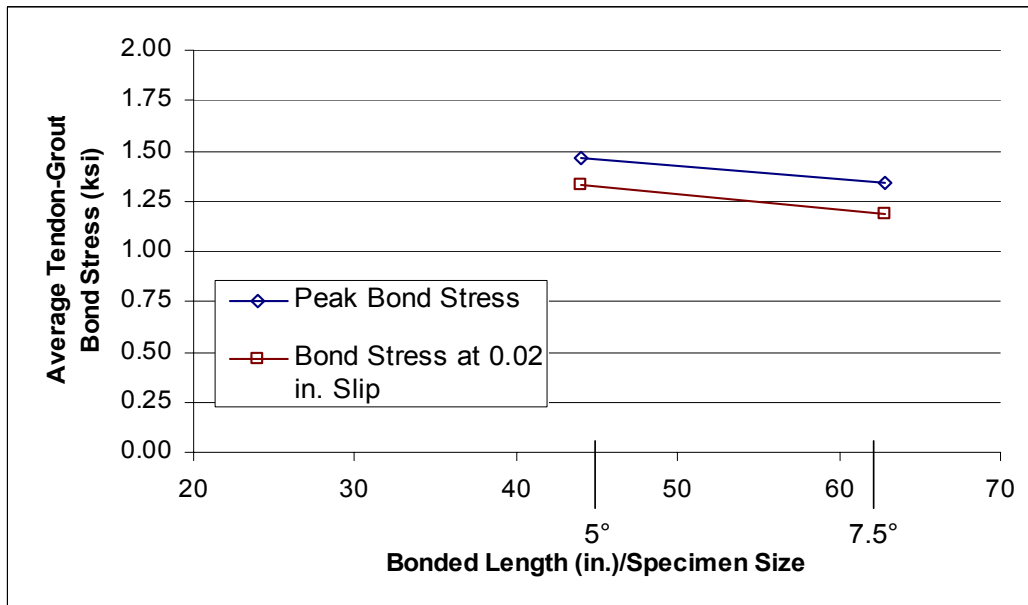
Failure was achieved in high density polyethylene duct specimens deviations of 10° and 7.5° (bonded lengths of 62.8 in. and 44.0 in., respectively). Testing was performed on specimens with two different transverse reinforcement spacings. For specimens with the standard transverse reinforcement spacing and this testing procedure, it can be concluded that the development length for a 12-strand tendon in an HDPE duct is less than or equal to 94.2 in., because all specimens of that length or longer were essentially fully developed.

Figure 5-5 shows the average pullout load for the two bonded lengths and Figure 5-6 shows the average bond stresses at the tendon-grout interface at failure for the two bonded lengths. The results plotted in the figures include both modes of failure. When more than one uncoiled specimen of a certain bonded length was tested, the value plotted is the average for all tests. The loads corresponding to the dead end slip failure mode were roughly 10% lower than those corresponding to the peak failure mode. The figures, which include data only from specimens with the standard transverse reinforcement spacing, indicate behavior that would be expected. The shorter bonded length had a lower ultimate load, while both bonded lengths exhibited similar ultimate bond stresses.

Just as the peak load failures of the galvanized metal duct specimens were controlled by splitting of the concrete, so were the failures of the HDPE duct specimens. Splitting cracks appeared in all specimens just as the peak load occurred and resistance was lost. This behavior suggests that confinement would play a role in peak load capacity. As with the galvanized metal duct specimens, the fact that the splitting cracks propagated from the dead end toward the live end, and did not always reach the face of the live end, indicates that the hydraulic ram likely provided a confining effect as it reacted against the specimen.



*Figure 5-5 Failure Load vs. Bonded Length for HDPE Duct Specimens*

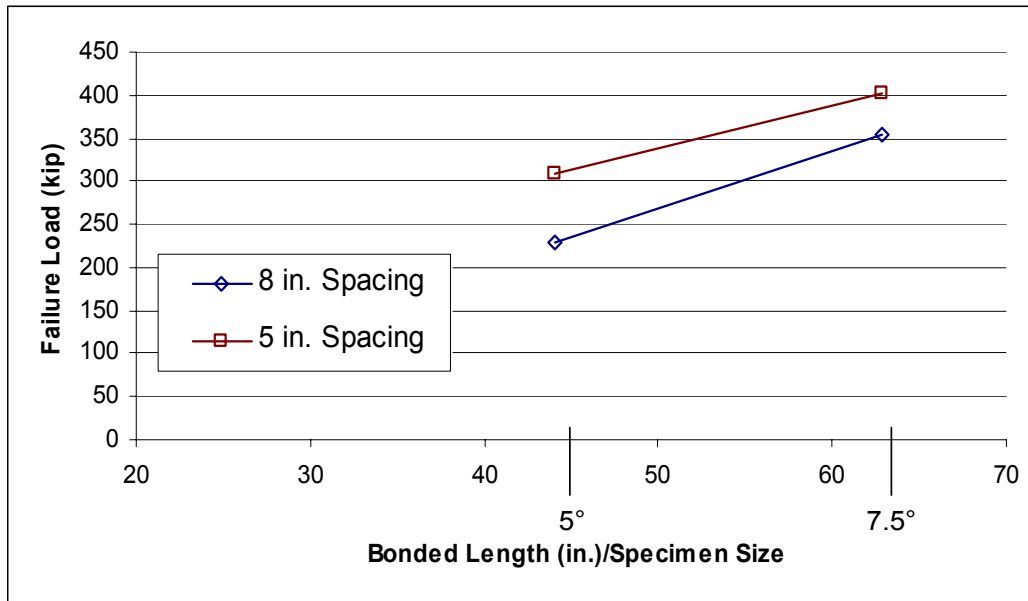


*Figure 5-6 Tendon-Grout Bond Stress vs. Bonded Length for HDPE Duct Specimens*

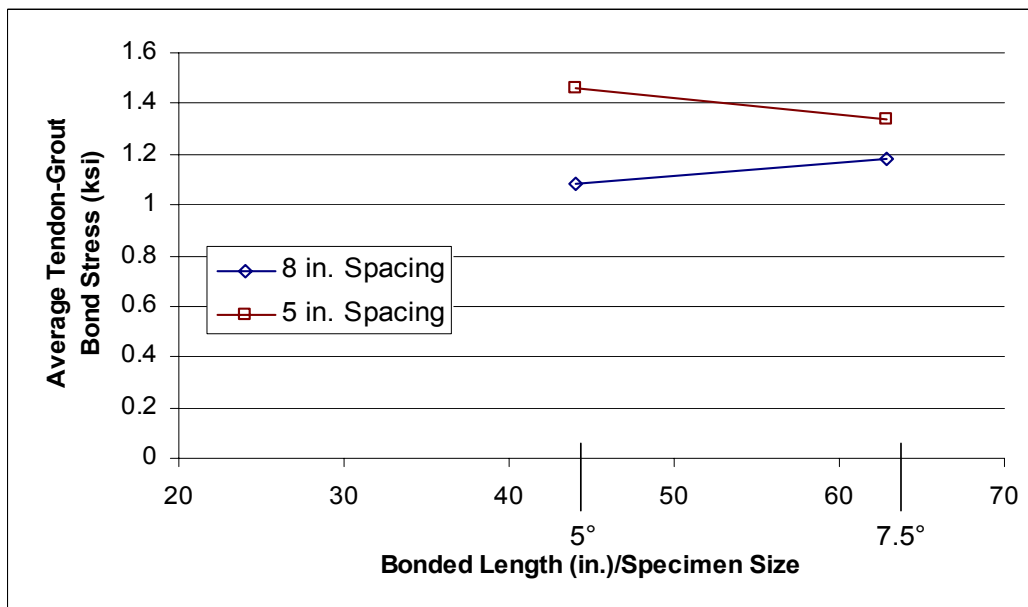


Since two different transverse reinforcement spacings were tested, some conclusions can be drawn with regard to the effect of confinement. Figure 5-7 shows the peak loads for the different combinations of bonded length and transverse reinforcement spacing that were tested. The figure indicates the peak load for more lightly reinforced specimens was lower. Figure 5-8 gives the bond stresses corresponding to the peak loads. While all specimens exhibited similar patterns of splitting cracking, the specimens with less transverse reinforcement developed significantly wider cracks. Additionally, observation of the load-slip curves from each specimen in Chapter 4 shows that specimens with more confinement tended to maintain a higher percentage of their ultimate load after a peak load failure had occurred.

Since the number of specimens was very limited, quantitative assessments of the effect of confinement cannot be drawn, but it appears as though confinement does play a role in the bond of post-tensioning tendons. Certainly the fact that splitting controlled the peak failure of the specimens confirms the effect evidenced in the figures.



**Figure 5-7 Peak Failure Load vs. Bonded Length for Different Transverse Reinforcement Spacings**



**Figure 5-8 Tendon-Grout Bond Stress vs. Bonded Length for Different Transverse Reinforcement Spacings**

### 5.3 COMPARISONS AMONG DUCT TYPES

Since 7.5° (44.0 in. bonded length) specimens were successfully tested for all duct types, the effect of duct type on bond capacity can be assessed. At this point only uncoiled specimens will be compared; an oiled specimen discussion is included in Section 5.4. Figure 5-9 summarizes the average pullout loads for these specimens. The figure includes failure loads for both modes. Since multiple specimens of each type were tested, average values are reported. The galvanized steel pipe specimens failed by peak load at less than 0.02 in. dead end slip. The values included in the plot for failure of galvanized steel pipe specimens according to the dead end slip criterion are peak load failure values, and are included for reference only.



*Figure 5-9 Average Failure Loads for 7.5° Specimens with Different Duct Types*

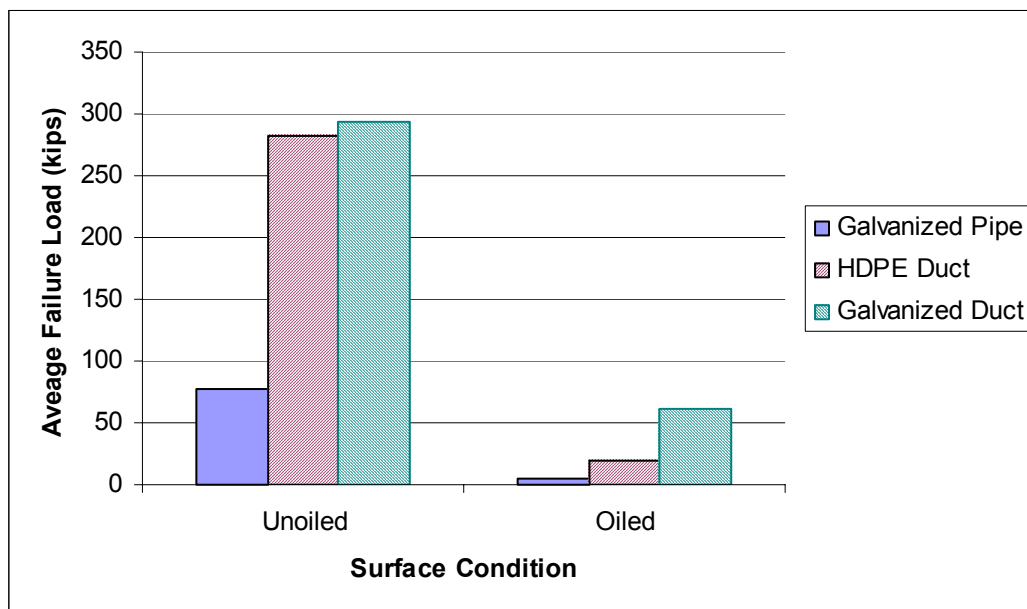
The failure interface in the galvanized steel pipe specimens resulted in very poor performance compared with the galvanized metal and HDPE duct specimens. The failure loads for galvanized steel pipe specimens were more than 70% lower than loads observed in specimens with the other duct types. The average galvanized steel pipe specimen failure load displayed in the figure corresponds to the irregular concrete-duct failure that is under further investigation. It is therefore possible that the failure loads could be even lower, as would be expected based on the trend discussed in Section 5.2.1. The literature suggests that behavior of galvanized steel pipe specimens could be improved to the level of the corrugated duct specimens by using a larger diameter steel pipe and correspondingly lower tendon steel area to duct cross-sectional area ratio. However, using a larger pipe would not be consistent with current post-tensioning practice, as the size tested in this program is typical for a 12-strand tendon with ½-in. strands.

The figure indicates that the galvanized metal duct performed somewhat better than the HDPE duct when compared based on the peak load criterion, as it provided a 17% increase in failure load. Improved bond performance is also evidenced by the fact that the 10° specimen (62.8 in. bonded length) essentially developed the tensile capacity of the tendon in the galvanized metal duct specimens but did not develop the tensile capacity of the tendon in the HDPE duct specimens. Examining the load-displacement plots for the two duct materials reveals that the galvanized metal duct specimens tended to maintain a higher percentage of their load after a peak load failure than the HDPE duct specimens. While post-slip behavior is not particularly important, maintenance of higher loads is desirable. The improved peak load and post-peak performance of the galvanized metal duct specimens may be due to confinement provided by the galvanized steel duct material.

When comparing the two duct types on a the dead end slip failure mode basis, the galvanized metal duct provided less improvement over the HDPE duct, offering a mere 4% increase in capacity. This indicates that while galvanized metal duct provides better peak load performance, each duct would provide similar service-level performance.

#### 5.4 COMPARISONS BETWEEN OILED AND UNOILED SPECIMENS

All specimens treated with Citgo Trukut NC 205 emulsifiable oil failed according to the dead end slip mode. Each specimen exhibited significant dead end slip at very low load levels. Figure 5-10 shows the average minimum failure loads for oiled and unoiled specimens of each duct type. The values reported in the figure correspond to the minimum failure load of the two modes.



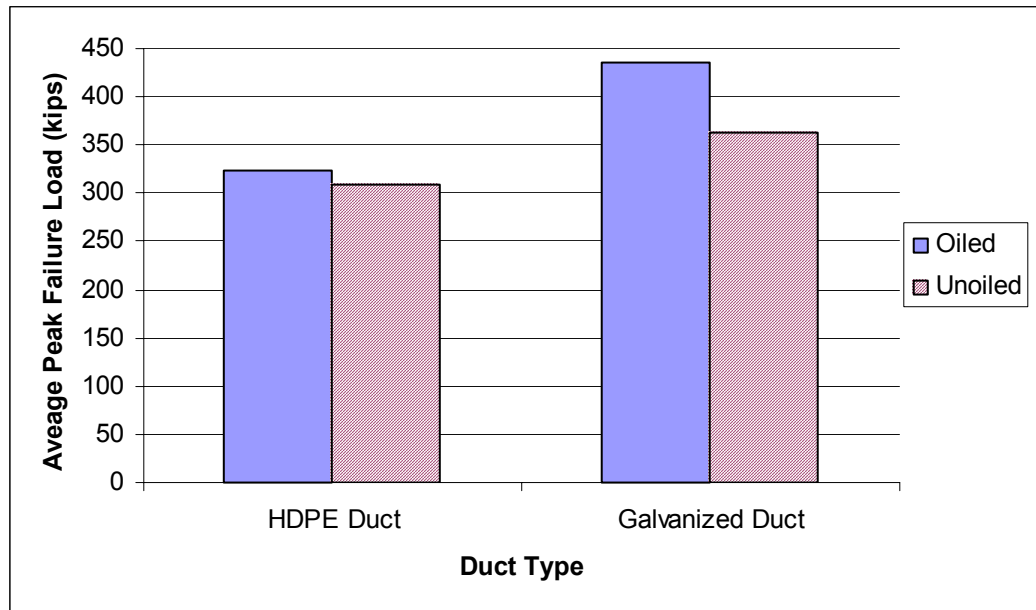
**Figure 5-10 Average Failure Loads for 7.5° Specimens with Oiled and Unoiled Tendons**

Galvanized pipe specimens began to slip immediately with the application of load, and had average failure loads reduced by 95%. Excess oil on the inner surface of the pipe likely destroyed adhesion between the grout and the duct. Since the inner surface of the galvanized pipes was smooth, there was little mechanical resistance to slip in these specimens. Upon inspection of the displaced grout plug in the oiled specimens, the underside was slightly darker than usual and had a greasy residue. This residue was a remnant of the emulsifiable oil and likely contributed to the reduced capacity.

The galvanized metal duct specimens exhibited an 80% reduction in capacity when oiled. The oiled HDPE duct specimens also performed more poorly than their unoiled counterparts, exhibiting a 93% decrease in capacity.

It is interesting to note, however, that both oiled galvanized metal duct and oiled HDPE duct specimens achieved higher maximum loads than their unoiled counterparts. Figure 5-11 shows peak load failure data for both duct materials. Since the oiled galvanized metal duct specimens did not experience a peak load failure, the load value displayed in the figure is the maximum load which the specimen resisted. Testing was halted at that load due to the breakage of wires in the tendon. The figure indicates that the increase in peak load capacity for HDPE ducts is about 5%, and the increase in peak load capacity for galvanized metal ducts is at least 20%.

Comparing Figure 5-10 and Figure 5-11 suggests that while oiled tendons may perform well from a peak capacity standpoint, their service performance is unacceptable.



***Figure 5-11 Peak Loads for 7.5° Specimens with Oiled and Unoiled Tendons in Galvanized Metal and HDPE Ducts***

Since the peak load capacity of the galvanized metal and HDPE duct specimens was controlled by splitting of the concrete, it is believed that the oil destroyed adhesion between the tendon and the grout, which allowed some of the splitting pressure to be relieved by tendon slippage. Mechanical interlock then provided a level of load resistance similar to that achieved by the unoiled specimens. The fact the crack growth in the oiled galvanized metal duct specimens was from the live end towards the dead end supports this idea, as splitting stresses would have been totally relieved by slippage of the free end. This phenomenon illustrates that adhesion is paramount to acceptable bond behavior, even if mechanical interlock is sufficient to develop the force.

## **5.5 SUMMARY OF FINDINGS**

This section makes overall observations based on the results discussed in the previous section.

### **5.5.1 Effect of Duct Type**

Galvanized steel pipes provided poor bond performance because of the inability of the smooth inner and outer surfaces to bond with the concrete or grout. For this reason it may be desirable to provide some sort of anchorage between the pipe and the concrete. While this would not improve the bond conditions at the duct-grout interface, it would at least eliminate one potential source of bond failure.

The corrugations of galvanized metal duct and HDPE duct allowed for adequate bond between both the concrete and the duct and the grout and the duct. The galvanized metal duct provided a small increase in bond capacity over the HDPE duct. For specimens of the same length, the galvanized metal duct provided between 5% and 15% higher peak load capacities. For this reason, the development length for tendons in galvanized metal ducts was shorter. The fact that the bond performance increase in galvanized metal duct specimens was relatively small means that, in most applications, either material will provide adequate performance.

### **5.5.2 Effect of Emulsifiable Oil**

Galvanized steel pipe specimens with oiled tendons experienced slip at the duct-grout interface immediately upon loading. Peak loads were achieved when the pipes broke free at the concrete-duct interface. Anchoring the pipes to the concrete would likely allow for development of loads similar to that of unoled specimens.



Galvanized metal duct and HDPE duct specimens with oiled tendons experienced slip at very low loads, but exhibited an increase of 5% or more in peak load capacity, as compared to their unoiled counterparts. The fact that slip occurred in the pullout specimens at very low loads indicates that deformations and crack widths may be significantly larger in a flexural member post-tensioned with oiled tendons. The fact that the peak load capacity was similar or improved means that flexural members post-tensioned with oiled tendons will likely provide similar ultimate flexural capacity.

The question of whether or not emulsifiable oils are appropriate for use lies then with the designer. If the designer is relying on the bond of the post-tensioning system to limit cracking and deformation, emulsifiable oils should not be used. If the designer is relying on the bond of the post-tensioning system only to provide adequate ultimate flexural capacity, emulsifiable oils may be used without hesitation.

### **5.5.3 Effect of Confinement**

Because testing of this variable was very limited only qualitative assessments can be made. Providing more transverse reinforcement limits bursting crack widths, allows development of higher failure loads and bond stresses, and allows a higher percentage of the peak load to be maintained after failure.

# CHAPTER 6

## Summary and Conclusions

### 6.1 INTRODUCTION

The research presented in this thesis was part of The University of Texas at Austin, Center for Transportation Research Project 0-4562: “Effect of Emulsifiable Oils Used as Temporary Corrosion Protection in Grouted Post-Tensioned Tendons, and Investigation of Alternate Corrosion Resistant Post-Tensioning Systems.” This research is associated with the first phase of the project which involves the effect of emulsifiable oils on grouted post-tensioned systems. The overall objectives of this phase of the project are the following:

1. Identify emulsifiable oils or other suitable products for providing temporary corrosion protection.
2. Assess the performance of the corrosion-inhibiting products.
3. Investigate how the products affect friction loss during post-tensioning.
4. Determine the impact of corrosion-inhibiting products on bond strength and behavior of multi-strand tendons.
5. Determine how flexural capacity is affected by any changes in bond strength or behavior, and make recommendations for the use of temporary corrosion protection.

The author’s involvement with Project 0-4562 began in August of 2002. The scope of this thesis is limited to the fourth and fifth objectives only, and the following section includes a summary of results and findings toward their completion.

## **6.2 SUMMARY AND CONCLUSIONS**

Twenty-eight, multi-strand tendon, pullout specimens were tested to investigate the effects of several variables on bond performance of multi-strand post-tensioning tendons. The variables tested in this program included bonded length, duct type, tendon surface condition, and amount of transverse reinforcement.

### **6.2.1 Effect of Duct Type**

Three duct types were tested in this program: smooth galvanized steel pipe, corrugated galvanized metal duct, and corrugated high density polyethylene (HDPE) duct. The following conclusions can be drawn:

- Failure loads for smooth galvanized steel pipes were more than 70% lower than for either of the corrugated ducts. The poor performance was due to the fact that the smooth surfaces of the pipe did not allow for adequate bonding of the grout to the duct or the duct to the concrete.
- Corrugated galvanized metal ducts provided slightly better bond performance than HDPE ducts. Higher failure loads, in the range of 5%-15%, were achieved in galvanized metal duct specimens than in HDPE duct specimens of the same length.

### **6.2.2 Effect of Tendon Surface Condition**

Two tendon surface conditions were tested in this program: unoiled tendons and tendons oiled with Citgo Trukut NC 205. The following conclusions can be drawn:

- Specimens treated with the emulsifiable oil failed at extremely low loads when using a dead end slip failure criterion. Loss of capacity was on the order of 80-95%.

- Specimens with corrugated duct materials and tendons treated with the emulsifiable oil exhibited at least 5% higher peak failure loads. These higher loads were accompanied by significantly increased tendon slip.

### **6.2.3 Effect of Confining Reinforcement**

Two HDPE duct specimens were tested with a larger transverse reinforcement spacing than was used in all other specimens in this program. The following conclusions can be drawn:

- Providing more transverse reinforcement resulted in narrower cracks.
- Providing more transverse reinforcement resulted in slightly higher peak failure loads and better maintenance of load after failure.

### **6.3 OVERALL CONCLUSIONS AND SUGGESTIONS FOR IMPLEMENTATION**

- Because of the poor bond performance of the smooth galvanized steel pipes, measures should be taken to anchor the pipes to the concrete.
- Since the increase in bond strength observed between galvanized metal ducts and HDPE ducts was moderate, either duct can be relied on to provide adequate performance in most situations.
- Because of the significant slip exhibited by tendons treated with emulsifiable oil, oiled tendons should not be used in situations where the bond of the post-tensioning system is being relied upon to control flexural cracking or deformation.
- Because oiled tendons were able to develop large forces despite their significant slip, they may be used in situations where bond of the post-tensioning system is being relied upon only for ultimate flexural capacity.

#### **6.4 DIRECTIONS FOR FUTURE RESEARCH**

Using emulsifiable oils as temporary corrosion protection in bonded post-tensioned systems has a marked effect on the bond behavior of multi-strand tendons. While this research has shed much light on the topic, there are still some questions which must be addressed. The author recommends the following additional work:

- Tests using at least one other emulsifiable oil to determine whether the trends found thus far are applicable to emulsifiable oils in general.
- Determination of the effect, if any, of emulsifiable oil on grout strength.
- Experimental or analytical analysis to determine the effect of tendon slip on the flexural behavior of post-tensioned elements.
- Development of design guidelines or recommendations for the use of emulsifiable oils as temporary corrosion protection.

# Appendix A

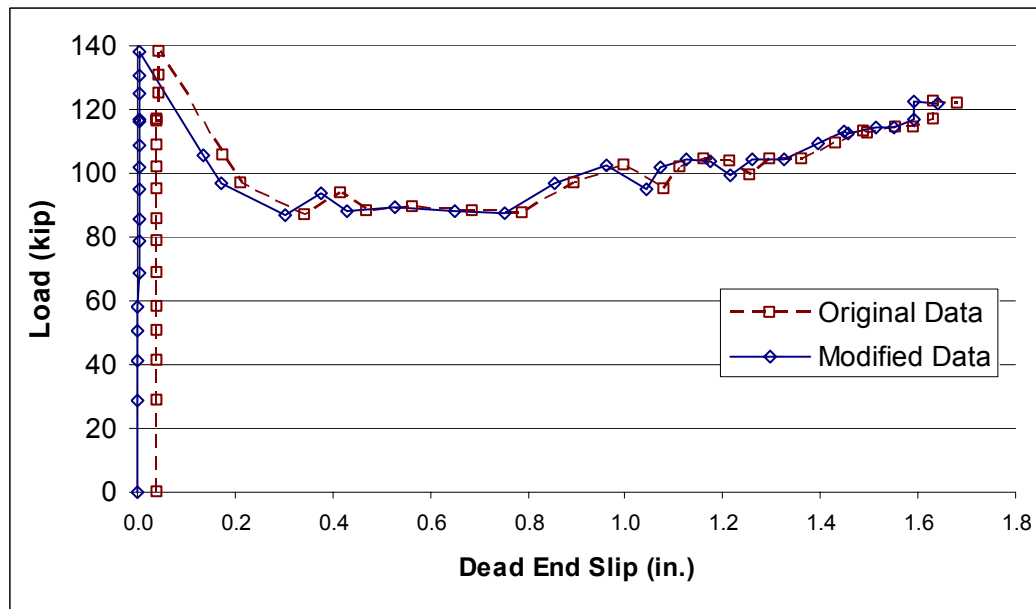
## Original and Modified Test Data

### A.1 GALVANIZED STEEL PIPE SPECIMEN DATA

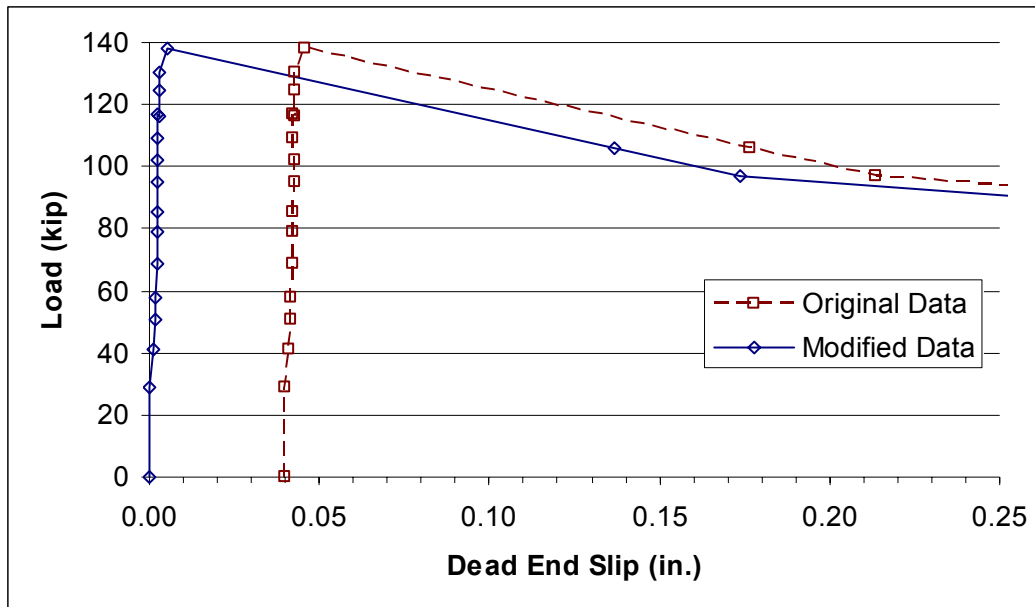
This section presents, in graphical form, the original and modified data for the galvanized steel pipe specimens.

#### A.1.1 0-SP-20°-1

Only dead end data were modified for this specimen.



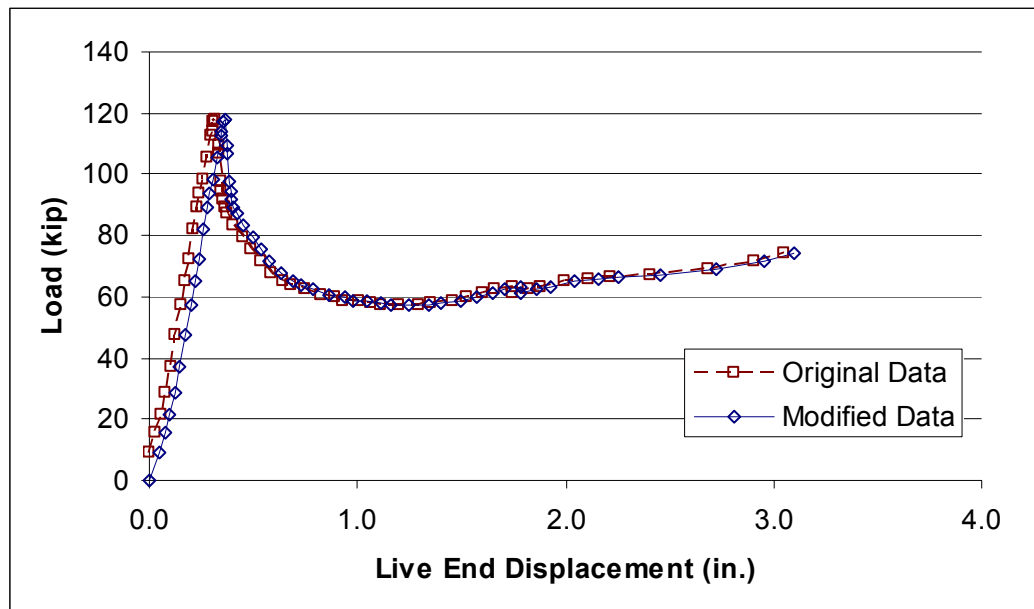
*Figure A-1 Original and Modified Dead End Load-Slip Response for Specimen 0-SP-20°-1*



**Figure A-2 Original and Modified Dead End Load-Slip Response for Specimen 0-SP-20°-1, Amplified Scale**

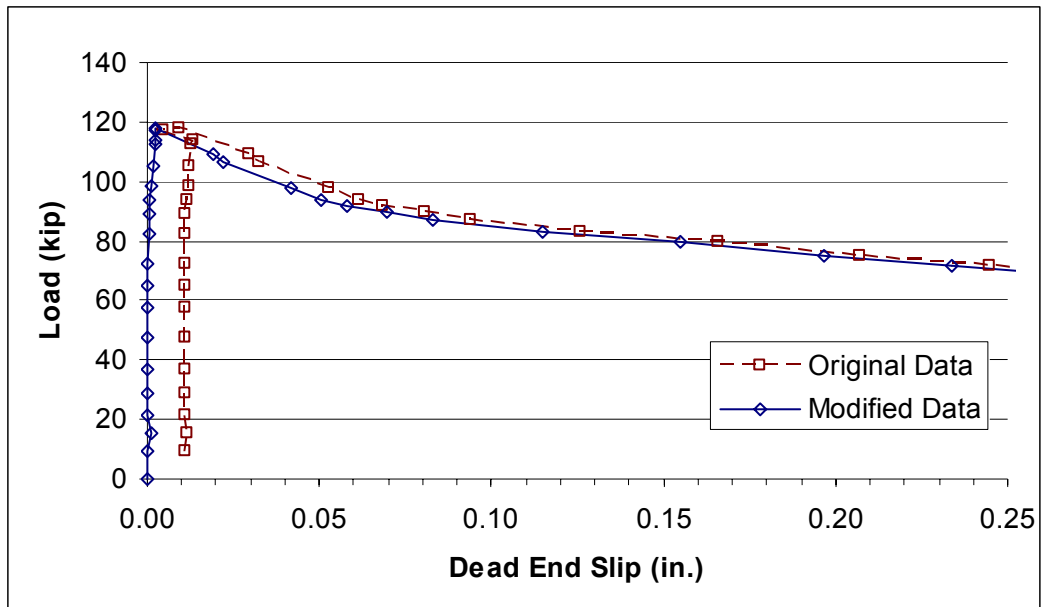
### A.1.2 0-SP-15°-1

Both live and dead end data were modified for this specimen. Because the dead end modification was so slight, the plot over the full range of slip values is not included because it is not possible to perceive the difference between the two curves at that scale.



*Figure A-3 Original and Modified Live End Load-Displacement Response for Specimen 0-SP-15°-1*

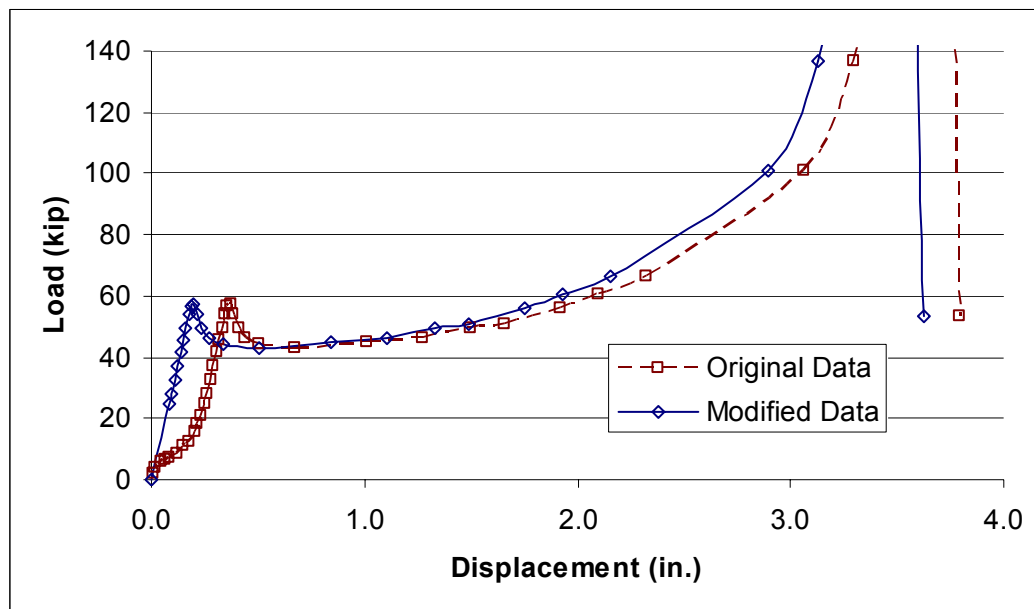




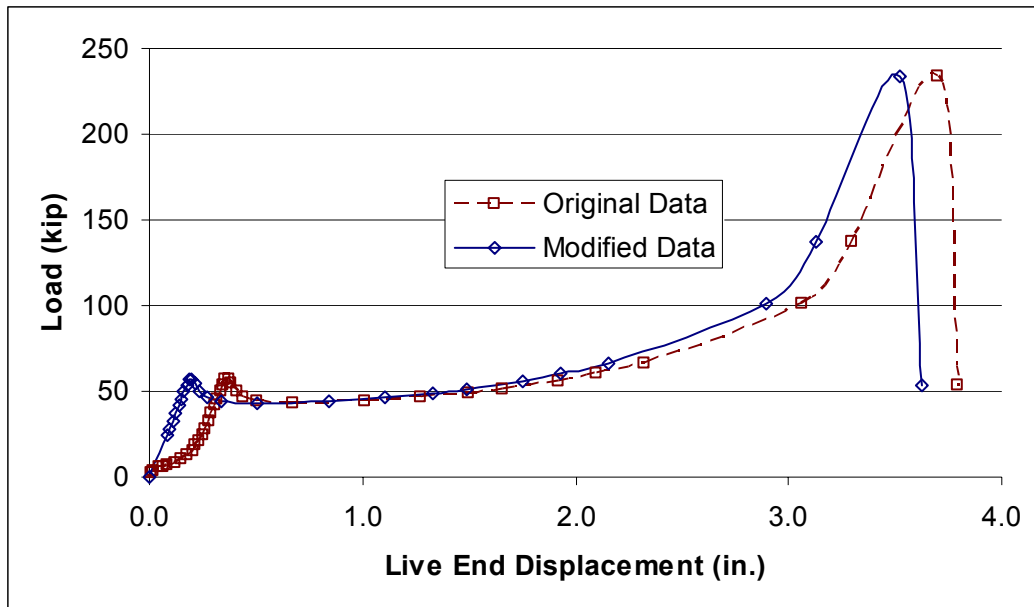
**Figure A-4 Original and Modified Dead End Load-Slip Response for Specimen 0-SP-15°-1, Amplified Scale**

### A.1.3 0-SP-10°-1

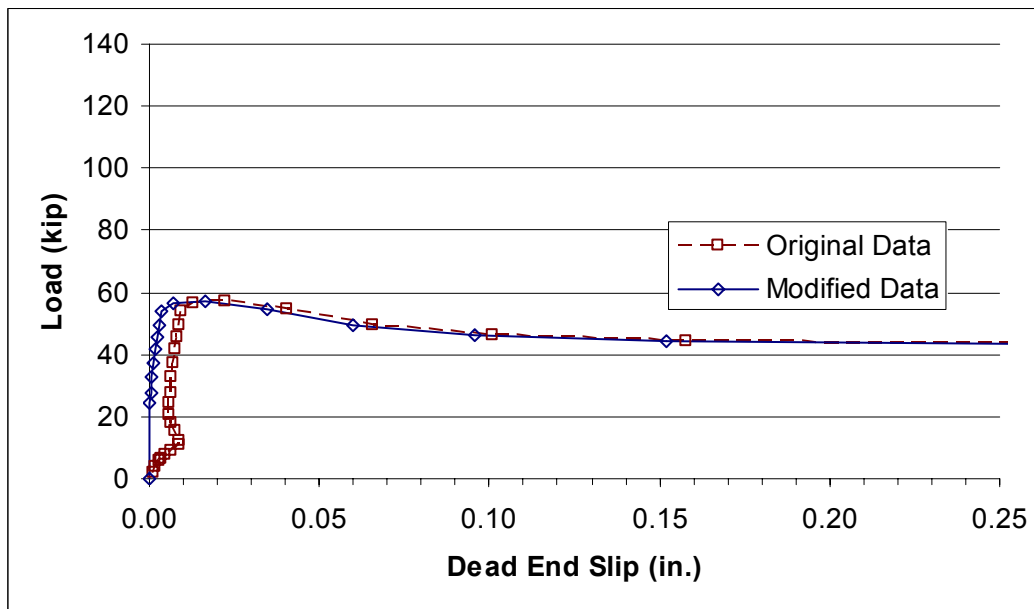
Both live and dead end data were modified for this specimen. The first live end load-displacement curve is plotted on the typical scale used for all galvanized steel pipe specimens. The second plot is over a greater load range to show all data points. Because the dead end modification was so slight, the plot over the full range of slip values is not included because it is not possible to perceive the difference between the two curves at that scale.



*Figure A-5 Original and Modified Live End Load-Displacement Response for Specimen 0-SP-10°-1*



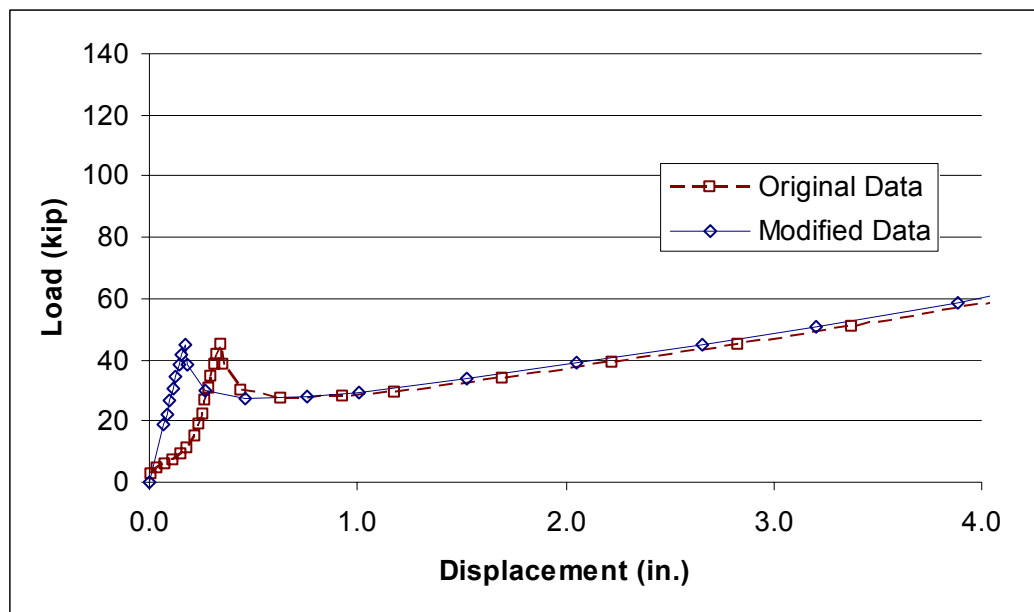
**Figure A-6 Original and Modified Live End Load-Displacement Response for Specimen 0-SP-10°-1, Full Range**



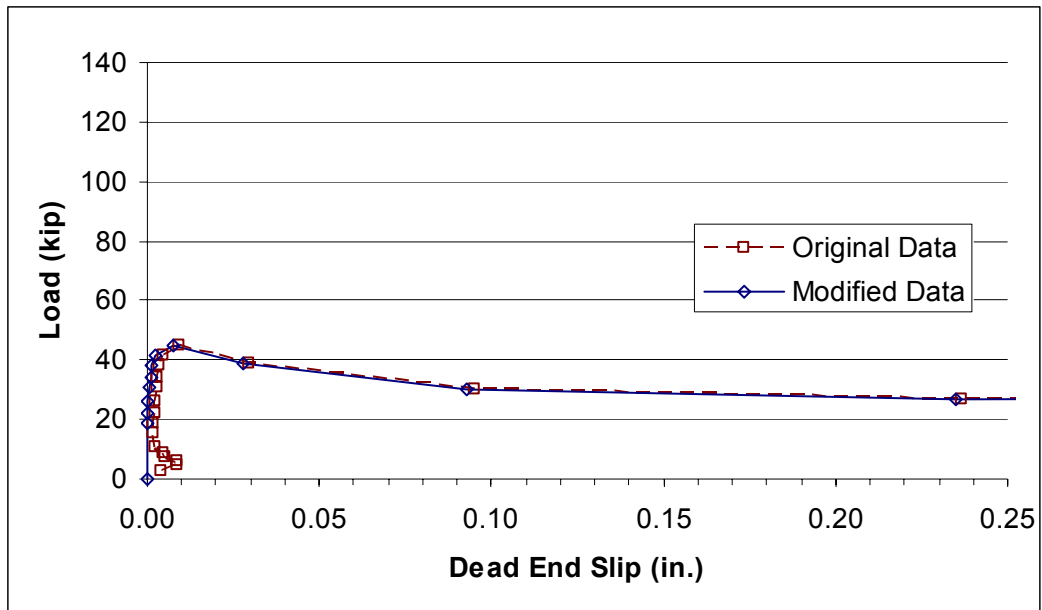
**Figure A-7 Original and Modified Dead End Load-Slip Response for Specimen 0-SP-10°-1, Amplified Scale**

#### A.1.4 0-SP-10°-2

Both live and dead end data were modified for this specimen. Because the dead end modification was so slight, the plot over the full range of slip values is not included because it is not possible to perceive the difference between the two curves at that scale.



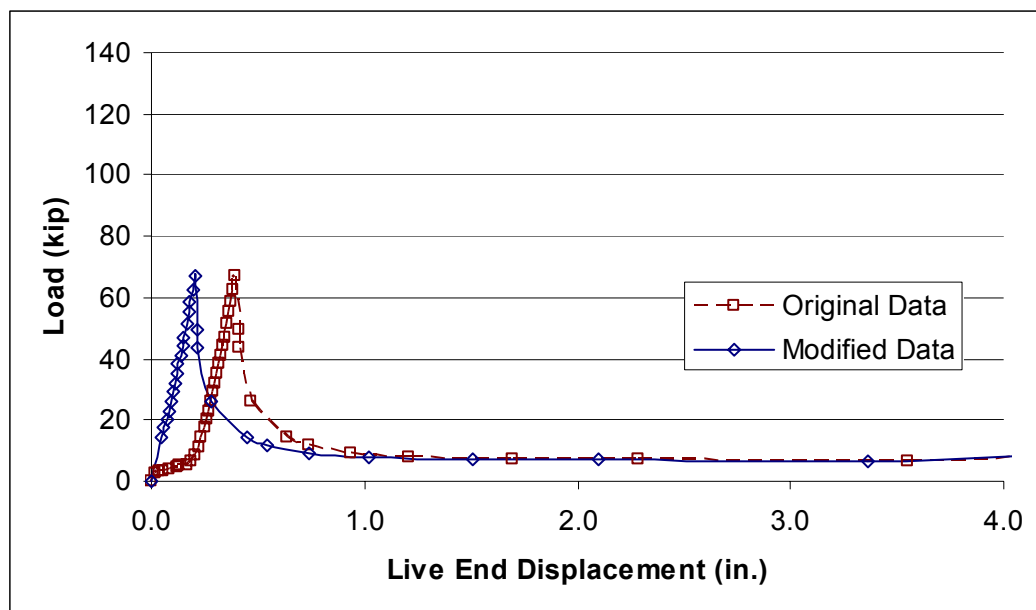
*Figure A-8 Original and Modified Live End Load-Displacement Response for Specimen 0-SP-10°-2*



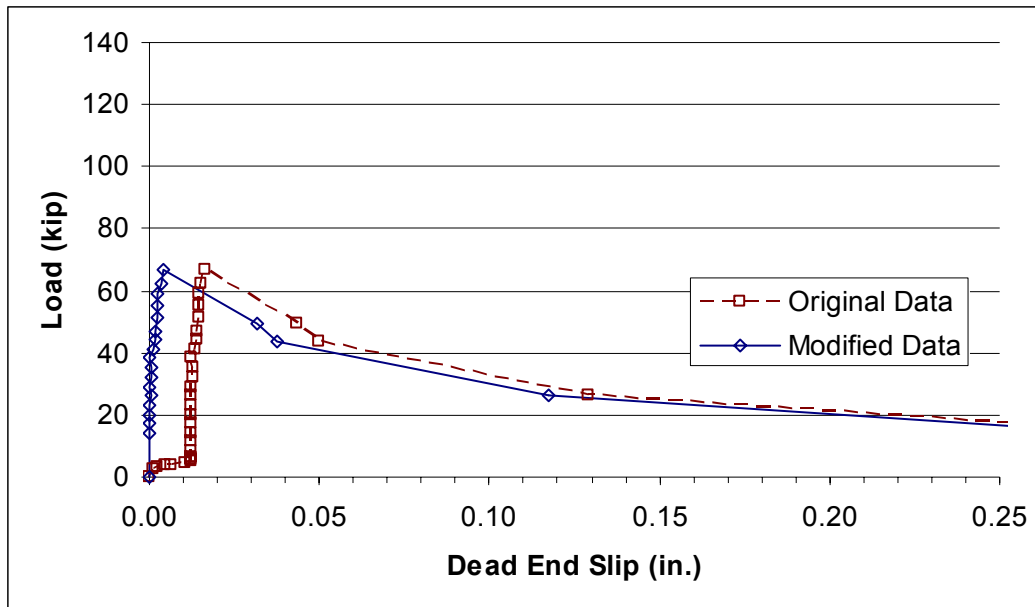
**Figure A-9 Original and Modified Dead End Load-Slip Response for Specimen 0-SP-10°-2, Amplified Scale**

### A.1.5 0-SP-7.5°-1

Both live and dead end data were modified for this specimen. Because the dead end modification was so slight, the plot over the full range of slip values is not included because it is not possible to perceive the difference between the two curves at that scale.



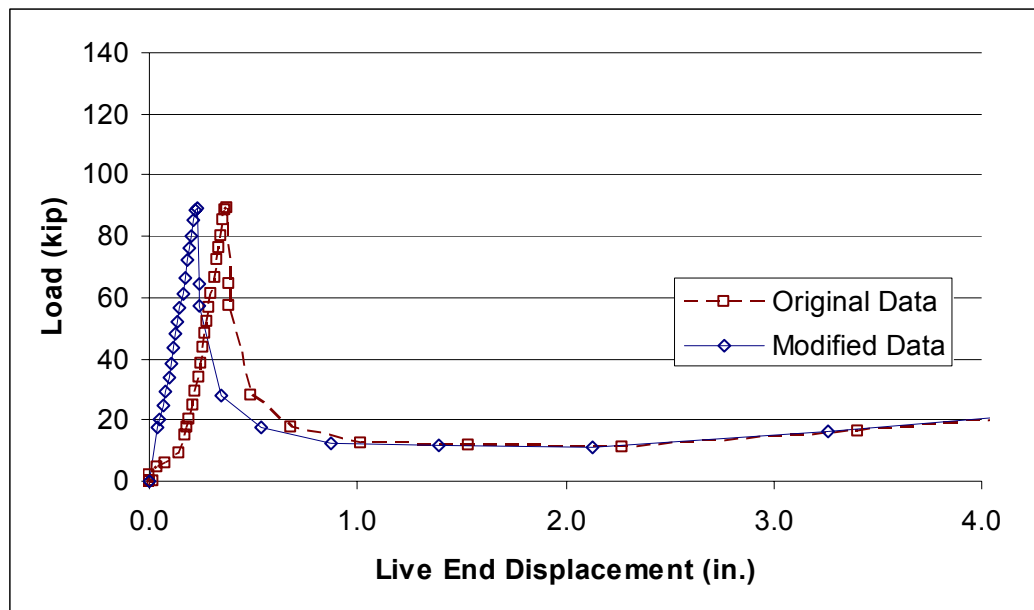
*Figure A-10 Original and Modified Live End Load-Displacement Response for Specimen 0-SP-7.5°-1*



*Figure A-11 Original and Modified Dead End Load-Slip Response for Specimen 0-SP-7.5°-1, Amplified Scale*

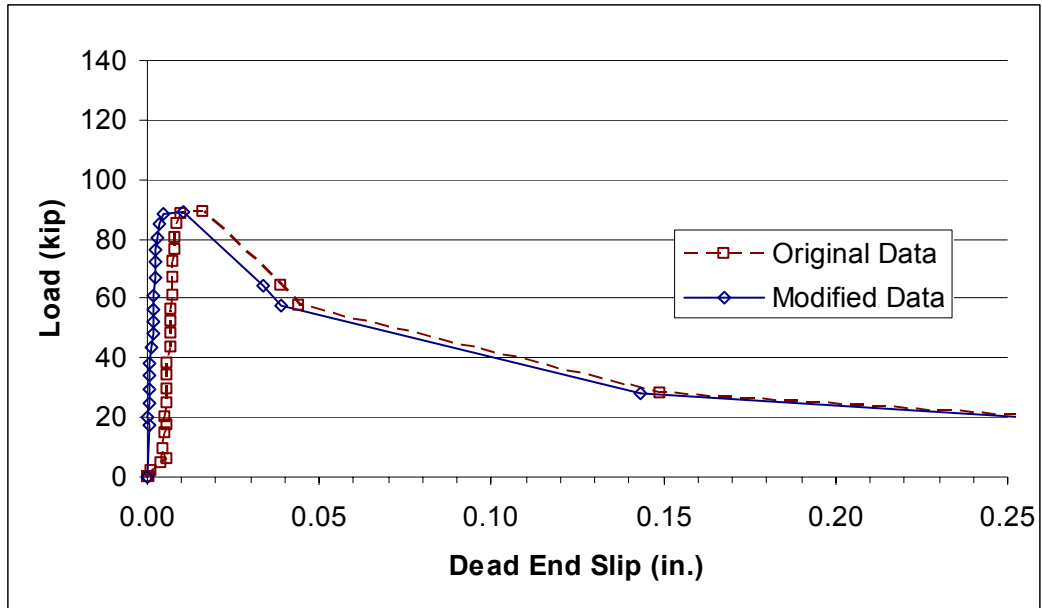
### A.1.6 0-SP-7.5°-2

Both live and dead end data were modified for this specimen. Because the dead end modification was so slight, the plot over the full range of slip values is not included because it is not possible to perceive the difference between the two curves at that scale.



*Figure A-12 Original and Modified Live End Load-Displacement Response for Specimen 0-SP-7.5°-2*





*Figure A-13 Original and Modified Dead End Load-Slip Response for Specimen 0-SP-7.5°-2, Amplified Scale*

**A.1.7 1-SP-7.5°-1**

The data from this specimen required no modification.

**A.1.8 1-SP-7.5°-1**

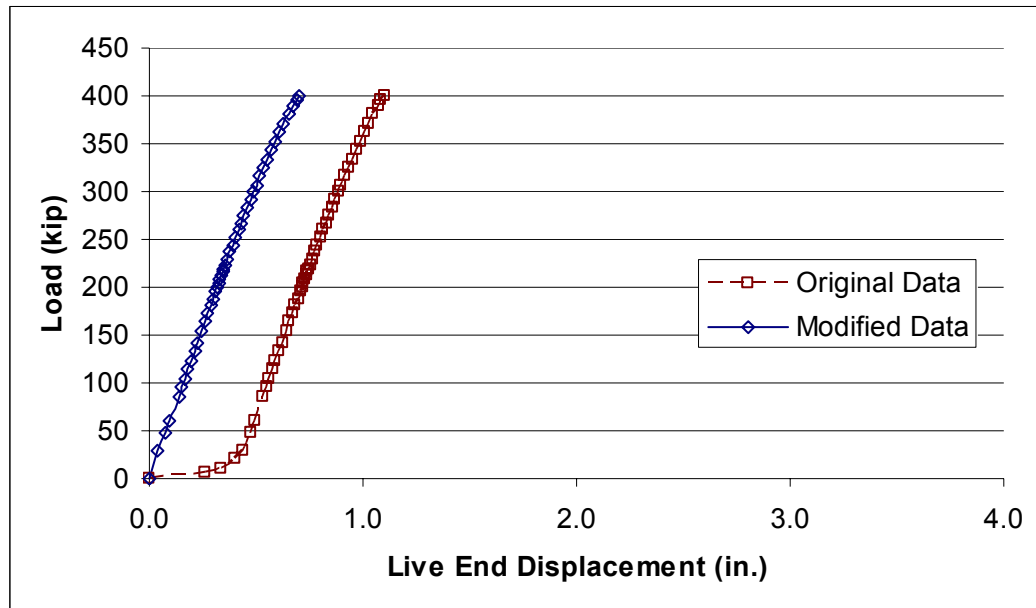
The data from this specimen required no modification.

## A.2 GALVANIZED METAL DUCT SPECIMEN DATA

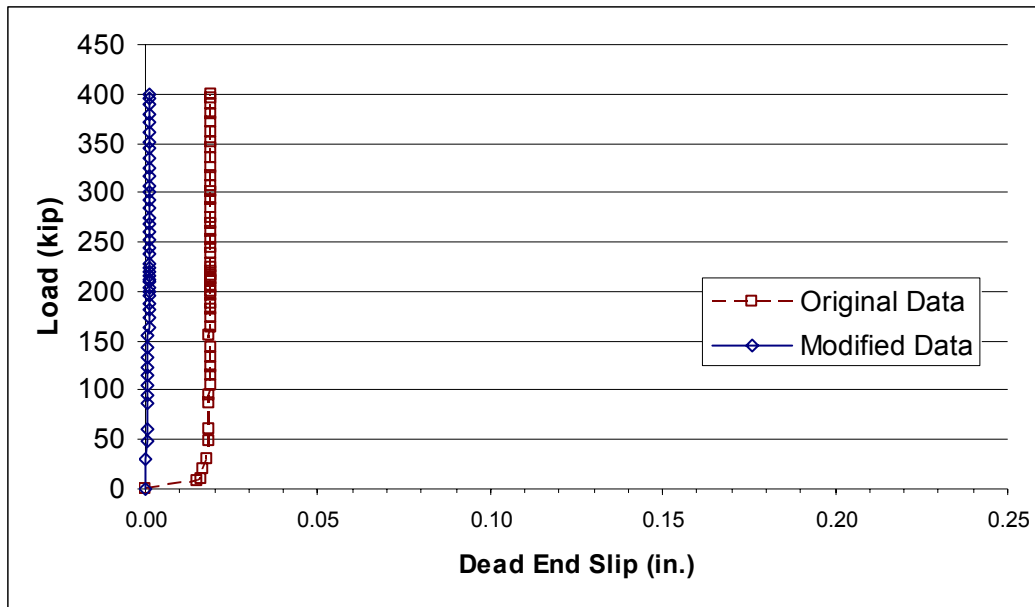
This section presents, in graphical form, the original and modified data for the galvanized metal duct specimens.

### A.2.1 0-GD-20°-1

Both live and dead end data were modified for this specimen. Because dead end data not does exist beyond the range of the amplified scale, the plot on the standard scale is not included.



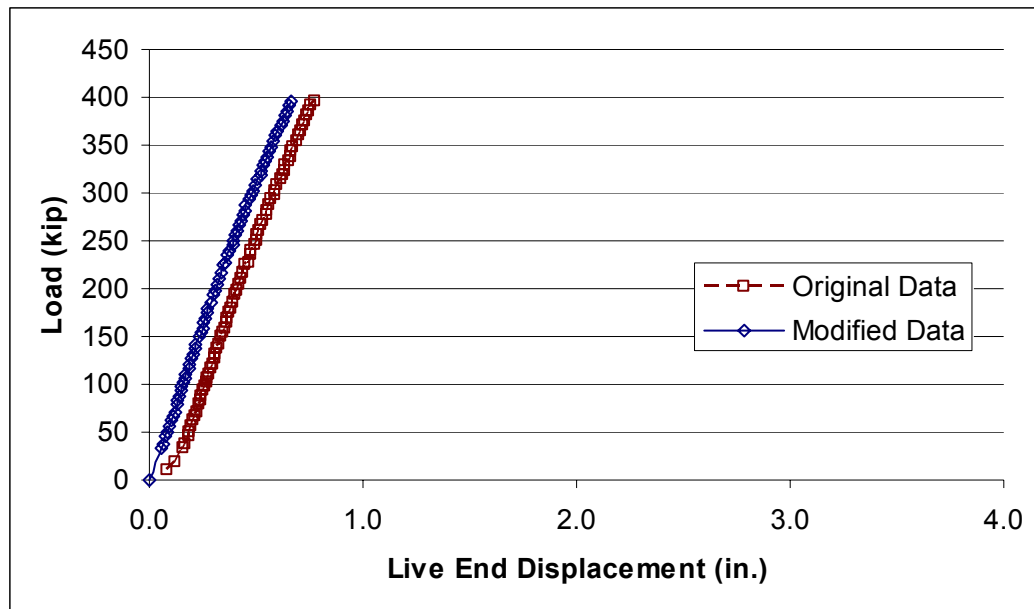
*Figure A-14 Original and Modified Live End Load-Displacement Response for Specimen 0-GD-20°-1*



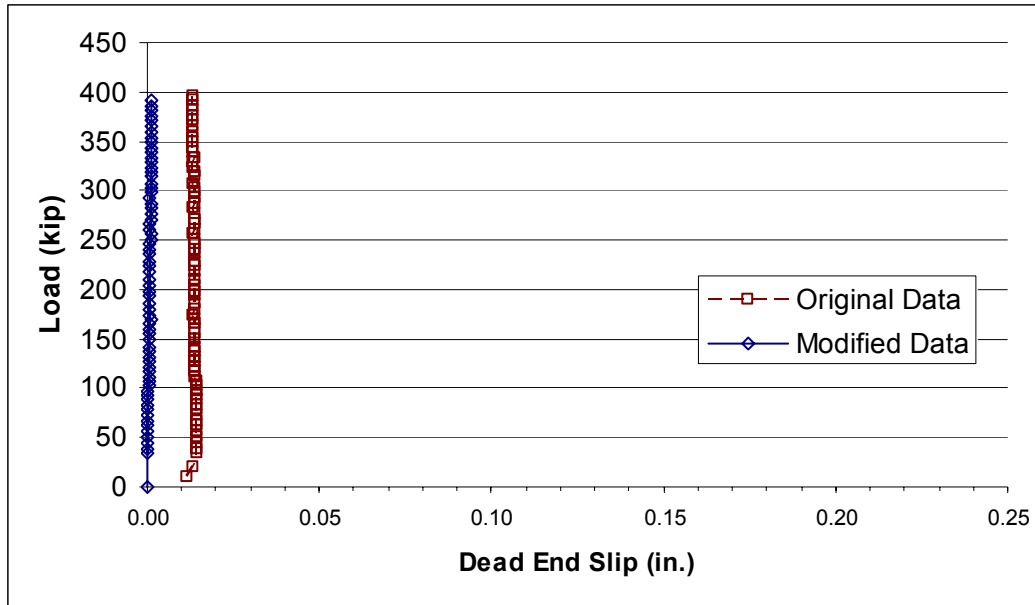
*Figure A-15 Original and Modified Dead End Load-Slip Response for Specimen 0-GD-20°-1, Amplified Scale*

### A.2.2 0-GD-15°-1

Both live and dead end data were modified for this specimen. Because dead end data does not exist beyond the range of the amplified scale, the plot on the standard scale is not included.



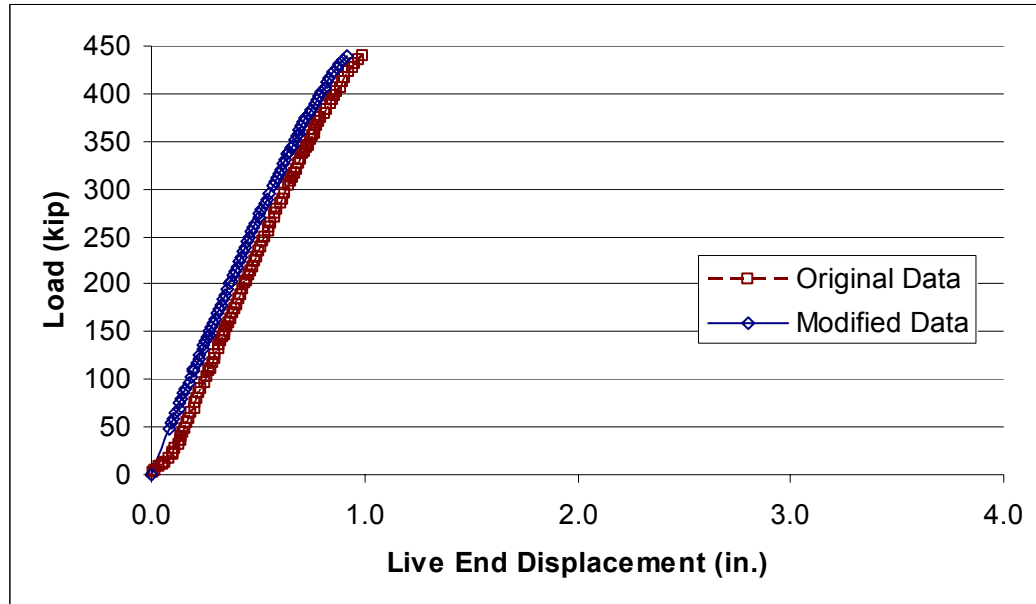
*Figure A-16 Original and Modified Live End Load-Displacement Response for Specimen 0-GD-15°-1*



*Figure A-17 Original and Modified Dead End Load-Slip Response for Specimen 0-GD-15°-1, Amplified Scale*

### A.2.3 0-GD-10°-1

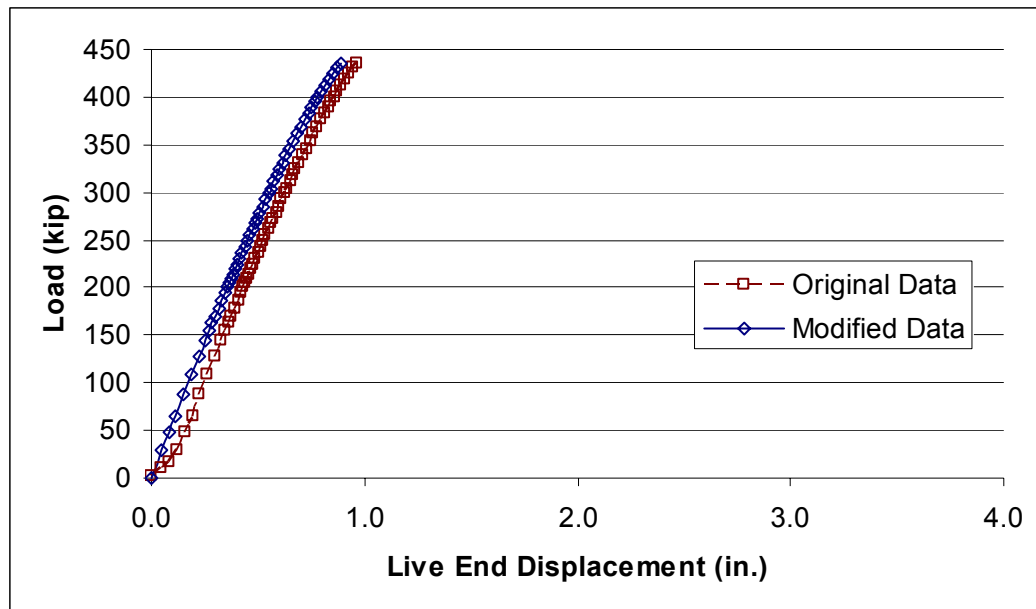
Only live end data were modified for this specimen.



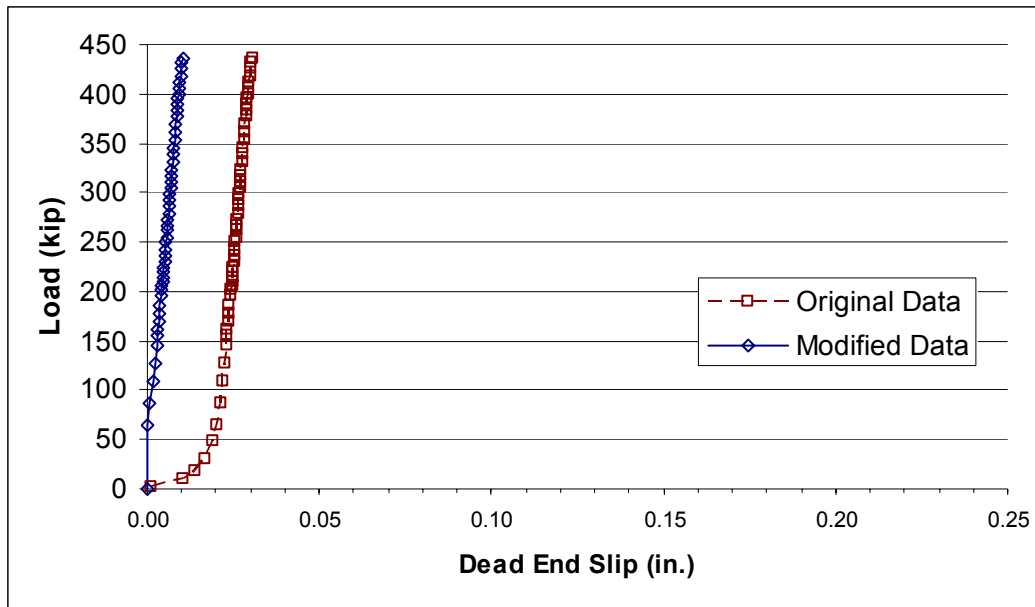
*Figure A-18 Original and Modified Live End Load-Displacement Response for Specimen 0-GD-10°-1*

#### A.2.4 0-GD-10°-2

Both live and dead end data were modified for this specimen. Because dead end data does not exist beyond the range of the amplified scale, the plot on the standard scale is not included.



*Figure A-19 Original and Modified Live End Load-Displacement Response for Specimen 0-GD-10°-2*

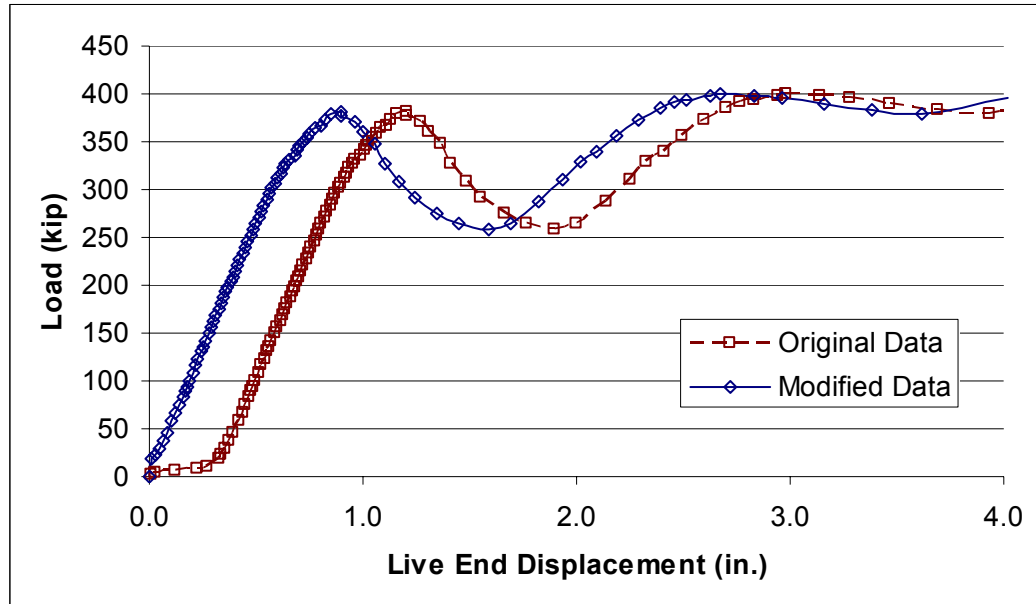


*Figure A-20 Original and Modified Dead End Load-Slip Response for Specimen 0-GD-10°-2, Amplified Scale*

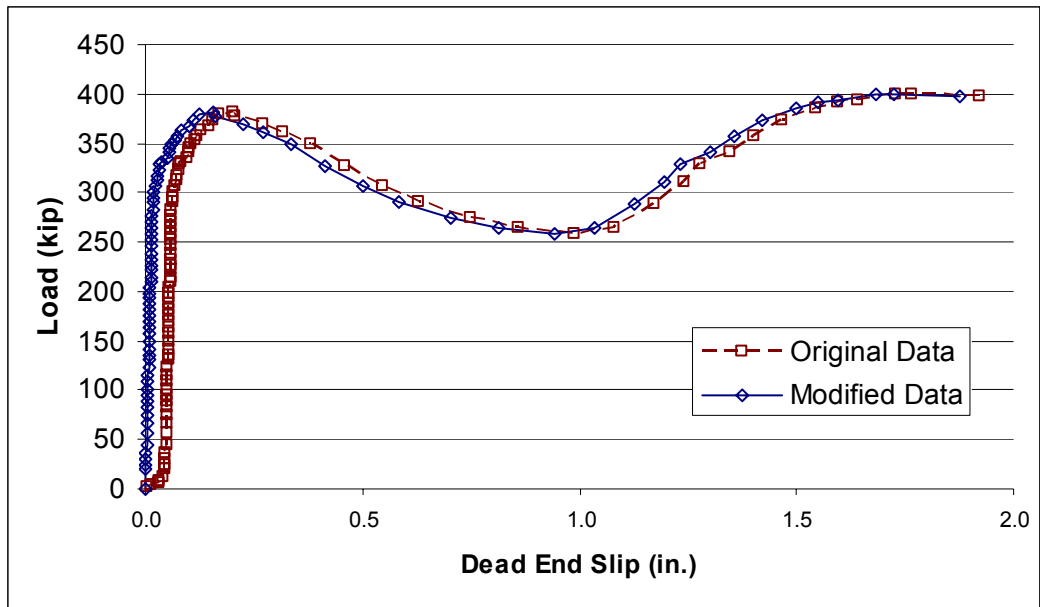


### A.2.5 0-GD-7.5°-1

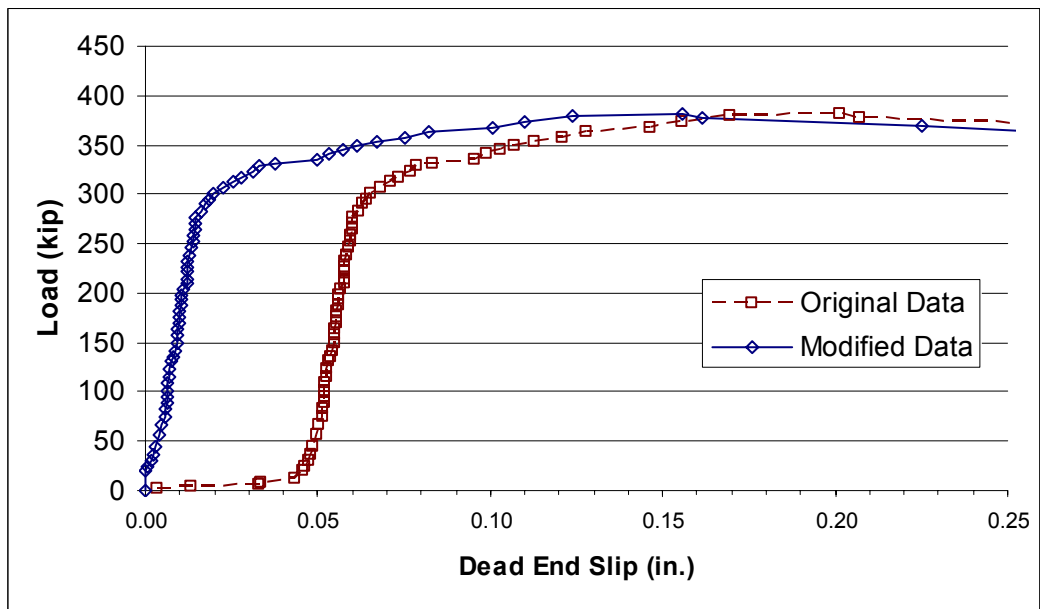
Both live and dead end data were modified for this specimen.



*Figure A-21 Original and Modified Live End Load-Displacement Response for Specimen 0-GD-7.5°-1*



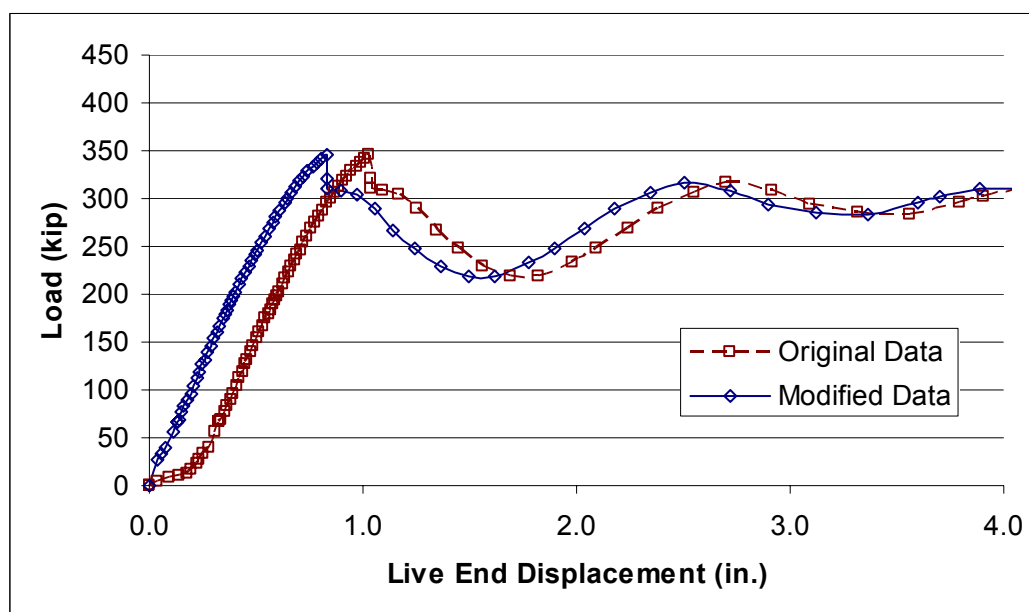
**Figure A-22** Original and Modified Dead End Load-Slip Response for Specimen 0-GD-7.5°-1



**Figure A-23** Original and Modified Dead End Load-Slip Response for Specimen 0-GD-7.5°-1, Amplified Scale

### A.2.6 0-GD-7.5°-2

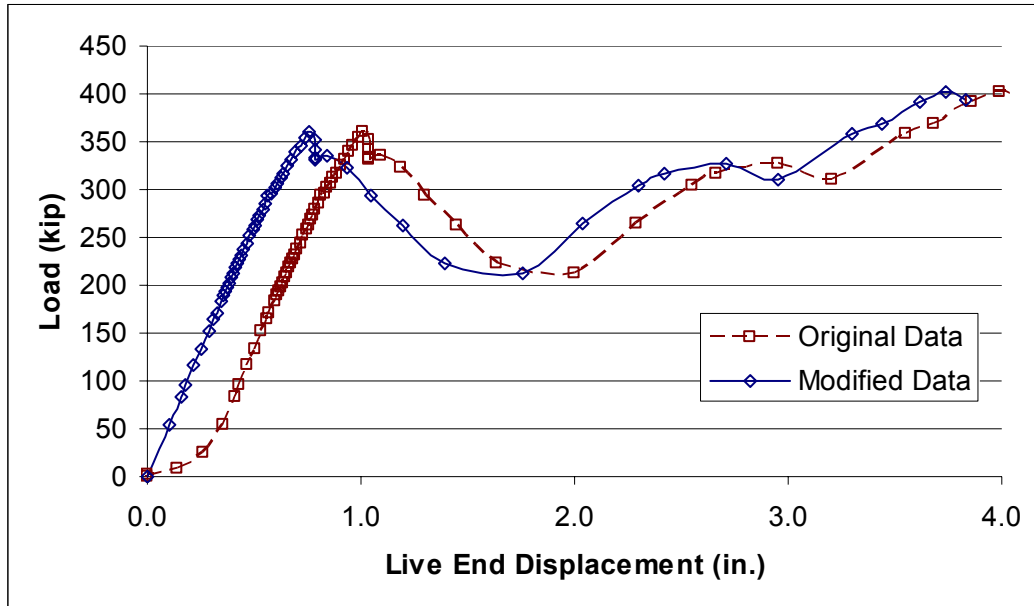
Only live end data were modified for this specimen.



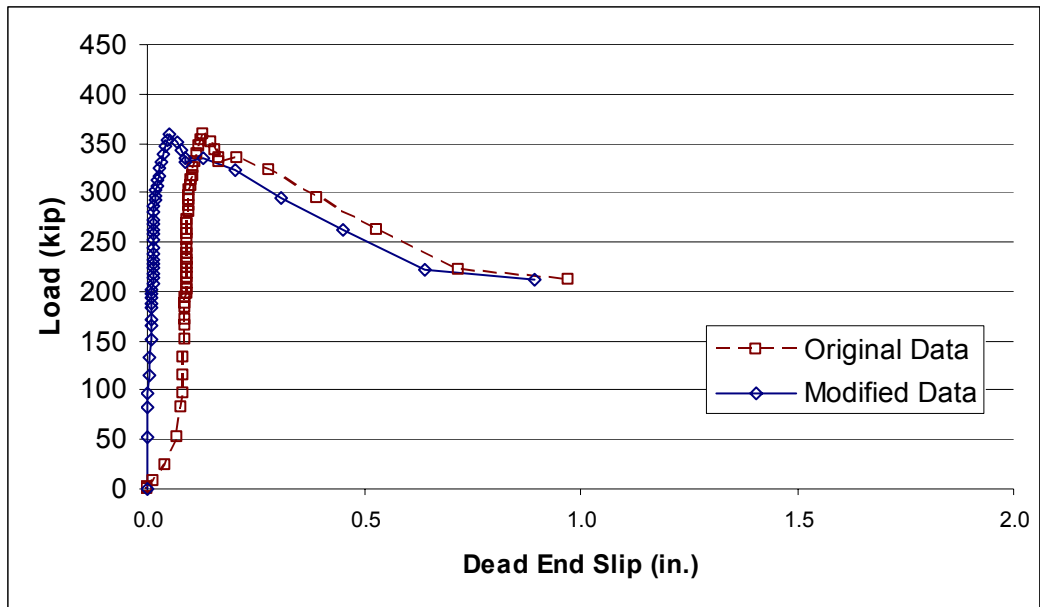
*Figure A-24 Original and Modified Live End Load-Displacement Response for Specimen 0-GD-7.5°-2*

### A.2.7 0-GD-7.5°-3

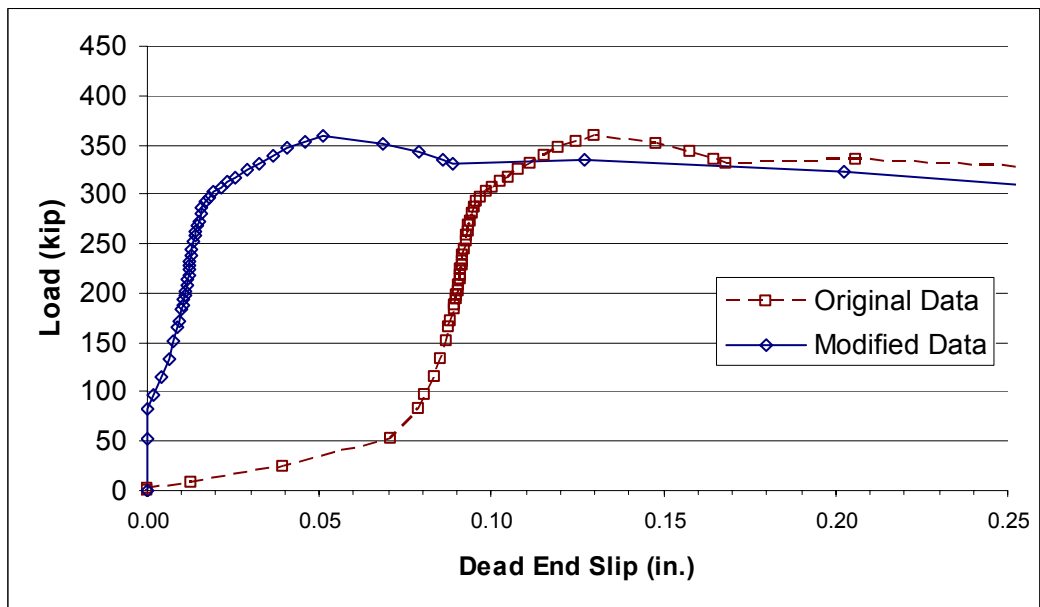
Both live and dead end data were modified for this specimen.



*Figure A-25 Original and Modified Live End Load-Displacement Response for Specimen 0-GD-7.5°-3*



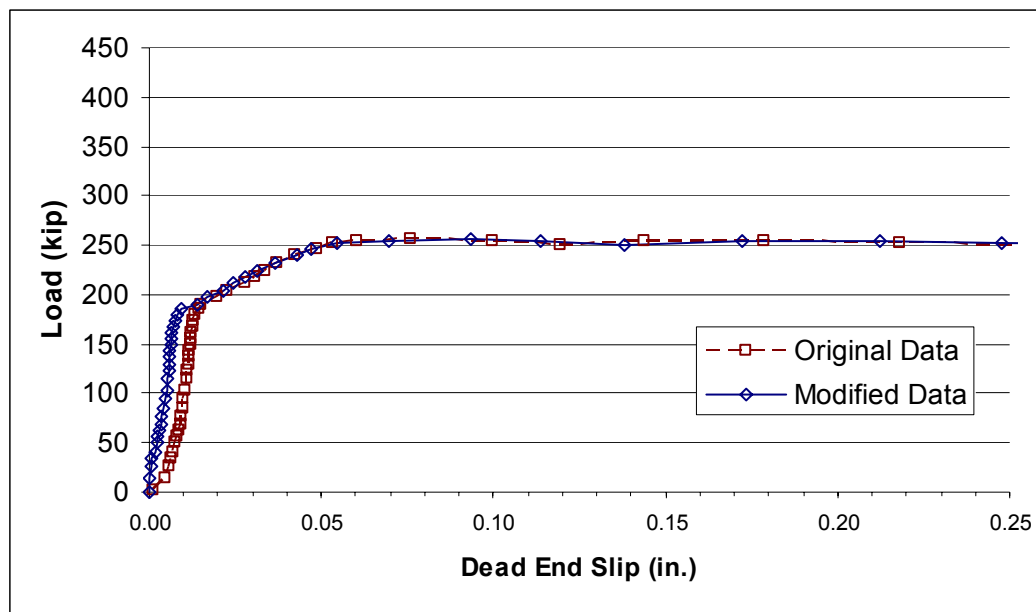
**Figure A-26 Original and Modified Dead End Load-Slip Response for Specimen 0-GD-7.5°-3**



**Figure A-27 Original and Modified Dead End Load-Slip Response for Specimen 0-GD-7.5°-3, Amplified Scale**

### A.2.8 0-GD-5°-1

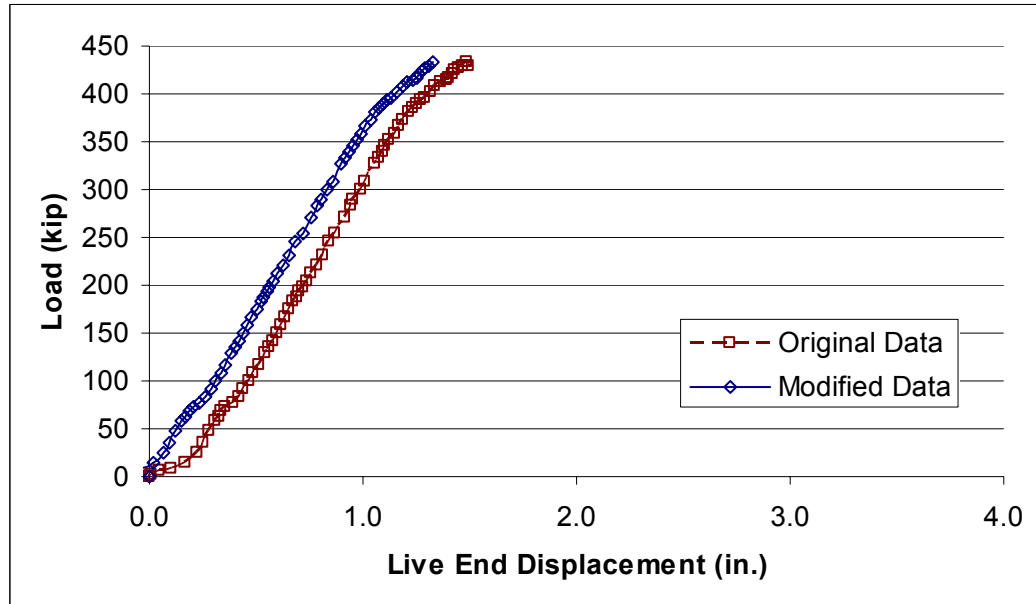
Only dead end data were modified for this specimen. Because the dead end modification was so slight, the plot over the full range of slip values is not included because it is not possible to perceive the difference between the two curves at that scale.



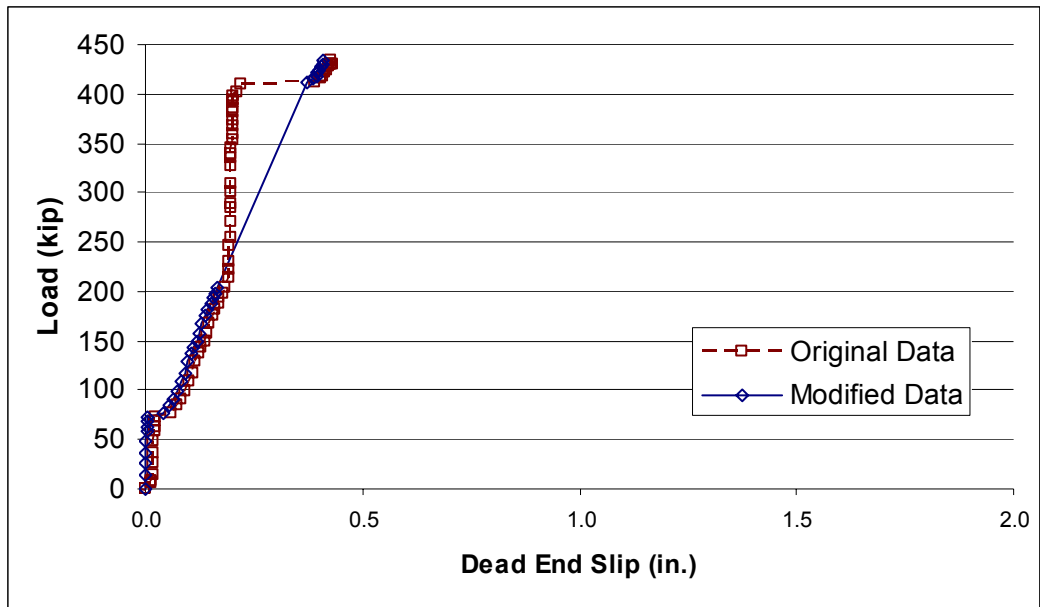
*Figure A-28 Original and Modified Dead End Load-Slip Response for Specimen 0-GD-5°-1, Amplified Scale*

### A.2.9 1-GD-7.5°-1

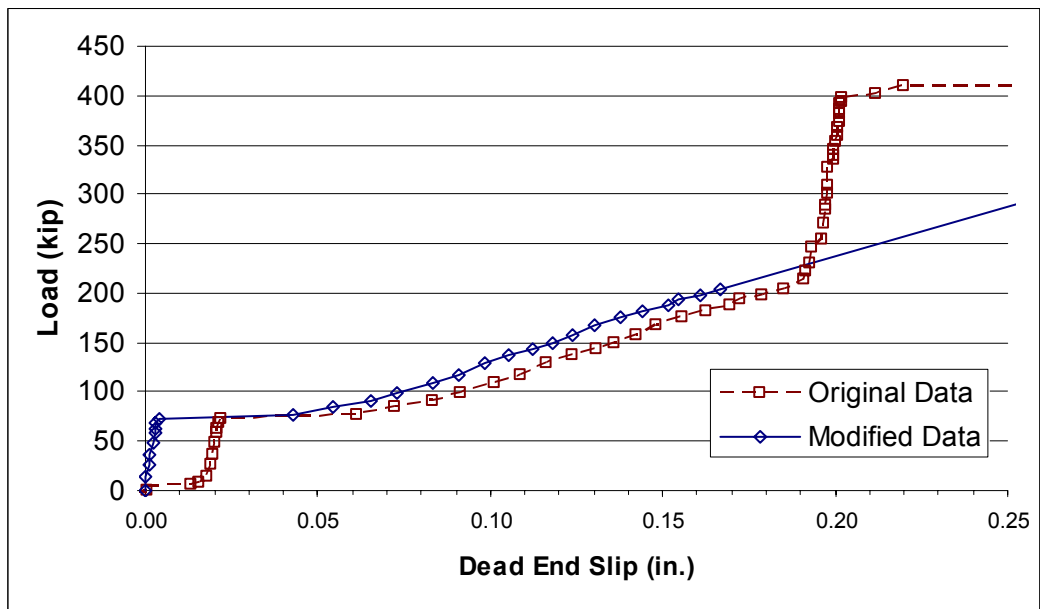
Both live and dead end data were modified for this specimen.



*Figure A-29 Original and Modified Live End Load-Displacement Response for Specimen 1-GD-7.5°-1*



**Figure A-30 Original and Modified Dead End Load-Slip Response for Specimen 1-GD-7.5°-1**



**Figure A-31 Original and Modified Dead End Load-Slip Response for Specimen 1-GD-7.5°-1, Amplified Scale**



**A.2.10 1-GD-7.5°-1**

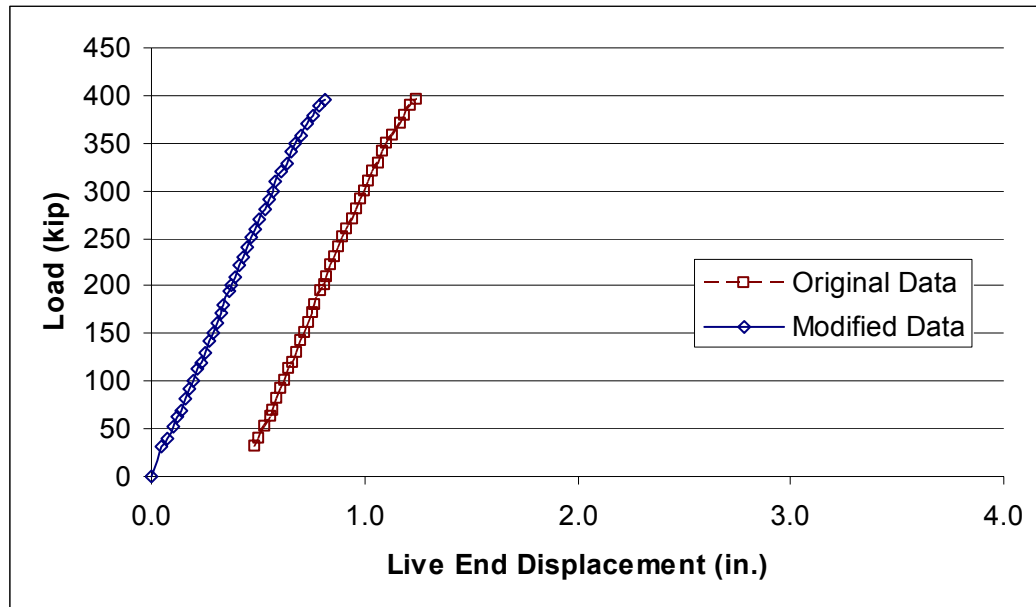
The data from this specimen required no modification.

### A.3 HDPE DUCT SPECIMEN DATA

This section presents, in graphical form, the original and modified data for the high density polyethylene duct specimens.

#### A.3.1 0-HD-20°-1

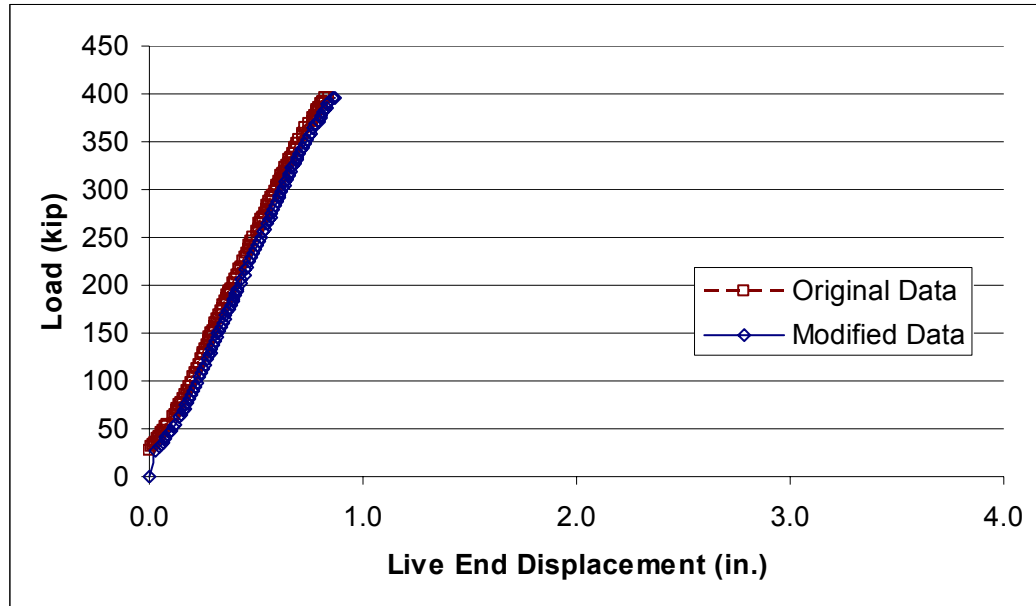
Only live end data were modified for this specimen.



*Figure A-32 Original and Modified Live End Load-Displacement Response for Specimen 0-HD-20°-1*

### A.3.2 0-HD-15°-1

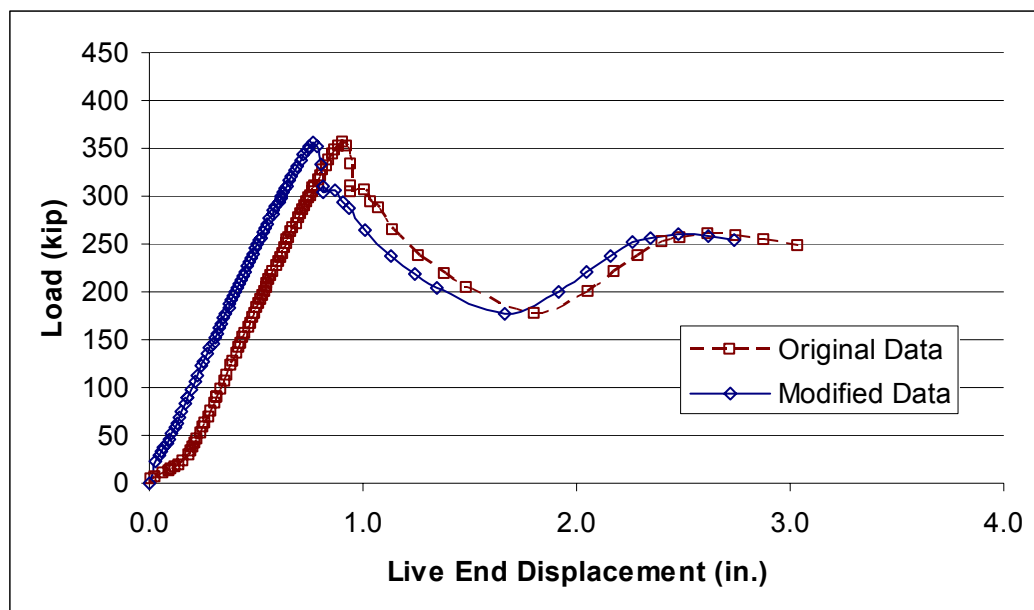
Only live end data were modified for this specimen.



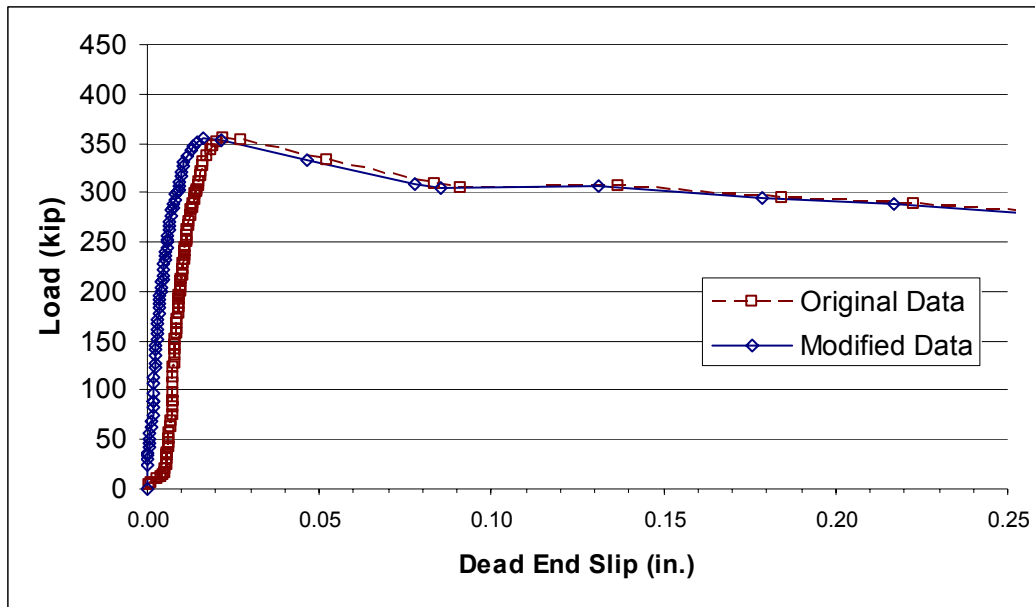
*Figure A-33 Original and Modified Live End Load-Displacement Response for Specimen 0-HD-15°-1*

### A.3.3 0-HD-10°-1

Both live and dead end data were modified for this specimen. Because the dead end modification was so slight, the plot over the full range of slip values is not included because it is not possible to perceive the difference between the two curves at that scale.



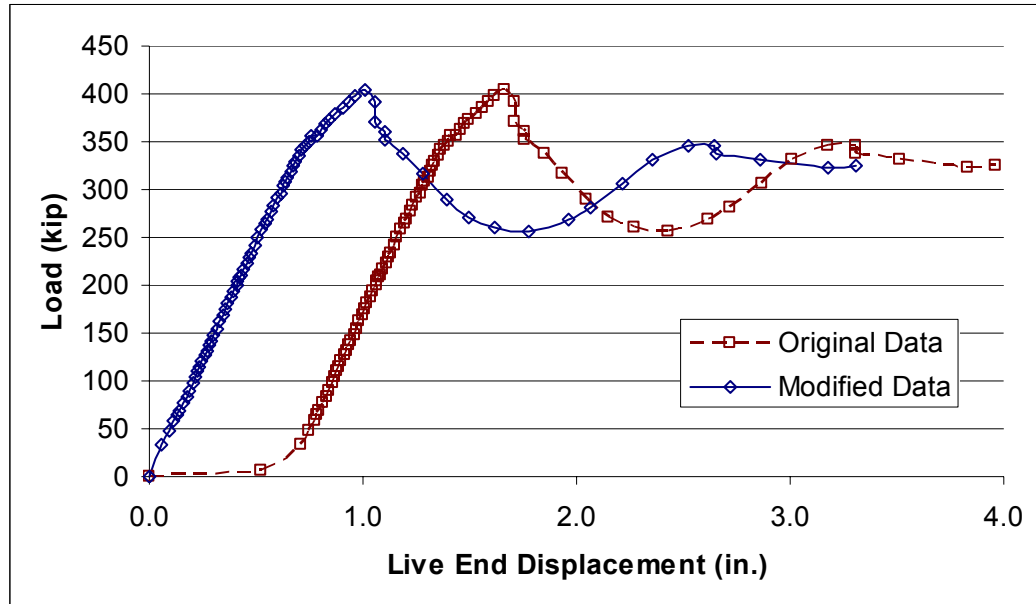
*Figure A-34 Original and Modified Live End Load-Displacement Response for Specimen 0-HD-10°-1*



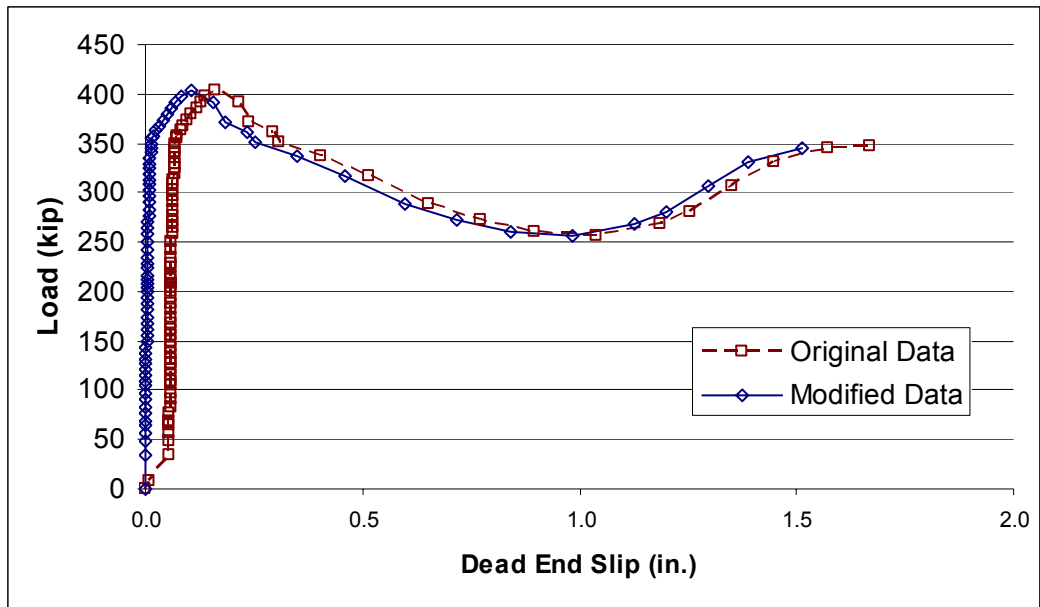
*Figure A-35 Original and Modified Dead End Load-Slip Response for Specimen 0-HD-10°-1, Amplified Scale*

### A.3.4 0-HD-10°-2

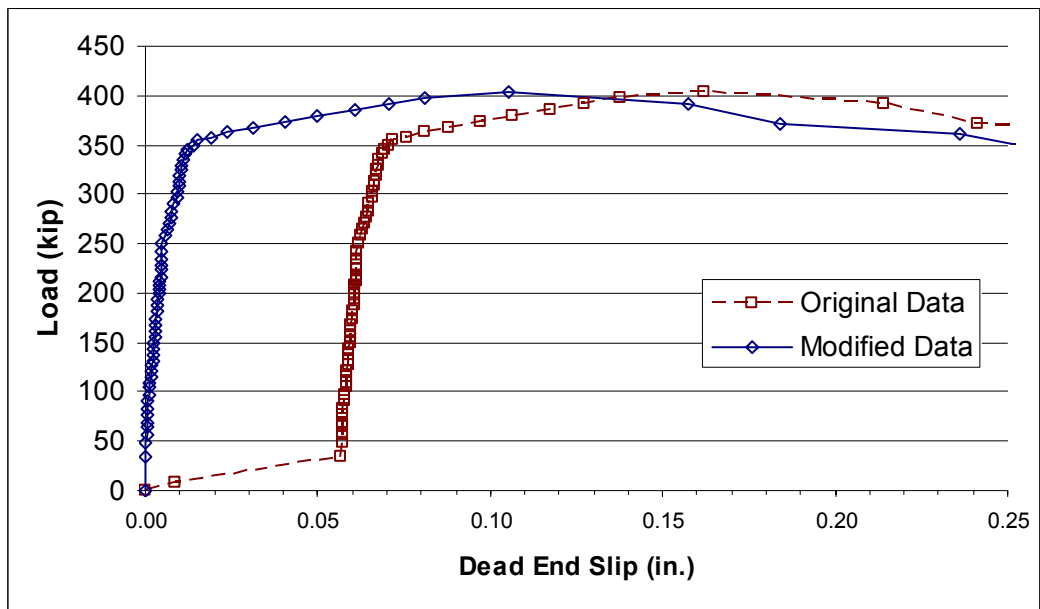
Both live and dead end data were modified for this specimen.



*Figure A-36 Original and Modified Live End Load-Displacement Response for Specimen 0-HD-10°-2*



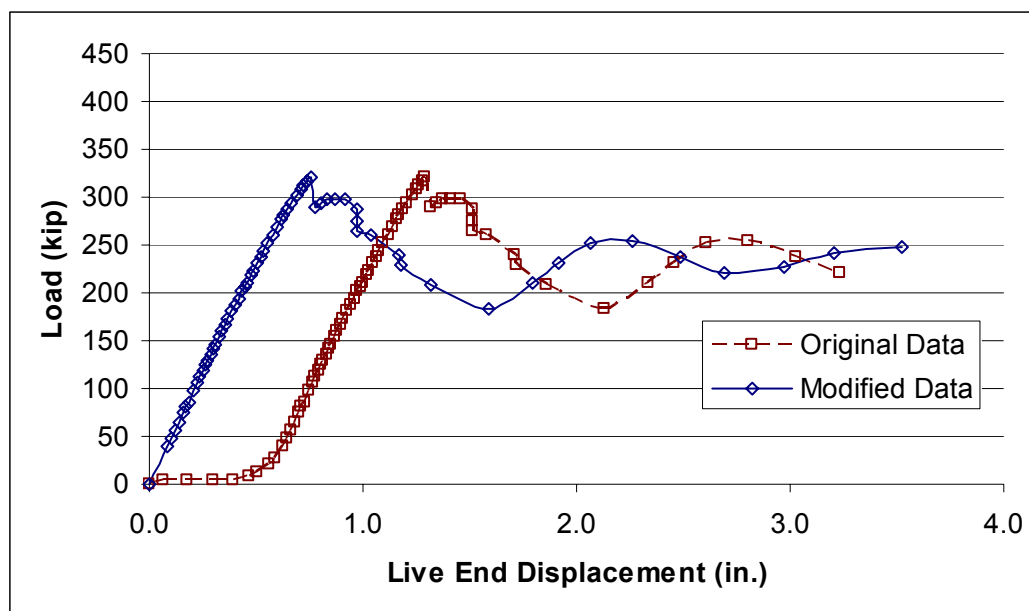
**Figure A-37** Original and Modified Dead End Load-Slip Response for Specimen 0-HD-10°-2



**Figure A-38** Original and Modified Dead End Load-Slip Response for Specimen 0-HD-10°-2, Amplified Scale

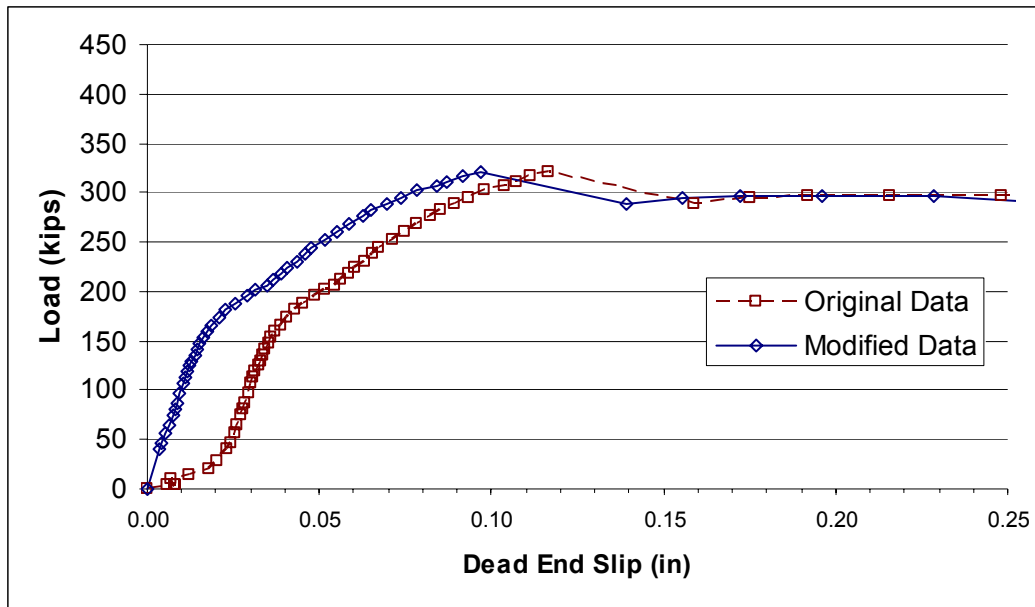
### A.3.5 0-HD-10°-3

Both live and dead end data were modified for this specimen. Because the dead end modification was so slight, the plot over the full range of slip values is not included because it is not possible to perceive the difference between the two curves at that scale.



*Figure A-39 Original and Modified Live End Load-Displacement Response for Specimen 0-HD-10°-3*

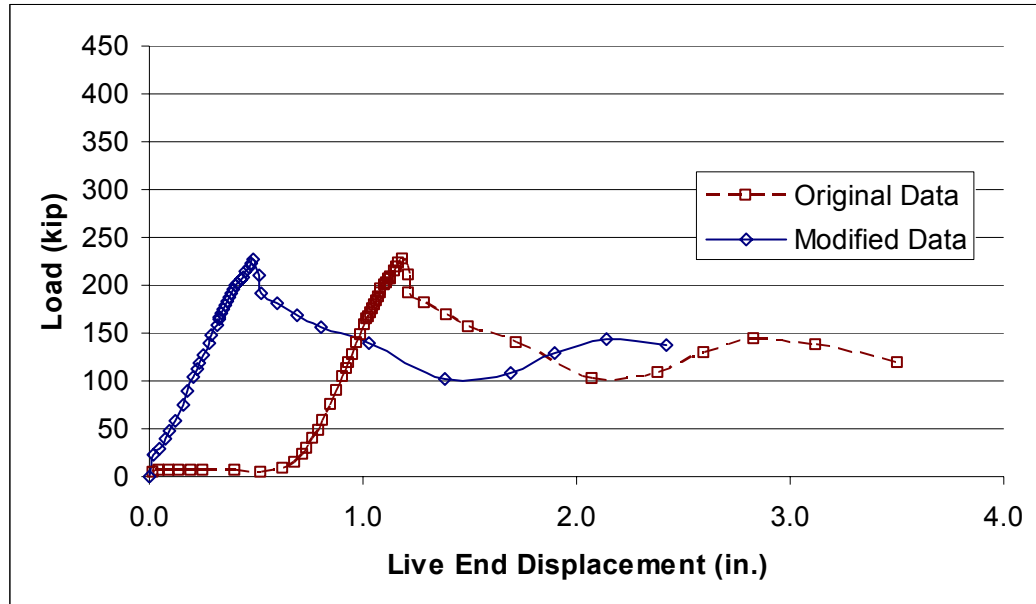




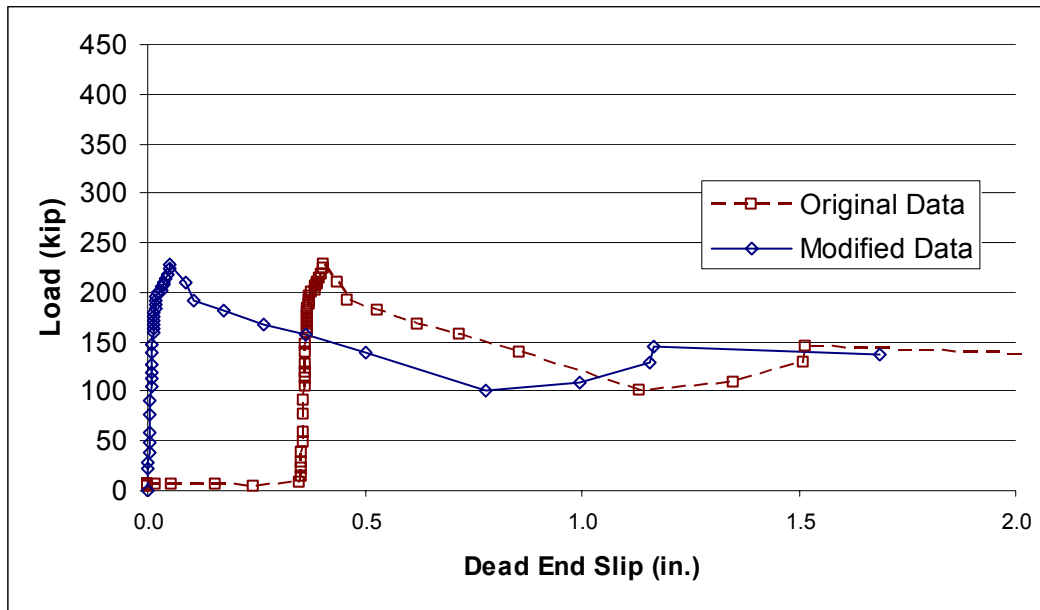
*Figure A-40 Original and Modified Dead End Load-Slip Response for Specimen 0-HD-10°-3, Amplified Scale*

### A.3.6 0-HD-7.5°-1

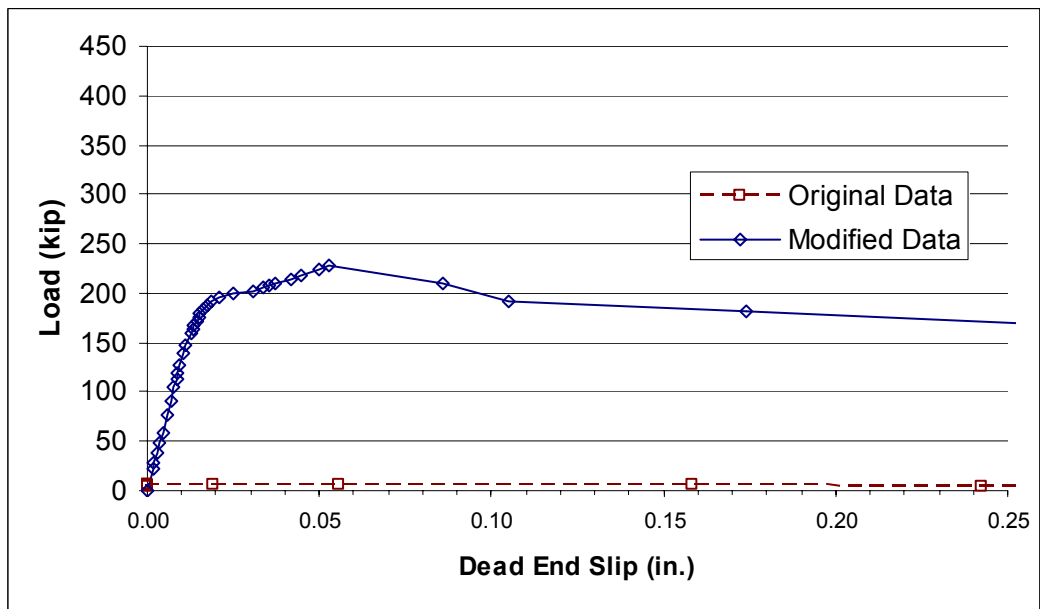
Both live and dead end data were modified for this specimen.



*Figure A-41 Original and Modified Live End Load-Displacement Response for Specimen 0-HD-7.5°-1*



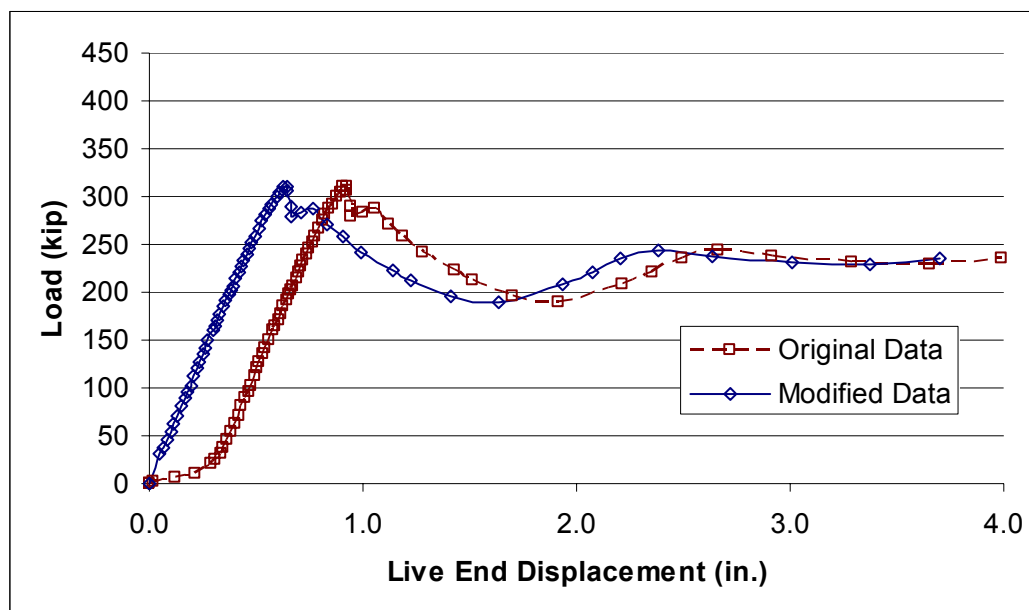
**Figure A-42 Original and Modified Dead End Load-Slip Response for Specimen 0-HD-7.5°-1**



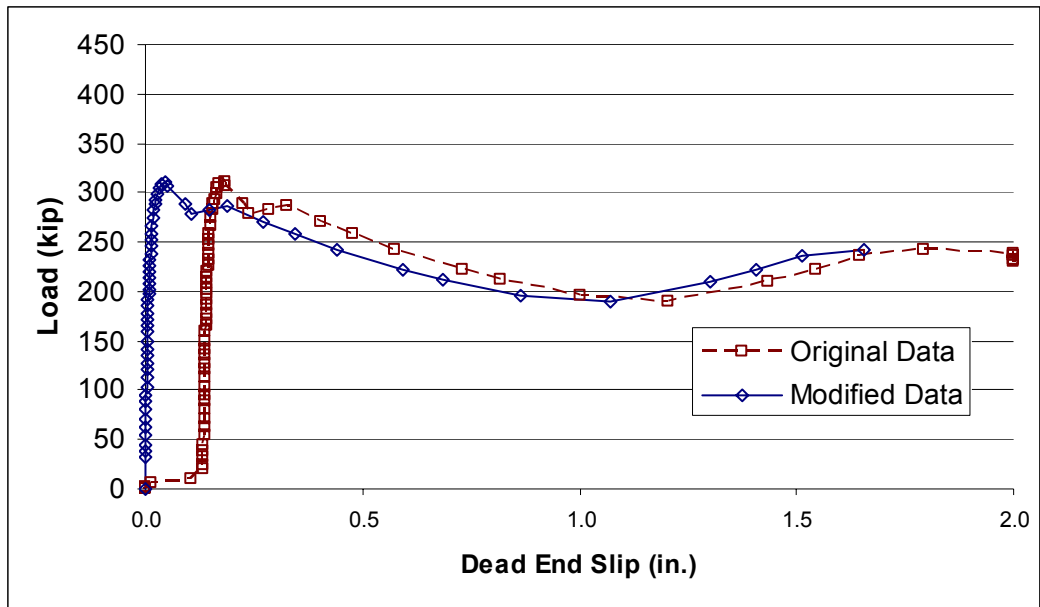
**Figure A-43 Original and Modified Dead End Load-Slip Response for Specimen 0-HD-7.5°-1, Amplified Scale**

### A.3.7 0-HD-7.5°-2

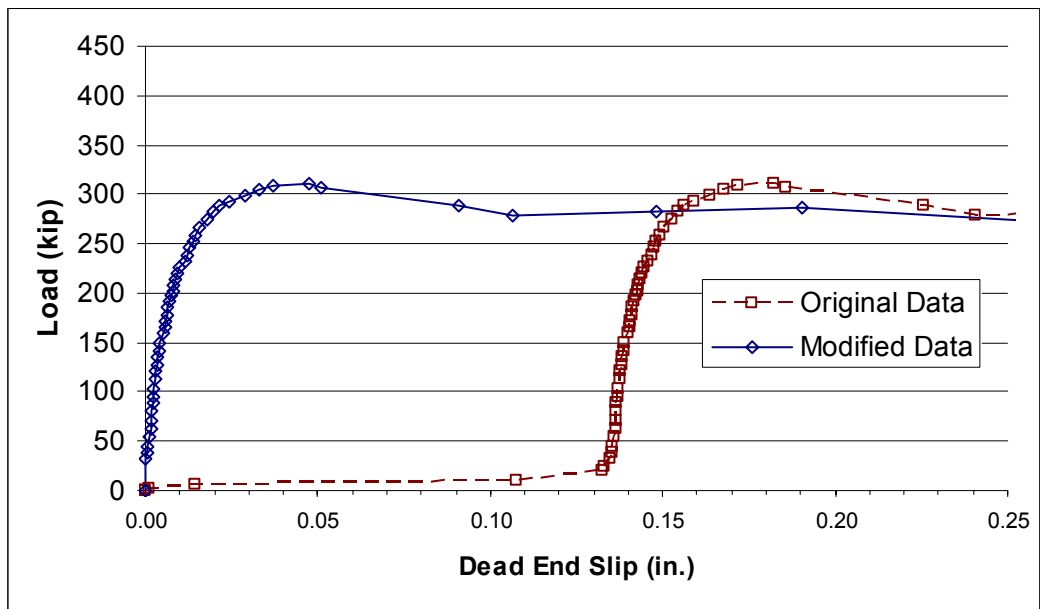
Both live and dead end data were modified for this specimen.



*Figure A-44 Original and Modified Live End Load-Displacement Response for Specimen 0-HD-7.5°-2*



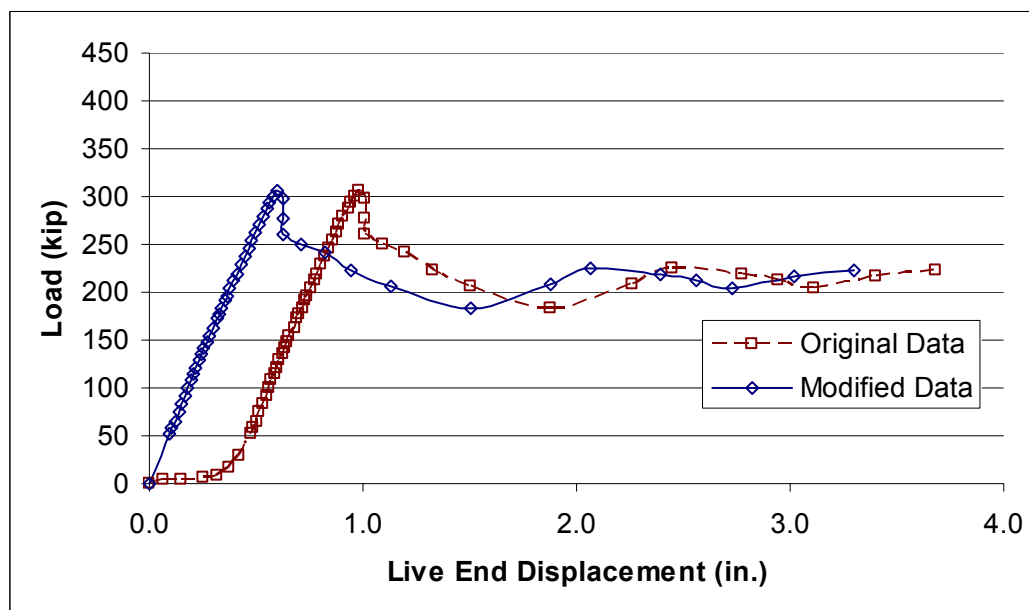
**Figure A-45 Original and Modified Dead End Load-Slip Response for Specimen 0-HD-7.5°-2**



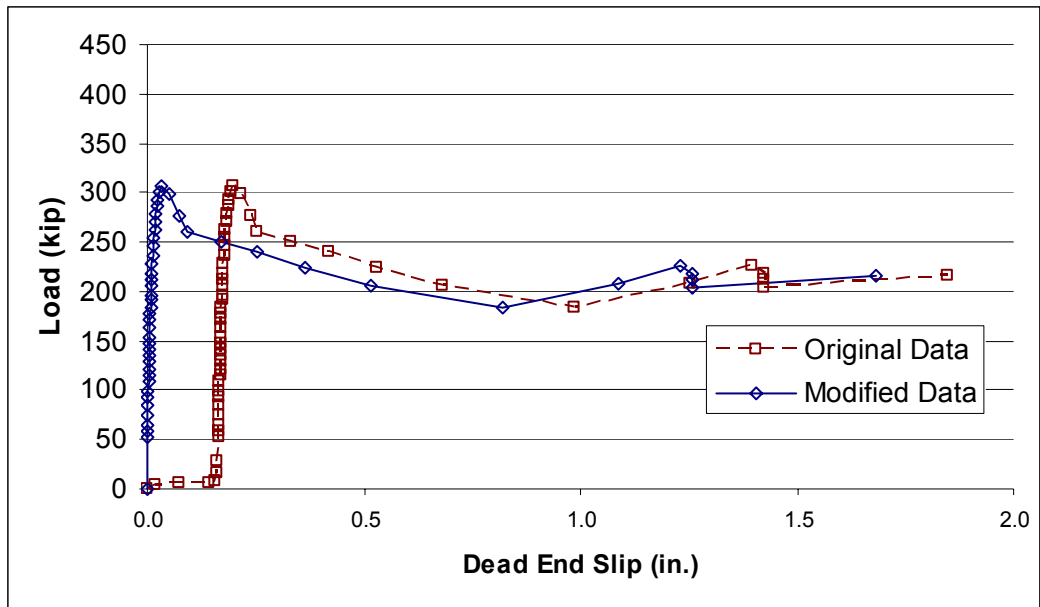
**Figure A-46 Original and Modified Dead End Load-Slip Response for Specimen 0-HD-7.5°-2, Amplified Scale**

### A.3.8 0-HD-7.5°-3

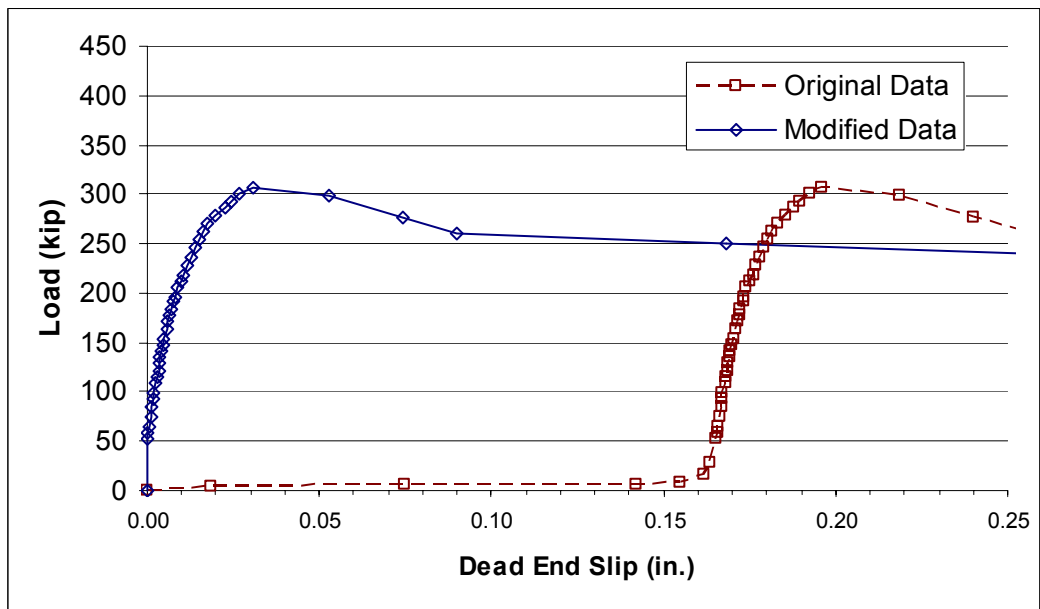
Both live and dead end data were modified for this specimen.



*Figure A-47 Original and Modified Live End Load-Displacement Response for Specimen 0-HD-7.5°-3*



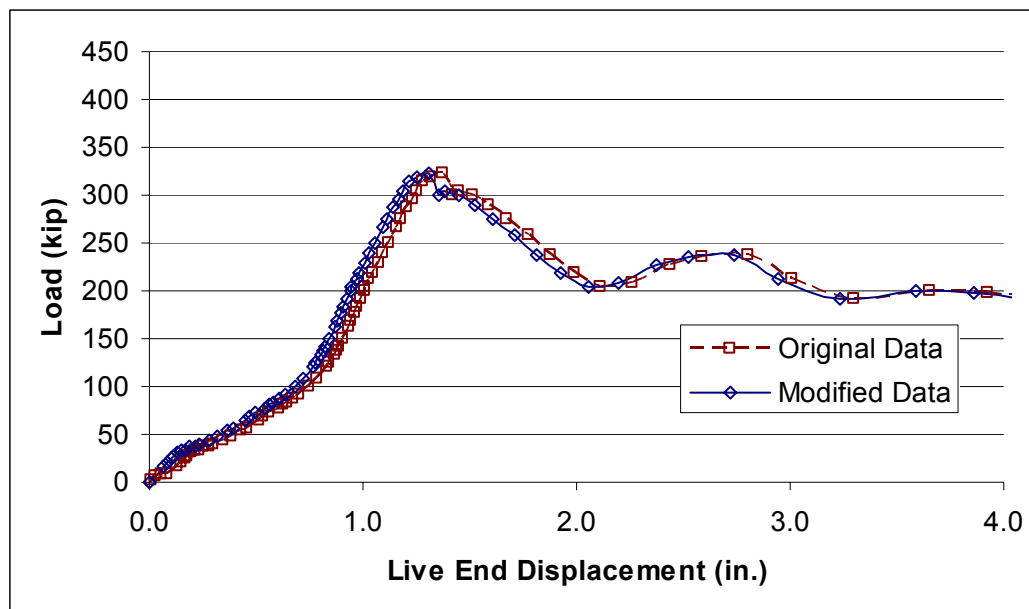
**Figure A-48 Original and Modified Dead End Load-Slip Response for Specimen 0-HD-7.5°-3**



**Figure A-49 Original and Modified Dead End Load-Slip Response for Specimen 0-HD-7.5°-3, Amplified Scale**

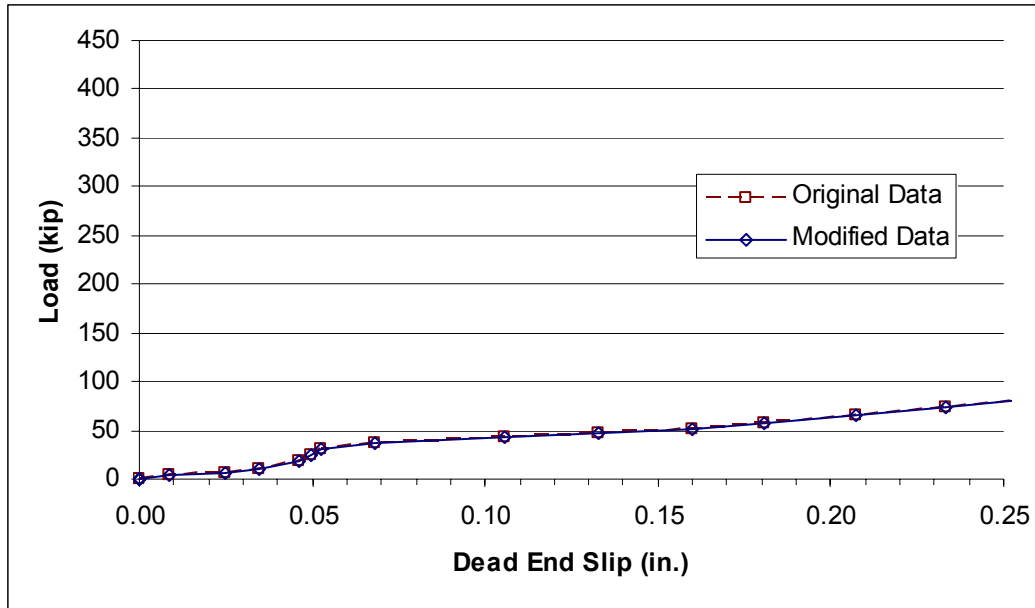
### A.3.9 1-HD-7.5°-1

Both live and dead end data were modified for this specimen. Because the dead end modification was so slight, the plot over the full range of slip values is not included because it is not possible to perceive the difference between the two curves at that scale.



*Figure A-50 Original and Modified Live End Load-Displacement Response for Specimen 1-HD-7.5°-1*





*Figure A-51 Original and Modified Dead End Load-Slip Response for Specimen 1-HD-7.5°-1, Amplified Scale*

**A.3.10 1-HD-7.5°-2**

The data from this specimen required no modification.

## **Appendix B**

### **Specimen Summary**

Table B-1 provides all relevant information about each specimen tested in this program.

**Table B-1 Complete Specimen Summary**

Specimen Name Scheme 1	Specimen Name Scheme 2	Duct Type	Surface Condition	Angle Change (deg)	Cage Type	Longitudinal Bar Size (#)	Transverse Reinforcement Spacing (in.)	Date Cast	Date Grouted	Date Released	Date Test	Grout Strength Release (psi)	Grout Strength Test (psi)	Nearest Concrete Cylinder Test Date	Concrete Comp. Strength (psi)
BT2-1	0-SP-20°-1	SP	Dry	20	H	9	5	1/22/2004	1/29/2004	2/3/2004	2/4/2004	8130	8400	2/3/2004	6440
BT2-2	0-SP-15°-1	SP	Dry	15	H	9	5	1/22/2004	1/29/2004	2/3/2004	2/4/2004	8130	8400	2/3/2004	6440
BT3-1	0-GD-20°-1	GD	Dry	20	H	9	5	2/23/2004	2/26/2004	3/2/2004	3/3/2004	7880	8400	3/9/2004	5630
BT3-2	0-HD-20°-1	HD	Dry	20	H	9	5	2/23/2004	2/26/2004	3/2/2004	3/3/2004	7880	8400	3/9/2004	5630
BT4-1	0-HD-15°-1	HD	Dry	15	H	9	5	2/23/2004	3/4/2004	3/9/2004	3/10/2004	7520	8140	3/9/2004	5630
BT4-2	0-GD-15°-1	GD	Dry	15	H	9	5	2/23/2004	3/4/2004	3/9/2004	3/10/2004	7520	8140	3/9/2004	5630
BT5-1	0-HD-10°-1	HD	Dry	10	S	7	8	3/11/2004	3/17/2004	3/22/2004	3/23/2004	7660	7980	3/23/2004	7140
BT5-2	0-HD-7.5°-1	HD	Dry	7.5	S	7	8	3/11/2004	3/17/2004	3/22/2004	3/23/2004	7660	7980	3/23/2004	7140
BT6-1	0-GD-10°-1	GD	Dry	10	H	7	5	4/2/2004	4/7/2004	4/12/2004	4/13/2004	7200	8440	4/13/2004	6490
BT6-2	0-GD-10°-2	GD	Dry	10	H	7	5	4/2/2004	4/7/2004	4/12/2004	4/13/2004	7200	8440	4/13/2004	6490
BT7-1	0-HD-10°-2	HD	Dry	10	H	7	5	4/2/2004	4/14/2004	4/19/2004	4/20/2004	8280	8580	4/13/2004	6490
BT7-2	0-HD-10°-3	HD	Dry	10	H	7	5	4/2/2004	4/14/2004	4/19/2004	4/20/2004	8280	8580	4/13/2004	6490
BT8-1	0-SP-10°-1	SP	Dry	10	H	7	5	4/2/2004	4/21/2004	4/26/2004	4/27/2004	8350	8660	4/27/2004	7400
BT8-2	0-SP-10°-2	SP	Dry	10	H	7	5	4/2/2004	4/21/2004	4/26/2004	4/27/2004	8350	8660	4/27/2004	7400
BT9-1	0-GD-7.5°-1	GD	Dry	7.5	S	7	5	4/29/2004	5/1/2004	5/6/2004	5/7/2004	8210	8530	5/7/2004	5650
BT9-2	0-GD-5°-1	GD	Dry	5	S	7	5	4/29/2004	5/1/2004	5/6/2004	5/7/2004	8210	8530	5/7/2004	5650
BT10-1	0-GD-7.5°-2	GD	Dry	7.5	S	7	5	5/12/2004	5/19/2004	5/24/2004	5/25/2004	8380	8655	5/24/2004	5980
BT10-2	0-GD-7.5°-3	GD	Dry	7.5	S	7	5	5/12/2004	5/19/2004	5/24/2004	5/25/2004	8380	8655	5/24/2004	5980
BT11-1	0-HD-7.5°-2	HD	Dry	7.5	S	7	5	5/12/2004	5/26/2004	5/31/2004	6/1/2004	8520	8370	6/1/2004	6600
BT11-2	0-HD-7.5°-3	HD	Dry	7.5	S	7	5	5/12/2004	5/26/2004	5/31/2004	6/1/2004	8520	8370	6/1/2004	6600
BT12-1	0-SP-7.5°-1	SP	Dry	7.5	S	7	5	5/12/2004	6/2/2004	6/7/2004	6/8/2004	8680	9110	6/8/2004	7160
BT12-2	0-SP-7.5°-2	SP	Dry	7.5	S	7	5	5/12/2004	6/2/2004	6/7/2004	6/8/2004	8680	9110	6/8/2004	7160
BT13-1	1-GD-7.5°-1	GD	NC 205	7.5	S	7	5	6/7/2004	6/10/2004	6/15/2004	6/23/2004	8620	7600	6/23/2004	7450
BT13-2	1-GD-7.5°-2	GD	NC 205	7.5	S	7	5	6/7/2004	6/10/2004	6/15/2004	6/23/2004	8620	7600	6/23/2004	7450
BT14-1	1-HD-7.5°-1	HD	NC 205	7.5	S	7	5	6/7/2004	6/17/2004	6/22/2004	6/30/2004	8560	9780	6/30/2004	8080
BT14-2	1-HD-7.5°-2	HD	NC 205	7.5	S	7	5	6/7/2004	6/17/2004	6/22/2004	6/30/2004	8560	9780	6/30/2004	8080
BT15-1	1-SP-7.5°-1	SP	NC 205	7.5	S	7	5	6/7/2004	6/24/2004	6/29/2004	7/1/2004	8360	8290	6/30/2004	8080
BT15-2	1-SP-7.5°-2	SP	NC 205	7.5	S	7	5	6/7/2004	6/24/2004	6/29/2004	7/1/2004	8360	8290	6/30/2004	8080

## REFERENCES

1. American Association of State Highway and Transportation Officials (AASHTO), "Standard Specification for Highway Bridges" 17<sup>th</sup> Ed., Washington D.C., 2002.
2. American Segmental Bridge Institute (ASBI), "2002 Grouting Certification training Manual", Phoenix, AZ, 2002.
3. Anderson, A.R. and Anderson R.G., "An Assurance Criteria for Flexural Bond in Pretensioned Hollow Core Units", ACI Journal, Proceedings Vol. 73, No. 8, Aug. 1976.
4. Barnes, R. W., Grove, J. W., and Burns, N. H., "Experimental Assessment of Factors Affecting Transfer Length", ACI Structural Journal, Vol. 100, No. 6, November/December 2003.
5. Braverman, F., "Pull-Out Tests of Prestressing Strands Grouted Inside Smooth-Wall Steel Ducts", Master's Report, The University of Texas at Austin, October 1985.
6. Collins, M. P., Mitchell, D., "Prestressed Concrete Structures", Response Publications, Toronto Canada, 1997.
7. Ferguson, P. M., Breen, J.E., and Thompson, J.N., "Pullout Tests on High Strength Reinforcing Bars", Journal of the American Concrete Institute, Vol. 62, No. 8, August 1965.
8. fib, "Corrugated Plastic Ducts for Internal Bonded Post-Tensioning", Federation International du beton (fib) Technical Report Bulletin No. 7. January 2000.
9. Freyermuth, C.L., "Status of the Durability of Post-Tensioning Tendons in the United States", Durability of Post-Tensioning Tendons. fib-IABSE Technical Report, Bulletin 15. Workshop 15-16 November 2001, Ghent (Belgium), 2001.
10. Ganz, H.R. "Recent Developments in the Protection of Prestressing Steels", Proceeding of the 1<sup>st</sup> fib Congress: Concrete Structures in the 21<sup>st</sup> Century, Session 7, Osaka, Japan, 2002.

11. Hanson, Norman, W. and Kaar, Paul, H., "Flexural Bond Tests of Pretensioned Prestressed Beams," ACI Journal, V. 30, No. 7, January 1959.
12. Janney, Jack R., "Nature of Bond in Pre-Tensioned Prestressed Concrete," ACI Journal, V. 25 No. 9, May 1954.
13. Karr, Paul H., Lafrugh, R.W., and Mass, M.A., "Influence of Concrete Strength on Strand Transfer Length", PCI Journal, Vol. 8, No. 5, October 1963.
14. Kittleman, William Marley, "Evaluation of Emulsifiable Oils for Lubrication and Temporary Corrosion Protection of Seven-Wire Strand," Unpublished Masters Thesis, The University of Texas at Austin, December 1992.
15. Laldji, S. and Young, A. G., "Bond Between Steel Strand and Cement Grout in Ground Anchorages," Magazine of Concrete Research, V. 40, No. 143, June 1988.
16. Losinger, AG. (VSL International), "Zugversuche an Felsanker E 6-52.," Berne, Switzerland, December 1977.
17. Osborne, W. R., "Bond Performance of Grouted Untensioned Multi-Strand Bundles During Pullout Tests", Master's Report, The University of Texas at Austin, December 1986.
18. Pielstick, B.H., "Grouting of Segmental Post-Tensioned Structures in America", Proceedings of the 1<sup>st</sup> fib Congress: Concrete Structures in the 21<sup>st</sup> Century, Session 8, Osaka, Japan, 2002.
19. Post-Tensioning Institute (PTI), Specification for Grouting of Post-Tensioned Structures, 2000.
20. Radloff, Brock Jordan, "Bonding of External Tendons at Deviators", Unpublished Masters Thesis, The University of Texas at Austin, December, 1990.
21. Russell, B. W., and Burns, N. H., "Measurement of Transfer Lengths on Pretensioned Concrete Elements", Journal of Structural Engineering, Vol. 123, No. 5, May 1997.
22. Salcedo, Edwin Rueda, "Effects of Emulsifiable Oils Used as Temporary Corrosion Protection in Grouted Post-Tensioned Tendons", Master's Thesis, The Pennsylvania State University, August 2003.

23. Salmons, J. and McCrate, T., "Bond Characteristics of Untensioned Prestressing Strand," PCI Journal V. 22, No. 1, Jan-Feb 1977.
24. Schokker, A.J., Koester, B.D., Breen, J.E., and Kreger, M.E., "Development of High Performance Grouts for Post-Tensioned Structures", Research Report 1405-2, Center for Transportation Research, Bureau of Engineering Research, The University of Texas at Austin, December 1999.
25. Schupack, M. and Johnston, D.W., "Bond Development Length Tests of a Grouted 54 Strand Post-Tensioning Tendon", ACI Journal, Vol. 71 No. 10, October 1974.
26. Tourneur, S., "Prestressing: 60 Years of Innovation", Compact Disc: The French Technology of Concrete, The 1<sup>st</sup> fib Congress 2002, Osaka, Japan.
27. Trost, H., Cordes, H., and Hagen, H., "Auswirkungen des Verbundverhaltens Zwischen Spannglied und Einpressmörtel Bei Verwendung Von Spanngliedern Mit Über 1500 Kn Zulässiger Spannkraft", Technischen Hochschule Aachen, July 1978.
28. Trost, H., Cordes, H., Thormahlen, U., and Hagen, H., "Verbundfestigkeit von Spanngliedern und ihre Bedeutung für Ribbilung und Ribbreitenbeschränkung", Deutscher Ausschuss Für Stahlbeton, Heft 310, W. Ernst and Sohn, Berlin, West Germany, 1980.
29. Vos, E. and Reinhardt, H.W., "Bond Stress-Slip Behavior of Deformed Bars, Plain Bars, and Strands Under Impact Loading", *Bond in Concrete*, Ed. P. Bartos, Applied Science Publishers, London, 1982.
30. VSL International, "Considerations Concernant le Dimensionnement et L'arrangement de la Zone de Scellement du Tirant"
31. Woodward, R., "Durability of Post-Tensioned Tendons on Road Bridges in the UK", Durability of Post-Tensioned Tendons. fib-IABSE Technical Report, Bulletin 15. Workshop 15-16 November 2001, Ghent (Belgium), 2001.

## VITA

Jeffrey Roger Diephuis was born in Grand Rapids, Michigan on March 13, 1980, to Daniel James and Betty Jo (Lindemulder) Diephuis. He graduated from Grand Rapids Christian High School in the spring of 1998. Entering Grand Rapids Community College the following fall, he earned an Associate of Science degree with honors in the spring of 2000. In the fall of that year he transferred to Michigan Technological University, in Houghton, Michigan. He was awarded the degree Bachelor of Science in Civil Engineering, summa cum laude in the spring of 2002. The following August he entered The Graduate School of The University of Texas at Austin.

Permanent Address: 622 Steketee RD NE  
Ada, MI 49301  
USA

This thesis was typed by the author.